University of East Anglia

Preventing the anti-angiogenic escape through the endothelial adhesome.

Aleksander M. Gontarczyk

A thesis submitted for the degree of Doctor of Philosophy (Ph.D.) in Biomolecular Science

University of East Anglia

School of Biological Sciences

January 2019

Dedication

To my family

Mamo, Tato, Martyna

You have always encouraged me to aim higher

Thank You

Abstract

αVβ3 integrin is a promising target for therapy due to its upregulation in angiogenic vasculature. However, Cilengitide, an αVβ3 integrin inhibitor (RGD mimetic), has failed late stage clinical trials due to lack of overall survival benefit. We have previously shown that depleting β3-integrin acutely in the mouse endothelium leads to smaller tumours *in vivo*, whereas constitutive depletion of endothelial expression of this molecule causes an increase in tumour angiogenesis. In the context of cancer therapy, long-term depletion or inhibition of β3-integrin is subject to treatment escape via unknown mechanisms of resistance. At the molecular level, much of the regulation of endothelial cell migration and adhesion, and therefore angiogenesis, occurs via the 'adhesome' – the sub-proteome present in focal adhesion complexes. We isolated and compared WT, β3-HET, β3-KO and αVβ3-inhibitor-treated adhesomes by mass spectrometry. Among approximately 300 proteins whose abundance significantly changed, three intermediate filament proteins were upregulated in the β3-integrin depleted adhesome, namely: nestin, plectin and vimentin. All three molecules are known to regulate integrins and play a role in angiogenesis.

Given this upregulation of intermediate filaments in the adhesome, I set out to determine whether they are playing a differential role in angiogenesis depending on β3-integrin depletion. At first, I took an siRNA approach to determine the functional consequence of knocking down each target, but, overall, results from this approach were inconclusive. However, I observed that Withaferin A, an inhibitor of vimentin, impaired proliferation and migration of β3-HET, but not WT, endothelial cells. I then decided to look at the effects of Withaferin A on subcutaneous tumour growth *in vivo*, in combination with long-term endothelial-specific depletion of β3-integrin (via the β3-floxed Tie1.Cre model). The drug did not significantly inhibit tumour growth, but tumour angiogenesis was significantly reduced in the Cre +ve, and not in the Cre -ve background. Similarly, Withaferin A inhibited microvascular sprouting of β3-floxed Tie1.Cre +ve aortic rings, but not of Cre -ve rings. I also utilised pSico technology as an shRNA delivery system and observed impaired microvascular sprouting when depleting nestin. Additionally, I generated tdTomato-labelled nestin constructs which could be utilised to visualise nestin *in vitro*. Overall, the findings described in this thesis suggest co-targeting β3-integrin and intermediate filaments, such as those made up of vimentin, as an improved anti-angiogenic strategy.

Contents

List of Figures

List of Tables

Acknowledgements

Dr Stephen Robinson. From start to end, your supervisory input was fantastic. Thank you for securing funding for this project from BigC and allowing me to work on it. You have planned it so well, I have not strayed from the original plan much at all. For all the many suggestions, motivation and help. I am very grateful for you always having time to listen. No doubt, the best PhD supervisor award is well deserved. Also, big thanks for organising the climbing course. That was an amazing lab activity.

Special thanks to Professor Ulrike Mayer as my secondary supervisor. Her feedback and suggestions also shaped this project. At the same time, it would not be possible to do this work without her dissection microscope and cryostat.

Professor Dylan Edwards for his intellectual input when I presented my work to the group. Also, thank you for the drinks at lab outings and the coffee!

Everyone in the lab that I had a pleasure to work with. Initially: Veronica, Tim, Christian, Julie and Liz, thank You! And then Sophie, Jordi, Kate, Sally, Tim (again), Sam, Ben, Abdu, Rob, Wez, Ali, Chris and James, thank You!

Sam, you laid the foundations for this project, taught me many things, thanks for your help and advice on all the aspects of the project. Tim, thanks for the conversations and teaching me lots of things. Abdu, thanks for always offering to help. Rob and Wez thank you for preparing all those 'cheesecakes'. Ben, thanks for your intellectual input. Kate, thanks for the real-time PCR work and proofreading of this thesis. Jordi, thanks for the ICC work. Last but not least, Sally, for the very many corrections that this thesis needed and the H&E's. Thanks to everyone that helped with this project.

It was fun having students around in the lab, especially Rosie and Ali. Thanks to James for his work on Adamts4 and the BIO hoodie.

I am grateful to Dr Paul Thomas for his help with microscopy on this project.

Martina, thanks for your help with molecular biology, for the very many coffees, pizzas and sweet edibles we shared.

Big thanks to the Fountain and Clark labs, for the conversations and saving our experiments several times.

Special thanks to BigC, Norfolk's cancer charity and those who donate to it. You do great work and big thank you for funding this PhD studentship.

Thanks to Pint of Science for letting me organise one of your events and give a talk the following year. Such a nice experience that opened me up to science communication.

Thanks to the Jicarilla Awkward Buddies: Andra, Barbora, Jon, Katka, Michelle, Smilyan, Svetlana, Tilak, Vlad C and Vlad O. Our reunions are priceless, give me new ideas and recharge my life energy levels, so thank you.

Cheers to Towers and Wolves volleyball teams. Auuu!

Thanks to fellow boulderers and climbers.

Mamo, you inspire me to do my best, you are always there for me in time of need, and any other time. Thank you. Also, I was envied by many, because of the lunches you prepared.

Tato, without your support I could not do many things that I had a privilege to do, including the Master's and this PhD.

Martyna, thank you for being the kind of sister that you are and helping me get a grip on life.

Finally, to Archana, the crazy Indian, my buddy, force of nature, the love of my life, the best human being there ever will be. I love you and thank you for taking care of me while writing and any other time.

1 Introduction

1.1 Preface

One of the hallmarks of cancer – angiogenesis – is a process of new blood vessel formation from ones that already exist. Tumours need a continuously expanding vascular network to meet the nutrient demand for rapid growth. Endothelial cells are the main drivers of this process, while their adhesion and migration are key for angiogenesis to proceed. At the molecular level, these processes are mediated by the 'adhesome' – the sub-proteome making up the focal adhesion complexes. A prominent member of the adhesome is αVβ3-integrin. Due to its role in angiogenesis, attempts have been made to target this protein in the battle against cancer. Unfortunately, long-term inhibition is subject to treatment escape. This thesis describes an investigation of the molecular detail of this phenomenon and proposes a dual-targeting approach for an improved anti-angiogenic strategy. The introduction chapter begins with a description of tumour angiogenesis, moves onto the endothelial cell adhesome, followed by a discussion about the current anti-angiogenic strategies.

1.2 Angiogenesis and Cancer

1.2.1 Vasculogenesis

Most cell types cannot survive further than 100 µm away from an oxygen source, as the diffusion rate of oxygen through the tissue beyond this thickness becomes not efficient enough to satisfy the needs of the cells [1]. Therefore, a vast network of blood vessels that reaches every part of the body at the microscopic level is required to meet respiratory needs, as well as to remove metabolic waste products. This vascular network is laid down in the embryo before the heart starts beating [2]. Embryonic growth depends on the cardiovascular system, therefore this organ system is the first functional one in the vertebrate embryo [3]. Vasculogenesis, or *de novo* blood vessel formation is a process where mesoderm, the middle germ layer of the primary embryo, gives rise to the vascular plexus [4]. More specifically, the haemangioblast lineage arises from mesodermal precursors, which subsequently differentiates into haematopoietic stem cells (HSCs) and endothelial cell (EC) precursors – angioblasts. The latter give rise to vascular ECs which arrange into a primitive network of vessels – the vascular plexus [3]. Angioblasts can migrate to distant sites before creating a new vascular plexus in response to the right cues [3], [5]. Haemangioblast induction appears to begin with expression of Vascular Endothelial Growth Factor Receptor 2 (VEGFR2) [6]–[8]. HSCs subsequently turn off VEGFR2 expression at a later stage of differentiation, while ECs express VEGFR2 throughout their lifetime [3]. VEGF, VEGF receptor 1 (VEGFR1) and VEGFR2 are all necessary for vasculogenesis.

The importance of VEGF in vasculogenesis was demonstrated by generation of the VEGF KO allele. The lack of one copy of the gene (in VEGF KO heterozygous mice) is enough to cause death *in utero* due to blood vessel network malformation [9], [10]. VEGF is secreted by the endoderm-derivatives in the embryo, while the angioblasts originating from the mesoderm express the VEGF receptors [3]. Both VEGFR1 KO and VEGFR2 KO mice also die *in utero* due to inability to generate an organised blood vessel network [11], [12]. Upon binding VEGF, VEGFR2 tyrosine kinase activity results in survival, proliferation and migration, thus promoting blood vessel formation [13]–[15]. VEGFR1 mainly contributes to the assembly of functional vessels as a negative regulator of the process [16], [17]. Vasculogenesis is a process limited to the embryo, except one controversial postnatal mechanism, where bone-marrow-derived cells are incorporated into the endothelium [18].

1.2.2 Angiogenesis

Once the vascular plexus is established, further expansion of the vascular system occurs by generation of new blood vessels from pre-existing ones, a process termed angiogenesis. Two types of angiogenesis can occur: sprouting or non-sprouting (intussusception). The latter is a process of splitting of an existing vessels into smaller ones, a phenomenon first described in the development of the complex network of bronchi and bronchioles in the lung [19], [20].

Here, the focus is on sprouting angiogenesis inducible by growth factors, such as VEGF, where vasculature chemotactically extends into the tissue. When a human body reaches adulthood this process is limited to the proliferative phase of the uteral cycle, wound healing and disease, most notably cancer [21].

Angiogenesis is a multi-step process orchestrated by a plethora of molecular players within the participating cells. Below, a section each of this introduction is dedicated to integrins and VEGFs (and their receptors). Other key players include: angiopoietins (Ang1 and Ang2) and their receptors (Tie1 and Tie2), CD31, CD34, fibroblast growth factors (FGFs), endothelial nitric oxide synthase (eNOS), ephrins, hypoxia inducible factors (HIFs), matrix metalloproteinases (MMPs), Neuropilin-1 (Nrp1), platelet-derived growth factor B (Pdgfb), Slits, transforming growth factor β (TGF-β), tissue inhibitors of metalloproteinases (TIMPs) and VE-Cadherin.

In inflamed and hypoxic tissue, there is an accumulation of HIFs, such as HIF-1α [22]. This leads to an upregulation of genes encoding secreted angiogenic factors such as VEGFs, FGFs and angiopoietins, to initiate the 'angiogenic switch' [23]. VEGF is upregulated up to 30-fold in response to HIFs [24]. Also, Notch signalling plays an important role. Membrane-embedded Notch receptors in ECs are cleaved and release a fragment inside the cell, upon interaction with ligands from neighbouring cells, such as Delta-like or Jagged [25], [26]. The cleaved fragment becomes a transcription factor, which is translocated to the nucleus to promote expression of genes, such as CD31, VE-Cadherin, Nrp1 and VEGFR2 [27].

As a result of the pro-angiogenic signalling, pericytes detach from micro-vessels in response to Ang2, MMPs make way for the new vessels by degrading the basement membrane (BM) and EC junctions loosen, a consequence of endocytosis of VE-Cadherin [18], [28]. At the same time, VEGF leads to an induction of eNOS, which causes vasodilation of vessels, increased permeability and extravasation of some of the cargo [29]. Next, ECs switch to a proliferative and migratory phenotype, as a consequence of combined action involving VEGFs, FGFs, Ang2, Nrp1, integrins and other factors [30]. According to the current dogma, a tip cell emerges, which leads the way in the formation of a new blood vessel [31]. ECs compete for the tip cell position based on their expression of VEGF receptors. The cell which is best equipped to respond to VEGF, takes the

lead, while the neighbouring ECs follow and become the stalk cells [31]. Tip cell guidance and adhesion involve ephrins, Slits and integrins, while VEGFR1, PGF, FGFs, Notch and other factors regulate stalk elongation [30]. VEGF, VE-Cadherin and CD34 ensure lumen formation in the stalk of expanding vessel [32]. ECs physically migrate, to form new blood vessels, while remodelling the ECM in the process, in a chemotactic manner, guided by the pro-angiogenic factors [23], [33]. This EC migration is mediated by integrins. This continues until two sprouting vessels meet, leading to a process of joining, or anastomosis of the lumen, thus expanding the blood vessel network [34]. Finally, new vessels enter the maturation stage. EC junctions are re-established in response to Ang1 and VE-Cadherin, while Pdgfb, Ang1, FGF and Notch signalling ensure that pericytes wrap around the newly formed vessels to provide stability [35], [36]. Also, TGF-β induces fibronectin and collagen deposition by the surrounding cells [37]–[39]. This is aided by TIMPs, which inhibit BM degradation and thus enable the BM to be rebuilt [34].

New blood vessels reach the cells which had an insufficient oxygen supply and lack of waste removal. In healthy angiogenesis, when the oxygen demands are met, further VEGF, Ang1, FGF and Notch signalling leads to maintenance of newly built vessels. This involves further recruitment of supporting cells, generation of matrix, fenestration where required, as well as expansion, branching and pruning of vessels [30]. Vessels without a pericyte coating undergo regression [40].

Notch signalling, via receptors such as Notch-1, drives ECs towards a more angiogenic potential and promotes EC maturation [18]. Notch signalling is a process evolutionarily conserved from sea urchins to humans, fundamental in development [41]. It lies at the heart of deciding cell fate, with consequences in cell growth, proliferation, migration and death [42]. Malfunction leads to heavy repercussions including disrupted neuro-, lympho- and angiogenesis [43]. Moreover, Notch signalling promotes the arterial fate of ECs during the process of differentiation of embryonic stem cells (ESCs) into ECs and is critical for proper maintenance of arteries [27].

1.2.3 Tumour Angiogenesis

Angiogenesis within the tumour microenvironment is much more chaotic than during physiological angiogenesis. In the late 1800s German pathologists noticed that tumours are highly vascularised [44]. A prominent study from 1927 described varying vascular architecture in different tumour types and led to the conclusion that tumour environment must have an impact on blood vessel growth and morphology [45]. Cells within a tumour mass often grow at a rapid rate and thus use up all the resources, creating a hypoxic environment. In order for a tumour to grow beyond 1–2 mm in diameter it needs to recruit new vasculature to supply it with sufficient amount of nutrients and oxygen [46]. The prevalent characteristics, such as disrupted vasculature, inflammation, necrosis and thick stroma, has led tumours to be described as "wounds that do not heal" [47]. The interactions between integrins, growth factor receptors and cytokine receptors in tumour and tumour-associated host cells (ECs, pericytes, fibroblasts, monocytes and myeloid cells) play a major role in tumour progression [48].

Chaos in the genome and the gene expression profile of cancer cells is reflected at the level of the tumour microenvironment, including the vasculature [49]–[51]. Heightened and prolonged abundance of pro-angiogenic factors leads to pathological levels of sprouting and abnormally high fenestration of the vessel wall [52]–[54]. ECs are forced to maintain high metabolism to meet the demands for their migration and proliferation [55]. Constant stimulation does not allow for mature vessels, with proper morphology and function, to form (**Fig. 1.1**) [56]. As the tumour expands pro-angiogenic signalling continues and the vasculature expands with it. The vessels are tortuous, leaky, highly disorganised and fragile (**Fig. 1.1**) [49], [57], [58].

Once the vascular barrier is compromised, blood perfusion is impaired and there is increased extravasation of leukocytes. The prominent subsets present in the tumour microenvironment include both myeloid cells (macrophages, eosinophils, dendritic cells) and lymphoid cells (T cells), although the composition varies between tumours [59], [60]. It can be said that tumours recruit myeloid cells, which release stimulatory factors for tumour cell survival and angiogenesis, including VEGF, TGF-β, MMPs, nitric oxide, but also pro-inflammatory cytokines [61], [62]. Typically, the extent of immune cell infiltration correlates with the progression stages of cancer. Indeed, the tumour microenvironment is typically in the state of inflammation, due to presence of immune cells attempting to fight the tumour, initially perceived as a foreign body [63], [64].

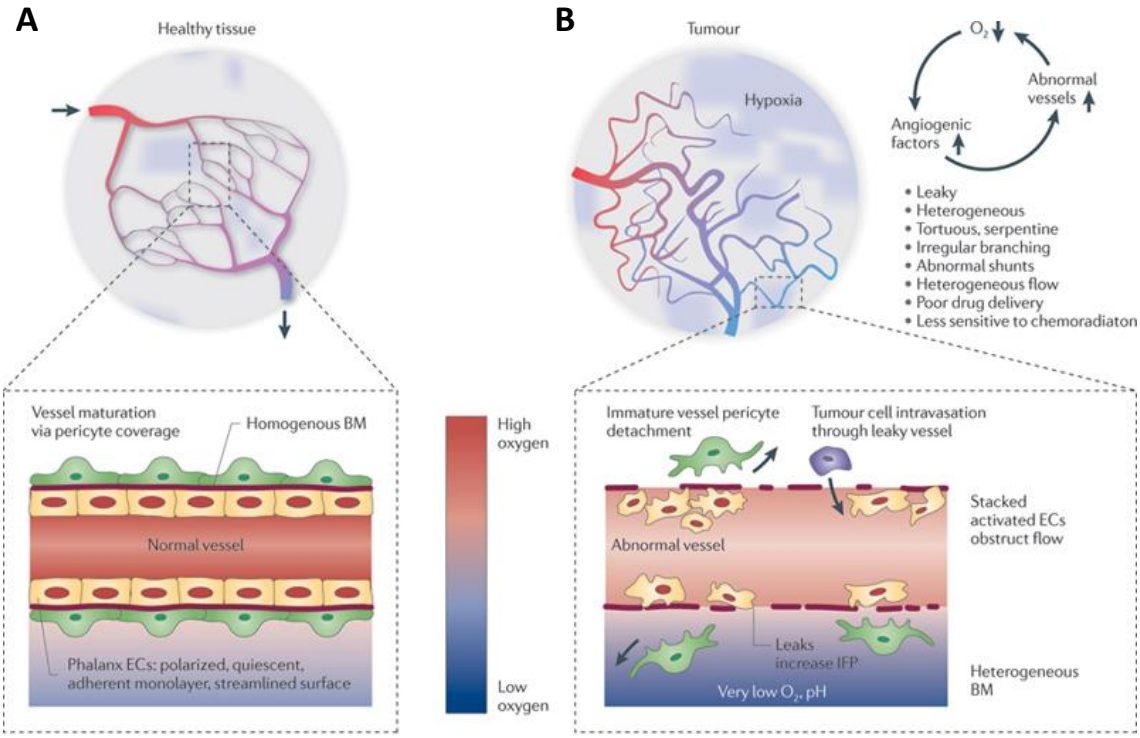

Figure 1.1 Comparison of normal and tumour vasculature.

(**A**) In normal tissue small blood vessels consist of highly organised layers of ECs, basement membrane and pericytes whereas (**B**) within a tumour, blood vessels are always expanding due to constant stimulation by angiogenic factors induced by hypoxia. This takes place too rapidly, resulting in leaky vessels with a very chaotic architecture. Adapted from [65].

At the same time, a key cell type linked with tumour progression is the M2 macrophage: polarised to the anti-inflammatory phenotype, also referred to as the tumour-associated macrophage (TAM). Presence of M2 macrophages in the tumour promotes angiogenesis and correlates with reduced patient survival [66]. However, pro-inflammatory, anti-tumour M1 macrophages are also present, and the latest understanding is that there is no clear-cut differentiation between M1 and M2 [67]. There is rather a spectrum of polarisation with a range of overlapping functions [68].

It has been suggested that a form of vasculogenesis can occur in the adult organism, whereby circulating bone-marrow-derived cells differentiate into ECs and participate in neovascularisation at a site of injury [69]. Others have shown that this recruitment of EC precursor cells also occurs in the tumour and impairing this process has the potential to inhibit tumour growth and angiogenesis [70].

Moreover, tumour angiogenesis promotes disease progression, as increased vessel permeability enables metastasis. In order for a primary tumour to spread, cancer cells from the primary site must enter the blood or lymphatic vessel by intravasation, travel to the secondary site and leave the vessel by extravasation [71]. Many of these cancer cells will fail to metastasise, unable to cross one of the barriers or unable to colonise a particular secondary site, or due to being captured by the immune system [71], [72]. However, as the primary tumour expands, more entry points in the growing vasculature are created increasing the chances of successful metastasis. A chaotic and dynamic angiogenesis of the tumour vascular network produces leaky vessels which allow tumour cells to enter much more easily than into normal vasculature. Angiogenesis and metastasis are both fundamental hallmarks of cancer, while metastasis can be viewed as the primary reason of cancer patient death [73], [74]. The fact that angiogenesis enables metastasis, highlights this process for targeting in the battle against cancer. The hope is that if we target tumour angiogenesis, tumour growth is halted at an early, benign stage.

1.2.4 VEGFs and Their Receptors

In the 1980s it was observed that conditioned media from a guinea pig tumour cell line contained a protein which enhanced vascular permeability, EC growth and angiogenesis [75]. A few years later this was identified as VEGF [76], [77]. Undoubtedly, it can be described as the most prominent among all the pro-angiogenic factors. However, the mammalian genome contains four VEGF genes: VEGF-A, -B, -C and -D. These four along with placenta growth factor (PGF) constitute the VEGF sub-group of the platelet-derived growth factor (PDGF) family [78]. VEGFR1, 2 and 3 are the three type III receptor tyrosine kinases that initiate intracellular signalling upon binding to VEGFs [78].

1.2.4.1 VEGF Types

VEGF-A is the most studied isoform due to its involvement in both developmental and pathological angiogenesis. The human VEGF-A gene possesses three widely expressed splice variants: $VEGF_{121}$, $VEGF_{165}$ and $VEGF_{189}$; and two rare variants $VEGF_{145}$ and $VEGF_{206}$ [79]. The numbers refer to the length of amino acids within their structures, excluding the signal sequence required for extracellular secretion, which is cleaved off [80]. VEGF refers to VEGF-A_{165} throughout this thesis, which is the most studied isoform. VEGF binds receptors VEGFR1, VEGFR2, as well as co-receptors Nrp1 and Nrp2 to promote survival, proliferation, migration and sprouting of ECs in developmental and pathological angiogenesis [78], [81]. Also, VEGF upregulates expression of eNOS, which generates nitric oxide, a vasodilator contributing to vascular permeability [29]. The lack of a single VEGF allele is sufficient for embryonic lethality in mice due to the dramatic impairment of angiogenesis and blood island formation [10]. Keshet *et al.* reported that VEGF was hypoxia inducible [82]. Soon after, a region within the structure of VEGF (and erythropoietin) was proven to be the binding site of HIF-1α thus further elucidating the mechanism [83], [84]. Hypoxia in the tumour microenvironment induces angiogenic factor production, including VEGF, the key driver of angiogenesis, to make tumours highly vascularised [77], [78], [85]. Monoclonal antibody inhibition of VEGF has been shown to dramatically suppress tumour growth *in vivo* [86]. At the same time, neither VEGF nor VEGF inhibition affect tumour cell growth *in vitro*, leading to a conclusion that it is a vasculature-specific mitogen [87]. This portrays VEGF as an excellent vasculature-specific therapeutic target. Indeed, a number of VEGF-targeting agents are in use in the clinic. These will be covered in Section 1.4.2.

VEGF-B binds only VEGFR1 and Nrp1 [88]. One study reported VEGF-B to be needed for correct development of the myocardial tissue [89]. On the other hand, most studies have shown VEGF-B KO mice are healthy and fertile under normal conditions [89]–[91]. Some argue that it may be a useful target in anti-angiogenic therapy, as it contributes to angiogenesis in pathological conditions as a survival factor [92], [93]. VEGF-C mainly stimulates vasculogenesis and lymphangiogenesis via VEGFR3, but it can also bind VEGFR2, although not as efficiently as VEGF-A [94], [95]. VEGF-D has some angiogenic and lymphangiogenic potential and acts through VEGFR2 and VEGFR3 [81], [96]. PGF is a VEGFR1 ligand, implicated in vasculogenesis, wound healing and cancer [97], [98].

1.2.4.2 VEGF Receptors

VEGFR1, also known as fms related tyrosine kinase 1 (FLT1), gene encodes a transmembrane receptor, but also a shorter, soluble isoform, which gets released into the extracellular space [99]. The membrane-bound variant can exert a weak tyrosine kinase activity upon binding its ligands, VEGF-A, VEGF-B and PGF [78], [100]. As a result, VEGFR1 appears to act as both a mild stimulator of vasculogenesis and a negative regulator of angiogenesis [101]–[103]. Its antagonistic role is carried out by sequestering VEGF, which would otherwise bind and activate VEGFR2 [16], [17]. VEGFR1 KO in mice is embryonic lethal, due to excessive proliferation of angioblasts [11], [16]. Interestingly, mice lacking the tyrosine kinase domain of VEGFR1 develop into adulthood with no overt abnormalities to the vasculature [104]. Therefore, the VEGF decoy function appears to be an essential step in angiogenesis for mature, functional vessels to form. Both the tyrosine kinase activity of VEGFR1 and sequestering VEGF can contribute to pathological conditions [105], [106].

The affinity of VEGFR2, also referred to as fetal liver kinase 1 (FLK1) and kinase domain receptor (KDR), to bind VEGF is two-fold weaker than that of VEGFR1, but the tyrosine kinase activity is estimated to be ten-fold more potent [107], [108]. This signalling potential makes it a key receptor in VEGF-dependent angiogenesis and hematopoiesis. Its importance was demonstrated by VEGFR2 KO in mice, which causes death *in utero* due to failure to form blood islands and disruption of vasculature [12]. VEGFR2 is found embedded in the membrane of early haemangioblasts and post-embryogenesis becomes mostly limited to ECs, although there are reports of its expression in a sub-population of cardiovascular stem cells and macrophages [109]–[111]. VEGFR2 can also weakly bind VEGF-C [112].

VEGFR2 consists of seven extracellular immunoglobulin(Ig)-like domains, a transmembrane linker and intracellular tyrosine kinase region, followed by the C-terminal end domain (**Fig 1.2**) [113]. VEGF binds at the second and third Ig-like domains, leading to a receptor dimerisation and phosphorylation at multiple tyrosine (Y) sites [114]. The major phosphorylation residues are Y951, Y1054, Y1059, Y1175 and Y1214 [113]. The rat sarcoma (RAS)/rapidly accelerated fibrosarcoma (RAF)/mitogen-activated protein kinase kinase (MEK)/extracellular signal-regulated kinase (ERK) pathway downstream of VEGFR2 stimulates EC proliferation, while survival is promoted by the phosphoinositide 3-kinase (PI3K)/phosphoinositide-dependent kinase (PDK)/protein kinase B (PKB, Akt) pathway (**Fig 1.2**) [114], [115]. Multiple pathways downstream of VEGFR2 promote EC migration: proto-oncogene tyrosine-protein kinase (Src)/SH2 domain-containing adaptor protein B (SHB)/focal adhesion kinase (FAK) pathway, PI3K/Rac Family Small GTPase (RAC) pathway and P21 activated Kinase 2 (PAK2)/cell division cycle 42 (Cdc42)/p38 mitogen-activated protein kinase (p38 MAPK) pathway [114], [116]–[120]. VEGFR2 signalling is influenced by dimerisation, endocytosis and recycling of the receptor [121]–[123]. Also, its co-receptors, such as integrins and neuropilins, contribute to cellular events downstream of VEGR2 [124]–[127].

VEGFR3, also knowns as fms-related tyrosine kinase 4 (FLT4), binds VEGF-C and VEGF-D to stimulate vasculogenesis and lymphangiogenesis [96], [128]. VEGFR3 KO mice die during embryogenesis due to defects in the cardiovascular system, before the lymphatic system emerges [129]. Post-embryogenesis its expression becomes largely restricted to lymphatic ECs [78].

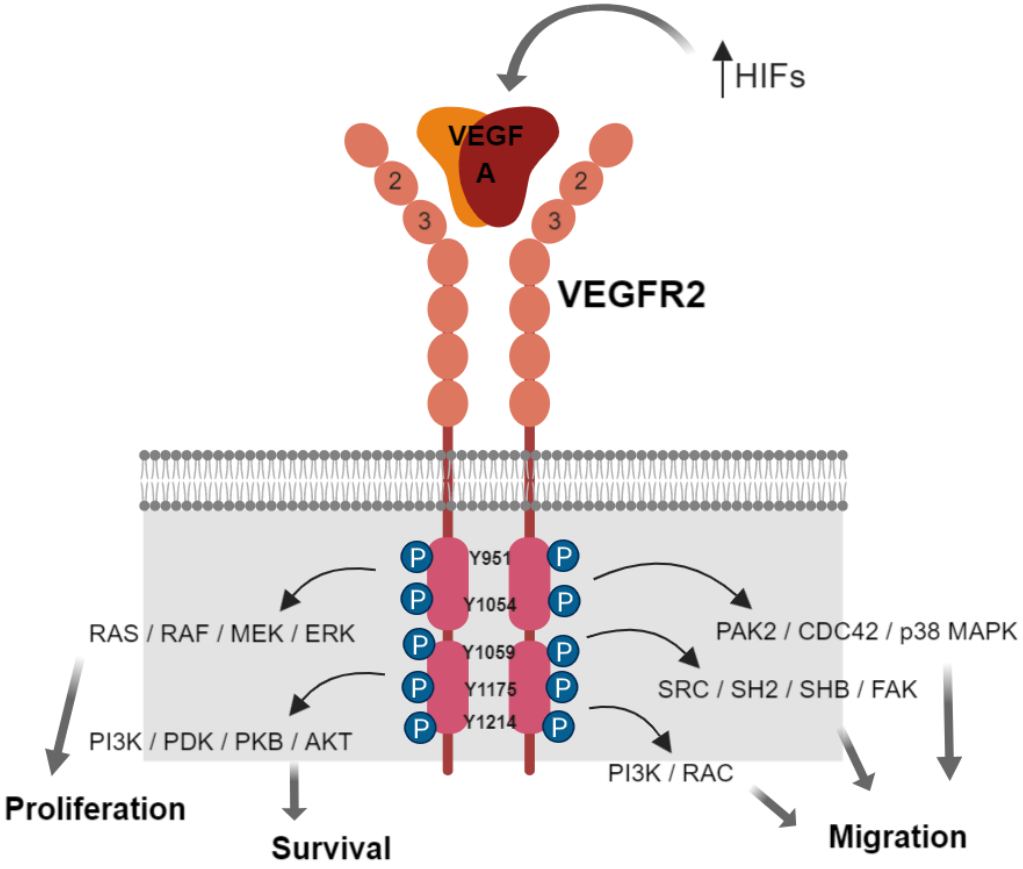

Figure 1.2 VEGF / VEGFR2 complex and downstream signalling.

Hypoxic tissue accumulates HIFs causing an upregulation and release of VEGF. VEGFR2 is embedded in the cell membrane of endothelial cells and binds VEGF via the 2nd and 3rd Ig-like domain. VEGF-bound VEGFR2 undergoes auto- and transphorylation at multiple tyrosine (Y) sites. This initiates a number of signalling pathways which promote endothelial cell migration, proliferation and survival. Figure adapted from Koch *et al*. (2011) and generated with BioRender.com [114].

1.2.5 Integrins

Integrins are a family of cell surface glycoproteins, present in most cell types, which mediate cell adhesion to the ECM or immunoglobulins [130], [131]. An integrin receptor is made up of non-covalently associated α and β subunits, forming a heterodimer (**Fig 1.3 A**). Typically, an α monomer is approximately 1000 amino acids long, while a β monomer tends to be made up of 750 amino acids [132]. Both monomers possess a short cytoplasmic tail, a transmembrane helical domain and a large, multi-domain extracellular region (**Fig 1.3 A**) [133]. In vertebrates, the integrin family comprises of eighteen α and eight β monomers which pair to form at least 24 distinct heterodimeric integrin receptors (**Fig 1.3 B**) [134]. The number of binding partners vary. For instance, β1 integrin has 12 binding partners, whereas β5 integrin can only associate with αV integrin (**Fig 1.3 B**). Pairing of different subunits ensures specificity for different ligands, e.g. α1β1 is a collagen receptor, αVβ3 and α5β1 are Argininine-Glycine-Aspartic acid (RGD) receptors, while α6β4 is a laminin receptor [135]–[137]. Integrin heterodimers assume two main conformational states: bent, inactive state with low affinity for ligand-binding and upright, active, high affinity conformation [138], [139]. The inactive state can be pro-apoptotic, while the active, ligand-bound state is typically stimulatory [140], [141].

To fulfil their role in mediating cell adhesion and movement, integrins undergo clustering and recruit cytoskeletal, adaptor and signaling proteins [142]–[144]. Thus, they are normally found complexed with many other proteins into structures named focal adhesions (FAs) to mediate cell attachment, migration and signaling [145]. Integrin signal transduction is bi-directional. External cues can be transmitted from outside of the cell to the intracellular integrin binding partners ('outside-in signalling'), but integrins also change their conformational state in response to cytoplasmic stimuli, thus affecting their binding with the ligands in the extracellular space ('inside-out' signalling) [146], [147]. Recently, a third mode of anchorage-independent 'inside-in' signalling has been proposed [148]. The authors observed β1-integrin, present on endosomal membranes inside the cell, to promote sustained c-Met/ERK1/2 phosphorylation, thus influencing cell survival, invasion and tumorigenesis.

Integrin structure does not include an enzymatic domain. The regulatory role of integrins is achieved through interaction with enzymatic receptors, such as growth factor (VEGF, FGF and EGF) receptors with tyrosine kinase activity [149]–[151]. Integrin function is in turn regulated by membrane trafficking, i.e. endocytosis, recycling and degradation, which determines the amount present at the cell surface, available for clustering and interaction with ECM ligands [152].

A

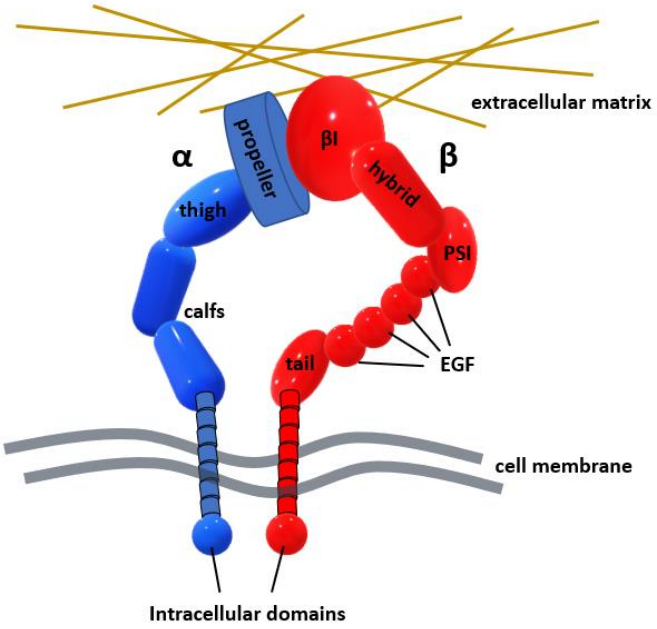

B

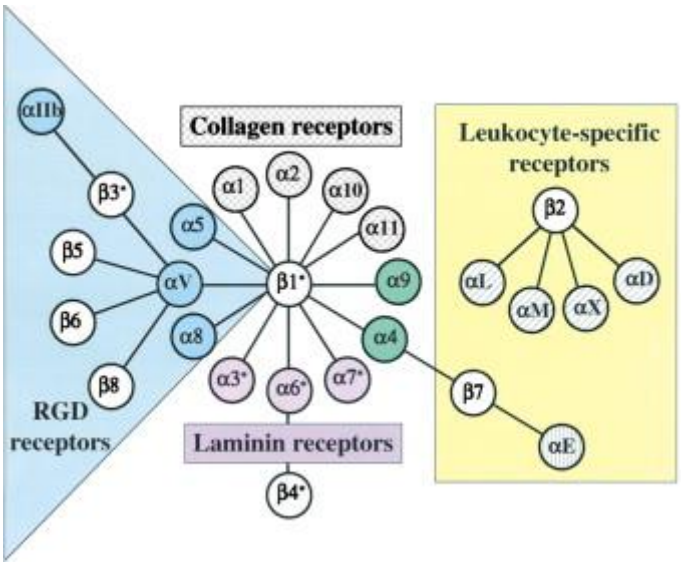

Figure 1.3 Integrin structure and domain pairing.

(**A**) Cartoon representation of the heterodimeric integrin in its active state. α and β subunits interact, assume an upright conformation and engage with the matrix via the propeller and the βI domain. EGF – epidermal growth factor module, PSI – plexin-semaphorin-integrin. Adapted from [132], [153]. (**B**) The integrin family showing all known pairs of α and β subunits grouped according to the type of ligand they bind to, adapted from [134].

Integrins are expressed in multiple cell types contributing to angiogenesis: ECs, fibroblasts, pericytes and BMDCs [48]. In these cells, numerous angiogenesis-contributing integrins have been found: α1β1, α2β1, α4β1, α5β1, α6β1, α6β4, α9β1, αvβ3, αvβ5 and αvβ8 [131]. These integrins stimulate angiogenic sprouting but are also able to regulate responses to pro- and anti-angiogenic growth factors, proteases, cytokines and receptors, to influence proliferation, remodelling of the ECM, migration and cell-cell interactions [48], [140]. Endothelial αvβ3 integrin, in particular, has received a lot of attention from researchers, due to its importance in angiogenesis.

1.2.6 αVβ3-integrin

αVβ3 integrin has become a prominently-studied member of the integrin family, since it was found upregulated in angiogenic vasculature [154]. It is also highly expressed in many tumour types: breast, lung, kidney, ovary, skin and prostate [155]. When bound to its canonical ligand, vitronectin, αVβ3 integrin associates with platelet-derived growth factor receptor β (PdgfRβ) and VEGFR2, via the extracellular domain, to promote proliferation and migration in ECs [156]. Phosphorylation sites Y747 and Y759, within the cytoplasmic tail of the integrin, also play an important role in the cross-talk with VEGFR2 and subsequent downstream signalling [157], [158]. αVβ3 integrin will also bind to other substrates: fibronectin, von Willebrand factor (vWF), thrombospondin, fibrillin, tenascin, osteopontin, bone sialoprotein (BSP); crosslinkers - fibrinogen, lactadherin (Mfge8); as well as Del-1 and the LAP-TGF-Beta complex [159].

Early research on this integrin portrayed it as pro-angiogenic. Vitronectin and fibronectin, both recognised by αVβ3 via the RGD-motif, are typical matrices laid down for migrating ECs in angiogenesis [18], [160], [161]. Numerous studies revealed it to be a positive regulator of VEGFR2, a main angiogenic receptor. When clustered and activated, αVβ3 leads to an increase in p38 MAPK and FAK activation, through its interaction with VEGFR2 [162]. Similarly, the αVβ3-VEGFR2 complex correlates with PI3K activity [124], [163]. Moreover, VEGF stimulation of VEGFR2, induces Src to phosphorylate β3 tyrosine residues, thus activating it and promoting the β3-VEGFR2 complex, which leads to VEGFR2 phosphorylation [164]. Early studies showed that blockade of αVβ3 integrin using RGD-mimetic compounds has the potential to inhibit angiogenesis-relevant processes *in vitro*, such as VEGF-dependent EC invasion in 3D culture and differentiation of progenitor cells into ECs [165], [166]. Cilengitide, a prominent inhibitor of αV integrins, was shown to inhibit tumour angiogenesis, progression and metastasis in pre-clinical models *in vivo* [167]–[170]. The mechanism of action behind these exciting findings involves dampening of FAK, Src and Akt signalling, cellular detachment and induction of apoptosis in angiogenic blood vessels (expressing integrin αVβ3) [167], [170], [171]. Strieth *et al*. observed a synergy in inhibition of tumour angiogenesis, growth and metastasis when using another αV inhibitor (EMD 270179) in combination with a VEGFR2 inhibitor (SU5416) [172]. In addition, Cilengitide prevented brain tumour cell lines from interacting with the surrounding matrix and induced apoptosis [173].

However, genetic manipulation of αVβ3 provided surprising results. It is important to point out that depleting β3-integrin is the more specific approach of targeting the αVβ3 heterodimer, as the only other partner of β3 is αIIb (not expressed in ECs), while αV has four additional β partners, including β5 (present in ECs) (**Fig. 1.3 B**) [174]. β3-KO mice develop into adulthood, are fertile, exhibit a bleeding disorder and high bone mass, but developmental angiogenesis in these

animals is unaffected [175]. It was later shown, using cell-lineage-specific knockouts, that the bleeding phenotype was due to β3 integrin deletion in platelets, while the bone phenotype was attributed to myeloid β3 integrin knockout [176]. Surprisingly, β3-KO mice exhibit enhanced pathological angiogenesis and tumour growth [177]. This may be explained by overexpression of VEGFR2 observed in β3-KO ECs, and as a result, elevated sensitivity to VEGF, accompanied by increased vascular permeability [175], [178]. Moreover, low doses of Cilengitide also promoted angiogenesis and tumour growth, due to increased presence of αVβ3 in FAs and enhanced VEGFR2 recycling [179]. Cilengitide and other αVβ3 antagonists will be discussed in detail in Section 1.4.3.

Thus, the involvement of αVβ3 in angiogenesis is complex and context dependent, whilst efficacy of inhibitor-based anti-angiogenic targeting of this integrin is dose dependent. In the light of the above findings, our research group investigated the effects of endothelial-specific depletion of β3 integrin on angiogenesis and tumour growth in two Cre-lox mouse models: the inducible β3-floxed Pdgfb.CreER model and the constitutive β3-floxed Tie1.Cre model. We have observed that acute depletion of β3-integrin (Pdgfb.CreER) impairs pathological angiogenesis and tumour growth, whereas long-term depletion of the molecule from birth (Tie1.Cre) results in similar sized tumours between Cre -ve and +ve animals with enhanced microvascular sprouting [180]. Moreover, inducing β3-integrin depletion for an extended period of time in the Pdgfb.CreER model prior to tumour cell implantation, results in a loss of tumour growth inhibition, turning this into a long-term depletion mode, eliciting a phenotype much like that seen with Tie1.Cre mediated deletion [180]. This suggests that long-term anti-angiogenic depletion directed at β3-integrin is subject to an escape mechanism. Interestingly, Robinson *et al*. observed an upregulation in Nrp1 in β3-KO ECs, promoting Nrp1-VEGFR2 complex formation and elevated ERK signalling [181]. The same study showed that αVβ3 and Nrp1 co-immunoprecipitate and proposed that αVβ3 sequesters Nrp1, preventing its interaction with VEGFR2 and downstream signalling. Furthermore, co-targeting β3 and Nrp1 is an effective way of inhibiting EC migration, VEGFR2 signalling, pathological angiogenesis and tumour growth [181], [182]. Another potential escape mechanism was identified in a study that observed a requirement for Rac1 in tumour angiogenesis and growth, in the absence of αVβ3 integrin only [183]. More answers can be found by analysing endothelial FAs, where αVβ3 integrin functions to mediate cell adhesion and migration. We recently characterised β3-depleted and control EC adhesomes, to understand the compensation mechanism further. This will be discussed in detail in Section 1.3.3.

1.3 The Endothelial Cell Adhesome

1.3.1 General Comments

Regulation of EC attachment and migration occurs via the integrin adhesome – a multi-molecular collection of proteins present at or associated with FA complexes at the cell membrane [184]–[186]. The term 'adhesome' coined by Prof. Richard Hynes (MIT, Boston) refers to the "complement of adhesion-related genes/proteins" [187]. More specifically, it is the set of proteins localised to and/or able to regulate adhesion complexes on the cell surface. A pivotal role in these complexes is played by integrins, therefore this sub-proteome is often referred to as the integrin adhesome. A prominent meta-study of the integrin adhesome, combining findings from various mammalian cell types, identified 690 interactions between 156 components, which belong to one of the following categories: adaptor, cytoskeletal, serine/threonine kinase or phosphatase, tyrosine kinases or phosphatase, actin-binding, GAP, GEF, receptor, adhesion protein, GTPase; and 32 other uncategorised components [188]. A more recent study, made possible thanks to advancements in mass spectrometry, reported over 2000 members of the adhesome [189]. Analysis of the adhesome helps us understand angiogenesis and improves our chances of designing more effective anti-angiogenic therapies.

1.3.2 Focal Adhesions

There are four conventional types of adhesion complexes. Nascent adhesions are the basic, smallest type which rapidly disassemble or develop into slightly more complex focal contacts [190]. Both are capable of causing membrane protrusions. Focal contacts mature into larger, 1 – 5μm long, FAs linked to the cytoskeleton, which allows them to mediate cell migration forces [191]. Fibrillar adhesions are large and stable, typically found in fibroblasts, arranged along fibronectin fibres, mostly containing β1 integrins as their adhesion receptors [192]. Here we are most interested in the FAs, containing both β1 and β3 integrins, dynamically assembling and disassembling to orchestrate progressive movement of the leading edge and retraction of the rear end of the cell [193]. Overall, FAs are the adhesion, migration and signalling hubs on the cell surface made up of numerous, adhesion, structural, adaptor and signalling proteins [194], [195].

Integrins are some of the key members of the FA complexes, among the 2000+ proteins that can be recruited there. Additional well-studied key players resident in FAs are: cytoskeletal – actin (Acta2); adaptor – α-actinin (Actn1), paxillin (Pxn), talin (Tln1), tensin (Tns1), vinculin (Vcl) and signalling – FAK (Ptk2) and Src [196]. **Fig 1.4 A** represents a simplified view of a FA complex,

depicting the likely arrangement of these proteins. Actin assembles into stress fibres, which when anchored to FAs provide membrane protrusion and contraction forces in cell migration [197]. This process is regulated by numerous signalling pathways, including tyrosine kinases and Rho GTPases [196]. α-actinin was originally identified as an actin crosslinking protein, but it has a variety of other binding partners, e.g. vinculin, integrins and PI3K to name a few [198]. In FAs, it acts mainly as a scaffold for structural stability [199]. Paxillin is a multi-domain adaptor protein primarily present in FAs (**Fig 1.4 B**) [200]. It becomes phosphorylated by Src and FAK, which leads to recruitment of further adaptor and signalling proteins with consequences in regulating the dynamics of FAs [201]. Talin binds the cytoplasmic tail of β-integrins, leading to their activation, thus influencing integrin-dependent signalling [202]. It also mediates the interaction between integrins and the actin cytoskeleton [203]. Talin KO in mice is embryonic lethal [204]. Another FA adaptor protein, tensin is considered an anchor for actin fibres, a stabiliser of FAs and a mediator of signalling, phosphorylated by tyrosine kinases such as Src, FAK and protein kinase C (PKC) [205]. Furthermore, it has been shown to bind β-integrins and regulate cell migration [206]. Vinculin, another FA stabiliser, has been shown to bind talin, α-actinin, paxillin, actin and PKC, among other proteins, but not integrins directly [207], [208]. It is recruited to FAs under tension, and further tension exerted on the vinculin structure correlates with FA assembly [209]. FAK is considered a fundamental tyrosine kinase in angiogenesis-relevant processes, such as EC proliferation and migration [210]. Deletion of endothelial FAK leads to an increase in EC apoptosis upon VEGF stimulation and dramatically inhibits tumour angiogenesis and growth [211]. It associates with other kinases, such as Src and PI3K [210]. FAK and Src activity is stimulated by integrins and VEGFR2 and feeds into the signalling network, e.g. enhancement of the RAS/RAF/MEK/Erk pathway with consequences in cell proliferation and motility or PI3K/Akt pathway to promote survival [212]. Also, FAK and Src phosphorylate multiple proteins in FAs, such as paxillin and tensin, thus regulating FA stability and dynamics [201], [205]. Interestingly, Src was the first proto-oncogene and protein tyrosine kinase to be discovered in the vertebrate genome [213]. Upregulation of its expression and/or activity has been linked to many types of cancer [214]–[216].

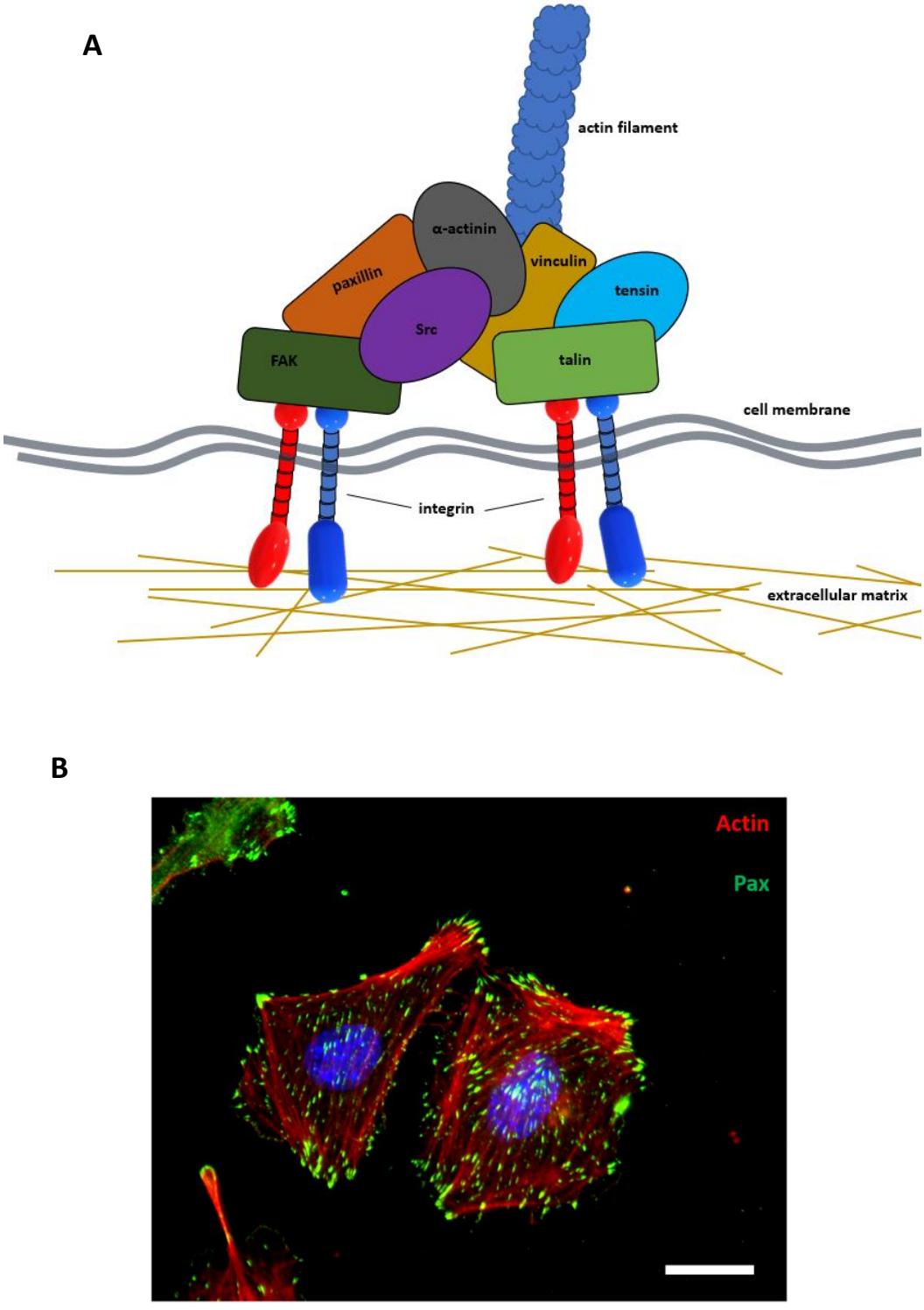

Figure 1.4 The focal adhesion complex, simplified.

(**A**) The integrin heterodimers span the membrane and bind the extracellular matrix via their head domains. The integrin cytoplasmic domains interact with several other proteins, such as: FAK, paxillin, Src, α-actinin, vinculin, tensin and talin; thus forming a complex at the end of an actin filament. Not to scale, adapted from Dash *et al*. [217]. (**B**) FAs in green and actin cytoskeleton in red, in ECs adhered for 180 min on fibronectin (63x, scale bar = 40 μm).

Many other members of FAs are kinases or other signalling proteins, whose activation and deactivation leads to modulation of a wide variety of downstream signalling pathways throughout the cell. For example, Rac1 and Cdc42, which can be found associated with FAs, most often at the leading edge of the cell, stimulate actin polymerisation to generate membrane protrusions during cell spreading and migration [190], [218].

FAs are dynamic, and the rate of their assembly and disassembly (turnover) is linked to cell migration, adhesion, proliferation and survival [195], [219]. A typical FA is positioned at the end of an actin fibre (**Fig 1.4**) [220]. However, microtubules (MTs) and intermediate filaments (IFs) have also been shown to complex with integrin-based FAs [221], [222]. We can gain further understanding of EC biology and angiogenesis by analysing the EC integrin adhesome.

1.3.3 Endothelial Integrin Adhesome and Angiogenesis

β1 integrins are found in both the dynamic FAs and the stable fibrillar adhesions, while the presence of β3 integrins in FAs is a distinguishable factor between them [190]. Fibrillar adhesions, typically present in fibroblasts, mostly contain β1 integrins [192]. Different affinity for binding ECM substrates, such as fibronectin and vitronectin, leads to different nanoscale organisation and dynamics of β1 and β3 integrins within FAs [223]. Additionally, there is differential stimulation of RhoA activity, a modulator of actin filament structure, between the two integrin types during FA translocation [224]. All these factors determine differential functionality of these two integrin types in FAs and the overall structure of FAs. α5β1 integrin promotes adhesion strength and more stable FAs, while αVβ3 integrin enables mechano-transduction [225].

In summary, FA assembly proceeds by integrins binding the ECM and recruitment of actin with the help of adaptor and signalling proteins [226]. Integrin-containing FAs in ECs are the adhesion, migration and signalling hubs which drive angiogenesis [227]. In addition, integrins can directly interact with growth factor receptors to enhance their signalling. A prominent example of such interaction is the αVβ3-VEGFR2 partnership [124].

αVβ3 has been proposed as a good target for anti-angiogenic therapy [154], [170], [228]. However, the most prominent αVβ3 inhibitor, Cilengitide, showed promising results in early clinical trials in cancer patients, but failed to provide overall benefit in phase III trials (discussed in detail in section 1.4.3), suggesting that an escape mechanism arises upon long-term inhibition of the molecule [229], [230]. Similarly, long-term genetic depletion of this integrin is subject to a compensation mechanism [180]. This may be occurring via Nrp1 and/or Rac1, as there is an

increased angiogenic dependence on these proteins in the absence of β3 integrin [181]–[183]. The escape mechanism phenomenon could be addressed further by creating a full picture of the EC adhesome. Recently, we have conducted FA enrichment, using a protocol by Schiller *et al*. [231], followed by mass spectrometry to profile adhesomes of control, β3-HET, β3-KO and RGD-mimetic-treated ECs [232]. We were then able to look for potential compensation pathways triggered by the depletion of β3 integrin. There was an upregulation of tubulins (building blocks of MTs) in the β3-depleted adhesome, associated with changes in active (GTP-bound) Rac1, regulator of chromosome condensation 2 (Rcc2) and annexin A2 (Anxa2) [232]. We observed that in the absence of αVβ3 integrin the Rac1/Anxa2/Rcc2 complex associated with α5β1 integrin and active Rac1 promoted stable MTs. Indeed, migration became more MT-dependent in the β3-depleted ECs, as β3-HET and β3-KO cells were more sensitive to MT-targeting agents than WT cells. Furthermore, MT inhibitors were more efficacious at reducing pathological angiogenesis and tumour growth in endothelial β3-KO (β3-floxed Tie1Cre +ve) mice, than in the vehicle-treated control littermates.

With this work, we created a comprehensive EC adhesome mass spectrometry dataset, which could be re-visited to further elucidate other potential pathways/molecules regulating the escape which accompanies β3 integrin depletion/inhibition. Indeed, the investigation of other pathways involved in this escape is the main thrust of this thesis.

1.4 Current Anti-angiogenic Therapies

1.4.1 General Comments

Cytotoxic strategies, i.e. chemo- and radiotherapy, effective in many cancers, come with severe side effects. Since the 1970s when it was officially proposed that cancer could be treated by targeting angiogenesis there have been enormous advances in the research field which led to development of continuously improving therapies [46]. When targeting angiogenesis, one can expect a much milder response from the body, since it is a process relatively limited to the tumour microenvironment [21]. There has been some success in using anti-angiogenic agents in the clinic. However, some are associated with side effects more severe than initially anticipated and some are subject to treatment escape. The most clinically effective way of targeting angiogenesis in the context of tumour progression is by combinatorial approach of targeting blood vessels in the tumour with anti-angiogenic agents alongside established chemo- and radiotherapy [233]. Indeed, this approach is often taken in the clinic, e.g. combining anti-VEGF bevacizumab and two cytotoxic drugs (fluorouracil and oxaliplatin) in patients with metastatic colorectal cancer [234].

Here, we briefly review the anti-angiogenic strategies designed to date. Paradoxically, part of the success with such therapies may be due to normalisation of the disturbed tumour vascular architecture, as a result of treatment with anti-angiogenic agents [58]. Normalised vessels may improve the efficiency of delivering therapeutic agents against cancer cells to the whole tumour mass. Currently, all the anti-angiogenic agents approved for clinical use are targeting the VEGF pathway [235]. Over 200 anti-integrin agents have entered clinical trials, in the hope of treatment of multiple sclerosis (MS), Crohn's disease, arthritis, osteoporosis, stroke, ischaemia, fibrosis, thrombosis, age-related macular degeneration and cancer, as well as other inflammatory and autoimmune conditions [236]. The integrin antagonists approved for use in patients are either targeting αIIbβ3 in thrombosis or α4β1 and α4β7 in MS, Crohn's and ulcerative colitis [237]. All of these prevent the integrin-ligand interaction, while most are remarkably safe to use in patients [237]. αVβ3 integrin remains a potential target in anti-angiogenic therapy, with Cilengitide making it to late stage clinical trials and new promising agents being developed [238], [239].

1.4.2 Anti-VEGF Treatments

The first agent approved for use in the clinic that inhibits angiogenesis was a VEGF inhibitor bevacizumab (Avastin®). It is a monoclonal antibody that binds all soluble isoforms of VEGF-A and prevents their interaction with VEGF-receptors [240]. It is now used to treat a wide variety of cancers: colorectal, lung, kidney and glioblastoma [241]. Patients that would benefit from this treatment are carefully selected as there are multiple associated risks. For example, wound healing and collateral circulation may be affected [241]. In contrast, its use in breast cancer patients in combination with paclitaxel was revoked in 2011 in the USA, due to life-threatening side effects [242]. This strategy remains in use for breast cancer patients in Europe. It was concluded by the European Medicines Agency (EMEA) that there is prolonged progression-free survival, which outweighs the risks [243], [244]. A number of other drugs targeting the VEGF pathway are currently in use in a whole range of cancer types [245], [246]. Most of them inhibit tyrosine kinase activity: axitinib, cabozantinib, pazopanib, regorafenib, sorafenib, sunitinib and vandetanib [247]. The remaining two are aflibercept which, like bevacizumab, binds VEGF directly, and everolimus that leads to reduced VEGF production [248].

Unfortunately, VEGF-pathway inhibitors can all induce a wide range of unwanted severe side effects, including renal toxicity, bleeding, abnormal platelet and leukocyte counts, wound healing complications, leukopenia and gastrointestinal perforation [249]. Moreover, in some instances these agents may cause initial tumour shrinkage, followed by an aggravated tumour growth and metastasis [235]. At the same time, they sometimes prove ineffective due to acquired resistance via escape mechanisms. One attempt to overcome this was a clinical trial co-targetting VEGF and Nrp1, a VEGFR2 co-receptor, in combination with chemotherapy [250]. This involved bevacizumab, paclitaxel and an anti-Nrp1 monoclonal antibody that prevents it from binding VEGF. Unfortunately, this strategy failed due to severe proteinuria, in more than half of the trial participants. In comparison with VEGF-pathway blockers, integrin inhibitors are generally less toxic and well tolerated [251].

1.4.3 αVβ3 as a Target

The advantage of targeting αVβ3 integrin is the specificity, which limits potential adverse effects. It is highly expressed in very few cell types: angiogenic ECs, mature osteoclasts, some neutrophils, activated macrophages, migrating smooth muscle cells and tumour cells [252]–[254]. In quiescent vasculature its expression is low [154]. The upregulation of αVβ3 expression in vessels undergoing angiogenesis prompted efforts to develop inhibitors against it. To date, several of these have been developed, while a few have made it to the clinical trials [255]. A very prominent inhibitor targeting αV integrin, Cilengitide (EMD 121974), effectively inhibited angiogenesis, tumour growth and metastasis *in vivo* [256]. It is an RGD-motif-mimetic, preventing ECM binding and capable of inducing apoptosis and downregulating the FAK/Src/AKT signalling pathway [167], [168]. It was taken forward for clinical trials and showed promising results at phase II in combination with chemo- and/or radiotherapy, with some anti-tumour activity, extended progression-free survival period with only sporadic toxicity [229], [257]. However, in phase III clinical trials no overall benefit in patient survival was observed [230]. A few other αVβ3 inhibitors, which were successful in inhibiting angiogenesis and tumor growth in animal models, should be highlighted here, namely: EMD 270179, MK-0429, vitaxin (MEDI-523) and etaracizumab (MEDI-522) [258]–[260]. Interestingly, RGD-mimetic EMD 270179 was shown to improve drug delivery selectively to the tumour by transiently increasing vascular permeability in this microenvironment of increased αVβ3 expression [259]. MK-0429, is a non-peptide RGD-mimetic, which has been evaluated in two clinical trials, in the context of osteoporosis and bone metastasis due to its role in bone resorption [261]–[263]. Monoclonal anti-αVβ3 antibody vitaxin and its improved derivative etaracizumab have been taken forward for clinical trials in patients with a variety of cancers and showed some promising ability to stabilise solid tumours [258], [264]. Unfortunately, the overall clinical trial outcomes with all these inhibitors have been disappointing, as there is a lack of long-term, meaningful improvements, most likely due to acquired resistance to the treatment [258].

Recently, a new kind of αVβ3 antagonist has been developed, also potent in inhibiting of angiogenesis and tumour growth and non-toxic in mice even at high doses [238], [265]. The novelty of ProAgio is that it binds the integrin outside the ligand binding site [238]. This potentially overcomes the problem of integrin activation, for instance, seen with a low dose of Cilengitide which elicits a pro-angiogenic effect [179]. ProAgio induces apoptosis of ECs by recruiting and activating caspase 8 [238]. Further research is needed to determine whether resistance to treatment with ProAgio arises, as is often the case with anti-angiogenic agents.

There were also attempts at combination therapies in mouse models to improve efficacy. Co-targeting αVβ3 and VEGFR2 using etaracizumab and bevacizumab or EMD 270179 and SU5416 (VEGFR2 antagonist) was more effective in reducing vessel density, tumour growth and metastasis than individual agents [172], [266]. Furthermore, one of the novel approaches in the pharmaceutical industry is to develop multi-specific drugs, such as a construct engineered to contain both VEGF- and RGD-mimetic region, able to bind both VEGFR2 and αVβ3 integrin simultaneously [267]. In a tumour growth experiment this dual-targeting agent showed remarkable inhibition of tumour angiogenesis and growth [267]. This type of strategy has the potential to improve potency and selectivity, as well as reducing the cost associated with production, testing and regulatory approval [267]. Similarly, vitaxin derivative (ScFv) was conjugated with a peptide which selectively binds human lung carcinoma cells [268]. It was demonstrated that this peptide-ScFv conjugate inhibited lung carcinoma xenograft growth significantly more than ScFv alone [268].

The problem of escape remains a key aspect that needs to be addressed to further understand the limited success of anti-angiogenic therapies. As discussed in section 1.3.3, we have recently undertaken a mass spectrometry approach to analyse the β3-depleted endothelial adhesome, in search for potential mediators of the escape from targeting αVβ3 integrin [232]. We identified a Rac1-dependent upregulation of MTs, as a potential mechanism of this kind, and showed that β3-depletion coupled with MT inhibition is more effective at inhibiting EC migration, tumour angiogenesis and growth then MT inhibitors alone [232]. Many more interesting targets emerged from the mass spectrometry data. This thesis re-visits these datasets to further understand the EC adhesome and the escape mechanism from anti-angiogenic targeting of αVβ3-integrin and pursue other candidate proteins that have emerged, which may serve as effective targets or co-targets.

1.5 Research Aims and Objectives.

The overarching aims of this project were to:

1. Further characterise the endothelial cell adhesome and how it changes upon β3-integrin depletion.
2. Narrow down the list of candidate genes/proteins and define a limited number of interesting ones that may be mediating the escape mechanism seen with long-term targeting of β3-integrin.
3. Carry out comprehensive testing of chosen candidates in combination with β3-integrin depletion, using angiogenesis relevant assays, to test them for involvement in the escape mechanism.
4. Generate molecular tools for testing chosen candidates if needed.
5. Provided a suitable candidate emerges, assess co-targeting of β3-integrin and one of the chosen candidates in a tumour growth model, as a proof-of-concept improved anti-angiogenic strategy.

2 General Materials and Methods

2.1 Reagents, Materials, Antibodies and General Comments

All chemicals used were purchased from Sigma-Aldrich (Poole) unless otherwise stated. Tissue culture materials and cell media were acquired from Thermo Fisher Scientific group (Loughborough) that supplies products from Thermo Fisher, Invitrogen, Life Technologies, Corning and Gibco unless otherwise stated. **Tables 2.1** and **2.2** contain information of all antibodies (Ab's) used.

Experimental protocols often involve steps conducted at various temperatures. Temperatures other than room temperature (RT) are specified in each case. If the temperature is not stated, the step was conducted at RT, i.e. ~20°C.

Some methods precede or are not directly linked to the work presented here, in which case they are cited and explained briefly. The methods carried out to generate results for this thesis are explained in detail in this chapter, as well as chapter 3.2, 4.2, 5.2 and 6.2 in the case of chapter-specific methods.

VEGF-A^{164} was made in-house according to the protocol by Krilleke *et al.* [269]. Briefly, plasmid pPICZαC-VEGF164 was transformed into competent yeast using the *Pichia* expression kit (Invitrogen). High secreting colonies were chosen and grown in 500 mL of BMGY medium at 30°C until the culture reached an Absorbance of 3 at 600 nm. To induce expression, yeast pellets were then resuspended in 100 ml of BMMY and grown at 30°C for 36 hours (hrs), and methanol was added to a final concentration of 1% every 12 hrs to maintain induction of transgene expression. Supernatants were cleared, concentrated, equilibrated in nitrilotriacetic acid chromatography binding buffer and incubated with acid-agarose (Qiagen) for 60 min at 4°C. The beads were collected by centrifugation and washed with binding buffer. Bound proteins were eluted with NaCl / imidazole buffer and analysed by SDS-PAGE and Coomassie staining.

Table 2.1 List of primary antibodies

Antigen	Reactivity used	Host	Application	Source	Clone / Cat. #
Akt	Mouse	Rabbit	WB	Cell Signalling Technology	#9272
β3-Integrin	Mouse	Rabbit	WB	Cell Signalling Technology	#4702
CD31	Mouse	Rat	ECS	Abd Serotec	ER-MP12
Endomucin	Mouse	Rat	ECS, IHC	Santa Cruz Biotechnology	V.7C7
ERK1/2 (p44/42 MAPK)	Mouse	Rabbit	WB	Cell Signalling Technology	137F5 / #4695
FAK	Mouse	Rabbit	WB	Cell Signalling Technology	#3285
GAPDH	Mouse	Mouse	WB	Sigma-Aldrich	G8795
HSC-70	Mouse	Mouse	WB	Santa Cruz Biotechnology	B-6 / sc-7298
ICAM-2	Mouse	Rat	ECS	AbD Serotec	#MCA2295EL
p38 MAPK	Mouse	Rabbit	WB	Cell Signalling Technology	#9212
Paxillin	Mouse	Rabbit	ICC, WB	Abcam	ab32084
Phospho Akt	Mouse	Rabbit	WB	Cell Signalling Technology	#4060
Phospho ERK1/2	Mouse	Rabbit	WB	Cell Signalling Technology	D13.14.4E #4370
Phospho FAK (Y407)	Mouse	Rabbit	WB	Thermo Scientific	#OPA1-03887
Phospho p38 MAPK	Mouse	Rabbit	WB	Cell Signalling Technology	3D7 / #9215
Phospho Paxillin (Y118)	Mouse	Rabbit	ICC, WB	Cell Signalling Technology	#2541
Phospho VEGFR-2 (Y1175)	Mouse	Rabbit	WB	Cell Signalling Technology	19A10 / #2478
Phospho Vimentin (S56)	Mouse	Rabbit	WB	Cell Signalling Technology	#3877
Plectin	Mouse	Rabbit	WB	Abcam	E398P / ab32528
VEGFR2	Mouse, Human	Rabbit	WB	Cell Signalling Technology	55B11 / #2479
Vimentin	Mouse	Rabbit	WB	Abcam	ab92547

WB – Western blot, IHC – immunohistochemistry, ECS – endothelial cell sort, ICC – immunocytochemistry

Table 2.2 List of secondary antibodies and directly labelled reagents

Host / name	Anti-	Application	Cat. #	Conjugate	Source
Rabbit	Goat	ICC	A-21222	Alexa®-488	Invitrogen
Rabbit	Goat	ICC	A-21223	Alexa®-594	Invitrogen
Donkey	Mouse	WB	715-035-151	HRP	Jackson Immunoresearch
Donkey	Rabbit	IHC, ICC	A-21206	Alexa®-488	Invitrogen
Donkey	Rabbit	WB	711-035-152	HRP	Jackson Immunoresearch
Donkey	Rat	IHC	A-21209	Alexa®-594	Invitrogen
Sheep	Rat	ECS	11035	Dynabeads	Invitrogen
BS1-lectin	blood vessels	ARA	L2895	FITC	Sigma-Aldrich
phalloidin	actin	ICC	A12380	Alexa®-568	Invitrogen

WB – Western blot, IHC – immunohistochemistry, ECS – endothelial cell sort, ICC – immunocytochemistry, ARA – aortic ring assay

2.2 Immortalised Lung Endothelial Cells (IMMLECs)

The immortalised lung ECs (IMMLECs) used extensively in this project came from in-house stocks. They were previously isolated from adult mice on a mixed C57BL6/129 background according to the protocol by Reynolds and Hodivala-Dilke [270]. Briefly, mouse lungs were aseptically removed and placed in Ham's F12 medium, then rinsed in 70% ethanol, minced using scalpel blades and digested with 0.1% collagenase I in PBS for 1 hr at 37°C. This was followed by a mechanical separation using a needle and syringe, passing through a 70 µm filter and centrifugation at 300 g for 5 minutes (mins). Cells were resuspended in MLEC medium – a 1:1 mixture of DMEM low glucose and Ham's F12 medium supplemented with 20% FBS, 4 mM GlutaMAX™, 50 µg/mL heparin and 50 mg/L of EC growth supplement (Bio-Rad, Watford). They were then seeded into a tissue culture flask, previously coated with 0.1% gelatin, 30 µg/mL collagen I and 10 µg/mL fibronectin (FN); and incubated at 37°C 5% CO_2 overnight (o/n). The next day, cells were washed with PBS to remove red blood cells and fed fresh MLEC medium. ECs were positively selected by magnetic activated cell sorting (MACS) using magnetic Dynabeads (Thermo Fisher, Loughborough) coated with a sheep anti-rat Ab (Invitrogen) and a rat anti-mouse ICAM2 Ab (endothelial marker, Invitrogen). The positively sorted cells were seeded onto a pre-coated tissue culture flask as above. Once cells reached near-confluency, the positive sort was repeated.

Subsequently, the cells were immortalised according to the protocol outlined by Robinson *et al.* [181]. GgP+E cells were used for virus production. Conditioned medium from these cells, containing the retroviral polyoma-middle-T-antigen (PyMT), was filtered (0.45 µm) and stored at −80°C. When required, the medium was thawed and placed on primary cells in combination with 8 µg/mL polybrene, which increases transduction efficiency, for 6 hrs at 37°C and changed back to MLEC medium o/n. PyMT conditioned medium treatment was repeated the following day. Subsequently, media was switched to IMMLEC – a 1:1 mixture of DMEM low glucose and Ham's F12 medium supplemented with 10% FBS, 2mM GlutaMAX™ and 50 µg/mL heparin. Cells were passaged for 4 weeks to ensure immortalisation. Finally, frozen stocks were prepared as described below.

To confirm their endothelial phenotype, IMMLECs were assessed for expression of ICAM2, CD31 and VECAD to ensure their endothelial identity. Cells were used for experiments between passages 5 to 25, provided a normal endothelial morphology was maintained.

2.2.1 Cell Culture

Cells were grown on tissue culture flasks pre-coated with 0.1% gelatin for 1 hr at 37°C or o/n at 4°C to promote cell adhesion. Once cells reached confluency (2 - 4 days) they were passaged using 0.25% trypsin-EDTA. The cell suspension was centrifuged at 300 g for 5 min to remove the trypsin, cells were resuspended in culture medium and seeded into to a freshly coated flask and incubated at 37°C with 5% CO_2. IMMLECs were cultured in IMMLEC medium, described above in section 2.2. Mouse lung carcinoma (CMT19T, CR-UK Cell Production) and human embryonic kidney cells possessing the SV40 large T antigen (HEK293FT) were cultured in DMEM high glucose, 10% FBS, 2 mM GlutaMAX™. Penicillin/Streptomycin (P/S, 100 units/mL) was added to all culture media unless otherwise stated. For most cell-culture-based assays tissue culture plates or dishes were pre-coated with 10 µg/mL FN at 4°C o/n.

2.2.2 Freezing and Thawing Cells

Cells were trypsinised and counted using a haemocytometer. Cells were centrifuged at 300 g for 5 min then resuspended at 1 - 2 x 10^6 viable cells/mL in freezing medium. For IMMLECs the freezing medium was composed of 90% FBS and 10% dimethyl sulfoxide (DMSO) whilst for HEK293FT, CMT19T the freezing medium consisted of 50% culture medium, 40% FBS and 10% DMSO. Cryovials containing 1 mL aliquots were placed in a freezing container (Mr. Frosty™, Thermo), which was stored at −80°C o/n or longer. For long-term storage, cryovials were banked in a liquid nitrogen DryStore™.

To defrost cells, cryovials were warmed in a 37°C water bath until thawed and immediately transferred to a falcon tube containing cold culture medium then centrifuged at 300 g for 5 min. The supernatant containing DMSO was removed and the cells resuspended in 5 mL of medium, then transferred to a T25 tissue culture flask.

2.3 Endothelial Cell Transfection

The amount of plasmid DNA transfected into the cells ranged from 3 to 12 µg. For targeted gene knockdown, 5.6 µL of 40 µM siRNA (Dharmacon, Cambridge) was 'nucleofected' into the cells. **Table 2.3** is a list of all siRNAs used.

To transfect IMMLECs, the Amaxa™ Nucleofector™ technology (Lonza, Slough) was used. It is an electroporation-based method that delivers nucleic acids to the cytoplasm and the nucleus using a specific voltage and buffer [271]. ECs were trypsinised, counted using a Neubauer counting chamber (Hawksley, Lancing), centrifuged at 300 g for 5 min then resuspended at a density of 10^6/ 100 µL of pre-warmed nucleofection buffer (200 mM Hepes, 137 mM NaCl, 5 mM KCl, 6 mM D-glucose and 7 mM Na_2HPO_4 in nuclease-free water; filter sterilised). 100 µL of the cell suspension was mixed with either siRNA or DNA (depending upon the assay) transferred into an electroporation cuvette then 'zapped' with T-005 voltage. Cells recovered in 1.9 mL of culture medium for 10 min at 37°C and then were utilised for functional assays according to the required protocol.

Table 2.3 List of siRNA oligos used

Gene name	Gene Accession	siRNA sequence	Pool Cat No.	Unique Cat No.
Atp5a1	NM_007505	GGUUGACGCCCUCGGUAAU	L-042902-01	J-042902-09
		UGGUGAUGGUAUUGCGCGA		J-042902-10
		ACGAUGGGACCGACGAGAA		J-042902-11
		GCAGCCAAGAUGAACGAUU		J-042902-12
Cltc	NM_001003908	GGAAAGCAAUCCAUACAGA	L-063954-00	J-063954-05
		UCAGAAGAAUUGCUGCUUA		J-063954-06
		GACAAAUUCAUCUGCAUUA		J-063954-07
		ACAAAGCAAUCCAGUUCUA		J-063954-08
Col4a2	NM_009932	CGGAAAGAAAGGCGACCAA	L-064498-01	J-064498-09
		GGAGUUUGUGGAUCGGAUA		J-064498-10
		AAACAGGAGCACCGGGAUU		J-064498-11
		CAGAAAGGGGAGCGGGGAA		J-064498-12
Gvin1	NM_029000	GAAAUUACUCCAACGUCUA	L-063733-00	J-063733-05
		UCUCUAAACUUUCCAUUUG		J-063733-06
		CAAGGAAAGUUUGAAAUCA		J-063733-07
		GUUGUAAUCUCUUGUGUGA		J-063733-08
Hspa12b	NM_028306	CCGAUGUCUUUGAGCGCUU	L-060987-01	J-060987-09
		GAGCGGAGGUCUAUCGACU		J-060987-10
		GCGUUGUGGUCCCGCAUGA		J-060987-11
		UCUGGAAACAACCGGCUAA		J-060987-12
Naa15	NM_053089	GAAUCAAGUUCUUCGGGAA	L-056607-01	J-056607-09
		AGCUAAAGAAACUGCGUAA		J-056607-10
		CAAUAGAGCUGGCGACAAC		J-056607-11
		ACACAGAAUGAGAGGAGUA		J-056607-12
Nes	NM_016701	GCGACAACCUUGCCGAAGA	L-057300-01	J-057300-09
		GGAGGAAGGUCAAGCGAUU		J-057300-10
		GGAACAGAAACUCGAACAA		J-057300-11
		CCAAAGAGGUGUCCGAUCA		J-057300-12
Plec	NM_201392	GCACUGAACUUGCGACACA	L-057830-01	J-057830-09
		UGAAUAAAGUGUAUCGACA		J-057830-10
		GGGAAGAUGUGUACCGGUA		J-057830-11
		UGGAGGAACACGAGCGGAA		J-057830-12
Serpinh1	NM_009825	GGUAAAGCCACCACAGCGU	L-043051-01	J-043051-09
		CCGUGAGCUUCGCCGAUGA		J-043051-10
		AAGCUAAGUUCCAAGGCGA		J-043051-11
		GCAACUCCACUGCGCGCAA		J-043051-12
Slit3	NM_011412	GGAUCAAGGAAGUGCGGGA	L-063651-01	J-063651-09
		GCUCUGAGGAUUAUCGCAA		J-063651-10
		AGAAUCAGAUAUCGGACAU		J-063651-11
		UCUUUGAGAUUCAGAACGA		J-063651-12
Tcp1	NM_013686	GCAAGGAAGCGGUGCGUUA	L-040339-01	J-040339-09
		GAUUAUUAACGCAGACGAA		J-040339-10
		GAUGUUGGGACAAGCGGAA		J-040339-11
		AAGUGAACCCGGAACGUAA		J-040339-12
Vim	NM_011701	CCAGAGAGAGGAAGCCGAA	L-061596-01	J-061596-09
		AGGAAGAGAUGGCUCGUCA		J-061596-10
		GUCUUGACCUUGAACGGAA		J-061596-11
		AAGCAGGAGUCAAACGAGU		J-061596-12

2.4 Western Blotting

Cells or tissue were washed in PBS and lysed in EB buffer (3% SDS, 60 mM Sucrose, 65 mM Tris-HCL, pH 6.8), e.g. 75 µL per well for a 6-well plate. Acid-washed glass beads were added to each sample and lysis was aided by using a Tissue Lyser LT (Qiagen, Manchester) for 2 min at 50 Hz. Protein content was quantified using the DC™ protein assay kit (Bio-Rad, Watford), a colorimetric method whereby amino acids reduce Folin's reagent causing it to change colour. 5 µL of protein sample was mixed with 25 µL of solution A (+S) in a 96-well plate, followed by 200 µL of solution B. Absorbance at 670 nm was determined using a VersaMax spectrophotometer (Molecular Devices, San Jose, US). Concentration was determined by comparison to the absorbance of the standards by using linear regression.

Protein sample (10 - 25 µg) was mixed with NuPAGE™ Sample Buffer and Reducing Agent, then heated to 95°C for 5 min on a heat block. Next, samples were loaded onto an 8 - 12% polyacrylamide gel and subjected to SDS-PAGE using the Bio-Rad Electrophoresis system for 1 hr+, depending on the degree of separation needed, at 100 V, followed by electro-transfer of the protein onto Amersham™ Protran™ 0.4 µm nitrocellulose membrane (GE Healthcare, Amersham) using the Bio-Rad Mini Trans-Blot® Cell kit with an ice pack at 35 V for 150 min or 115 V for 75 min.

Protein transfer was assessed by incubating the membrane for 5 min with a 0.1% Ponceau S stain in 5% acetic acid. To allow immuno-blotting of different size proteins with their corresponding Ab's, the membrane was cut, then blocked in 5% skimmed milk in PBS 0.1% Tween-20 (PBS/T) for 30 min, washed in PBS/T and incubated at 4°C o/n with primary Ab's (**Table 2.1**) made up in 5% Bovine Serum Albumin (Thermo Fisher). The membrane was washed with PBS/T and incubated with HRP-labelled secondary Ab (**Table 2.2**) in 5% milk (as above), for 2 hr at room temperature (RT). After washing the membrane with PBS/T, Pierce™ ECL substrate (Thermo Fisher) was added then the membrane was imaged using Fujifilm LAS-3000 darkroom (Fujifilm, Bedford).

Image J™ software was used to perform densitometry on the Western blot (WB) images. The signal was normalised according to loading controls, i.e. Hsc70 or Gapdh. The signal obtained from phosphorylated proteins was normalised to the total amount of the protein of interest in the same sample.

2.5 Adhesion Assay

To perform an adhesion assay, 96-well plates were pre-coated with 10 µg/mL FN at 4°C o/n. ECs were serum starved in minimal medium (Opti-MEM™ - Invitrogen) for 3h at 37°C, while the pre-coated plates were blocked with 1% BSA at RT for 1 hr. Cells were trypsinised, resuspended and counted, then 3 x 10^4 cells were seeded into each well. The plates were incubated for 90 min at 37°C, followed by three PBS washes, fixation in 4% paraformaldehyde (PFA) for 10 min and another PBS wash. Cells were stained with 1% Methylene blue, 10 mM borate, 50% methanol (pH 8.5) solution for 30 min, then washed by submerging in distilled water. Once the plates were air-dried, 100 µL per well of de-stain solution (50% ethanol, 50% 0.1 M HCl) was added and absorbance was read using a spectrophotometer at 670nm.

2.6 Wound-Closure Migration Assay

To assess migration, 6-well plates were pre-coated with 10 µg/mL FN at 4°C o/n. ECs were seeded at a density of 4 x 10^5 per well and allowed to reach 100% confluence o/n. They were serum starved in Opti-MEM™ for 3 hrs at 37°C. A P200 tip was then run in a straight line across the centre of each well to create a 'wound'. Medium was then supplemented with 2% FBS and 30 ng/mL VEGF. The bottom of each well was marked using a permanent pen to aid the process of taking images. Using an inverted Axiovert microscope (Zeiss), phase contrast images were taken at time 0 (T0) at marked positions and assay plates were returned to the incubator. Cells were fixed 24 hrs later in 4% formaldehyde and T24 images were taken in the same marked positions as at T0.

Image J™ software was used to quantify the scratch-wound closure. To analyse, three measurements of the gap width per image was averaged, with the difference between the time points calculated and expressed as % closure.

2.7 Proliferation Assay

To assess cell proliferation, 96-well plates were coated with 0.1% gelatin o/n or for 1 hr at 37°C. Cells were seeded at a density of 7 x 10^3 cells per well in 100 µL of IMMLEC medium and incubated at 37°C for 24 - 96 hrs. To each well, 10µL of tetrazolium salt reagent (WST-1, Abcam, Cambridge) was added then incubated with the cells for 2 hrs at 37°C. The reagent is cleaved into formazan dye by metabolically active cells [272]. Absorbance at 450 nm was determined using a spectrophotometer to quantify the amount of dye and thus cell proliferation in each sample.

2.8 Immunocytochemistry

Acid-washed sterile coverslips were placed into 24-well plates (1 per well), coated with FN o/n at 4°C, washed with sterile PBS then blocked with filter-sterilised 1% BSA in PBS for 1 hr at RT. Cells were trypsinised, counted and seeded at 2 x 10^4 per well for 90 min. All washing steps were done with PBS at RT. Next, cells were washed and fixed in 4% PFA for 10 min at RT and washed again. Fixed cells were permeabilised with 0.5% Nonidet™ P-40 in PBS for 10min at RT. This was followed by two washes and a blocking step using 0.5% BSA, 2% goat serum, 0.2% Triton-X100 in PBS and another washing step. A 15 cm dish was lined with moist filter paper (for a humid environment) followed by parafilm (provides a hydrophobic border) and coverslips were moved onto it. 60 µL of primary Ab (**Table 2.1**) in PBS was added to each coverslip at 4°C o/n: anti-vimentin at 1 in 250 and anti-paxillin at 1 in 200. The dish was covered with a lid to maintain a humidity. Coverslips were washed three times by immersion in PBS. Secondary Ab's or fluorescently labelled phalloidin (**Table 2.2**) made up in PBS were added onto the coverslips for 45 min at RT in the dark: secondary Ab's at 1 in 500 and phalloidin at 1 in 300. Once again coverslips were washed three times by dipping and air-dried for 5 min. They were then mounted using Prolong Gold + DAPI (Thermo Fisher) onto glass slides and edges were sealed using nail polish. Slides were stored at 4°C in the dark. Images of fluorescently-labelled cells (Section 6.2.7) were taken using the Axioplan Epifluorescent microscope (Zeiss, Cambridge) and the AxioCam MRm camera (Zeiss). The Multidimensional Acquisition tool within Axiovision software was used for fluorescence microscopy and imaging. Images of different colour channels were merged using the Image J™ software.

2.9 PCR and Agarose Gel Electrophoresis

PCR and agarose gel electrophoresis were used to amplify and separate DNA based on size. A typical PCR reaction mix consisted of: 10 µL of MegaMix-Blue (Microzone, Haywards Heath, UK), which contains DNA polymerase, dNTPs, buffer and salts at optimal concentrations, as well as a loading dye for electrophoresis; 0.8 µL DNA and 0.08 µL each of Forward and Reverse primer (Invitrogen) at the working concentration of 0.8 µM per well in a 96-well plate (Corning®, Flintshire). To amplify the DNA, thermocyclers (Life Touch, Bioer Technology, Binjiang, China) and Veriti™ (Applied Biosystems/Thermo Fisher) were programmed as follows: an initialisation step at 95°C, then 35 cycles each of: denaturation at 95°C, primer annealing at 50 - 60°C and elongation at 72°C. At the end there was an additional, extended elongation step.

A 1.8% agarose (Thermo Fisher) gel was prepared, as follows: 2.7 g of agarose was dissolved in 100 mL of distilled water in a microwave for 2 – 3 min. 50 mL of a 3X TAE buffer was added to reach a working concentration (1X) of 10 mM Tris, 200 mM acetic acid and 1 mM EDTA, pH 8.0, with 7.5 µL of 10 mg/mL ethidium bromide (Thermo Fisher).

Using the Choice Horizontal Gel System (Alpha Laboratories, Eastleigh, UK) the gel solution was poured into a casting tray, a comb was inserted, and the gel was left to set for 30 min. Then it was placed into a running tank, submerged in 1X TAE buffer and 10 µL of sample per well was loaded. For size reference, 3 µL of HyperLadder™ 1 kB (Bioline, London, UK) was added to a well. The gel was run for 1 hr+ at 100 V using a 75 W power pack (Bio-Rad, Watford) then a ChemiDoc-It®2 imager (UVP, Cambridge, UK) was used to visualise and photograph bands on the gel under UV light.

2.10 Graphing Data and Statistics

GraphPad Prism 6 and Microsoft Excel were used to graph and perform Student's t-test on the generated data to determine statistically significant differences between conditions. Bar charts represent the mean + the standard error of the mean (SEM), unless otherwise stated. Asterisks represent P values as follows: * $P < 0.05$, ** $P < 0.01$, *** $P < 0.001$ and **** $P < 0.0001$.

3 The Search for Candidate Genes in the Adhesome

3.1 Introduction

Tumours cannot grow beyond 2 mm in diameter without recruitment of new blood vessels, a process termed angiogenesis [273]. Since αVβ3-integrin (αVβ3) was seen upregulated in neovasculature it became a promising target for therapy [274]. Small molecule inhibitors achieved impaired blood vessel formation in various models, including intratumoural [252]. Surprisingly, β3-integrin-KO mice exhibited enhanced angiogenesis and tumour growth [275]. By comparing two endothelial-specific Cre mouse models of β3-depletion, we have shown that acute depletion (inducible, β3-floxed Pdgfb.CreER) impairs angiogenesis and tumour growth, whereas in the long-term depletion model (constitutive, β3-floxed Tie1.Cre) this impairment is revoked [180]. Similarly, the most prominent small molecule inhibitor of αVβ3 – Cilengitide – promising up to early stage clinical trials, failed to provide overall benefit alongside chemotherapy in late stage clinical trials [276]. Both the genetic and chemical inhibition studies suggest that a mechanism of escape arises upon long-term depletion or inhibition of αVβ3-integrin. We felt it was important to 'dissect' WT and β3-depleted endothelial cells (ECs) to understand what these changes are at the molecular level. Investigation of the escape mechanism began by observing changes which occurred alongside depletion of β3-integrin in the endothelial focal adhesions (FAs), where it resides. The most unbiased and in-depth way to dissect potential changes within FAs would be by performing mass spectrometry on FA complexes isolated from WT and β3-depleted cells. As previously communicated by Ellison *et al.* [182], we adapted the protocol of FA enrichment for ECs based on the work in fibroblasts by Schiller *et al.* [231]. This protocol, mass spectrometry and the analysis of the β3-depleted EC adhesome are extensively discussed by Atkinson S. J. [232], [277]. β3-depletion was achieved by genetic means (β3-HET and β3-KO ECs) as well as treatment using an αVβ3-integrin inhibitor – a Cilengitide-like cyclic mimetic of the RGD motif (cRGD, EMD66203, Bachem, Bubendorf, Switzerland). These various depletion methods were investigated to strengthen any conclusions (if any changes occurred in more than one β3-depletion model) and ultimately compare the modes of depletion. In addition, there was hope for an explanation of the disappointing outcomes of clinical trials testing αVβ3-integrin inhibitors. The investigation in this chapter is directly linked to the findings from the mass spectrometry experiments mentioned above, therefore it needs to be summarised here.

The initial mass spectrometry data set consisted of label-free quantification (LFQ) values assigned to 1497 proteins. Removing contaminants, false discoveries and proteins that were not detected by all three repeat runs of the same pooled sample (to improve stringency), reduced the list to 1064. Next, LFQ values were converted to log base 2 of LFQ and missing values generated by the log calculation of 0's (undetected) were replaced with a low value. This was necessary to allow statistics to be performed on the data later. At this stage, datasets were arranged into unsupervised hierarchical clusters. As a result, the adhesome data was grouped in terms of VEGF-induction and matrix dependent enrichment, i.e. fibronectin vs. poly-L-lysine (PLL, a non-specific cell adhesion matrix). Unsupervised hierarchical clustering, based on Euclidian distance, identified 3 main groups of clusters: VEGF-induced (clusters A, B, C), fibronectin-enriched (D, E, F) and poly-L-lysine-enriched (G – L) (**Supp. Fig. 1**). Finally, the WT and β3-depleted adhesome data sets were compared using the significance analysis of microarrays (SAM) method. After eliminating false positives this method identified 143 downregulated and 263 upregulated proteins in the β3-depleted adhesome [277].

In this refined data set, an upregulation of all detected tubulins was observed in the β3-depleted adhesome, compared with the WT control adhesome. Further experimental analysis showed that microtubule targeting agents are more effective at inhibiting angiogenesis in the β3-depleted background, both *in vitro* and *in vivo*, via a Rcc2/Anxa2/Rac1-dependent mechanism [232].

The mass spectrometry of the IMMLEC adhesomes confirmed their endothelial identity, as many endothelial-specific proteins, such as VE-Cadherin and Tie1, were present [232]. The role of β3-integrin is context dependent, as discussed in the first chapter of this thesis [278]. Most of the *in vitro* work in this study was performed in IMMLECs on tissue culture plastic coated with fibronectin – a ligand of αVβ3-integrin. This matrix is typically present in the basement membrane around angiogenic blood vessels, but not around quiescent vasculature [161].

Initially, β3-integrin inhibition in tumour angiogenesis seemed promising, but long-term targeting of this integrin was subject to a compensatory mechanism [180], [251]. The work undertaken in this chapter is a further in-depth analysis of the aforementioned mass spectrometry data sets. We mined the data for further proteins with altered presence in the β3-depleted endothelial adhesomes (models of long-term inhibition) in search for other potential mediators of compensation. Precisely 12 out of 104 proteins that were upregulated in at least two of the three models of β3-depletion were followed up experimentally. These potential co-targets all belong to the intermediate filament (IF) protein family. As a result, we discovered another potential avenue of targeting the cytoskeleton alongside β3-integrin.

3.2 Materials and Methods

3.2.1 Focal Adhesion Enrichment

This method was performed as described by Ellison *et al.*[182] and Atkinson *et al.* [232]; adapted from Schiller *et al.* [231]. First, 10 cm plates were coated with 10 µg/mL FN at 4°C o/n, then blocked with 1% BSA at RT for 1 hr. ECs were serum starved for 3 hrs in Opti-MEM™ prior to seeding $6x10^6$ cells per plate. Cells were allowed to adhere for 90 min to allow formation of mature, β3-rich, adhesions. For VEGF stimulated samples, 30 ng/mL of VEGF was added to the plates for the last 10 min of the adhesion step. Next, plates were washed with PBS supplemented with 1 mM $CaCl_2$ and 1 mM $MgCl_2$ (PBS++), followed by treatment with 0.5 mM Dithiobis(succinimidyl propionate) (DSP) and 0.05 mM 1,4-Bis[3-(2-pyridyldithio)propionamido] butane (DPDPB) for 5 min. This reaction was stopped by addition of 1 M Tris-HCl pH 7.5 and the cells were lysed on ice for 30 min using RIPA buffer (20 mM Tris pH 7.4, 50 mM NaCl, 0.1% SDS, 1% Triton, 1% Deoxycholate, 1% NP40). Lysate was collected without scraping and the plates were subjected to a high-sheer flow of distilled water to wash off cell debris. Dithiothereitol (DTT) buffer was used for 1 hr at 60°C to elute the cross-linked material in a humidified chamber. This was followed by 8 mL of acetone per plate and storage o/n at -20°C with 10 µl of GlycoBlue™ as a co-precipitant (ThemoFisher). Protein samples were spun down at 13'000 g for 40 min and the acetone layer was discarded. Pellets were resuspended in 30 µL EB buffer (see Section 2.4). 2 µL of the DTT eluent and 2 µL of the total cell lysate as a control were run on a 10% SDS-PAGE gels. The eluents were assessed for focal adhesion enrichment by silver staining using the Pierce™ Silver Stain Kit (ThermoFisher).

3.2.2 Mass Spectrometry and Analysis

Silver stain was used to confirm successful isolation of FA complexes. Less content and enrichment of bands of particular size in the crosslinked material compared to the whole cell lysate indicated a successful enrichment. Also, silver stain allowed to assess enrichment on FN compared to poly-L-lysine, an integrin independent adhesion factor. Three preferred samples were pooled and analysed three times by mass spectrometry, which was carried out by the Fingerprints Proteomics Facility (University of Dundee) as described by Schiller *et al*. [231]. Briefly, protein samples were digested using 12.5 ng/µL trypsin, dehydrated using acetonitrile and subjected to liquid chromatography tandem mass spectrometry (LC-MS/MS) using LTQ Orbitrap mass spectrometer (Thermo Electron, Bremen, Germany). Ion spectrum data was analysed using MaxQuant software, linked to the Andromeda database for peptide identification. Subsequent analysis was done using Perseus software, a bioinformatics toolbox for MaxQuant [279]. GO [280] and KEGG [281] databases were used to annotate the protein data set. Statistically significant change between conditions was determined by using the significance analysis of microarrays (SAM) method [282], with a false discovery rate of 0.01, based on 250 data permutations and an S_0 cut-off of 1.

3.2.3 Network Analysis

Protein interaction networks were illustrated using Search Tool for the Retrieval of Interacting Genes/Proteins (STRING), an online database of known and predicted protein-protein interactions, a joint project between the Swiss Institute of Bioinformatics (SIB), Novo Nordisk Foundation Center for Protein Research (NNFCPR) and the European Molecular Biology Laboratory (EMBL). These diagrams were generated using a tool built into the website with default parameters, i.e. medium confidence setting (0.4) and using all available active interaction sources for mouse proteins.

https://string-db.org/cgi/input.pl

3.3 Results

3.3.1 Differential Gene Expression in the β3-integrin-depleted Adhesome

Endothelial FAs from β3-depleted and WT/control IMMLECs were isolated and subjected to mass spectrometry, as described above. False discoveries were removed using Perseus software. The raw data and the full lists of proteins detected in each of the adhesomes has previously been presented in the PhD thesis by Atkinson S.J. [277]. I revisited these datasets and decided to focus on upregulated proteins, as these were more likely to represent members of a compensatory escape pathway. Also, upregulated genes/proteins could be targeted more readily with siRNA, while re-introducing a gene/protein into the cells is a much more complex strategy. Therefore, this approach was more feasible in terms of time and cost, allowing me to test more potential candidates.

The DMSO- vs cRGD-treated adhesome comparison highlighted only a single significantly altered candidate protein, as discussed below. The WT vs β3-HET endothelial adhesome comparison was deemed more meaningful than the WT vs β3-KO comparison. The complete loss of β3 integrin (in the β3-KO ECs) is subject to drastic, developmental changes, such as upregulated VEGFR2 expression that we felt might skew results [277]. We felt that, at least initially, focusing on the β3-HET EC adhesome, where β3 levels are reduced to 50%, would allow us to pinpoint the most β3-relevant changes. Despite this, all three comparisons were considered here, but I focused on the WT vs β3-HET comparison in particular. Of the 726 proteins detected in this comparison, 175 were upregulated and 94 were downregulated to a significant degree as determined by the SAM method [277]. This is depicted by the volcano plot in **Fig. 3.1**. All proteins upregulated in the β3-HET adhesome compared to the WT are listed in **Table 3.1**.

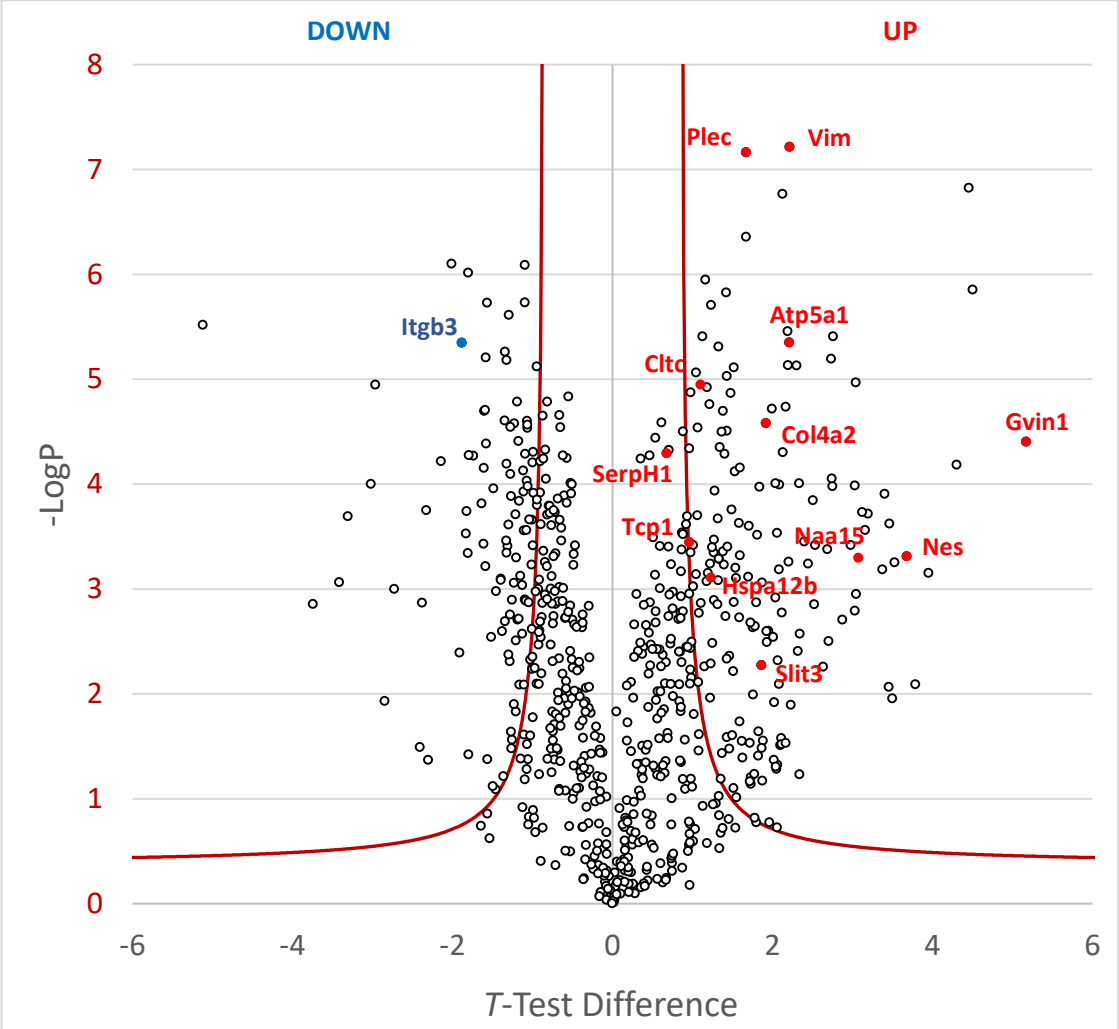

Figure 3.1 WT vs. β3-HET endothelial adhesome.

A volcano plot of *t*-test difference and – log of P value for each of the proteins detected by mass spectrometry analysis of the focal adhesion enrichment samples (n=3). Dark red lines represent the significance cut-off, as dictated by the significant analysis of microarrays (SAM). 12 candidate genes taken forward are highlighted in red and β3-integrin in blue.

Table 3.1 List of upregulated proteins in the β3-HET vs WT endothelial adhesome.

				LFQ NORMALISED TO WT β3			
GENE NAME	PROTEIN ID	PROTEIN NAME	CLUSTER	WT	β3-HET	-LOG P VALUE	DIFFERENCE
Itgb3	**O54890**	**Integrin beta-3**	**F**	**100.000**	**21.008**	**4.190**	**-2.257**
…							…
Gm4832	Q3UTE1	(pseudogene)	F	0.000	139.167	5.394	6.928
Gvin1	**L7N451**	**Interferon-induced very large GTPase 1**	**I**	**0.000**	**78.046**	**3.083**	**5.354**
Copb2	O55029	Coatomer subunit beta	I	0.550	37.927	2.999	5.013
Thbs1	Q3TR40	Thrombospondin-1	F	47.229	1363.428	6.235	4.856
Slc25a3	Q3THU8	Phosphate carrier protein, mitochondrial	C	0.000	51.578	5.481	4.181
Lmna	P48678	Prelamin-A/C;Lamin-A/C	F	10.750	172.698	6.756	4.006
Rtn4	Q8BH78	Reticulon;Reticulon-4	C	8.554	116.196	3.934	3.809
Palld	K0BWC3	Palladin	F	7.986	67.778	1.456	3.627
Actc1;Acta1;Actg2;Acta2	Q9CXK3	Actin, α cardiac muscle 1;skeletal muscle;aortic/γ smooth muscle		1.925	42.226	3.171	3.505
Eprs	B9EIU1	Glutamyl-Prolyl-TRNA Synthetase	I	1.192	20.706	5.077	3.463
Snrnp200	Q6P4T2	U5 small nuclear ribonucleoprotein 200 kDa helicase	I	1.187	31.529	3.483	3.429
Canx	Q5SUC3	Calnexin	I	2.838	28.213	2.160	3.384
Map7d1	A2AJI0	MAP7 domain-containing protein 1	F	0.000	12.813	2.837	3.383
Atp5b	P56480	ATP synthase subunit beta, mitochondrial	C	14.518	141.982	3.174	3.356
Hspd1	P63038	60 kDa heat shock protein, mitochondrial	G	0.000	26.477	3.197	3.352
Dars	Q8BK18	Aspartate--tRNA ligase, cytoplasmic	I	0.000	11.786	3.397	3.333
Rpl10a	Q5XJF6	Ribosomal protein;60S ribosomal protein L10a	I	2.150	17.183	1.758	3.326
Col4a1	P02463	Collagen alpha-1(IV) chain;Arresten	F	6.995	71.651	3.316	3.306
Mcm7	Q3UDI8	DNA replication licensing factor MCM7	A	0.000	11.844	4.640	3.243
Cad	E9QAI5	CAD protein	I	0.000	11.699	3.715	3.232
Nes	**Q6P5H2**	**Nestin**		**0.000**	**28.776**	**3.278**	**3.200**

				LFQ NORMALISED TO WT β3			
GENE NAME	PROTEIN ID	PROTEIN NAME	CLUSTER	WT	β3-HET	-LOG P VALUE	DIFFERENCE
Bgn	Q3TNY9	Biglycan	I	0.108	0.962	3.202	3.191
Prpf8	Q99PV0	Pre-mRNA-processing-splicing factor 8	I	0.000	18.620	1.959	3.175
Lmnb1	P14733	Lamin-B1	C	0.000	14.800	2.309	3.133
Eif4b	Q3TDD8	Eukaryotic translation initiation factor 4B	I	1.083	16.565	2.560	3.109
Eftud2	Q543F1	116 kDa U5 small nuclear ribonucleoprotein component	I	3.453	28.546	3.546	3.096
Naa15	**Q80UM3**	**N-alpha-acetyltransferase 15, NatA auxiliary subunit**	**I**	**0.000**	**8.836**	**3.295**	**3.077**
Rpn2	Q61833	Dolichyl-di(P)oligosaccharide protein glycosyltransferase 2	I	0.000	19.257	3.731	3.053
Eif5b	Q05D44	Eukaryotic translation initiation factor 5B	F	0.000	12.472	3.760	3.014
Akap12	B2RRE0	A-kinase anchor protein 12	C	7.433	59.733	3.786	2.978
Eef1b;Eef1b2	O70251	Elongation factor 1-beta	L	0.000	13.311	2.923	2.908
Iars	Q8BU30	Isoleucine--tRNA ligase, cytoplasmic	I	0.000	16.284	2.949	2.904
Sdpr	Q63918	Serum deprivation-response protein	I	0.000	10.667	2.238	2.899
Copa	F8WHL2	Coatomer subunit alpha;Xenin;Proxenin	I	10.490	69.800	2.624	2.845
Hsp90b1	Q91V38	Endoplasmin	I	19.258	130.649	3.359	2.806
Rps29;Gm10126	P62274	40S ribosomal protein S29	C	0.000	9.173	3.896	2.800
Mvp	Q8C2S9	Major vault protein		0.000	10.963	2.934	2.760
Dync1i2	A2BFF7	Cytoplasmic dynein 1 intermediate chain 2	C	0.000	15.542	5.329	2.695
Rrbp1	A2AVJ7	Ribosome-binding protein 1	I	0.000	12.119	3.607	2.652
Copg1	Q9QZE5	Coatomer subunit gamma-1	I	2.905	26.141	4.171	2.616
Atp2a2	J3KMM5	Sarcoplasmic/endoplasmic reticulum calcium ATPase 2		0.000	7.177	4.186	2.561
Vars	Q7TPT7	Valine--tRNA ligase	I	4.720	24.415	1.593	2.518
Tmem43	Q9DBS1	Transmembrane protein 43	H	0.000	18.367	1.981	2.501
Phb2	Q3V235	Prohibitin-2	C	1.145	13.627	2.333	2.479
Atp1a1	Q8VDN2	Sodium/potassium-transporting ATPase subunit alpha-1	F	7.166	35.787	2.232	2.474
Tnc	Q80YX1	Tenascin	F	181.642	974.847	7.423	2.424

				LFQ NORMALISED TO WT β3			
GENE NAME	**PROTEIN ID**	**PROTEIN NAME**	**CLUSTER**	**WT**	**β3-HET**	**-LOG P VALUE**	**DIFFERENCE**
Eif3f	Q6IRT4	Eukaryotic translation initiation factor 3 subunit F	I	1.394	12.530	1.841	2.398
Phb;1700071K01Rik	P67778	Prohibitin	D	1.476	11.816	3.948	2.393
Mcm6	Q542I2	DNA replication licensing factor MCM6	G	2.893	15.616	1.374	2.387
Psmd3	Q8BK46	26S proteasome non-ATPase regulatory subunit 3	I	1.017	9.785	2.259	2.331
Rpn1	Q5RKP4	Dolichyl-di(P)oligosaccharide protein glycosyltransferase 1	I	3.177	15.769	1.680	2.327
Csnk2a1	Q61177	Casein kinase II subunit alpha	I	2.225	8.849	1.292	2.320
Tuba1a;Tuba3a	P68369	Tubulin alpha-1A chain;Tubulin alpha-3 chain	C	12.498	57.595	2.497	2.286
Myof	E9Q390	Myoferlin	C	20.545	99.759	5.704	2.278
Atp5a1	**D3Z6F5**	**ATP synthase subunit alpha**	**G**	**20.633**	**99.010**	**5.921**	**2.263**
Uba1	B9EHN0	Ubiquitin-like modifier-activating enzyme 1	F	8.123	23.382	0.787	2.260
Nap1l1	Q3TF41	Nucleosome assembly protein 1-like 1	I	6.489	31.062	4.935	2.259
Ctgf;fisp-12	P29268	Connective tissue growth factor	I	28.427	133.287	3.676	2.239
Trim28	Q5EBP9	Transcription intermediary factor 1-beta	L	0.000	7.819	2.846	2.231
Uso1	Q9Z1Z0	General vesicular transport factor p115		0.000	9.455	2.167	2.219
Vim	**Q5FWJ3**	**Vimentin**	**F**	**340.023**	**1580.909**	**6.510**	**2.216**
Nid1	P10493	Nidogen-1	L	14.349	65.531	3.864	2.206
P4ha1	Q3TN84	Prolyl 4-hydroxylase subunit alpha-1	D	0.000	13.990	3.749	2.206
Hsp90aa1	Q80Y52	Heat shock protein HSP 90-alpha	C	14.137	64.558	4.209	2.202
Sf3b3	B2RSV4	Splicing factor 3B subunit 3	I	3.439	19.926	2.692	2.201
Rnf213	F7A6H4	E3 ubiquitin-protein ligase RNF213	I	3.347	15.585	1.741	2.193
Rars	Q9D0I9	Arginine--tRNA ligase, cytoplasmic	I	5.557	22.518	1.834	2.182
Uggt1	Q6P5E4	UDP-glucose:glycoprotein glucosyltransferase 1		0.000	10.692	1.863	2.181
Hist1h3e/2h3b/1h3b	A1L0U3	Histone H3;Histone H3.2	C	39.501	178.752	3.150	2.145
Kars	Q8C292	Lysine--tRNA ligase	I	2.523	11.316	1.245	2.129
Copb1	Q9JIF7	Coatomer subunit beta	I	1.142	10.555	1.949	2.123

				LFQ NORMALISED TO WT β3			
GENE NAME	PROTEIN ID	PROTEIN NAME	CLUSTER	WT	β3-HET	-LOG P VALUE	DIFFERENCE
Cav1	P49817	Caveolin-1	E	7.728	33.095	3.474	2.119
Ganab	A1A4T2	Neutral alpha-glucosidase AB	B	0.000	9.771	2.908	2.092
Tinagl1	Q4FJX7	Tubulointerstitial nephritis antigen-like	L	11.928	50.420	3.970	2.092
Hist2h4;Hist1h4a	B2RTM0	Histone H4	I	52.128	219.157	4.503	2.066
Lamc1	F8VQJ3	Laminin subunit gamma-1	I	11.761	48.918	5.191	2.059
Ctps1	P70698	CTP synthase 1	I	6.293	25.524	3.288	2.047
Lamb1	Q3UHL7	Laminin subunit beta-1	F	6.126	24.941	3.897	2.030
Col4a2	**B2RQQ8**	**Collagen alpha-2(IV) chain;Canstatin**	**F**	**24.497**	**98.623**	**2.289**	**2.017**
Vps35	Q3TRJ1	Vacuolar protein sorting-associated protein 35	I	5.001	19.956	2.326	2.015
H2afv;H2afz	B2RVP5	Histone H2A;Histone H2A.V;Histone H2A.Z	I	0.000	7.210	2.515	2.012
Rab5c	Q3TJ39	Ras-related protein Rab-5C	I	1.617	9.463	1.689	1.991
Numa1	Q80Y35	Nuclear Mitotic Apparatus Protein 1	I	3.190	12.862	1.626	1.987
Cope	D3Z315	Coatomer subunit epsilon	I	0.000	4.449	2.123	1.985
Srrt	Q99MR6	Serrate RNA effector molecule homolog	F	0.000	10.179	2.699	1.982
Fasn	Q3UHT6	Fatty acid synthase	C	9.974	38.934	3.450	1.982
Psmd7	A1L3B8	26S proteasome non-ATPase regulatory subunit 7	I	2.740	10.181	1.378	1.935
Hspa9	P38647	Stress-70 protein, mitochondrial		0.000	5.945	3.186	1.919
Rpl12	Q5BLK0	60S ribosomal protein L12	I	2.801	9.398	1.363	1.893
Myo1d	Q5SYD0	Unconventional myosin-Id	C	0.000	9.041	3.832	1.888
Psmd2	Q3TXV1	26S proteasome non-ATPase regulatory subunit 2	I	8.677	31.581	3.298	1.884
Plod3	Q9R0E1	Procollagen-lysine,2-oxoglutarate 5-dioxygenase 3		0.000	7.951	2.916	1.881
Capns1	D3YW48	Calpain small subunit 1	I	10.225	37.310	4.608	1.870
Colgalt1	Q8K297	Procollagen galactosyltransferase 1	G	0.000	6.795	3.714	1.863
Plec	**Q6S390**	**Plectin**	**F**	**202.740**	**727.958**	**5.146**	**1.842**
H2afy;H2afy2	Q9QZQ8	Core histone H2A/H2A.1/H2A.2	L	0.000	6.222	2.713	1.789

				LFQ NORMALISED TO WT β3			
GENE NAME	**PROTEIN ID**	**PROTEIN NAME**	**CLUSTER**	**WT**	**β3-HET**	**-LOG P VALUE**	**DIFFERENCE**
Rplp2	P99027	60S acidic ribosomal protein P2	I	0.000	7.242	1.884	1.750
Top2b	Q64511	DNA topoisomerase 2-beta;DNA topoisomerase 2	L	0.000	7.179	2.996	1.718
Thbd	Q543W3	Thrombomodulin	I	0.000	5.856	1.431	1.711
Anxa6	Q99JX6	Annexin;Annexin A6	C	0.000	7.691	1.534	1.708
Dhx15	Q3UKJ6	DEAH-Box Helicase 15	C	1.898	10.203	1.285	1.706
Sptbn1	Q62261	Spectrin beta chain, non-erythrocytic 1	I	60.755	194.138	3.604	1.689
Usp9x	Q4FE56	Ubiquitin carboxyl-terminal hydrolase		0.000	5.864	2.093	1.680
Flnc	D3YW87	Filamin-C	F	35.723	114.187	3.190	1.675
Hsp90ab1	Q71LX8	Heat shock protein HSP 90-beta	C	194.174	617.413	7.252	1.669
Cttn	Q921L6	Src substrate cortactin	F	4.442	14.305	1.369	1.667
Serpinb9b	Q9DAV6	Serpin Family B Member 9	I	0.000	8.357	2.068	1.657
Rpl30	Q497D7	60S ribosomal protein L30	I	2.405	10.820	1.158	1.657
Pdlim5	D9J2Z9	PDZ and LIM domain protein 5	F	8.745	27.454	2.760	1.656
Capn1	Q3UF24	Calpain-1 catalytic subunit	L	0.000	7.153	2.599	1.640
Psmb3	Q545G0	Proteasome subunit beta type-3	I	6.707	20.415	2.932	1.627
Myh10	Q5SV64	Myosin-10	I	11.520	34.481	2.475	1.623
Cops3	Q8BX58	COP9 signalosome complex subunit 3	B	0.000	5.805	2.305	1.620
Slit3	**Q3UHN1**	**Slit homolog 3 protein**		**0.000**	**4.971**	**2.274**	**1.613**
Ssr1	Q3TV94	Translocon-associated protein subunit alpha	I	0.000	5.108	5.034	1.584
Arpc4	Q9D3C4	Actin-related protein 2/3 complex subunit 4	I	2.112	9.000	1.317	1.567
Col12a1	E9PX70	Collagen alpha-1(XII) chain		0.000	6.945	3.034	1.564
Sptan1	P16546	Spectrin alpha chain, non-erythrocytic 1	I	63.184	186.294	4.838	1.561
Capn2	O08529	Calpain-2 catalytic subunit	I	29.479	87.199	3.488	1.558
Slk	A2RRK3	STE20-like serine/threonine-protein kinase	L	0.000	5.894	1.967	1.556
Tpm4	Q6IRU2	Tropomyosin alpha-4 chain	F	8.625	25.024	4.342	1.541

				LFQ NORMALISED TO WT β3			
GENE NAME	**PROTEIN ID**	**PROTEIN NAME**	**CLUSTER**	**WT**	**β3-HET**	**-LOG P VALUE**	**DIFFERENCE**
Eif3l	Q8QZY1	Eukaryotic translation initiation factor 3 subunit L	I	10.820	31.941	2.537	1.535
Ddost	Q3UG68	Dolichyl-di(P)oligosaccharide glycosyltransferase 48 kDa	C	0.000	5.563	3.137	1.530
Nop58	Q6DFW4	Nucleolar protein 58	I	2.478	6.942	1.124	1.526
Upf1	Q9EPU0	Regulator of nonsense transcripts 1	L	0.000	6.683	2.141	1.515
Dpysl3	E9PWE8	Dihydropyrimidinase-related protein 3	C	37.671	105.735	3.516	1.497
Set;BC085271	A2BE93	Protein SET	I	4.258	13.483	1.551	1.496
Actn1	Q7TPR4	Alpha-actinin-1	F	163.561	454.165	4.273	1.477
Tubb2a	Q7TMM9	Tubulin beta-2A chain	C	14.716	37.932	1.196	1.476
Hspa5	Q3U9G2	78 kDa glucose-regulated protein	I	42.654	118.472	5.620	1.474
Rpsa	B2CY77	40S ribosomal protein SA	I	51.357	142.264	4.385	1.473
Eef1d	E9QN08	Elongation factor 1-delta	I	11.109	30.672	5.162	1.465
Ptrf	O54724	Polymerase I and transcript release factor	I	17.614	48.468	5.013	1.459
Mcm2	Q3UK39	DNA replication licensing factor MCM2	I	0.000	7.520	1.656	1.458
Hras;Kras;Nras	Q71SW8	GTPase HRas;GTPase Kras;GTPase Nras	F	0.000	6.002	1.527	1.456
Eef1g	Q4FZK2	Elongation factor 1-gamma	I	35.902	96.412	4.220	1.429
Sec23a	E9Q1S3	Protein transport protein Sec23A	F	5.797	15.478	3.168	1.428
P4hb	Q3UDR2	Protein disulfide-isomerase	A	8.150	21.413	2.686	1.418
Tubb6	Q3UMM1	Tubulin beta-6 chain	F	19.167	49.441	2.516	1.386
Psmc2	Q3UIH5	26S protease regulatory subunit 7	I	6.540	16.835	3.466	1.373
Rab7;Rab7a	Q4FJQ0	Ras-related protein Rab-7a	E	2.023	6.483	1.382	1.363
Kpnb1	Q3TFE8	Importin subunit beta-1	I	13.084	33.499	4.054	1.361
Psma2	Q3UWT6	Proteasome subunit alpha type-2	H	2.793	7.173	4.033	1.357
Tuba1b;Tuba4a	P05213	Tubulin alpha-1B chain;Tubulin alpha-4A chain	C	467.223	1194.949	4.989	1.356
Pdia6	Q3THH1	Protein disulfide-isomerase A6	I	11.955	29.981	2.501	1.354
Myadm	Q0VE46	Myeloid-associated differentiation marker	F	20.796	52.891	4.164	1.347

				LFQ NORMALISED TO WT β3			
GENE NAME	PROTEIN ID	PROTEIN NAME	CLUSTER	WT	β3-HET	-LOG P VALUE	DIFFERENCE
Rplp0	Q5M8R8	60S acidic ribosomal protein P0	I	23.489	58.974	4.042	1.332
Csnk2b	N0E4C0	Casein kinase II subunit beta	I	0.000	3.998	1.732	1.331
Hspa12b	**Q9CZJ2**	**Heat shock 70 kDa protein 12B**	**C**	**11.458**	**28.569**	**3.156**	**1.331**
Htra1	Q9R118	Serine protease HTRA1	F	36.808	91.134	3.684	1.307
Anxa5	P48036	Annexin A5	I	9.502	23.306	3.371	1.303
Tubb5	P99024	Tubulin beta-5 chain	C	95.502	231.405	3.456	1.284
Tagln2	Q9WVA4	Transgelin-2	E	8.208	19.747	3.135	1.270
Eif3a	P23116	Eukaryotic translation initiation factor 3 subunit A	I	37.211	87.588	3.973	1.239
Eif3k	Q9DBZ5	Eukaryotic translation initiation factor 3 subunit K	I	1.338	6.676	1.923	1.232
Eif3c	Q8R1B4	Eukaryotic translation initiation factor 3 subunit C	I	16.043	36.177	1.892	1.229
Kif5b	Q61768	Kinesin-1 heavy chain	I	8.925	20.724	4.328	1.218
Pcna	Q91ZH2	Proliferating cell nuclear antigen		0.000	4.629	2.622	1.216
Csde1	Q8JZN2	Cold shock domain-containing protein E1	I	4.322	9.958	2.797	1.214
Gsn	Q6PAC1	Gelsolin	F	24.718	56.962	3.004	1.195
Tubb4b;Tubb4a	P68372	Tubulin beta-4B chain;Tubulin beta-4A chain	C	303.360	686.271	4.785	1.179
Dhx9	A0A087	ATP-dependent RNA helicase A	L	17.786	39.696	2.687	1.170
Anxa7	Q922A2	Annexin;Annexin A7	I	6.376	14.115	3.175	1.154
Vdac2	G3UX26	Voltage-dependent anion-selective channel protein 2	C	7.169	15.793	3.059	1.132
Flna	B7FAU9	Filamin-A	F	549.006	1199.381	5.635	1.127
Psmc6	Q14AQ1	26S protease regulatory subunit 10B	I	5.809	12.528	2.604	1.124
Ipo7	Q9EPL8	Importin-7	I	14.741	31.896	2.871	1.114
Vcp	Q01853	Transitional endoplasmic reticulum ATPase	F	108.664	234.660	4.711	1.109
Cltc; mKIAA0034	**Q5SXR6**	**Clathrin heavy chain 1**	**I**	**172.585**	**369.487**	**4.786**	**1.098**
Rangap1	Q91YS2	Ran GTPase-activating protein 1	I	0.000	4.355	2.614	1.094
Cand1	Q6ZQ38	Cullin-associated NEDD8-dissociated protein 1	I	4.544	9.444	3.122	1.050

				LFQ NORMALISED TO WT β3			
GENE NAME	**PROTEIN ID**	**PROTEIN NAME**	**CLUSTER**	**WT**	**β3-HET**	**-LOG P VALUE**	**DIFFERENCE**
Myo1c	Q9WTI7	Unconventional myosin-Ic	F	104.111	215.457	5.039	1.050
Actn4	Q3ULT2	Alpha-actinin-4	F	491.279	988.789	4.899	1.009
Rps5	Q91V55	40S ribosomal protein S5	I	21.348	42.866	3.586	1.006
Tcp1	**P11983**	**T-complex protein 1 subunit alpha**	**I**	**35.550**	**71.295**	**3.883**	**1.002**

The second column contains one of the corresponding peptide IDs identified for each gene using the Andromeda database. The fourth column informs on inclusion to a particular cluster, as identified by unsupervised hierarchical clustering: A, B, C – VEGF-enriched; D, E, F – fibronectin-enriched and clusters G, H, I, J, K, L – poly-L-lysine enriched. LFQ – label free quantification value obtained from the mass spectrometer. The LFQ values presented here are averages from 3 runs of FA enrichment samples expressed relative to the average LFQ detected for β3-integrin in WT condition. The last 2 columns report the -log P value and the *t*-test difference from the Significance Analysis of Microarrays (SAM) carried out in Perseus. The table was sorted in descending order based on the last column. Chosen candidate genes taken forward for further analysis are highlighted and in bold. Adapted from Atkinson *et al*. (2018) [232].

In addition, FA enrichment comparison was performed on β3-KO and WT IMMLECs. Here, we detected 961 proteins of which 88 were upregulated and 49 were downregulated according to SAM [277]. More proteins were detected than in the β3-HET experiment, but significant change in their abundance was much less prevalent, ~15% compared to ~35%. Upregulated proteins in the β3-KO background compared to WT are listed in **Supp. Table 1**.

To further complement this analysis, we isolated FAs from Cilengitide-like αVβ3-integrin-inhibitor-treated (cRGD, EMD66203, Bachem, Bubendorf, Switzerland) WT IMMLECs. For these experiments, the 90 min adhesion step was carried out in the presence of cRGD (made up in DMSO) at 20 μM or DMSO as a control. β3-integrin appeared downregulated in cRGD treated cells, but not to a significant degree. Significance analysis of microarrays (SAM) analysis identified only a single protein that had changed significantly in response to cRGD treatment – Ncbp1, a protein required for mRNA processing and translocation [283]. We were uninterested in following up this nuclear protein as it is likely a false positive. Instead, we chose to search the list of detected proteins showing an upregulation trend for more angiogenesis-relevant candidates. To sum up the data set, 912 proteins were detected, of which 406 experienced a fold change of more than 1, these were considered upregulated, and the remaining 506 had a fold of less than 1, i.e. downregulated. Most of the upregulated proteins in the cRGD vs DMSO WT IMMLEC adhesome were listed in **Supp. Table 2**. This time the data was presented differently, because of the lack of statistical significance. Proteins were sorted according to their fold-change in the cRGD vs DMSO WT adhesome, and the top 150 proteins were included in **Supp. Table 2**. The last two genes on this list were Gvin1 and Tcp1, both significantly upregulated in the β3-HET and β3-KO adhesomes.

3.3.2 Candidate Search

An unbiased approach was taken to narrow down the resulting lists of candidate genes. The lists of upregulated proteins (**Table 3.1, Supp. Table 1 and 2**) were cross-referenced to generate a shorter list of candidate proteins that were upregulated in at least two of the three conditions of β3-depletion, and thus a list of candidates in which we had the most confidence (**Table 3.2**). The list of proteins upregulated in the cRGD adhesome used in this step consisted of the hits with fold change of 1.1 or above (292 out of the 406 with fold change of 1 or above). Thus, the pool of potential candidate genes could be reduced as follows (in comparison to WT/DMSO adhesome): (1) 23 proteins were upregulated in both β3-HET and β3-KO adhesomes; (2) 75 proteins were upregulated in both β3-HET and cRGD-treated adhesomes; (3) 36 proteins were upregulated in both β3-KO and cRGD-treated adhesomes (**Table 3.2**). This cross-referencing exercise left us with 104 unique proteins, while 15 of these were upregulated in all three β3-depleted adhesomes.

Several factors determined the outcome of the next stage of narrowing candidates. We searched the GO and KEGG annotations assigned to our gene lists for relevance in angiogenesis and EC biology, by using 'angiogenesis' and 'endothelial' as database search queries. Annotations reported which molecular function (GOMF) or biological process (GOBP) the genes/proteins participate in and which biological system are they part of (KEGG) [280], [281]. We also checked which cellular component (GOCC) does a given protein reside in [280]. These steps were further aided by using publication search engines to look for established links to angiogenesis and EC biology. At the same time, we preferred genes that were near the top of our lists, as they were the most significantly upregulated. Thus, the list shortened, and 12 candidate genes were chosen for further analysis (**Table 3.3**). ATP Synthase, subunit α (Atp5a1) and Interferon-induced very large GTPase 1 (Gvin1) were highly upregulated in all three β3-depleted EC adhesomes. N-α-acetyltransferase 15 (Naa15) and T-Complex 1 (Tcp1) were also upregulated in all three conditions. Naa15 has been previously seen expressed by ECs and has been suggested to regulate blood vessel development [284]. Mutations in Tcp1 disrupted actin and microtubule structure and function [285]. Collagen type IV α 2 (Col4a2) and Slit Homolog 3 (Slit3) were up in both genetically β3-depleted adhesomes. Collagen derived anti-angiogenic inhibitors have been designed, including Canstatin, which binds αVβ3 and αVβ5 integrins, and is based on a domain within Col4a2 [286]. Slit3 activation has been implicated in angiogenesis *in vivo* and in vascular network formation in engineered tissue [287]. Serpin Family H Member 1 (Serpinh1), also known as Heat Shock Protein 47, was up in β3-KO and the cRGD-treated adhesomes. It is a collagen-specific chaperone, shown to promote angiogenesis in gliomas [288]. The remaining five chosen candidates were upregulated in the β3-HET and the cRGD-treated adhesomes, namely: Heat

Shock 70kD 12b (Hspa12b), Clathrin heavy chain 1 (Cltc), nestin (Nes), plectin (Plec) and vimentin (Vim). Hspa12b is a predominantly endothelial, stress-response chaperone shown to be required for angiogenesis [289]. Cltc plays a role in endocytosis and intracellular trafficking, also shown to bind HIF-1α and promotes VEGF expression [290]. Nestin, plectin and vimentin are all intermediate filament (IF) proteins. Nestin forms type VI IFs and is a novel player in angiogenesis [291]. Plectin is a giant linker protein which binds all the major of types of cytoskeleton, i.e. actin filaments, IFs and microtubules [292]. It can also form a complex with β3-intergin and vimentin [293]. Vimentin forms type III IFs, which are the most abundant kind in this family [294]. In summary, the 12 chosen candidates were either highly upregulated in all three β3-depletions (Atp5a1 and Gvin1), or upregulated in all three β3-depletions and possess proven links to EC biology (Naa15 and Tcp1), or upregulated in at least two β3-depletions with links to angiogenesis or EC biology (Col4a2, Slit3, Hspa12b, Cltc, Serpinh1, Nes, Plec and Vim) (**Table 3.3**).

We focused on the proteins upregulated in β3-depleted adhesomes, but we also made other notable discoveries, which we did not pursue at this time. Some of the proteins significantly downregulated in both the β3-HET and the β3-KO endothelial adhesome that we observed were A Disintegrin And Metalloproteinase 10 (Adam10), ADAM with thrombospondin motifs 1 (Adamts1), Adamts4 and tissue inhibitor of metalloproteinase inhibitor 3 (Timp3). Notable examples of proteins decreased in both the β3-HET and the cRGD-treated (downregulation trend) adhesions were radixin (Rdx), moesin (Msn) and the Guanine nucleotide-binding protein subunit beta-1 (GNB1). Proteins downregulated in the β3-KO and cRGD-treated (trend) adhesome included the melanoma cell adhesion molecule (MCAM) and Vasohibin-1 (Vash-1). Another notable result seen was that β4-integrin, VEGF receptor 1 (VEGFR1 / Flt1) and ezrin (Ezr) were significantly decreased in the β3-HET adhesome but remained unchanged in the other two models of depletion. Also, von Willebrand factor (vWF) was significantly down in the β3-HET background and up in the β3-KO one, whilst Thrombospodin 1 (Thbs1) exhibited the reverse trend.

Table 3.2 Proteins upregulated in more than one type of β3-depleted EC adhesomes, compared to the WT EC adhesome.

HET and KO	HET and cRGD		KO and cRGD	HET, KO and cRGD
Atp2a2	Actn1	Lmnb1	Abcf2	**Atp5a1**
Atp5a1	Actn4	Myadm	Actg1	Canx
Canx	Anxa6	Myh10	**Atp5a1**	Ctps1
Col4a2	Atp1a1	Myo1c	Canx	Eif3f
Ctps1	**Atp5a1**	Myo1d	Cars	Gsn
Eif3f	Atp5b	Naa15	Cct5	**Gvin1**
Gsn	Cand1	**Nes**	Cct6a	H2afv
Gvin1	Canx	Pdia6	Cct7	Hsp90ab1
H2afv	Capn2	Pdlim5	Cd55	Hspd1
Hsp90ab1	Cav1	Phb	Ctps1	**Naa15**
Hspa9	**Cltc**	Phb2	Ddx58	Psmd3
Hspd1	Col4a1	**Plec**	Dnaja1	Rnf213
Htra1	Copb1	Psmd3	Drg2	Sdpr
Iars	Ctps1	Ptrf	Ehd4	Slc25a3
Naa15	Cttn	Rars	Eif3e	**Tcp1**
Psmd3	Dars	Rnf213	Eif3f	
Rnf213	Dpysl3	Rpl12	Gsn	
Rpn2	Eef1b;Eef1b2	Rpn1	**Gvin1**	
Sdpr	Eef1d	Rps5	H2afv	
Slc25a3	Eef1g	Rtn4	Hsp90ab1	
Slit3	Eif3a	Sdpr	Hspd1	
Tagln2	Eif3c	Sec23a	Impdh2	
Tcp1	Eif3f	Slc25a3	Lbr	
	Eif3k	Sptan1	Mdh2	
	Eif3l	Sptbn1	**Naa15**	
	Eprs	**Tcp1**	Ncbp1	
	Fasn	Tinagl1	Paics	
	Flnc	Tpm4	Prr11	
	Gsn	Tuba1a;Tuba3a	Psmd3	
	Gvin1	Tuba1b;Tuba4a	Rnf213	
	H2afv	Tubb2a	Sdpr	
	Hist1h3b;1h3e; 2h3b	Tubb4b;Tubb4a	**Serpinh1**	
	Hsp90ab1	Tubb5	Slc25a3	
	Hspa12b	Tubb6	Snx9	
	Hspd1	Vdac2	Surf4	
	Kars	**Vim**	**Tcp1**	
	Kif5b	Vps35		
	Lamb1			

This table is a result of comparison of upregulated proteins shown in Table 3.1, Supp. Table 1 and 2. For the cRGD condition, proteins increased at least 1.1-fold (the first 292) in the cRGD vs DMSO sample were deemed upregulated. 12 chosen candidate genes taken forward for further analysis are highlighted and in bold. Adapted from Atkinson S.J. [277].

Table 3.3 Summary of the 12 chosen candidate genes.

	Gene name	Protein name	Function	Upregulated in
1	**Atp5a1**	ATP Synthase, subunit α	ATP synthesis	HET, KO and cRGD
2	**Gvin1**	Interferon-induced very large GTPase 1	Unknown	HET, KO and cRGD
3	**Naa15**	N-α-acetyltransferase 15	Acetyltransferase, implicated in vascular development [284]	HET, KO and cRGD
4	**Tcp1**	T-Complex 1	Actin and tubulin chaperone [285]	HET, KO and cRGD
5	**Col4a2**	Collagen type IV α 2	One of the six subunits of type IV collagen [295]	HET and KO
6	**Slit3**	Slit Homolog 3	Neurogenesis signalling, also implicated in angiogenesis [296]	HET and KO
7	**Hspa12b**	Heat Shock 70kD 12B	Predominantly-endothelial, specific stress response chaperone [297]	HET and cRGD
8	**Cltc**	Clathrin heavy chain 1	Endocytosis, shown to promote angiogenesis [298]	HET and cRGD
9	**Nes**	Nestin	Regulation of assembly and disassembly of intermediate filaments [299]	HET and cRGD
10	**Plec**	Plectin	Giant cytoskeletal linker [300]	HET and cRGD
11	**Vim**	Vimentin	Class III intermediate filaments [294]	HET and cRGD
12	**Serpinh1**	Serpin Family H Member 1	Collagen-specific chaperone, promotes angiogenesis [301]	KO and cRGD

3.3.3 Further Narrowing Candidates Using a Semi-high-throughput Approach

To further narrow the condensed list of twelve candidates, and cherry-pick the most interesting for further analysis, we took an experimental approach. As discussed in Section 3.3.1, using β3-HET ECs, as a model of β3-depletion, overcomes the potential complications associated with higher order changes seen in β3-KO ECs, keeping the experiments more directly relevant to β3 integrin. At the same time, cRGD-treatment was less effective at inducing detectable changes than genetic depletion, as we saw only one statistically significant change in the DMSO vs cRGD-treated adhesome comparison. Therefore, we performed angiogenesis-relevant assays in WT and β3-HET IMMLECs, post-transfection with siRNAs directed against the 12 candidate genes, to test their involvement in compensation which accompanies β3-depletion. Each time, one million cells were transfected with target-specific siRNA. Fourty-eight hours post transfection, cells were split between an adhesion (protocol in Section 2.5) and a scratch-wound migration assay (Section 2.6).

In WT cells siRNA-mediated silencing of Col4a2 impaired adhesion, while silencing Gvin1, Nes, Plec, Serpinh1, Slit3, Tcp1 and Vim siRNA enhanced adhesion (**Fig 3.2**). In β3-HET cells, siRNAs directed against Cltc, Col4a2, Hspa12b, Naa15, Nes, Plec and Vim impaired adhesion, while siRNAs directed against Atp5a1, Gvin1, Serpinh1, Slit3 and Tcp1 enhanced adhesion (**Fig 3.2**).

In WT cells, scratch wound migration was inhibited with siRNAs directed against Col4a2, Nes, Plec, Slit3, Tcp1 and Vim, and enhanced with siRNAs against Atp5a1 and Gvin1 (**Fig 3.3**). In β3-HET ECs, migration was inhibited when Hspa12b, Naa15, Nes, Plec, and Vim were targeted (**Fig 3.3**).

This work needs to be caveated with two technical notes: (1) both assays have only been performed with 1 biological repeat, so results were interpreted only as trends, rather than hard statistical significance; (2) at this stage, we did not test knockdown efficiency – thus, where no biological response was observed, we cannot rule out the possibility that the intended target was not silenced. Nevertheless, we were particularly intrigued by the response of cells to the silencing of intermediate filament (IF) proteins. Collective migration in monolayer was impaired both in WT and β3-HET ECs transfected with siRNAs against IF proteins (Nes, Plec, Vim) (**Fig 3.3**). Moreover, we observed a differential response between WT and β3-HET cells to IF silencing with respect to adhesion (**Fig 3.2**). Adhesion in WT cells was moderately enhanced, whilst in β3-HET cells it was impaired. This suggests that IFs play more of a role in adhesion when β3 levels are reduced, and therefore co-targeting these IF proteins alongside αVβ3 is a potential improvement on the current anti-angiogenic strategies.

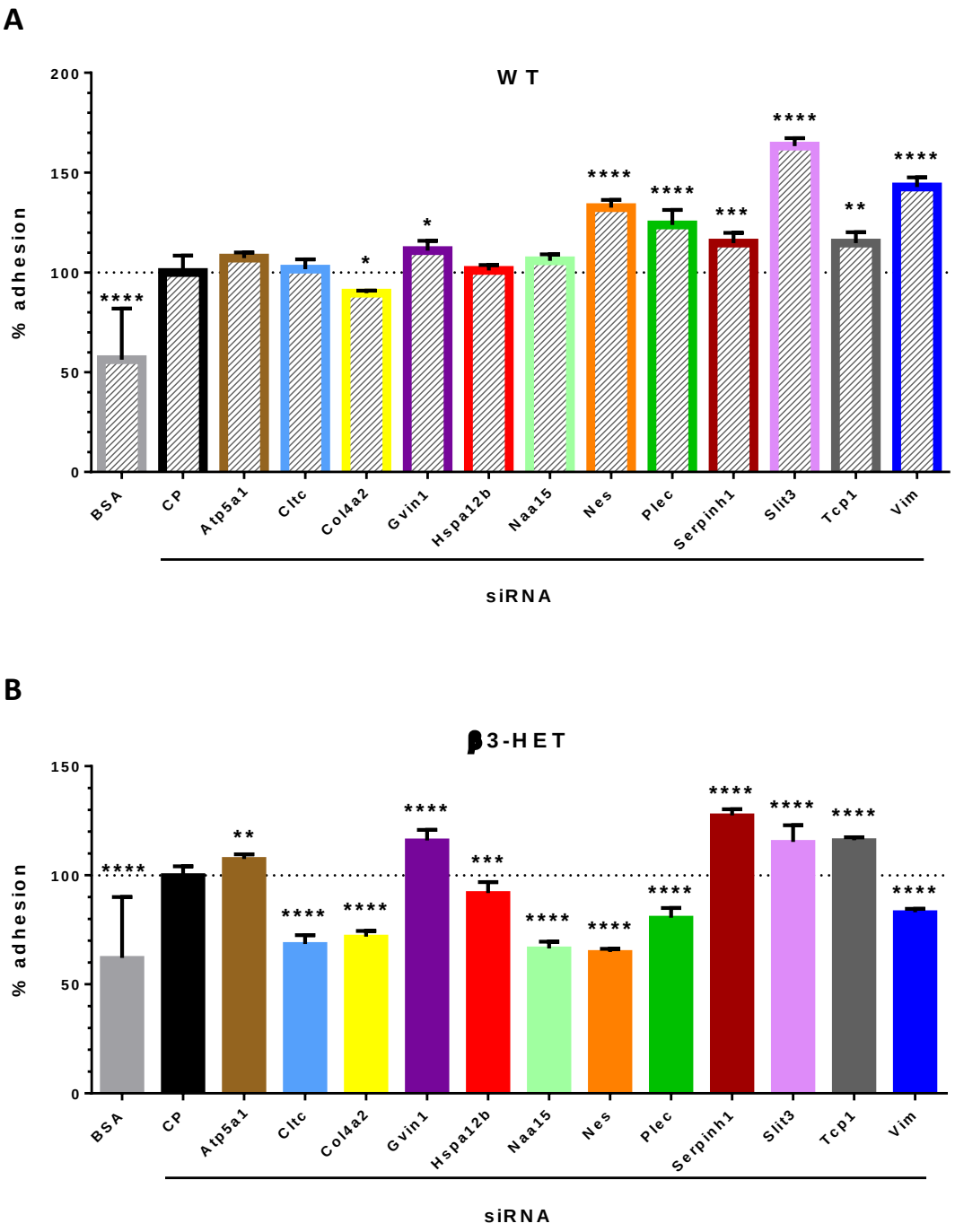

Figure 3.2 Adhesion assays of WT and β3-HET IMMLECs transfected with siRNA against candidate genes.

48 hrs post-transfection with siRNA against 12 chosen candidate genes, adhesion assay of (**A**) WT and (**B**) β3-HET ECs on FN was performed. Absorbance values were normalised to the CP (control pool of non-targeting siRNA) sample average. Therefore, bar charts represent % adhesion +SD of the control sample (4+ technical repeats). BSA only (no FN) control was included on the left.

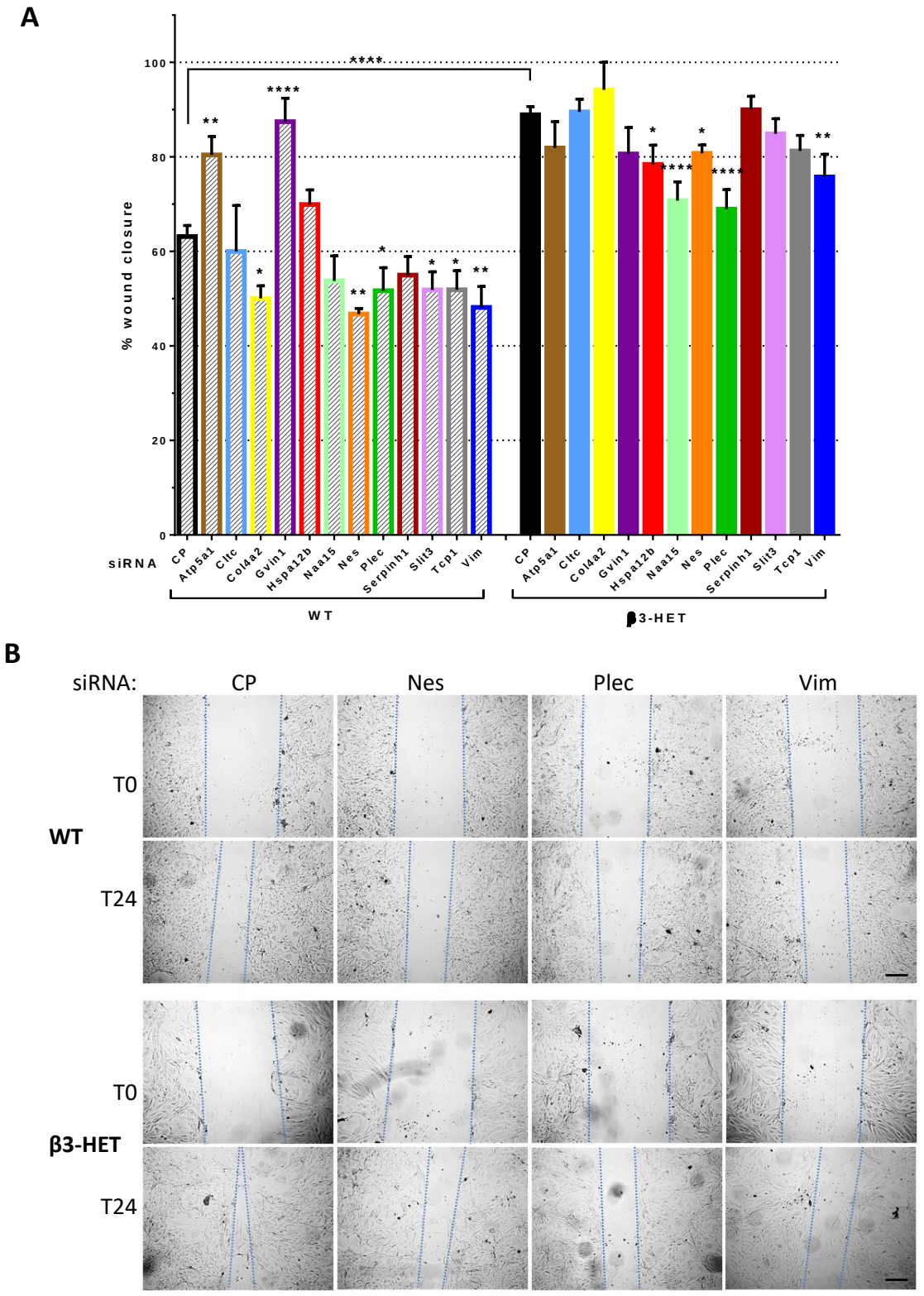

Figure 3.3 siRNA against IF proteins impairs directional migration in WT and β3-HET IMMLECs.

(**A**) 48 hrs post-transfection with siRNA against 12 chosen candidate genes, a 24-hr wound-closure migration assay on FN was performed on WT and β3-HET ECs. Bar chart represents % wound closure +SEM (6 technical repeats). * indicates P<0.05; ** P<0.01, *** P<0.001 and **** P<0.0001, as determined by an unpaired student's *t*-test. (**B**) Images corresponding to chosen conditions at T0 and T24 are shown. Scale bar = 200µm, CP – control pool of non-targeting siRNA.

3.3.4 Visualising Interactions of Intermediate Filament Proteins and Known Players of the Adhesome

We were interested whether the candidate genes that we have identified by mass spectrometry in the endothelial FAs, have been previously shown to be present there. One way to test this, is to check for interaction with known FA residents. Some of the well-studied ones, that are regarded as canonical FA proteins, are: β3-integrin (Itgb3), actin (Acta2), FAK (Ptk2), paxillin (Pxn), talin (Tln1), tensin (Tns1), vinculin (Vcl) and tyrosine-protein kinase Src. A list of 12 candidate proteins (**Table 3.3**) and the canonical FA residents mentioned above (described in more detail in Section 1.3.2) were analysed by the Search Tool for the Retrieval of Interacting Genes/Proteins (STRING). Interestingly, an interaction loop was identified between heat shock 12b (Hspa12b), T-complex 1 (Tcp1), ATP synthase α (Atp5a1), clathrin heavy chain 1 (Cltc) and tensin-1, which has been suggested to link the actin cytoskeleton to integrins thus enhancing pro-angiogenic signalling (**Figure 3.4 A**) [302]. Slit Homolog 3 (Slit3) was shown to interact with Src, a prominent proto-oncogene and tyrosine kinase shown to regulate angiogenesis and vascular permeability [303]. Another interaction chain – FAK - Col4a2 - Serpinh1 - Vim - Itgb3 – emerged from the network map. According to the STRING database, Gvin1, Naa15 and Nes had no known interactions within this pool of proteins.

Migration and adhesion data described in Section 3.3.3 guided us towards the IF proteins. The network maps in **Figure 3.4 A and B** illustrate known interactions of nestin, plectin and vimentin, but also other IF proteins: desmin (Des), syncoilin (Sync), synemin (Synm), lamin (Lmna) and Glial fibrillary acidic protein (Gfap); with the canonical FA players named above. The STRING database pointed out binding interactions of plectin with FA proteins, namely: actin, FAK (Ptk2), paxillin, vinculin, a putative interaction with talin and most interestingly, β3-integrin (**Figure 3.4 B**). No direct link was identified for nestin, although STRING suggested a link to the FAs via caspase-3, an apoptotic protease [304]. Gfap was shown to interact with Src, while desmin has links to actin and vinculin. Overall, the evidence for interactions observed between IF and FA proteins is sporadic, suggesting that further research on this subject is required.

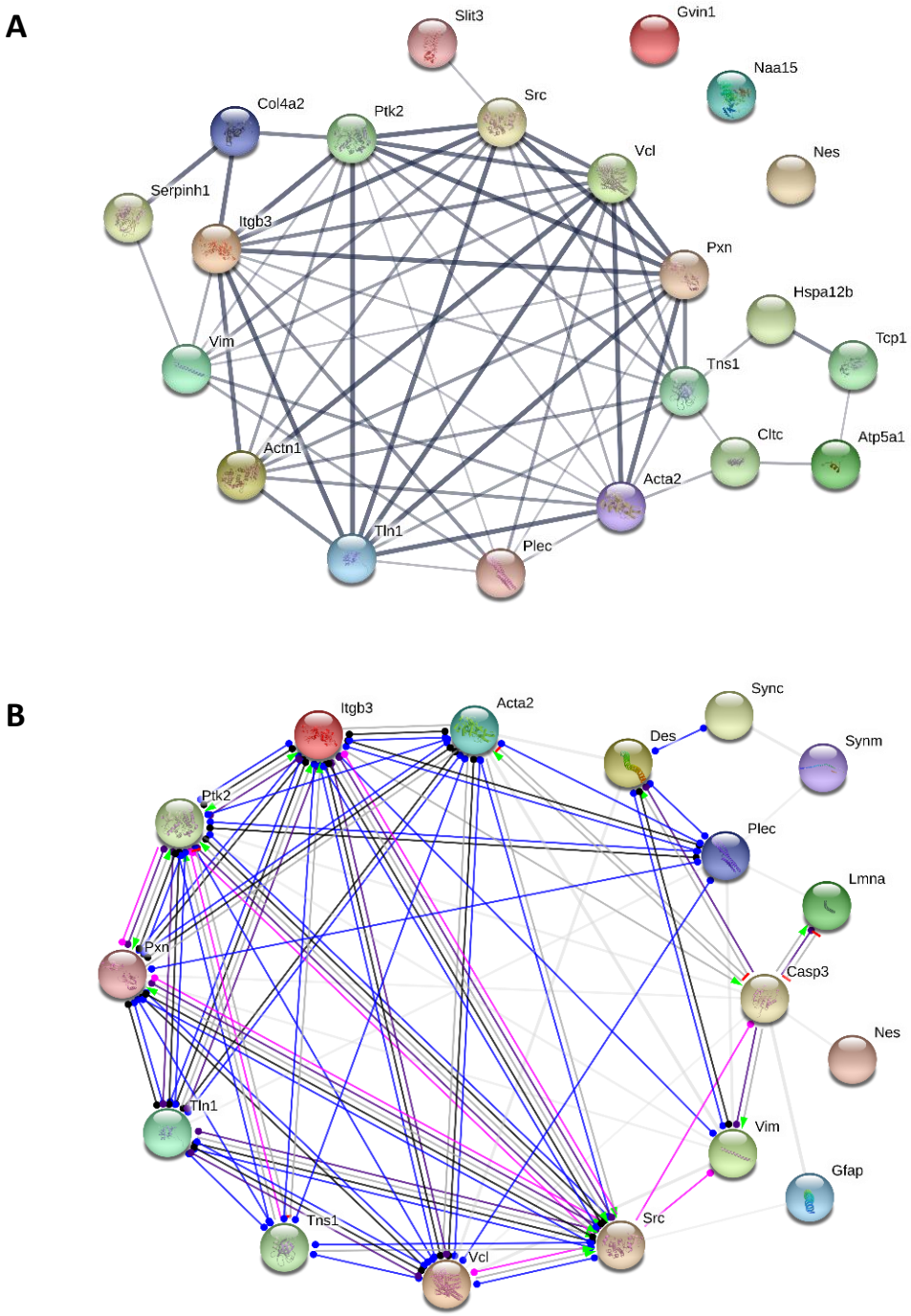

Figure 3.4 Visualisation of protein interaction networks of candidate genes using STRING.

(**A**) The canonical members of FAs: Itgb3 (β3-integrin), Ptk2 (FAK), Src, Vcl, Pxn, Tns1, Acta2, Actn2, Tln1; were tested for interaction with the 12 candidate genes that were seen upregulated in the β3-integrin adhesome. The width of the line correlates with confidence of interaction according to STRING mouse database. No interactions were identified for Gvin1, Naa15 and Nes in this pool of proteins. (**B**) IF proteins, namely: Nes, Plec, Vim, Des, GFAP, Lmna, Synm and Sync1 were tested for interaction with FA players. Casp3 was added, as it was identified by STRING as a link for Nes to this network. Blue link – binding, pink – post-translational modification, black – reaction and grey – unspecified. Green arrow indicates positive interaction, red line – negative and beaded end – unspecified. There is no indication here whether the interactions are direct or indirect. Diagrams were generated using STRING's built-in online tool with the default parameters, i.e. medium confidence setting (0.4) and using all available active interaction sources.

3.4 Discussion

In this chapter, we directed the most focus towards the changes observed in the endothelial adhesome induced by the genetic depletion of β3-integrin in the heterozygous background. Atkinson S. J. dissected both β3-HET and β3-KO endothelial adhesome in his thesis but eluded to a few problems which suggest a direct comparison between the two datasets should be interpreted with caution [277]. Firstly, the β3-HET and the β3-KO adhesome samples were collected on different days which could produce variations in the biological repeats leading to possible false discoveries. Many unexpected differences were observed by Atkinson between β3-HET and the β3-KO. Neither nestin, plectin nor vimentin were upregulated in the β3-KO adhesome, although the latter two were at least detected. It is also important to add, β3-KO studies have previously been criticised as not being physiologically relevant, thus not mimicking a treatment setting where depletion/inhibition of β3-integrin would be incomplete [180]. Nevertheless, β3-KO cells remain a useful tool. The power of our observations may be increased, if their phenotype is in agreement with that of β3-HET cells.

Surprisingly, out of the 912 proteins detected in the DMSO vs cRGD-treated adhesome comparison, only one protein (Ncbp1) significantly changed in abundance. This suggests that RGD-mimetics may not have a strong effect on the β3-dependent adhesome on fibronectin. However, there were some substantial fold changes in abundance of the detected proteins in this comparison, which were approaching significance, and these were used here for guidance in narrowing down candidates.

Here, we first identified 104 proteins upregulated in two or all three endothelial β3-depleted adhesomes. Then, guided by mass spectrometry data, GO and KEGG annotations, as well as publication searches, we identified 12 candidates that we felt could be the most promising β3-integrin partners for dual targeting. We tested them in that context, in the 90-min adhesion assay and the scratch-wound migration assay. We observed that targeting nestin, plectin and vimentin with siRNA in ECs inhibited both processes alongside β3-integrin depletion. Thus, they became the targets that we will pursue further. It is interesting and reassuring that they all belong to the same protein family – intermediate filaments. This class of proteins will be discussed in detail in the next chapter. Briefly, due to their roles as cytoskeletal proteins interacting with FAs and β3-integrin, plectin and vimentin have previously been implicated a role in angiogenesis [293], [305], [306]. In comparison, nestin is an emerging player in angiogenesis [291].

Other candidates that stood out were Col4a2 and Naa15. siRNA against the former inhibited migration in the WT but not in the β3-HET cells, as well as adhesion in both cell types. Collagens

are components of the basement membrane and integrin ligands [307]. They are present in almost all basement membranes and a plethora of vascular defects are associated with Col4a2 mutations [308]. Canstatin, an inhibitor based on a domain within Col4a2, binds αVβ3 and αVβ5 integrins and inhibits angiogenesis *in vitro* and *in vivo* [286]. A similar peptide, endostatin, based on collagen type XVIII, has been tested in clinical trials. At phase II, in patients with neuroendocrine tumours it did not result in significant tumour regression [309]. However, in stage III clinical trials, for patients with advanced Non-Small-Cell Lung Carcinoma, in combination with conventional chemotherapy it offered some improvement in response rate and progression time over chemotherapy alone [310]. It would be interesting to know if combining Canstatin and chemotherapy, and perhaps Cilengitide, could lead to better outcomes in patients. Interestingly, siRNA against Naa15 impaired adhesion and migration in the β3-HET but not in the WT cells. Naa15 carries out post-translational modifications of other proteins as part of a complex at the ribosomes [311]. It is surprising to see it in the adhesome of ECs, although it has been reported at non-ribosomal sites, as a potential regulator of actin polymerisation [312]. Also, it has been associated with blood vessel development and EC permeability [284], [313].

We also tested our 12 candidates for interaction with known endothelial proteins that reside in the FAs, as another way of testing their potential involvement in EC biology (**Fig. 3.4**). We saw numerous interactions of Plec and Vim with the canonical members of the EC adhesome. This increased our confidence in the IF proteins as targets for further testing in this study. Casp3 provides a link for Nes to the rest of the network in **Fig. 3.4 B**, an indirect link to β3-integrin and Vim. The evidence for the Nes-Casp3 interaction comes from a study of brain tissue injury, therefore it is likely not relevant here [314].

Cells respond to both internal and external forces, with FAs playing a central role of the mechanotransduction hub [315], [316]. This hub contains and links up to the members of the signalling network of the cell, leading to a diverse range of downstream actions [174], [317], [318]. Thus, the composition and regulation of FAs modulates a very wide range of cellular processes, i.e. metabolism, proliferation, migration, cell cycle regulation and cell division. The meta-adhesome on FN, which includes 2400+ proteins, has been defined using data from multiple cell types, mostly fibroblasts, and refined to identify the 'consensus adhesome' that consists 60 proteins [319]. This includes a number of confirmed complexes of integrin, actin, signalling and adaptor proteins, for example αVβ3 integrin, talin, paxillin and FAK [320], [321]. Neither Nes, Plec or Vim are considered as members of the 'consensus adhesome', but they have all been detected in multiple studies contributing to the meta-adhesome [319]. Morever, Plec has been shown to be a link between Vim and β3 integrin in FAs [293], [322].

As reviewed by Humphries *et al.*, FA enrichments in the adhesome studies to date comprise of various types of FAs from thousands of cells [323]. Efforts are made to be able to isolate uniform FA preparations, such as using a specific adhesion matrix, uniform cell culture conditions and length of adhesion, as we have done [323]. In the future, improvements in sensitivity of mass spectrometry and high-throughput analysis are likely to unravel adhesome composition and regulation further [323]. Also, novel techniques for researching FAs, such as the proximity-dependent biotinylation technique (BioID) hold promise for improved understanding of the adhesome [324]. FAs are dynamic structures, many proteins transiently interact with these complexes [322]. Also, the canonical FA players are found elsewhere in the cell, as a result of events, such as internalisation and recycling [325], [326]. The design of the protocol by Schiller *et al*. ensured capture of transient interactions, as it included the FA crosslinking step [231]. It also allows one to focus on what is present at the FAs specifically, as the non-crosslinked material was lysed and removed. We have adopted this protocol for ECs and, for the first time, defined the mature mouse EC adhesome on FN consisting of 1064 proteins [232].

We focused on the proteins that were upregulated in the β3-integrin-depleted EC adhesome. The rationale for this approach was as follows. One can confirm a role of an upregulated protein by siRNA knockdown or using an inhibitor. In this setting, we looked for inhibition of angiogenesis-relevant processes, i.e. impaired adhesion or migration. In addition, this already takes us one step ahead, as it stages a double-targeting treatment situation, if we carry out the KD or inhibition experiments in WT and β3-integrin-depleted cell models. A downregulated protein is more problematic in that sense. KD only has the potential to reproduce what we saw in the mass spectrometry, while overexpression (to stage a treatment situation, counter-acting the potential escape mechanism) is likely a more complex undertaking, too complex for the initial stages of narrowing candidates. Focusing only on the genes/proteins upregulated in the adhesome is limiting from the start. However, most cellular functions are not carried out by a single protein. They are part of a bigger complex or network of proteins. Indeed, this phenomenon is embedded in the very core of this project. When β3-integrin is targeted in the long-term, other players carry out its function in angiogenesis and tumour progression. Although, only looking at the upregulated proteins might lead to omission of some of the candidates of interest, which were downregulated, one can assume that their partners, agonists or antagonists, from the same complex or network, will be picked up by analysing 'the other half'.

Indeed, we have made several intriguing discoveries that we chose not to follow up experimentally at this time. Three members of the metalloproteinase family – Adam10, Adamts1, Adamts4 and Timp3 were seen downregulated in the β3-depleted EC adhesome.

Adam's are family of cell surface glycoproteins with metalloprotease potential [327]. In addition, their disintegrin-like domains are ligands for various integrins [328]. Adam10 cleaves ectodomains of proteins on the cell surface, which can have various consequences. It activates cell surface receptors, such as Notch-1 a driver of tumour and embryonic angiogenesis and Tie-1, necessary for developmental angiogenesis [329], [330]. On the other hand, it cleaves ephrins to release fragments which inhibit tumour angiogenesis in mice [331]. Adamts proteins possess the thrombospondin motif in addition to the disintegrin and metalloproteinase domains that Adam's have. Adamts1 inhibits angiogenesis *in vitro* and *in vivo* as result of binding and sequestering VEGF [332], [333]. Its family member, Adamts4 can be both pro- and anti-angiogenic [334]. Its upregulation in numerous cancers suggest its role in tumour progression by cleavage of extracellular proteoglycans to make way for the expanding tumour and blood vessels [335], [336]. However, it can also sequester VEGF and thus inhibit VEGFR2 signalling [337]. Timp3 regulates ECM composition by inhibiting matrix metalloproteinases, and thus influences cell migration, invasion and angiogenesis [338]. Interestingly, it inhibits a wide variety of Adam's and Adamts' including Adam10, Adamts1 and Adamts4 [339]–[341]. It suppresses tumour growth because of its potent pro-angiostatic mode of action [342]. It has also been suggested that it inhibits angiogenesis more directly, by preventing VEGF from binding VEGFR2 [343]. It is interesting to see a downregulation in a group of proteins that carry out similar functions and all have been previously linked to angiogenesis.

In addition, we noticed a decrease in the abundance of ezrin, moesin and radixin in the β3-depleted EC adhesome. These three proteins constitute the whole ERM family of paralogs. They provide the link between the cytoskeleton and the plasma membrane and thus play a role in adhesion and motility [344]. They do this via the FERM domain, also present in talin, a prominent member of the focal adhesions and neurofibromatosis 2 (NF2/merlin) a known tumour suppressor [345].

We also noticed Gnb1 was decreased in the β3-depleted adhesome. Downregulation of human Gnb1, as reported by a study in 500+ patients, correlates with worsened prognosis of clear-cell renal cell carcinoma [346]. The same study suggested an association of Gnb1 and the VEGF signalling pathway.

Two of EC markers, MCAM and Vash-1 were downregulated in the β3-KO and cRGD-treated adhesions. Research shows that MCAM is a pro-angiogenic co-receptor of VEGFR2 [347]. On the other hand, it has also been shown to inhibit breast cancer progression [348]. It would be interesting to investigate how it affects angiogenesis in further detail. Endothelial Vash-1 is an agonist of tumour angiogenesis. In a tumour growth experiment, Vash-1 KO mice exhibited tumour angiogenesis inhibition compared to the WT controls [349]. Further experiments in the

same study showed that supplying high levels of Vash-1 alongside chemotherapy (cisplatin) improved the outcome due to improved drug delivery, because of improved vessel maturation and inhibition of sprouting angiogenesis. It is therefore interesting to see it downregulated in our β3-depletion models.

It was surprising to see Integrin β4 and VEGFR1 (Flt1) also reduced, although only in the β3-HET adhesome. β4 normally partners with integrin α6 as a laminin receptor. Its signalling has been linked to pathological angiogenesis [350]. VEGFR1, like VEGFR2, is a tyrosine kinase that binds VEGF is a capable of proliferative signalling, but it is much weaker in doing so [100]. It has been suggested that it can be a negative regulator of angiogenesis by sequestering VEGF [351].

Perhaps the most intriguing findings from the mass spectrometry analysis are the changes we saw in vWF and Thbs1. The former was down in the β3-HET and up in the β3-KO adhesome, compared to the WT. vWF is a blood plasma clotting factor secreted by endothelium and megakaryocytes, but fraction of it is stored in ECs in the form of Weibel-Palade bodies [352], [353]. Moreover, vWF is a ligand of integrin αVβ3 [354]. ECs deficient in vWF had increased VEGFR2-dependent proliferation and increased release of angiopoietin-2, suggesting an inhibitory role of vWF in angiogenesis [354]. Interestingly, the same study found integrin αVβ3 downregulated in those cells. Thbs1 was up in the β3-HET and down in the β3-KO adhesome. Thbs1 inhibits neovascularization by sequestering VEGF and thus inhibiting VEGFR2 signalling [355], [356]. It was surprising to see such a potent inhibitor of angiogenesis downregulated in the adhesome of the β3-HET cells, our *in vitro* model of upregulated angiogenesis. Abundance of vWF and Thbs1 was altered in both directions depending on the β3 genotype. This highlights the difference between the β3-HET and the β3-KO cells. It served as a reminder that the compensatory changes due to total loss of β3-integrin may be different to those that we see in the partial depletion model (β3-HET) [277]. Explanation of the differential presence of vWF and Thbs1 in the β3-HET and the β3-KO remains to be determined.

Another limitation to our approach of targeting the candidate genes (or proteins) was with the siRNA knockdown, which at this point, had not been confirmed by means of RNA (qRT-PCR) or protein (WB) analysis. Therefore, it is possible that no migratory or adhesion phenotype was observed following siRNA transfection against some of the targets due to a lack of successful targeting by the siRNA pool used. In our multi-gene approach, it was more efficient to follow the phenotype rather than start with a confirmed knockdown and then investigate the phenotype.

The obvious improvement is that the experimental work could be corroborated by increasing the number of migration and adhesion assays repeats to a statistically significant degree. Overall, we trust the data presented in this chapter could be utilized to indicate the way forward. From here onwards, our efforts focused on investigating nestin, plectin and vimentin and their relationship with αVβ3 integrin in ECs in the context of angiogenesis.

4 Targeting the Adhesome *In Vitro*

4.1 Introduction

4.1.1 General Comments

Targeting β3 integrin as an anti-angiogenic strategy was initially promising but encountered a problem. However, there exists an escape when this molecule is targeted long-term. In the previous chapter, we identified three intermediate filament (IF) proteins that are upregulated in β3-depleted endothelial focal adhesions (FAs) (Section 3.3), and therefore may be a part of this mechanism of escape, namely: nestin (Nes), plectin (Plec) and vimentin (Vim). More specifically, we revealed by mass spectrometry an increase in the abundance of Plec, Nes and Vim in both β3-HET and cRGD-treated EC adhesomes. In the β3-KO EC adhesome, there was no upregulation of Vim, Nes or Plec. The potential reasons for these differences were discussed in detail in the previous chapter. β3-KO ECs differ from the β3-HET and cRGD-treated ECs in that 'higher order' changes are expected to have occurred in them, due to complete absence of β3-integrin, rather than a depletion, where changes are arguably more closely β3-dependent [A], [275], [357]. Here, we have chosen to focus on β3-HET ECs. The reasons for doing so are summarised below, at the beginning of the Results section.

We hypothesised that Nes, Plec and Vim may be upregulated in β3-depleted adhesomes as part of the mechanism of pro-angiogenic compensation observed in tumour vasculature with long-term depletion of β3. Furthermore, we propose that these may be good candidates for a dual-targeted anti-angiogenic strategy, in combination with β3-integrin inhibition. This chapter describes the efforts to conduct an *in vitro* experimental assessment of this proposal. In the first part we describe experiments conducted using siRNA knockdown of IF proteins in WT and β3-HET IMMLECs. The second part discusses experiments in which we investigated the effect of Withaferin A, an inhibitor of Vim, in WT and β3-depleted ECs. We begin with an overview of IFs and their roles in ECs and angiogenesis.

4.1.2 Intermediate Filament Types and Their Roles

The cytoskeleton of animal cells is made up of three major types of networks: microtubules (MTs), actin-microfilaments (MFs) and intermediate filaments (IFs). The latter, as the name suggests, are of intermediate size (10-12 nm), narrower than MTs (25 nm), but wider than MFs (5-8 nm) [358], [359]. MFs and MTs tend to break more readily than IFs under shear stress [360]. The IF structure is more irregular and adjusts in response to mechanical impact. Their monomers possess a long, central α-helical domain (coil) (**Fig. 4.1**) and assemble into dimers by co-translation [361]. The coil at the core of the filaments and irregular nature of chemical bonds between the dimers ensure viscoelastic properties, compared to a more defined and organised structure of MFs and MTs [359]. This elasticity points to the role of IFs in protecting the cell against stress and strain. There are 65 functional IF genes encoding protein monomers, which assemble into filaments [362]. Based on the building blocks and the roles, IFs are divided into 6 major types. In humans, the majority of IF genes (54) encode keratins, the structural components of hair, nails and outer layer of human skin that arrange into type I and type II IFs [363]. The monomers of type III IFs, found across multiple cell types, are: peripherin, syncoilin, desmin, glial fibrillary acidic protein (GFAP) and the most abundant – vimentin (Vim) [364], [365]. Type IV IFs include the muscular synemin-based filaments and a number of neuro-filaments [366], [367]. Type V are the structural filaments of the cell nucleus and they are made up of lamin monomers [10]. Finally, type VI IFs (related to type IV) are based on nestin (Nes), normally expressed in nerve cells [368]. Other proteins in the IF family include phakinin and filensin, which are expressed exclusively in the eye lens and form beaded-type filaments, instead of the classical-type IFs [369]. Also, several IF-associated proteins (IFAPs) exist. A prominent member of this group is plectin (Plec), initially identified as a general, giant cytoplasmic crosslinker of IFs [370]. Our interest was drawn towards Vim (type III), Nes (type VI) and Plec (IFAP), since we observed that they were upregulated in the β3-depleted endothelial FAs (Section 3.3).

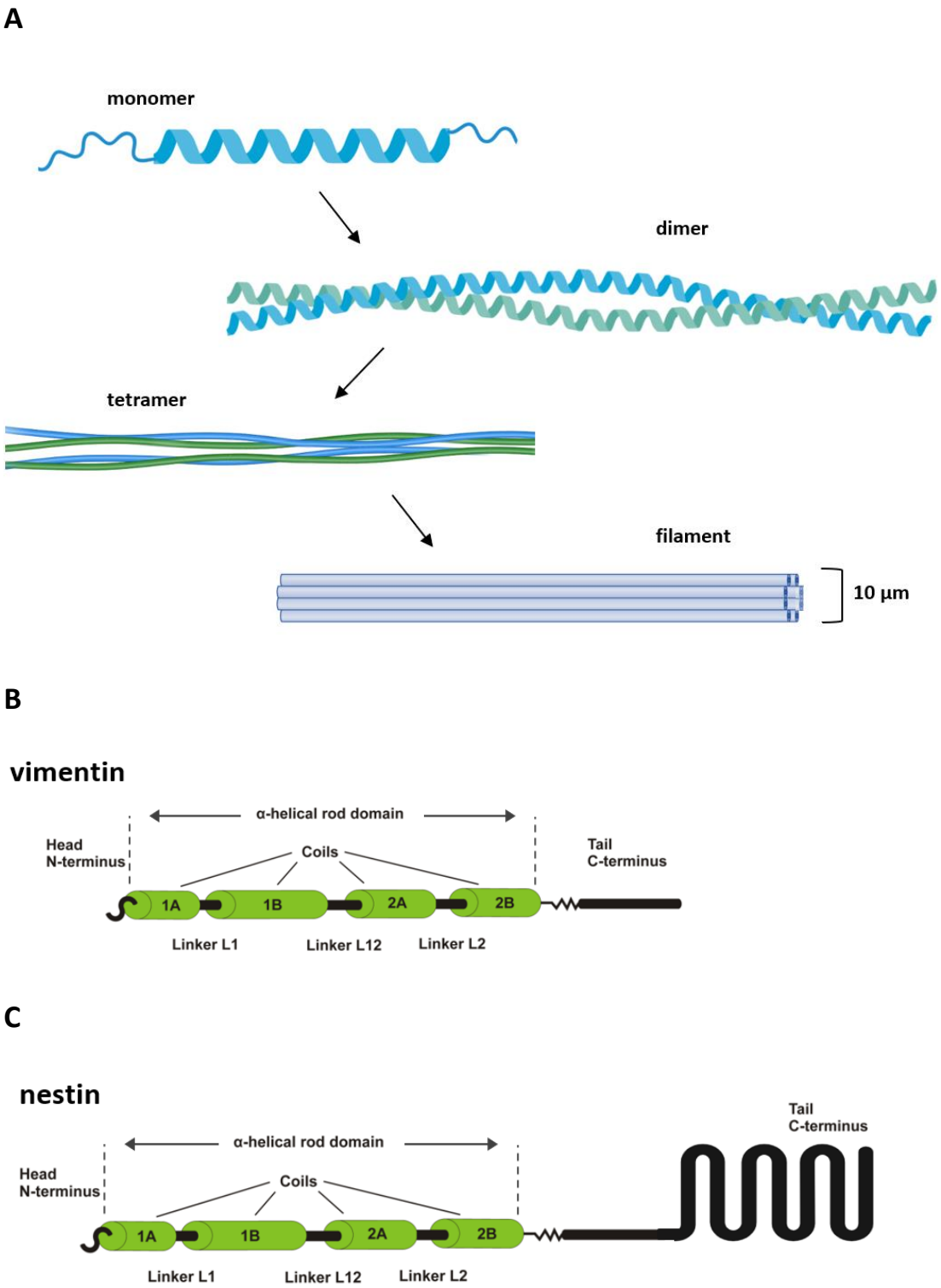

Figure 4.1 Intermediate filament structure.

(**A**) Intermediate filament monomers polymerise into a chain, pair up to form dimers, tetramers and are finally arranged into a 10-µm-wide filament. Summary of the structure of the (**B**) vimentin and the (**C**) nestin monomer. Figure adapted from Herrmann *et al*. (2007), Svachova *et al*. (2013) and Michalczyk and Ziman (2005), and generated using BioRender.com [299], [371], [372].

Type III IFs made up of Vim can be found in a variety of cell types including leukocytes, fibroblasts and ECs. It is the most widely distributed of all the IF proteins and a major IF type in ECs [373]. Vim monomers have the typical IF protein structure, i.e. a central α-helix coil domain and non-helical head and tail domains (**Fig. 4.1 B**) [374]. They arrange into dimers, which then assemble into tetramers, filaments (**Fig. 4.1 A**) and finally a network that spans the entire cell cytoplasm [358]. This network of Vim plays the classical IF type role of protecting cells from stress and strain, as well as the positioning of organelles inside the cell [375], [376]. Vim-IF cleavage amplifies pro-apoptotic signalling which suggests an important role in cell biology [377]. Surprisingly, Vim-KO mice develop into adulthood and breed normally, without exhibiting any drastic phenotype, except an impairment in wound healing [305]. Vim-KO cells have abnormalities in their MF and MT networks, which demonstrates that Vim interacts and acts together with actin and tubulin [375]. Together, all the three types of cytoskeleton regulate cell structure, shape and movement. Vim is a marker of the epithelial (settled, tightly adhered) to mesenchymal (migratory) transition (EMT) in development [378]. Also, Vim tends to be upregulated in migratory and invasive cancer cells, and for this reason it is used in the laboratory as a marker of metastasis [379]–[381]. We were interested in Vim in the context of ECs and FAs. The classical FA is positioned at the end of an actin MF, but FAs can also to be located at the sites of MT polymerization [220], [221]. Interestingly, the Vim-IF cytoskeleton also associates with integrins in the FAs [222], [382]. This interaction may be mediated by Plec, or direct, with the N-terminal head domain of Vim binding the cytoplasmic tail of β3-integrin [222], [383], [384]. Moreover, Tyr747 and Tyr759 within the tail of β3-integrin are essential for creating the link between Vim-IFs and FAs [383]. In β3-Y747F and β3-Y759F mutant CHO cells, Vim collapses around the nucleus and adhesion strength of the cells is compromised. Vim head fragment, which competes with Vim-IFs for binding to β3-integrin in the FAs led to reduced cancer cell migration and invasiveness in mice [384]. The metastatic potential of the triple-negative model of breast cancer in mice was significantly reduced, using 4T1 cells expressing the Vim head fragment. This is an exciting finding. It suggests that targeting the integrin-Vim interaction is a potential therapeutic approach against cell-adhesion-relevant disorders, such as pathological angiogenesis and cancer. In ECs, an association between Vim and αVβ3-integrin in the FAs was first observed in cells cultured on laminin [222]. It was suggested that this interaction was most likely mediated by Plec. Since then, it has been demonstrated that the recruitment of Vim-IFs to bind β3-integrin in the FAs requires Plec, and is a MT (kinesin) dependent process [383]. ECs under shear stress (subjected to flow) recruit an increased number of Vim-IFs to β3-integrin-FAs, which stabilises them for greater adhesion strength, needed to remain attached [385]. Vim knockdown ECs under flow conditions have smaller and less stable FAs, and as a consequence, their adhesion is impaired [385]. These findings demonstrate the importance of the IF-FA

interactions in cell-matrix adhesion strength, more specifically the interaction of Vim and β3-integrin; and highlight this interaction as a target in anti-angiogenic strategies.

The Nes monomer resembles Vim, as it also possesses a similar α-helical rod domain near the N-terminus, but in addition contains a very long C-terminal tail (**Fig. 4.1 C**) R. Nes homodimers and homotetramers have been observed, however they do not assemble into IF structures *in vitro* [386]. Instead, Nes co-assembles with a range of IF proteins, but preferentially with Vim (type III) or internexin (type IV) to form heterodimers, which constitute type VI IFs [387], [388]. Nes' role was initially implicated in the development of the central nervous system [387], [389]. Nes KO mice show embryonic lethality due to severe anomalies in the development of the neural tube [390]. In the adult, Nes expression appears to be restricted to defined locations or sites of injury [391]–[393]. Nes has a role in remodelling of IF network structure and correlates with proliferation and cell migration [391], [394]. Recently, Nes has been reported to be expressed in proliferating angiogenic vasculature, including that within tumours (glioma, hemangioblastoma, adenocarcinoma), whereas its expression in mature human ECs is sporadic [395]–[397]. Indeed, smaller, proliferating blood vessels within HCT-15 human colorectal tumours implanted into nude mice express Nes, whereas larger vessels do not [396]. Endothelial Nes has not been well studied beyond the observations of vascular expression. However, some of the cancer research findings provide information relevant to EC biology. One cancer study reported, that much like Vim, Nes can also be the driver of invasion and metastasis [398], [399]. On the other hand, it has been shown that Nes-depleted prostate cancer cells are more invasive due to FAK activation, increased α5-integrin clustering, regulation P-FAK and altered FA turnover [400]. The classical FA is positioned at the end of an actin MF [220]. However synemin, structurally similar to Nes, has been shown to bind two of the classical members of FAs (alpha-actinin and vinculin) [401]. Overall, Nes has become an emerging player in angiogenesis and a novel marker of neovasculature in the light of recent findings. Morever, Nes may be a promising target in the clinic, as a potential driver of proliferative and invasive phenotype, whilst its expression in the adult organism is limited to the sites of injury and regeneration.

Plec is a very large (500 kDa) protein, consisting of an actin binding site, plakin domain, rod domain and six plecin repear domains (**Fig. 4.2 A**) [402]. It is potentially the most versatile cytolinker, often classified as an IFAP (**Fig. 4.2 B**) [370]. Plec KO in mice causes blistering of the skin, heart and skeletal muscle defects, and death within the first few days after birth [403]. This demonstrates that it is required for structural reinforcement in cells and tissue under mechanical stress, which is often the role of IF proteins. As a cytolinker protein, Plec has a variety of interaction partners. This includes all three major types of cytoskeleton: IFs, MTs and MFs, as well as FA players: vinculin, β4- and β3-integrin (**Fig. 4.2 B**) [293], [404]–[406]. In ECs, this protein plays a role in connecting Vim-IFs and the laminin-binding α6β4-integrin [404], [406], [407]. Seifert *et al*. observed that Plec colocalised with actin stress fibres, vinculin and Vim in the FAs of rat fibroblasts and glioma cells [408]. Its interaction with Vim appears to be direct [409]. Moreover, it is required for the recruitment of Vim-IFs to FAs in a kinase- and MT-dependent manner, but not to maintain this link [383]. The same study also demonstrated that the cytoplasmic tail of β3-integrin is on the other side of this interaction, but it remains to be determined whether it is direct. Others have showed that Plec has a role in vascular integrity, as a link between Vim and Actin, needed for normal function of FAs and tight junctions [410]. Interestingly, Plec was suggested as a novel marker of pancreatic cancer [409], [411].

A

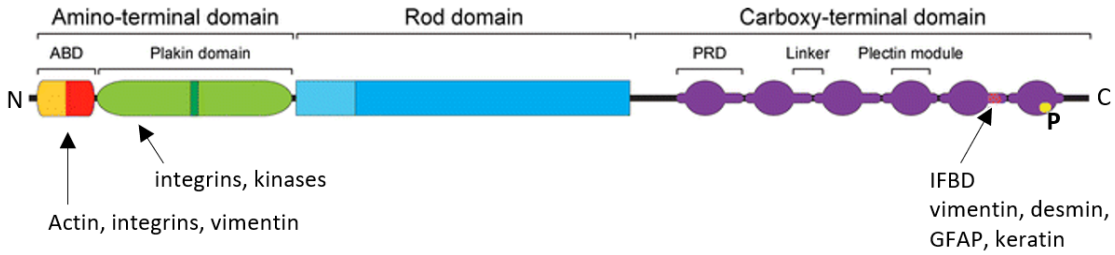

B

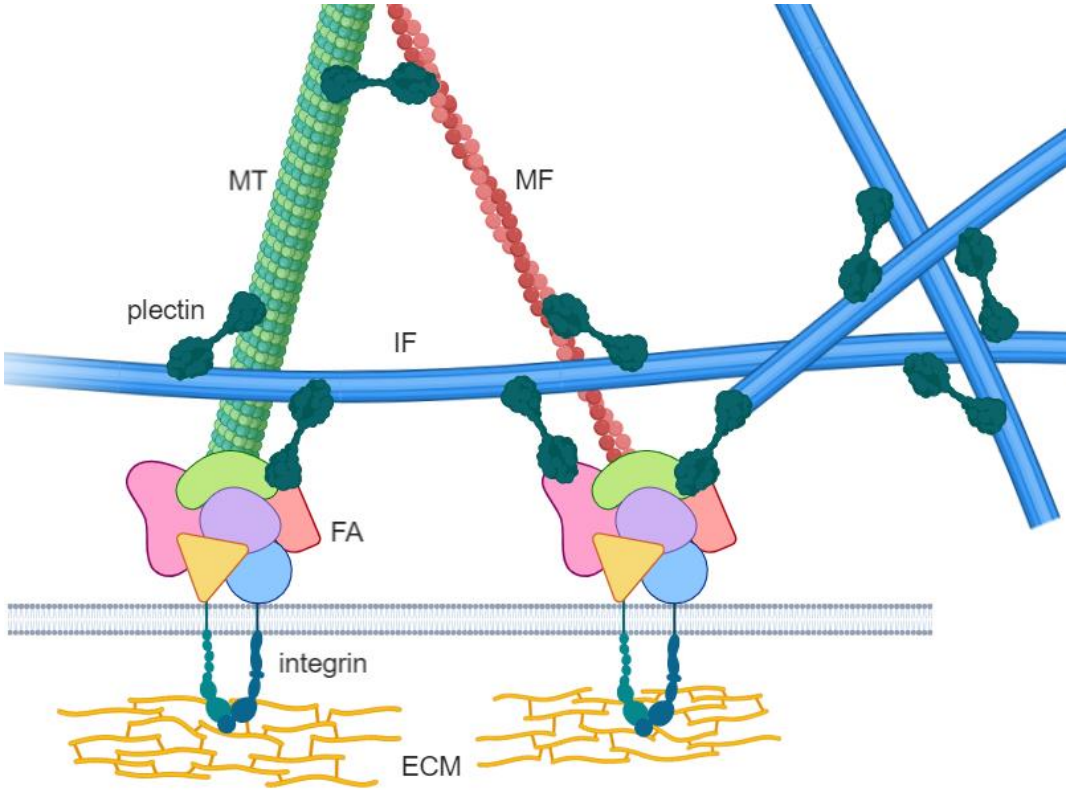

Figure 4.2 Plectin is versatile a cytolinker.

(**A**) Summary of plectin protein structure. ABD – actin binding site, IFBD – intermediate filament binding site, P – phosphorylation site, PRD – plectin repeat domain. (**B**) Plectin can provide a physical link between microtubules (MT), actin microfilaments (MF), intermediate filaments (IF) and focal adhesions (FA). ECM – extra-cellular matrix. Adapted from Winter and Wiche (2013) and Fuchs and Karakesisoglou (2001), and generated using BioRender.com [402], [412].

4.1.3 Withaferin A, an Inhibitor of Vimentin

Withaferin A (WFA) is one of 50+ chemicals identified in the extract of a medicinal plant *Withania somnifera* (also called ashwagandha or winter cherry) [413]. WFA is a steroidal lactone belonging to the withanolide family of compounds. The plant extract has been used in traditional Indian (ayurvedic) medicine for centuries to prevent and treat a wide range of conditions including stress, anxiety, inflammation, autoimmunity, cancer and aging [414]. Within the last two decades, WFA has been of interest to many research groups in context of diabetes, arthritis, cancer and angiogenesis [415]–[419]. Sub-cytotoxic levels of WFA showed promising anti-cancer effects in aggressive breast cancer cell lines [420]. Also, WFA was suggested as a preventative measure against mammary cancer due to its ability to suppress breast cancer stem cells [421]. Moreover, it was suggested as a potential drug for managing chronic inflammation in cystic fibrosis [416]. The anti-inflammatory and anti-tumour growth activity of WFA comes from the inhibition of NF-κB activation [417], [422]. NF-κB is a rapidly-acting transcription factor and known inducer of effectors in cell proliferation and cell survival [423], [424]. When de-coupled from its partner and inhibitor IκBα, as a result of IκBα phosphorylation or ubiquitination, it is activated and translocated into the nucleus, to regulate gene expression [425], [426]. One study proposes that WFA treatment interferes with the ubiquitin-mediated proteasome pathway to achieve NF-κB inhibition [417]. Another study proposes a different mechanism involving hyperphosphorylation of IKKB [422]. This prevents the phosphorylation of IκBα, which remains coupled to NF-κB, thus preventing NF-κB activation. However, the aspect of WFA which received the most interest from researchers is that it disrupts the Vim filament network [427]–[429].

It was demonstrated that WFA binds Vim at the cysteine 328 residue, which is normally the site of a disulphide bridge between two Vim dimers [428]. In this scenario, a WFA molecule physically prevents Vim filament cross-linking, thus disrupting the Vim network. A recent study has revisited this proposal for WFA's mechanism of action with respect to Vim. It showed that Vim lacking cysteine 328, not only assembles into networks but also responds to WFA as normal, suggesting that further investigation is required to determine putative (or other) WFA binding sites within the structure of Vim [427]. There is evidence that numerous kinases, including Akt, Cdk1 and PKA, phosphorylate one or more of 40+ Vim residues, which may regulate Vim-IF organisation [430]–[432]. Also, it has been shown that, through an unknown mechanism, WFA leads to phosphorylation of serine-38 of Vim, a target site for many kinases [427], [429]. It can be suggested that Vim phosphorylation, which prevents filament polymerisation, is a consequence of WFA-induced activity of these kinases [433]. However, clarification is needed since WFA has also been shown to downregulate some of these, e.g. Akt and Cdk1 [434], [435].

Furthermore, WFA-induced changes in Vim-IFs are accompanied by alterations in MFs and MTs [427]. This is not surprising, because there is evidence of direct interaction of Vim with the other two cytoskeletons [436], [437]. Also, WFA may bind actin and tubulin, although it remains to be determined whether this interaction is direct [428]. WFA also alters organisation of other IFs such as keratin and peripherin [427]. WFA at high concentrations may cause aggregation of various IFs in the perinuclear region which could have various unwanted, most likely neurological, consequences [438], [439]. However, finding a dose for targeted approach without disruption to the normal tissue function may be possible, as different IFs show different sensitivities to WFA [427].

Here, we are most interested in the anti-angiogenic properties of WFA. Indeed, WFA inhibits proliferation (12 nM) and sprouting in HUVECs (0.5 µM), as well as angiogenesis *in vivo* at a dose as low as 7 µg/kg/day [417]. This is most likely caused by the disruption of the Vim-IF network as a consequence of WFA-induced phosphorylation of Vim [428]. In Summary, WFA treatment has a wide range of implications on cellular processes but at the same time remains a valuable tool for researching the role of Vim and a promising compound for anti-cancer and anti-angiogenic strategies. Thus, it became a valuable tool for us, as we exploited its Vim-targeting properties in the context of αVβ3-integrin dependent angiogenesis.

4.2 Materials and Methods

4.2.1 General Comments

Some of the Materials and Methods used for the experiments in this chapter were previously described in Chapter 2, the General Materials and Methods. IMMLEC culture was done as described in Section 2.2 and nucleofection performed as in 2.3. WB protocol was outlined in Section 2.4. The scratch-wound migration assay was described in 2.6, the proliferation assay in 2.7 and ICC in 2.8. Data was graphed, and Student *t*-tests performed as described in Section 2.10. The Ab's used can be found in Table 2.1 and 2.2. siRNA used can be found in Table 2.3. Also, the focal adhesion enrichment protocol was conducted as described in Chapter 3, Section 3.2.1.

WFA was made up in 100% DMSO. The amount of DMSO used to treat cells (as the control condition) was equivalent to the amount needed in delivering the highest WFA dose in a given experiment, which was 0.1% v/v or less to avoid any DMSO toxicity.

Frozen stocks, of immortalised mouse lung ECs (IMMLEC), used here were isolated (protocol in Section 2.2) prior to the start of the project. Not surprisingly, some variability in cell morphology and behaviour were observed within any one genotype. All the available variants were assessed for β3-integrin expression, migration speed, adhesiveness and rate of cell division, i.e. how quickly 100% confluency was reached after a passage (data not shown). The most representative cell preps were selected and used in the majority the experiments in this project. Occasionally, when appropriate, other cell preps were used, for example in the VEGF-signaling assay.

4.2.2 RNA Isolation, cDNA Synthesis and Quantitative Real-Time PCR

Total cell RNA was extracted using the SV Total RNA Isolation Kit (Promega, Southampton) according to the manufacturer's protocol. RNA concentration and purity were determined using a NanoDrop™ 2000 spectrophotometer (Thermo Fisher). The 260/230 absorbance ratio reported any organic solvent contamination while the 260/280 ratio notified of protein contamination. cDNA was generated from RNA samples using the MMLV-Superscript reverse-transcriptase set (Sigma-Aldrich) resulting in a final concentration of 0.5 ng/µL. Quantitative real-time polymerase chain reaction (qRT-PCR) TaqMan™ was carried out using 5 ng cDNA for Vim and 1 ng cDNA for the 18S ribosomal RNA control gene. The cycle conditions in the 7500 Fast Real Time PCR System (Applied Biosciences, Thermo Fisher) were: 2 min at 50°C, 10 min at 95°C, then 40 cycles of 15 sec at 95°C and 1 min at 60°C. The primer/probe sets used were obtained from Applied Biosciences: 18S - Mm03928990_g1 and Vim - Mm01333430_m1.

4.2.3 Random Migration

ECs were trypsinised, counted and seeded at 10^4 cells per well onto 24-well plates, pre-coated with 10 µg/ml FN o/n and incubated at 37°C for 24 or 48 hours. The following day, cells were starved for 3 hours in serum-free Opti-MEM™, before replacing it with Opti-MEM™ supplemented with 2.5% FBS and 30 ng/mL VEGF. The plate was moved into an incubation chamber (37°C and 5% CO_2) mounted on an Axiovert (Zeiss, Cambridge) microscope where phase contrast images were taken at the same coordinates in each well every 20 min for 15 hours. This was done using the Multidimensional Acquisition tool in Axiovision software. Nuclei of single cells were manually tracked with the aid of the MTrackJ plugin for ImageJ software, which then allowed to calculate the speed of random cell migration.

4.2.4 Directional Migration

Information on directionality of EC migration was extracted from data generated during the random migration assay with the use of MTrackJ. The directionality of migration was quantified by dividing the maximum displacement value of a track (Max D2S) by the length of the track at that point (Len). Picking out D2S and Len values from data tables was aided by a Perl script.

4.2.5 VEGF Stimulation Assay

6-well plates were coated with 10 µg/mL FN o/n. IMMLECs were seeded at 2.5 x 10^5 cells per well and incubated o/n at 37°C. The following day the cells were washed with PBS and serum starved for 3 hours in Opti-MEM™. VEGF was added at for 0, 5 or 15 min and cells were lysed using buffer EB and protein samples were analysed using a WB (Section 2.4). Rabbit primary Ab's against P-ERK followed by total-ERK (Table 2.1) were used at 1 in 1000.

4.3 Results

In the previous chapter, I described our approach for narrowing the study of candidates present in the endothelial adhesome that might be responsible for mediating elevated angiogenic responses that occur in β3-integrin depleted cells (e.g. "resistance" in response to the long-term genetic deletion of the molecule). Having decided to focus on IFs (as described in chapter 3), in this chapter I further explore the consequences of siRNA-mediated knockdown of Nes, Vim and Plec in both WT and β3-depleted cells. Whilst β3-KO cells and RGD mimetic-treated cells were very useful in narrowing the list of targets to follow-up, we decided that subsequent studies should only profile responses in β3-HET ECs, which carry one wild-type allele of β3-integrin, and one knockout allele. These cells express 50% wild-type levels of β3-integrin. As in previous studies, we decided to use β3-HET cells for further analyses (rather than β3-KO cells, for example) because they circumvent potential developmental changes arising from the complete loss of the protein, which we felt might confound downstream quantitative interpretations. For example, we have shown these cells are a good model for studying the role of β3-integrin in cell migration, whilst evading changes arising from the complete loss of the integrin on both alleles (e.g. upregulated total VEGFR2 expression) [277].

4.3.1 siRNA Knockdown of Intermediate Filament Proteins Impairs Angiogenesis-Relevant Processes *In Vitro* in β3-depleted IMMLECs

I first set out to determine how effective siRNA-mediated knockdown of each IF target was. The fold decrease in Vim mRNA content was 20-fold in the WT cells and 17-fold in the β3-HET cells at 24 hours post-transfection (**Fig 4.3 A**). At 48 hours, this reduction in mRNA was ameliorated to about 5-fold in the WT and appeared to be abolished in β3-HET cells. Overall, Vim RNA expression shows signs of returning to baseline (untargeted) levels 48 hours post-transfection (**Fig 4.3 A**). I also measured Vim levels by WB (**Fig 4.3 B and C**), surmising that the turnover of Vim protein would be slower than its mRNA turnover, such that knockdown at the protein level would persist for longer than what was observed at the transcript levels. On average, 48 hours post-transfection, a 40% decrease in Vim protein level was detected in both WT and β3-HET cells. For this reason, alongside our empirical observation that for most targets the Robinson lab has examined, siRNA-mediated silencing begins to recover after 48 hours, I decided, wherever possible, to conduct knockdown experiments 48 hours post-transfection.

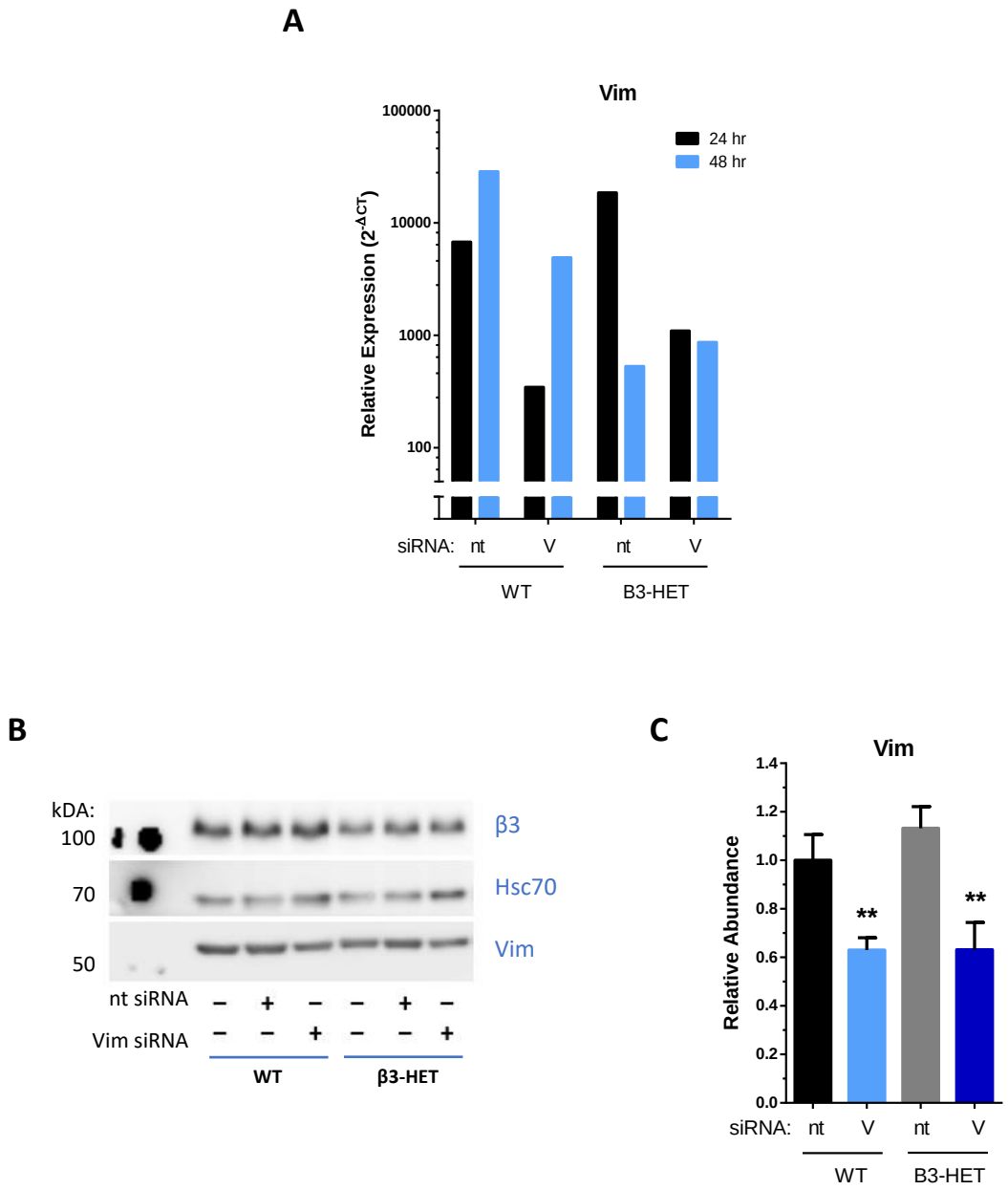

Figure 4.3 Vimentin knockdown in WT and β3-HET IMMLECs.

Vim siRNA-mediated KD in WT and β3-HET ECs was assessed by (**A**) real-time PCR 24- and 48-hrs post-transfection and (**B**) WB 48-hrs post-transfection. (**C**) Densitometry over 5 independent WBs relative to WT nt, error bars represent SEM, ** indicates P<0.01, as determined by an unpaired student's *t*-test. V – Vim siRNA, nt – non-targeting control siRNA.

I was able to efficiently knock down Plec, as measured by WB. On average, there was a 60% reduction of Plec in WT cells and 90% in β3-HETs 48 hours post-transfection (**Fig. 4.4 A and B**). I was intrigued by the observation that both Vim and Plec appeared to be overexpressed in β3-HET cells, compared to WT. One could speculate that the adhesome findings presented in chapter 3, which demonstrated the increased localisation of these proteins in the β3-HET adhesome was simply a consequence of the increased expression of the two proteins in these cells, rather than a consequence of increased recruitment to the adhesome when β3-integrin is depleted. Therefore, I examined the expression of Plec by WB in FA enriched samples. Here, I focused on Plec, as its increased expression in β3-HET total cell lysates was more dramatic than that of Vim. On average, the amount of Plec present in the β3-HET EC adhesome was approximately 2.5-fold more than that in the WT adhesome (**Fig. 4.4 C and D**); more than the approximate 1.3-fold difference noted in total cell lysates, suggesting more Plec is recruited to FAs upon β3-depletion.

Unfortunately, all attempts at assessing Nes knockdown were unsuccessful. I tested three anti-Nes Ab's by WB, which resulted either in many unspecific bands or no signal. However, given encouraging findings with Nes in chapter 3, I decided to continue to pursue this target, at least in the random migration assay presented below.

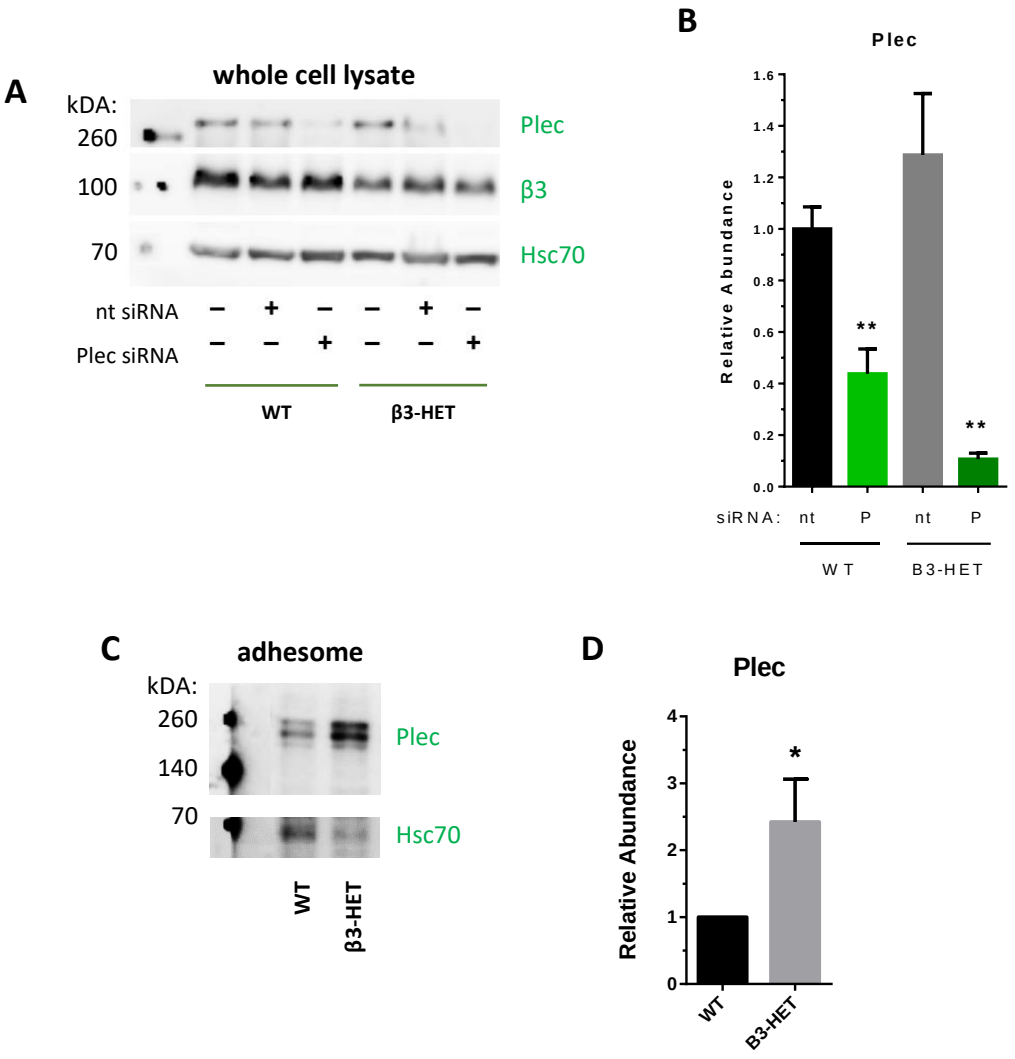

Figure 4.4 Plectin in WT and β3-HET IMMLECs.

(**A**) Plec siRNA-mediated KD in WT and β3-HET ECs was assessed by WB. (**B**) Densitometry representative of 3 WBs (5 samples per condition), P – Plec siRNA, nt – non-targeting control siRNA. (**C**) WT and β3-HET samples of FA enrichment on FN were subjected to WB to examine the levels of Plec in the EC adhesome. (**D**) Densitometry representative of 6 WBs (6 samples per condition) relative to the WT. Error bars represent SEM, * indicates P<0.05 and ** P<0.01, as determined by an unpaired student's *t*-test.

EC migration is a process that is crucial for angiogenesis. ECs sprout and migrate in response to pro-angiogenic factors to form new blood vessels [440]. In an attempt to corroborate preliminary studies (see chapter 3) showing changes in collective cell migration in response to Vim, Nes, and Plec knockdown, we decided to conduct random migration assays (for protocol see Section 4.2.3) following siRNA depletion of these targets. These assays were performed in the presence and absence of VEGF for all conditions, however minimal differences were observed between conditions with and without VEGF (**Fig. 4.5 A**). This lack of difference may be due to the long timespan (15 hours) of the assay, while most of VEGF's impact occurs within the first 1 hour of addition to the cell media; the half-life of VEGF, after administration *in vivo*, is approximately 1 hour [441]. Therefore, I chose not to include VEGF in subsequent random migration assays. To our surprise, the only significant noted change in random migration was following Nes knockdown in WT cells (**Fig 4.5 B – D**). Whilst this was a disappointing result with regards to Vim and Plec, I was at least reassured that Nes siRNA can elicit a biological response, even though I could not prove knockdown by WB.

Impaired directional migration in ECs could be correlated with impaired responsiveness to pro-angiogenic cues from within the tumour microenvironment or chaotic dysregulated angiogenesis, therefore we also investigated migration directionality (protocol - Section 4.2.4), using the data collected in the random migration assays. Similarly, few notable changes were observed (**Fig. 4.5 E**). There was a decrease in directionality of Plec siRNA transfected WT ECs, a trend in β3-HET cells for a less directional trajectory upon Vim knockdown and a trend in the WT cells for a more directional migration upon Nes knockdown. Representative tracks used to calculate random migration speed and migration directionality with Vim, Nes and Plec knockdown are shown in **Figure 4.5 F**.

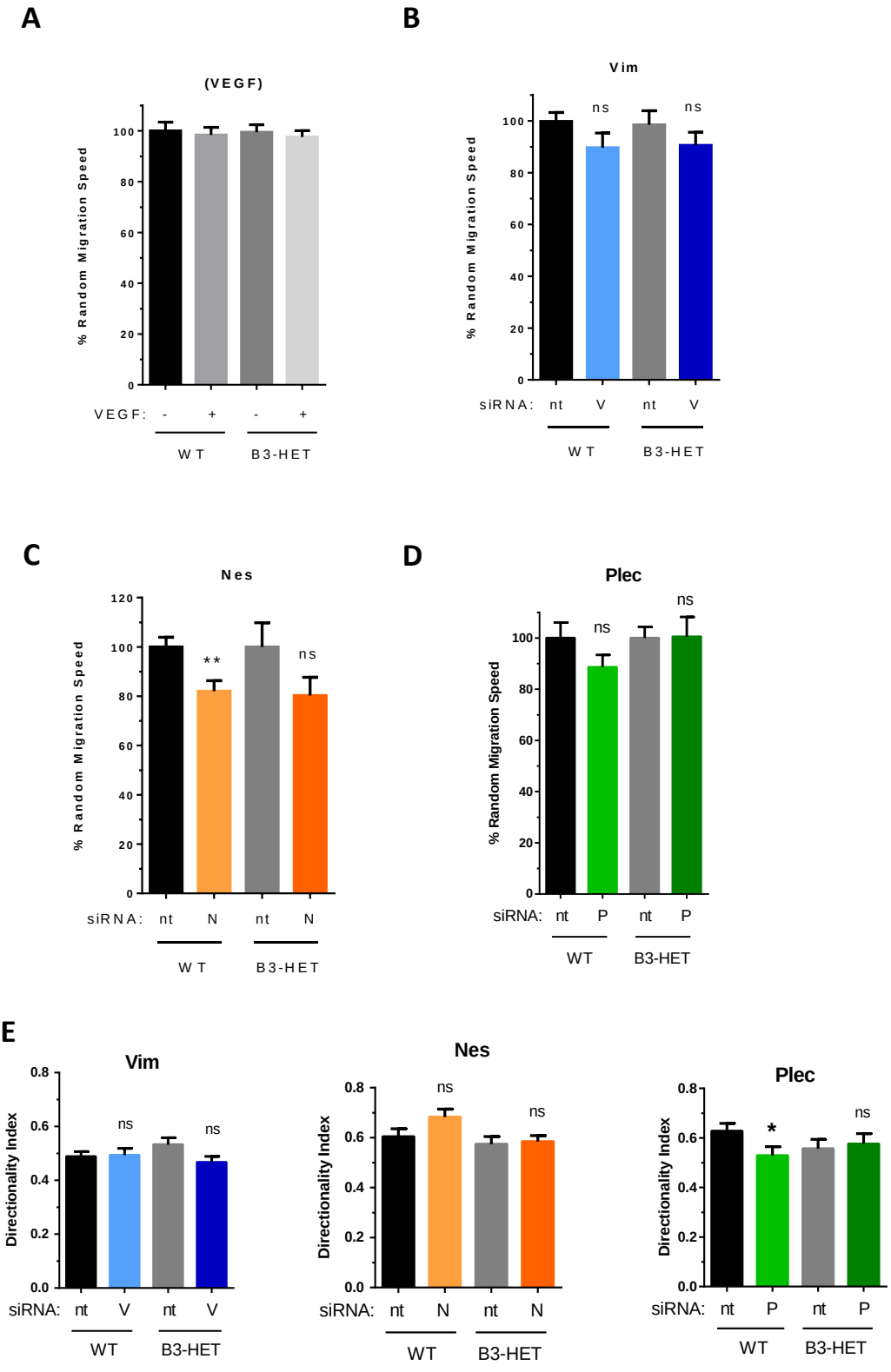
A
(VEGF)
% Random Migration Speed
VEGF: - + - +
WT
B3-HET
B
Vim
ns
ns
% Random Migration Speed
siRNA: nt V nt V
WT
B3-HET
C
Nes
**
ns
% Random Migration Speed
siRNA: nt N nt N
WT
B3-HET
D
Plec
ns
ns
% Random Migration Speed
siRNA: nt P nt P
WT
B3-HET
E
Vim
Directionality Index
ns
ns
siRNA: nt V nt V
WT
B3-HET
Nes
Directionality Index
ns
ns
siRNA: nt N nt N
WT
B3-HET
Plec
Directionality Index
*
ns
siRNA: nt P nt P
WT
B3-HET

F

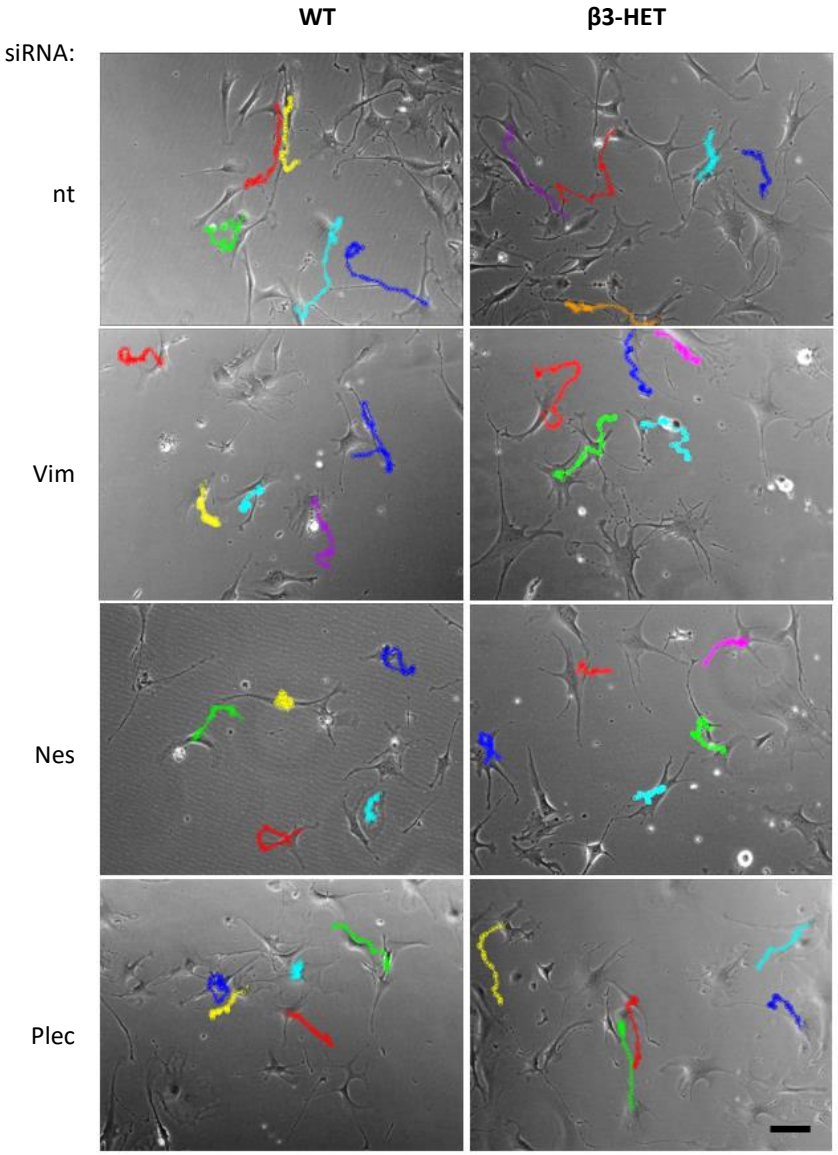

Figure 4.5 Vim, Nes and Plec knockdown has little or no effect on random or directional migration of WT and β3-HET IMMLECs.

Cells were transfected with non-targeting (nt), Vim (V), Nes (N) or Plec (P) siRNA and seeded into FN-coated 24-well plates for a random migration assay. Nuclei were tracked, using MTrackJ plug-in in ImageJ software, to quantify random migration. (**A**) shows random migration speed of WT cells +/- VEGF. (**B**), (**C**) and (**D**) summarise the effects of Vim, Nes and Plec siRNA, respectively, on random migration speed in WT and β3-HET cells relative to nt controls (no VEGF, n=20+). (**E**) Track data also allowed the quantification of migration directionality. Error bars represent SEM. * indicates $P<0.05$ and ** $P<0.01$, as determined by an unpaired student's *t*-test. (**F**) Representative cell tracks for each condition, scale bar = 100µm.

It was unexpected that knocking down Vim, Plec and Nes did not, in general, slow random migration, in a manner similar to the effects of these knockdowns on collective cell migration (see Chapter 3). However, these are two different assays. The random migration assay measures migration speed of individual cells, which rarely interact with one another, with no spatial constraints. In the wound-closure assay cells are migrating as a collective of closely interacting cells, in a defined direction to close the 'wound', which is more like angiogenesis *in vivo*. Therefore, I decided to investigate whether IF knockdown influenced VEGF-mediated signalling by performing WBs examining ERK1/2 phosphorylation. ERK1/2 sits at the bottom of the VEGF signalling cascade and is often used as a functional readout of overall VEGF-responses [114], [115], [442]. At this stage, I decided to exclude Nes, as I was not able to confirm knockdown.

In order to test whether Vim knockdown affects angiogenic signalling in ECs a VEGF time-course experiment was performed, according to the protocol described in Section 4.2.5, followed by a WB for phospho-ERK1/2. Briefly, WT and β3-HET ECs were transfected with Vim siRNA and incubated for 48 hours. They were then serum-starved, stimulated with VEGF and lysed for a WB. No augmentation to the normal pattern of ERK phosphorylation was observed with Vim knockdown (**Fig. 4.6**). Likewise, Plec knockdown did not impair ERK phosphorylation in either WT or β3-HET ECs (**Fig. 4.7**).

A

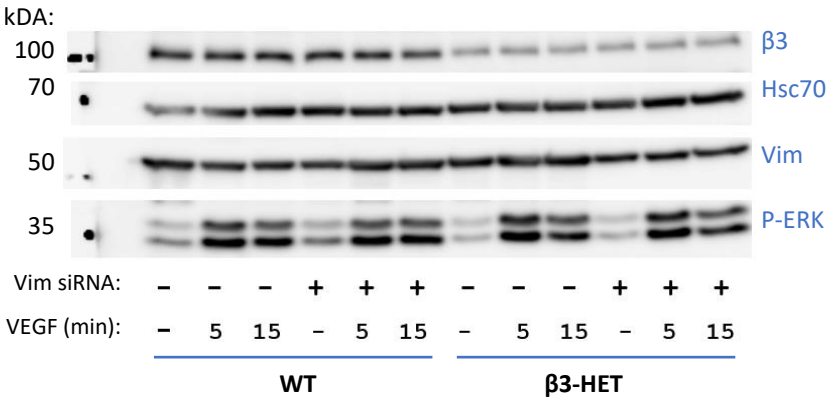

B

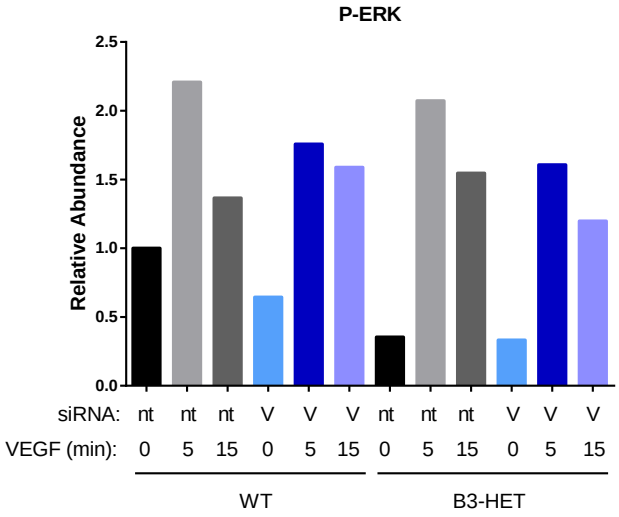

Figure 4.6 Knocking-down vimentin in IMMLECs has no effect on ERK1/2 phosphorylation.

(**A**) Cells were transfected with non-targeting (nt) or Vim (V) siRNA and seeded on FN. 48-hrs post-transfection, cells were stimulated with VEGF for 0, 5 or 15 min and lysed. 20 µg from each sample was used in a WB to compare ERK1/2 phosphorylation (P-ERK) patterns. (**B**) Densitometry values were normalised to the Hsc70 signal and shown relative to average WT nt 0 control. This figure is representative of 2 independent repeats.

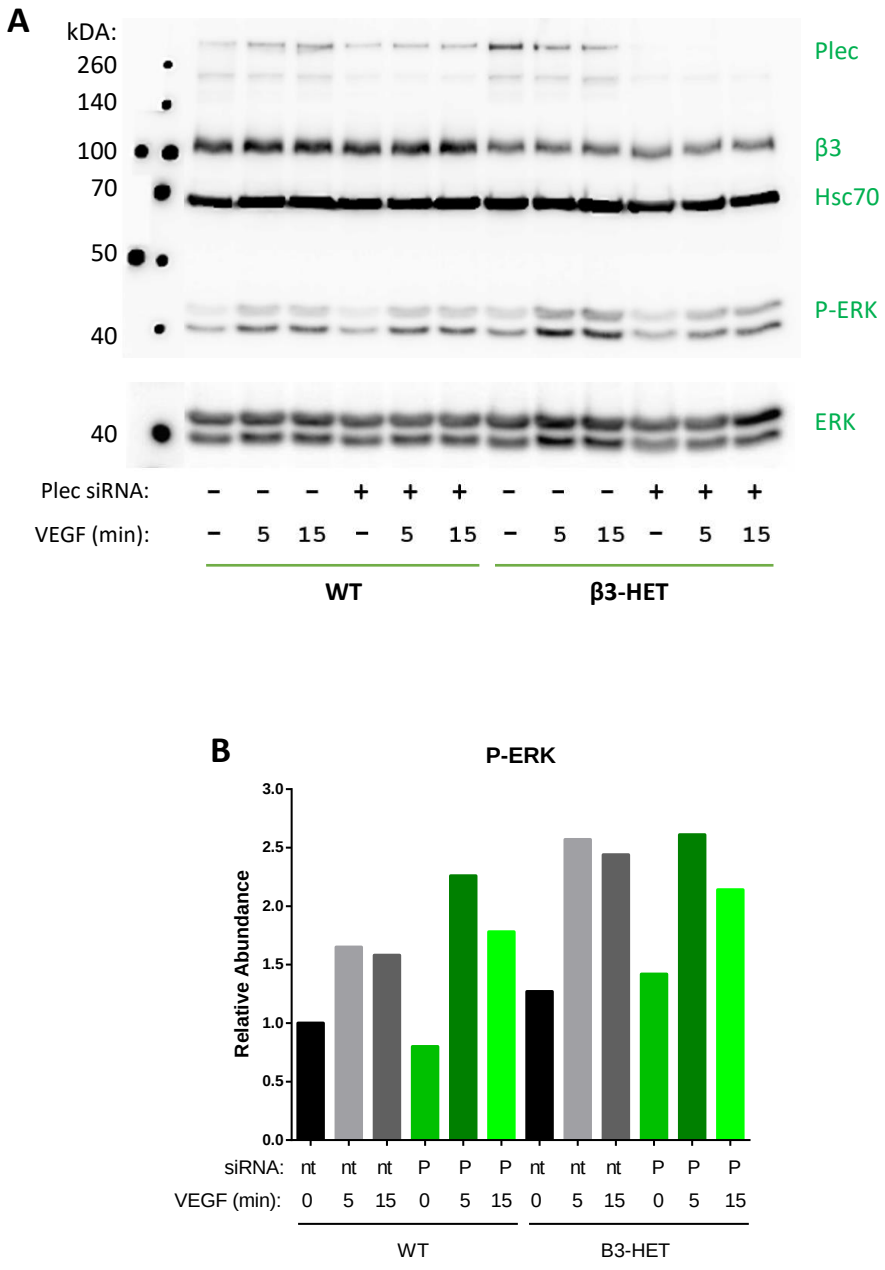

Figure 4.7 Plectin knockdown has no effect on ERK1/2 phosphorylation.

(**A**) Cells were transfected with non-targeting (nt) or Plec (P) siRNA and seeded on FN. 48-hrs post-transfection, cells were stimulated with VEGF for 0, 5 or 15 min and lysed. 20 µg from each sample was used in a WB to compare ERK1/2 phosphorylation (P-ERK) patterns. (**B**) Densitometry values were normalised to the Hsc70 signal and total ERK (ERK) and shown relative to average WT nt 0 control.

4.3.2 Vimentin Inhibition Using Withaferin A in Combination with β3-integrin Genetic Depletion.

Given the promising results shown in chapter 3, whereby siRNA depletion of IFs inhibited migration in both WT and β3-HET ECs, we were quite dismayed over the findings presented in the previous sections of this chapter. In my hands, it looks as if IFs play little, if any role in regulating EC migration, at least as assessed by siRNA-mediated target depletion. Whilst it is possible that IFs play a role in collective cell migration, but not random migration, the findings presented so far in this chapter go against a large body of evidence. As summarised by Leduc and Etienne-Manneville (2015), Nes, Plec and Vim all contribute to cell migration and invasion [443]. Overall, experiments utilising siRNA knockdown of IFs in the previous section were disappointing. Therefore, we decided to turn to chemical inhibition of IFs, rather than siRNA-mediated depletion, theorising that this approach would lead to more immediate and long-lasting effects. However, unlike microtubules and actin filaments, few destabilising drugs exist that target IFs specifically [443]. However, we did come across a generally non-toxic inhibitor, Withaferin A (WFA), which leads to Vim filament fragmentation, by inducing phosphorylation of Vim [428], [433]. From here onwards, much of the project became focused on Vim, as WFA proved to be a very useful tool.

Prior to using Withaferin A (WFA) in our experiments, a dose response curve needed to be established to determine an optimal, physiologically relevant dose for use *in vitro*. Suggestions can be found in the literature, but it was important to determine the right dose that works in our hands [444]. We wanted to find a concentration of the drug that would just inhibit proliferation of our IMMLECs. We conducted a proliferation assay (Section 2.7) in WT IMMLECs using a wide range of WFA doses (**Fig. 4.8 A**) and observed a sharp drop in the proliferation rate between the concentrations of 0.1 μM and 1.0μM. In order to tease out the optimal dose further, we performed another proliferation assay using WFA between 0 and 1.0 μM (**Fig. 4.8 B**). Thus, a working concentration of 0.5 μM was identified (**Figure 4.8 B**), which is also an experimental dose cited in the literature [444]. At this concentration, the proliferation rate of the WT IMMLECs is 90% of that at its highest, which is at 0.2 μM. It is worth noting that we observed an induction in proliferation between 0.1 and 0.6 μM. Therefore, at a concentration of 0.5 μM the drug is affecting biological processes of the cells but is not too detrimental to the rate of proliferation. Next, we conducted a time-course proliferation assay using the WT and β3-HET IMMLECs at 24, 48, 72 and 96 hours after the addition of 0.5 μM WFA to the cells. We saw a significantly lower rate of proliferation in the WFA-treated β3-HET cells compared to the WT cells, at 48 and 72 hours, while re-treating the cells daily with WFA (**Fig. 4.8 C**).

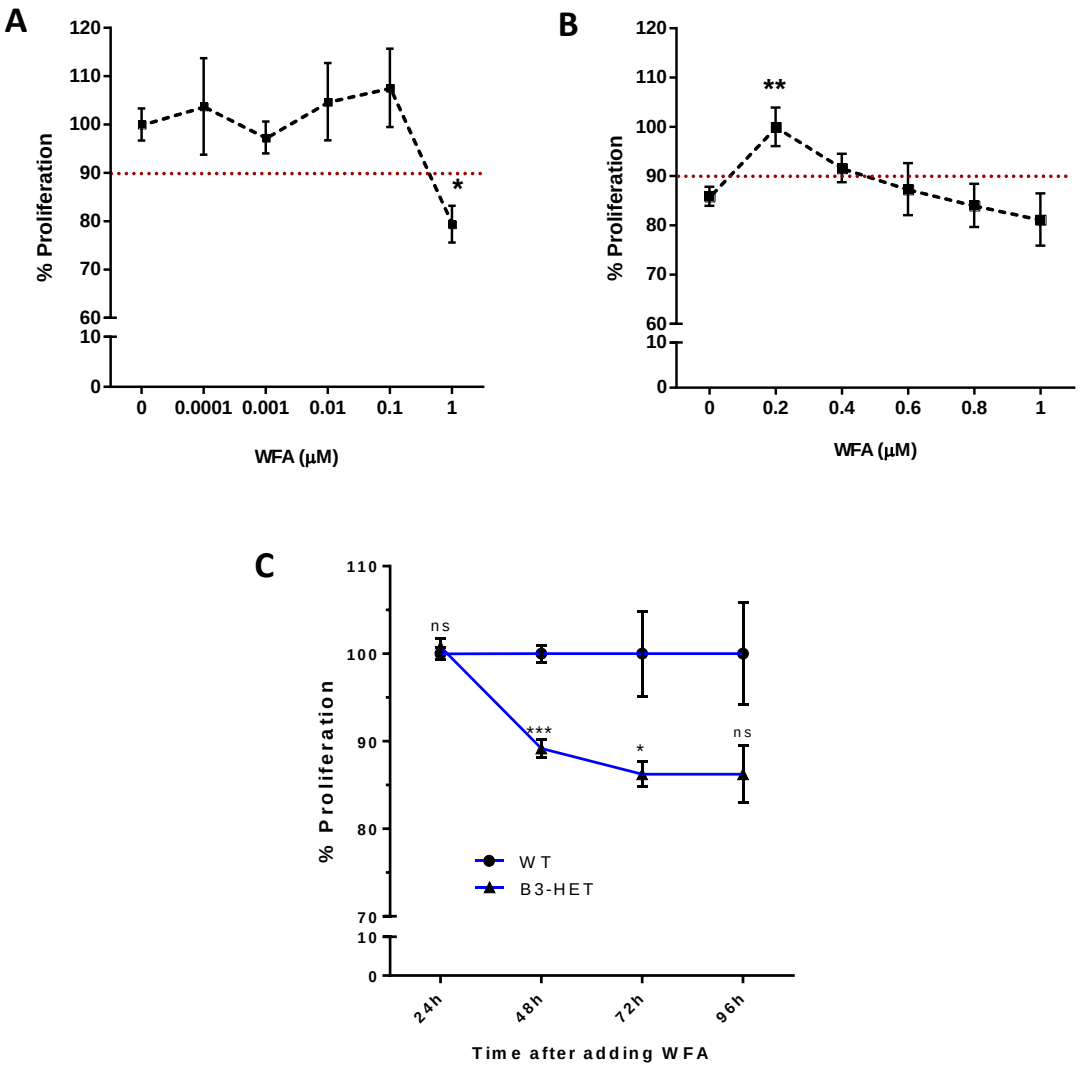

Figure 4.8 WFA dose and the impact of WFA on WT and β3-HET IMMLECs.

(**A**) Wide and (**B**) narrow dose range of Withaferin A (WFA) was used in the WST-1 proliferation assay of WT ECs to find an optimal experimental dose. (**C**) 96-hour WST-1 proliferation assay, with daily time-points, was carried out in WT and β3-HET ECs in the presence of 0.5 µM WFA. Absorbance values were normalised to the 0 µM value in A, 0.2 µM value in B and WT 24-hour value in C. Error bars represent SEM (N=1, n=4+ technical repeats), * indicates P<0.05, ** P<0.01 and *** P<0.001, as determined by an unpaired student's *t*-test.

We were interested to investigate how dual targeting of IFs using WFA and β3-integrin (by genetic depletion) affects migration of ECs, a process crucial for angiogenesis. In a 24-hour wound-closure assay, we observed that the WT cells collectively migrate faster when treated with WFA, whereas β3-HET ECs migrate slower upon WFA treatment (**Fig. 4.9**). It was interesting to observe a differential response in WT vs β3-HET ECs. In comparison, random cell migration speed was impaired in both cell types upon WFA treatment, although not significantly in the β3-HET ECs when compared to their DMSO controls (**Fig. 4.10 A and C**). WFA did not affect migration directionality in either of the cell types (**Fig. 4.10 B**).

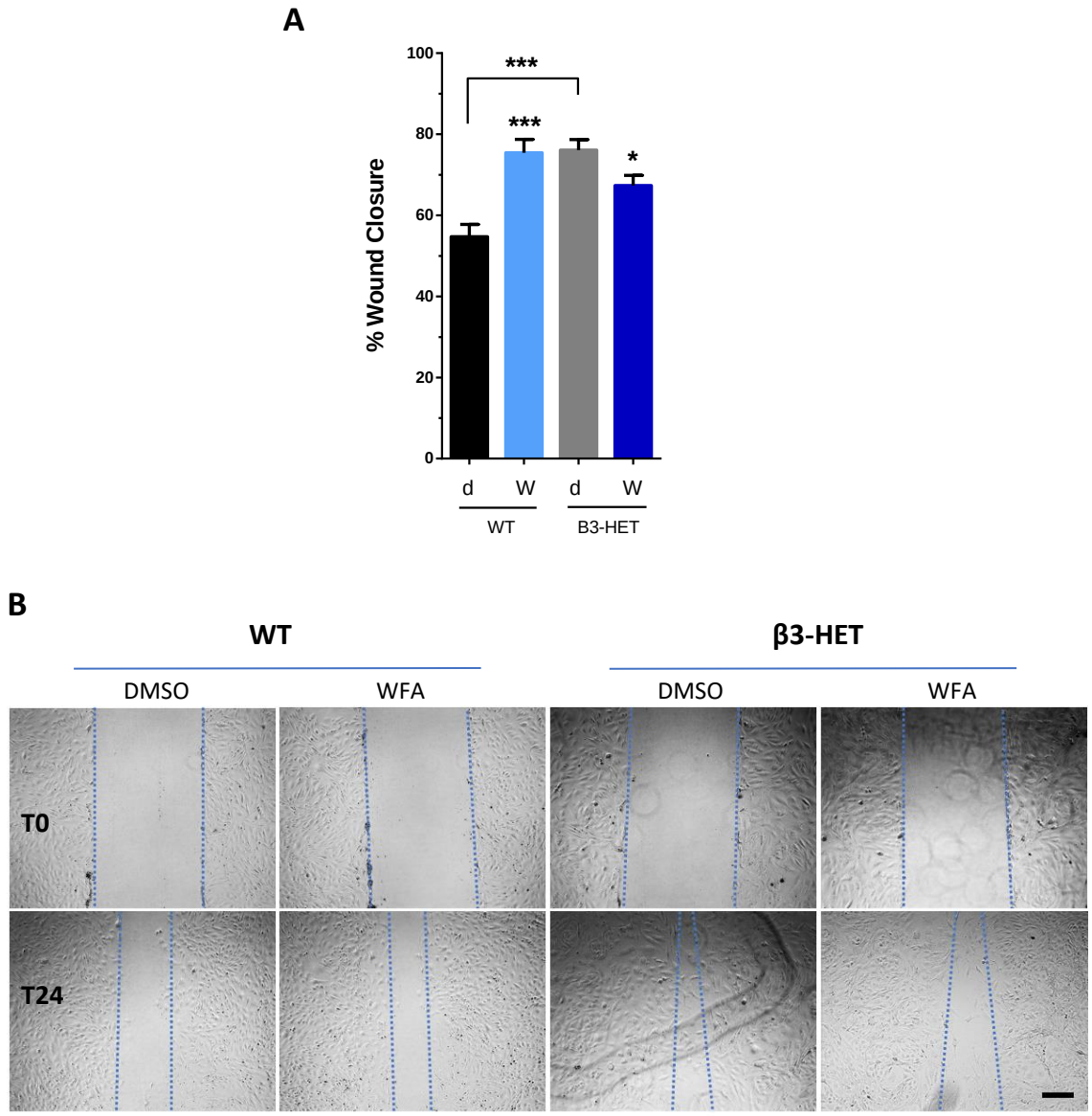

Figure 4.9 Withaferin A has a differential effect on migration of WT and β3-HET IMMLEC monolayers.

(**A**) Cells were pre-treated with DMSO (d) or 0.5 µM WFA (W) for 5 hours and subjected to a 24-hr wound-closure migration assay (+SEM; n=9+). * indicates P<0.05 and *** P<0.001, as determined by an unpaired student's *t*-test. (**B**) Representative images at T0 and T24, scale bar = 200 µm.

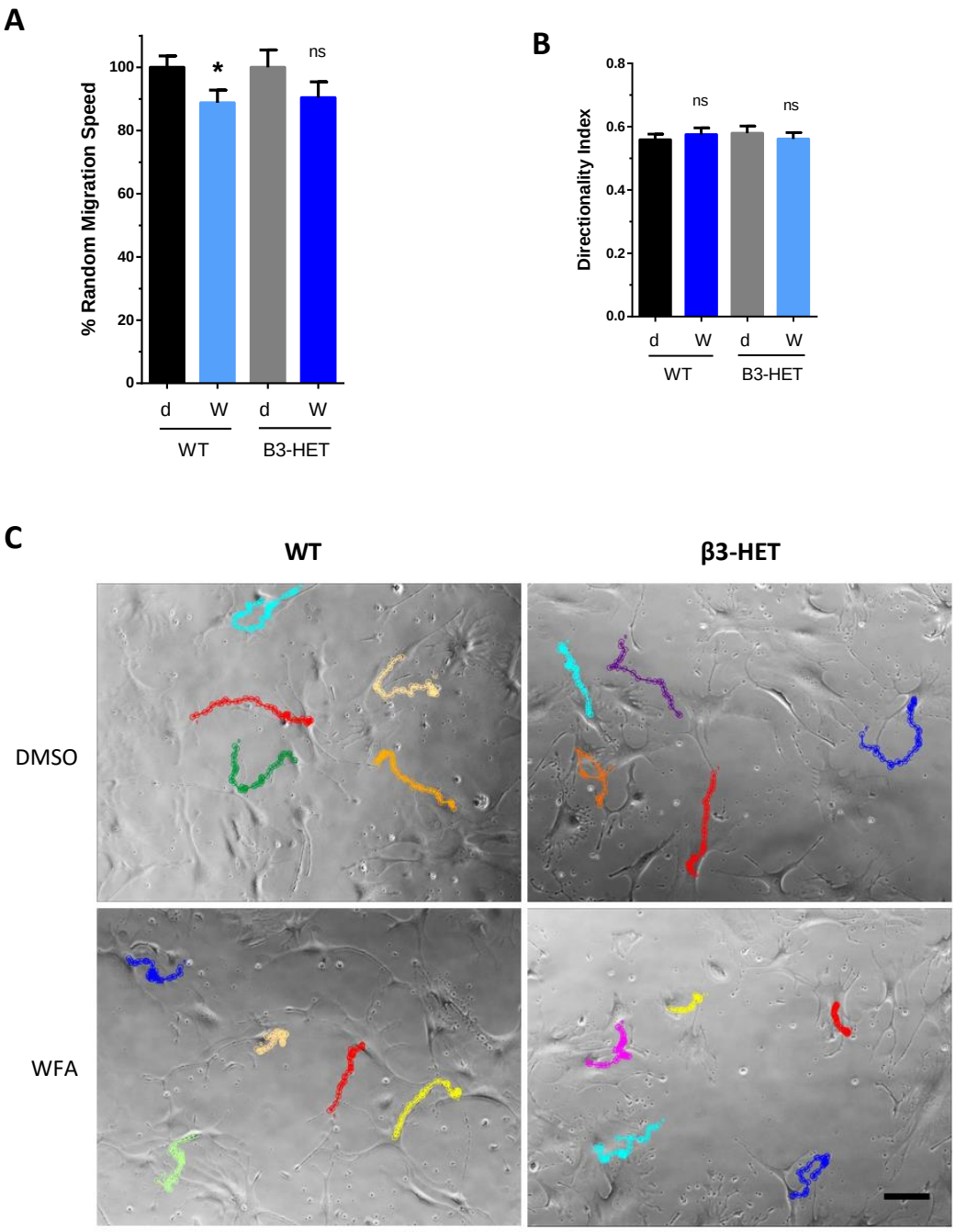

Figure 4.10 The effect of Withaferin A on random migration of WT and β3-HET IMMLECs.

(**A**) Cells were seeded into FN-coated plates and treated with DMSO (d) or 0.5 µM WFA (W) and subjected to a random migration assay. Individual cell nuclei (n=50+) were tracked using MTrackJ plug-in in ImageJ. Random migration speed of WT and β3-HET + DMSO/WFA is shown relative to the DMSO controls. (**B**) The same tracking data was used to quantify migration directionality. (**C**) 5 representative tracks from each of the conditions, scale bar = 100 µm.

WFA treatment leads to an increase in soluble, phosphorylated Vim in fibroblasts, which does not efficiently incorporate into filaments [445]. Therefore, we wanted to determine if there was a change in phosphorylated Vim (P-Vim) in ECs upon WFA treatment, using a WB. As shown in **Figure 4.11 A**, increasing the concentration of WFA (between 0 and 2 μM) appears to cause a continuous increase in the level of P-Vim. Quantitation of the signal by densitometry, whereby the P-Vim values were normalised to total Vim (Vim) and Hsc70 (housekeeping gene) appears to corroborate with the WB image (**Fig 4.11 B**). However, this is n of 1 and requires further repeats to confirm.

Vim-containing complexes have been shown to regulate focal adhesion kinase (FAK) in ECs [446]. Therefore, we were interested to determine whether WFA treatment of ECs affected FAK expression and phosphorylation. At first glance, the WB image in **Figure 4.11 C** suggested that there is a decrease in total levels of FAK (FAK) and phosphorylated FAK (P-FAK) with WFA treatment. However, having done this WB twice and performing densitometry with normalisation to Gapdh (housekeeping gene) this was no longer the case. On average, there was no decrease in P-FAK relative to total FAK (**Fig 4.11 E**). There is a trend for a decrease in total FAK levels as a result of WFA treatment, as cells treated with 0.2 μM and 1 μM WFA appear to have less total FAK than untreated cells (**Fig. 4.11 D**). Further repeats are needed to determine any changes in FAK with confidence.

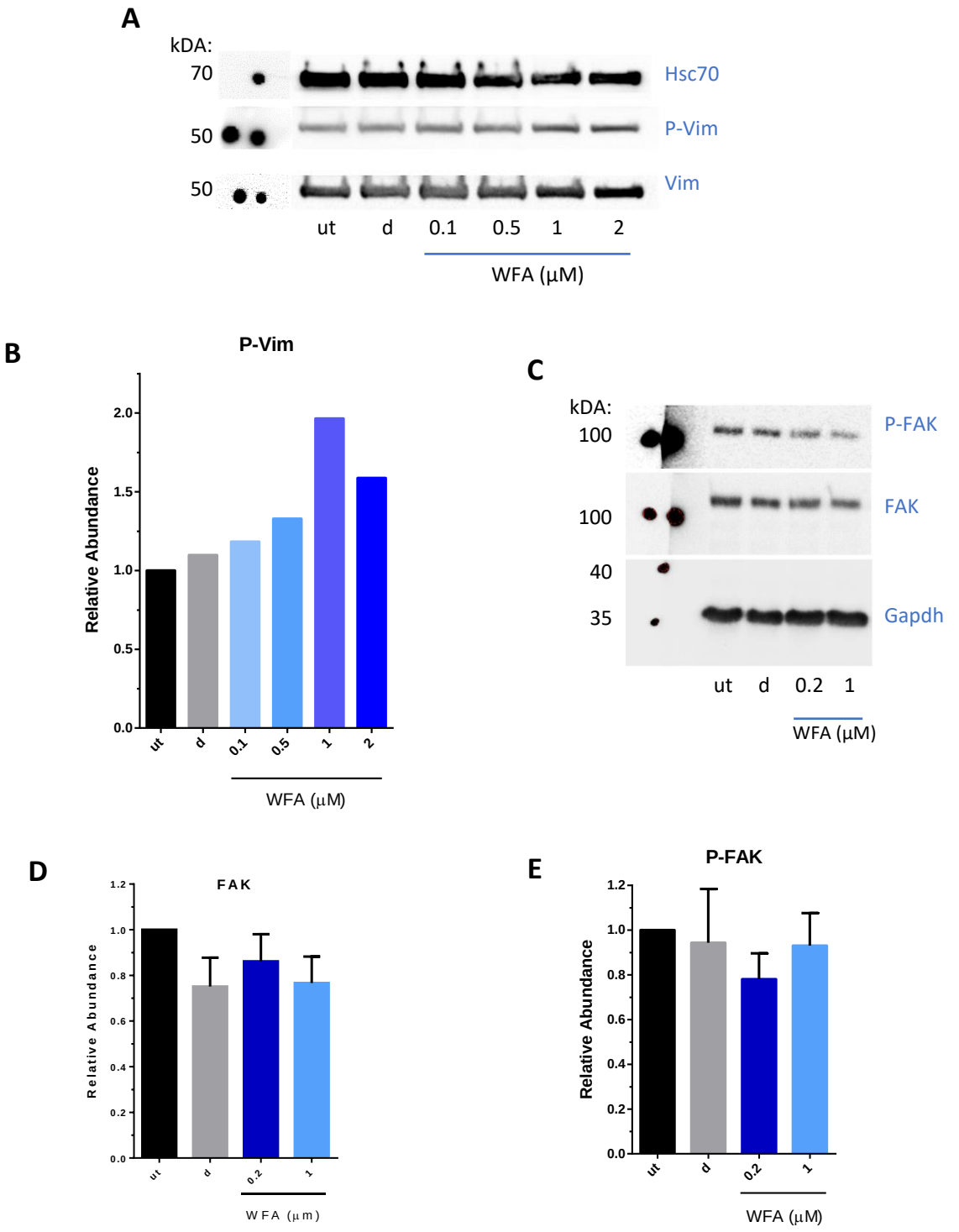

Figure 4.11 WFA treatment in ECs causes an increase in phospho-Vim and a decrease in FAK levels.

WT IMMLECs were treated with DMSO (d) or WFA o/n. Fresh full media + d or WFA was added the following day for 1 hour and the cells were lysed. 20 µg was used in a WB to determine the levels of total and (**A**) phospho-Vim (P-Vim), (**C**) total FAK (FAK) and phospho-FAK (P-FAK) upon WFA treatment. WB images were subjected to densitometry using ImageJ to quantify the signal. (**B**) P-Vim values were normalised to total Vim (Vim) and Hsc70 signal (n = 1). (**D**) FAK values were normalised to Gapdh, while (**E**) P-FAK signal was normalised to FAK and Gapdh (n = 2, +SEM). All values in B, D and E were expressed relative to the untreated sample (ut) in the same WB.

To visualise if and how WFA is affecting the Vim network in our ECs, we performed ICC. Indeed, WFA had a dramatic effect on the Vim filament structure. The Vim network collapsed towards the centre of the cell, unable to reach the cell membrane, in the horizontal plane, in both WT and β3-HETs ECs (**Fig. 4.12**).

Actin microfilaments (MFs) and actin stress fibres play a role in many cellular processes including adhesion and motility. Actin is a major component of FAs and interacts with Vim [186], [447]. Therefore, we hypothesised that Vim network collapse upon WFA treatment might have an influence on the actin network. Therefore, we also stained for F-Actin using directly-labelled phalloidin in ICC. We observed that actin was more concentrated around the nucleus, less so at the periphery, as if following the collapse of Vim to an extent, when the cells are treated with WFA (**Fig. 4.12**). Also, the actin fibres appeared to be shorter in the β3-HET WFA-treated ECs compared to their DMSO control, whereas this was less apparent in WT ECs. Classical FAs assemble at the end of actin stress fibres, while Vim has been shown to stabilise FAs [220], [385]. WFA is likely causing a de-stabilisation of FAs due to the impact that it has on IFs, but perhaps also on MFs. This reiterates its efficacy as an anti-angiogenic compound [417].

The images from the ICC illustrated in **Figure 4.12** were analysed further. By lowering the upper limit of the image display range in the green (Vim) channel in ImageJ, the peripheral Vim fragments were displayed, which are not visible with the normal settings (**Fig 4.13 A**). These fragments were counted. Their number was dramatically increased in both WT and β3-HET ECs upon WFA treatment, thus visually reiterating that the drug leads to the disruption of the Vim filament network (**Fig 4.13 B**). Integrity of the Vim network appears to be more affected by WFA in the β3-HET ECs then in the WT ECs (more fragments). It can be deduced that there is more phosphorylated and soluble Vim present in WFA-treated cells, which does not efficiently incorporate into the filament network [445]. We saw an indication that the amount of phospho-Vim in WFA-treated cells increases (**Fig. 4.11**) although, given the ICC results, it is surprising that this is not more apparent by WB.

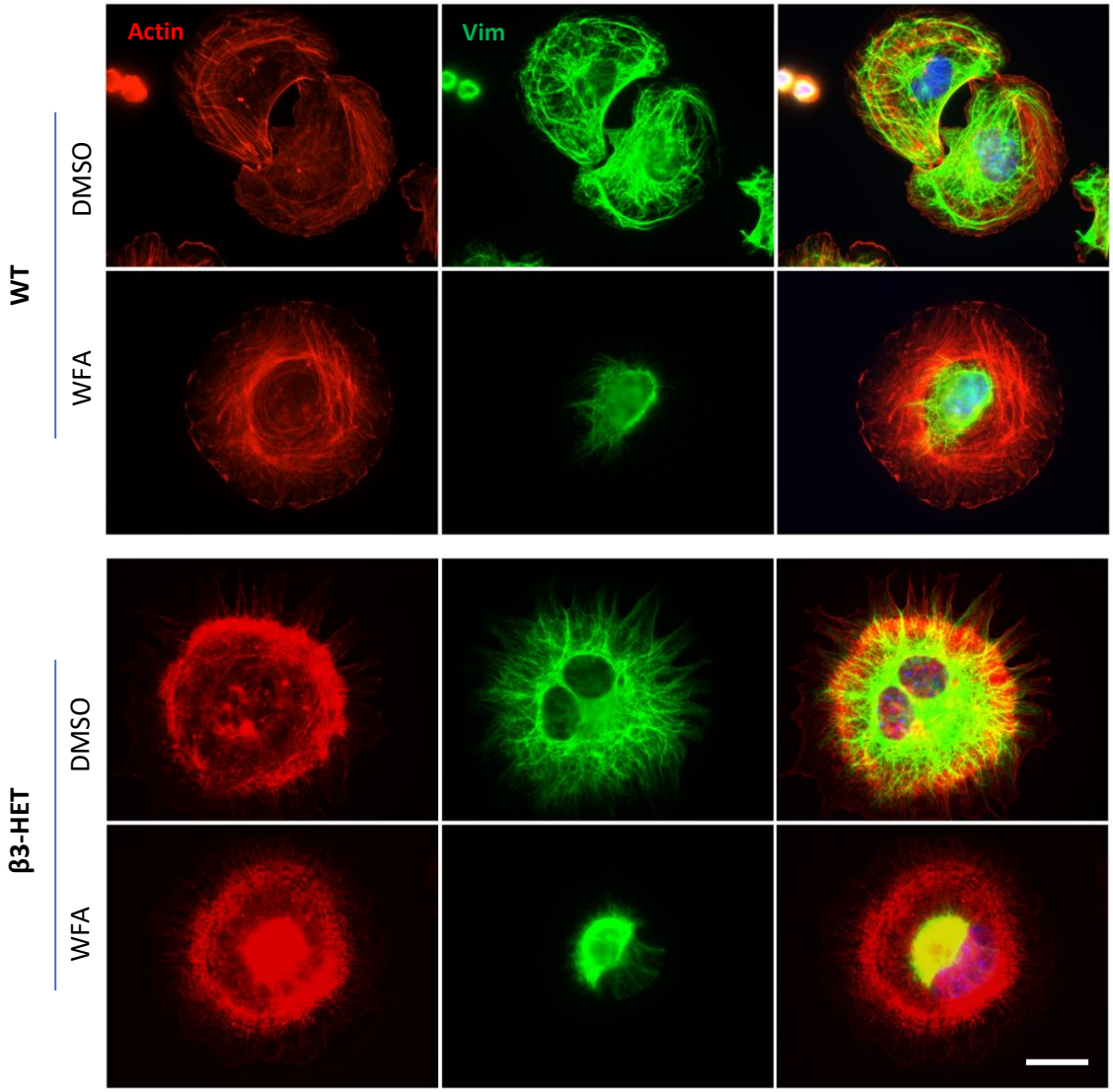

Figure 4.12 WFA disrupts peripheral Vim filaments and remodels actin network in IMMLECs.

WT and β3-HET ECs, pre-treated with DMSO or 0.5µM WFA, were adhered on FN-coated coverslips for 90 min in the presence of DMSO or WFA, then fixed and stained: actin (red), Vim (green) and DAPI (blue). Representative ICC images (63x) of stained cells are shown. Images were taken using the Axioplan epifluorescent microscope (Zeiss, Cambridge) and the AxioCam MRm camera (Zeiss). Scale bar = 50 µm.

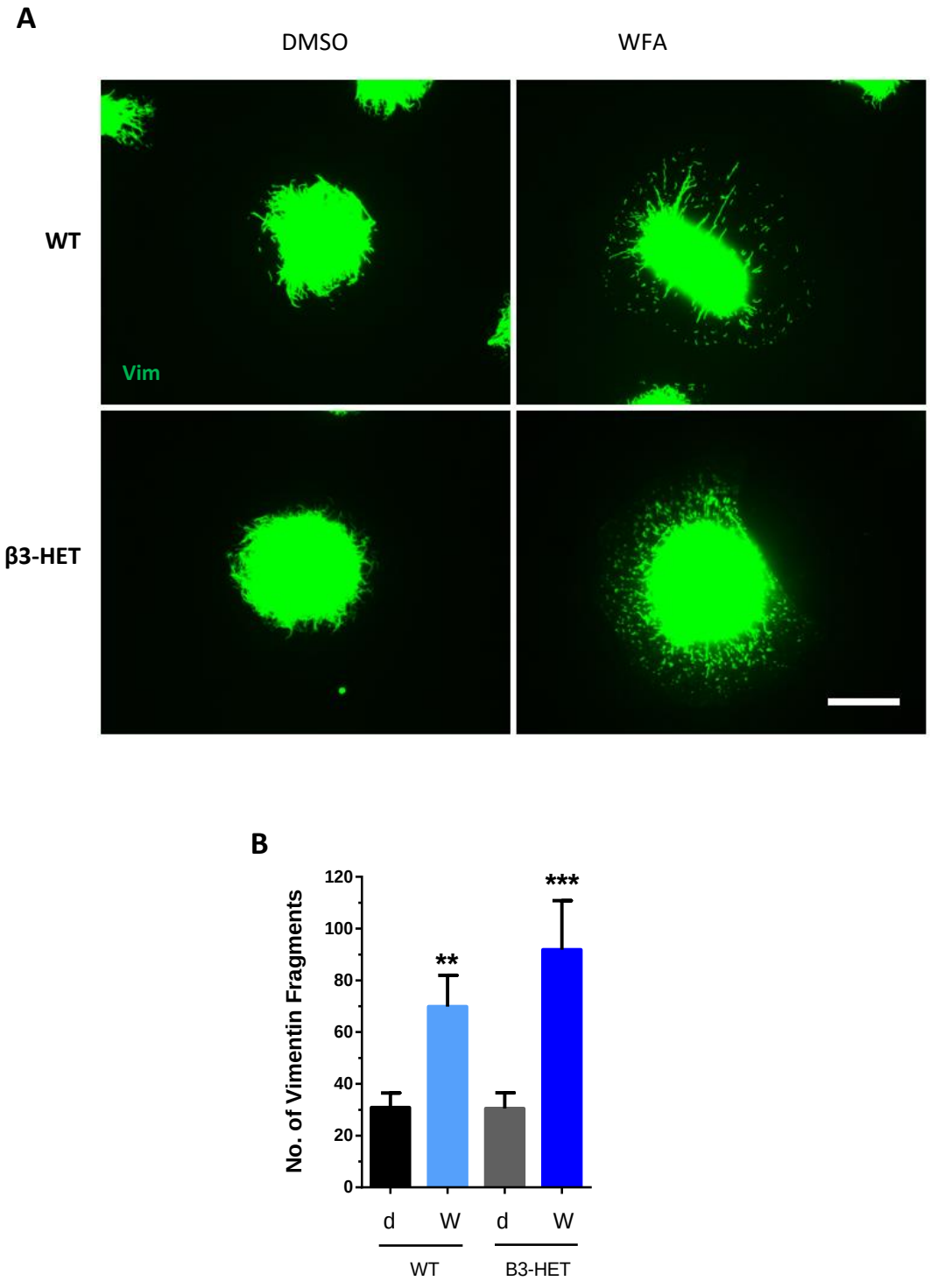

Figure 4.13 Quantification of vimentin filament integrity in WFA-treated IMMLECs.

(**A**) As in Fig 4.10, WT and β3-HET ECs were pre-treated with DMSO (d) or WFA (W) and seeded on FN in the presence of DMSO or WFA for 90 min, then fixed and stained: Vim (green). ICC images (63x) of these cells were taken and the maximum display range limit was decreased to enhance the peripheral fragments. (**B**) Average number of Vim fragments per cell (n=10+ cells per condition). * indicates P<0.05, ** P<0.01 and *** P<0.001, as determined by an unpaired student's *t*-test. Scale bar = 50 µm.

4.4 Discussion

Results of experiments with WFA, presented in this chapter, suggest that angiogenesis-relevant processes can be inhibited *in vitro* when co-targeting β3-integrin and IF proteins. We saw that WFA impaired proliferation and migration of β3-HET ECs more than that of WT ECs. We also visualised the effect WFA has on the Vim IF network, which may be accompanied by actin remodelling. However, additional experiments (e.g. VEGF-induced signalling) would benefit this study to give a more complete picture.

The abundance of Plec was assessed at the whole cell lysate and the FA level by WB. Plec was upregulated in the β3-HET cells compared to WT at both levels, in agreement with the mass spectrometry data discussed in Chapter 3. We achieved an effective Plec knockdown of 60 - 90%. In the literature Plec's influence on ERK signalling is cell-type and context dependent [448], [449]. In ECs Plec plays a pro-angiogenic role in connecting Vim-IFs to integrins, promoting adhesion and migration [383], [406], [443]. Therefore, we were disappointed not to see a decrease in random migration or ERK phosphorylation upon siRNA-mediated knockdown of Plec.

Unfortunately, none of the antibodies against Nes worked in my hands in ICC or WB. As a result, we decided to build tdTomato-labelled Nes constructs for use in ICC. This work constitutes the second half of the next chapter of this thesis. However, we were able to look at random migration WT and β3-depleted ECs transfected with Nes siRNA. Random migration was impaired only in WT ECs. Literature suggest that Nes expression correlates with cells proliferation and migration [391], [394]. The latter is in agreement with our observations. Lack of working Ab's prevented us from assessing Nes knockdown in our cells. With more time, we could also assess this using qRT-PCR.

Vim has been (successfully) looked at by WB only at the whole cell level. Analysing FA enriched samples would further complement the findings resulting from the mass spectrometry described in the previous chapter. With the limited level of Vim knockdown that we achieved here, we did not observe many changes in migration or VEGF-dependent (ERK) signalling. We attempted adhesion and proliferation assays post Vim siRNA transfection. Unfortunately, results from these tended to be confusingly inconsistent. Others have observed that Vim RNAi led to smaller FAs and decreased cell adhesion in ECs under shear stress, suggesting that Vim knockdown disrupts cell-matrix interaction [385].

We saw more dramatic changes when we used WFA in IMMLECs. Therefore, from then onwards, much of the project became focused on Vim, as WFA proved to be such a useful tool. There was a dose-dependent modulation of cell proliferation in WT ECs, an upregulation between 0.1 and 0.6 μM WFA and inhibition at 1.0 μM or above. We treated our cells with 0.5 μM WFA in most of our experiments. The increase in proliferation at low concentration of WFA may be the explanation for the increase in migration of WT IMMLECs in the wound-closure assay. We attempted adhesion assays in WT and β3-HET ECs with WFA treatment. Unfortunately, results from these tended to be inconsistent, and were not shown here. Random migration was impaired in WT, but not β3-HET ECs treated with WFA. However, in the more angiogenesis-relevant, wound-closure migration assay, we saw a decrease in cell migration with the WFA-treatment in the β3-HET, but not in the WT ECs. This is an interesting finding in favour of dual targeting of Vim and β3-integrin, as an anti-angiogenic strategy. Furthermore, we visualised disassembly of Vim-IFs in ECs treated with WFA by ICC. This appeared to be more dramatic in the β3-HET cells (more fragments) than the WTs. Not only did the Vim-IFs collapse to the perinuclear region, but also the actin MFs appeared to be following in a similar pattern, although to a smaller degree. Indeed, Vim-IFs and MFs have been shown to cross-link directly, as well as being linked by Plec [436], [450]. In addition, WFA may be a binding partner of MFs (and MTs) exerting a more direct influence on them rather than via Vim [428]. The collapse of IFs following WFA treatment is in line with published findings and further illustrates the anti-angiogenic potential of this compound [428], [444]. Indeed, low dose WFA holds promise for the clinic with few adverse effects [420]. The impact of WFA on Vim disassembly has interesting implications in the context of angiogenesis. Vim-IFs bind integrins and regulate FA structure and function [385], [451], [452]. Endothelial Vim promotes adhesion strength by stabilising cell-ECM interactions [383]. This contributes to the proliferative and migratory characteristics of ECs participating in angiogenesis. In the WFA-treated cells Vim filaments do not reach the FAs and angiogenic processes are impaired [427], [453]. The literature suggests Vim (together with RACK1) promote angiogenesis via FAK upregulation and activation [446]. We saw an indication of that by WB, as there appeared to be less total FAK in the WFA-treated cells. If we had more time, we would explore FAK signalling in both WT and β3-HET IMMLECs post WFA treatment.

We observed a 40% depletion of Vim using siRNA by WB and a 20-fold decrease by qRT-PCR. The level of Vim knockdown observed by WB appears ineffective. This could explain a lack of phenotype in some of the random migration, VEGF-signalling assay and ICC experiments (not shown). A pool of 4 siRNAs was used to achieve Vim knockdown, which increases the chances of using the correct one. On the other hand, we have not deconstructed the pool and made sure whether all the siRNAs are working. With that in mind, we may be diluting the effective ones with the ineffective when using the pool. There are two other factors which could have contributed to this outcome – low transfection efficiency and high abundance of Vim filaments. On one hand, it is surprising not to see a phenotype when knocking-down such a ubiquitous protein, on the other, there may be substantial levels of this protein remaining in the cell after siRNA silencing.

This highlights the importance of researching a chosen candidate gene using multiple approaches. In our case, the use of Withaferin A (WFA) treatment, an inhibitor of Vim. Not surprisingly, experiments with WFA are more conclusive, as we can presume that all the treated cells are exposed to it, which is not necessarily the case with siRNA which needs to be successfully delivered to the nucleus. The caveat that we needed to consider when using WFA, is that it does not only target Vim-IFs, which has been extensively reviewed by Vanden Berghe *et al*. [454]. Briefly, it regulates MFs, MTs and a number of IFs, including Vim [427], [428]. It also impacts kinase activity, targets the proteasome complex, as well as regulating acetylcholine (neurotransmitter) availability [417], [455]–[457]. These actions have potential to regulate angiogenesis, inflammation, cell cycle and apoptosis [454]. All these effects are dose-dependent and there is hope for clinical use at the right dose, as an anti-inflammatory or anti-tumour growth agent. Indeed, the use of WFA-containing extracts in traditional Indian medicine for centuries suggests so. At the same time, it remains a good tool for studying Vim-IFs in the laboratory.

A number of additional experiments to complement this study could be conducted. Firstly, adhesion assays using WFA and cells with confirmed Vim, Nes and Plec knockdown. During angiogenesis, ECs sprout into and invade the surrounding tissue forming new blood vessels. Therefore, a more angiogenesis-relevant assay than the migration assays conducted here, would be the invasion assay. The assessment of migration directionality that we have attempted here is limited. A chemotactic assay could provide additional data on the subject. Similarly, the tube-formation assay, which relates to the blood vessel formation in angiogenesis could be used [458], [459]. Further analysis of VEGF-dependent-signalling, such as Akt, ERK, FAK, Pax and VEGFR2 phosphorylation patterns, especially with WFA in β3-integrin depleted cells, would greatly contribute to this study. Moreover, all these experiments could be repeated with double

heterozygous or double knockout EC lines, e.g. β3-HET Vim-HET, which we did not have the chance to do. Although, it could be argued that siRNA transfection and treatment with a compound (WFA) is a more-clinically relevant approach than a genetic depletion, as they are active forms of targeting, like administering a drug.

Endothelial Nes, Plec and Vim have been investigated by others in the context of angiogenesis. The novelty of our research is that we co-target these three IF proteins (individually) alongside β3-integrin. Some evidence has been provided here that co-targeting β3-integrin and Vim is a valid *in vitro* anti-angiogenic strategy. Some exciting observations have been made. WFA differentially inhibited migration and proliferation in the WT and β3-HET cells, more so in the latter. Disruption of the Vim network appeared to be more pronounced in the β3-HET ECs (a trend for more Vim fragments) compared to the WTs. These observations suggest that IFs in the β3-depleted cells are more sensitive to targeting than in the WTs in the context of angiogenesis. Targeting β3-integrin alone is subject to an escape mechanism. A part of that mechanism is the upregulation of the IF proteins – Nes, Plec and Vim, as discussed in the previous chapter. The data presented in this chapter is largely in favour of dual targeting of β3-integrin and IFs, a possible route to overcome this escape mechanism. However, more definitive proof is needed. To investigate this further, we needed additional tools and more sophisticated models and assays of angiogenesis.

5 Building and Use of Molecular Tools for Studying Intermediate Filament Proteins

5.1 Introduction

In Chapter 3, we identified three IF type proteins, namely nestin, plectin and vimentin, as potential mediators of the escape observed with long-term anti-angiogenic depletion of β3-integrin [275], [276]. All three IF proteins appear to play a role in angiogenesis [222], [410], [460]. We described our investigation of these IF proteins *in vitro* in WT and β3-HET ECs in the context of angiogenesis, in Chapter 4. Our focus was drawn towards vimentin, while Withaferin A (WFA), an inhibitor of vimentin, proved to be an invaluable tool for our experiments [428].

We wanted to go beyond *in vitro* models and conduct experiments that are more clinically relevant than the work discussed in Chapter 4. Given our disappointing results with siRNA-mediated targeting of the proteins (chapter 4), we hypothesised we might achieve a more long-lasting depletion of each IF, if we took an shRNA approach. At the same time, we wanted to keep our focus on the endothelium. We realised we could do this by combining the endothelial-specific Pdgfb.Cre mouse model with the pSico technology of target depletion in the *ex vivo* aortic ring sprouting assay [461], [462]. First, we needed to build the pSico constructs, by inserting shRNA-encoding sequences against our genes of interest into the pSico backbone [463]. We then packaged these constructs into lentiviral particles for use in the Cre-inducible background. Also, we generated pSicoR plasmids, corresponding to some of the pSico constructs, i.e. containing the same shRNA. These could be utilised for testing the efficacy of the shRNA in easy-to-use cell lines, without the presence of Cre recombinase [463]. The first part of this chapter describes our efforts in generating and testing pSico and pSicoR constructs. The use of these constructs in the aortic ring assay is covered in the next chapter, section 6.3.1.

In addition, we wanted to investigate nestin in ECs and its interaction with FAs. We were unsuccessful with all the commercially available antibodies against nestin that we attempted in WB and ICC. Therefore, we also set out to generate constructs expressing dsTomato-labelled nestin that we planned to utilise in ICC. Our efforts in making, testing and using nestin constructs are described in the second part of this chapter. Thus, this chapter's focus is on the work related to molecular tools, which we generated in-house, for studying IF proteins in the endothelium.

5.2 Materials and Methods

5.2.1 General Molecular Biology Methods

5.2.1.1 Transformation of Plasmid DNA

Plasmid DNA was introduced into either One Shot™ Stbl3™ (pSico cloning) or One Shot™ OmniMAX™ 2-T1 (Nestin-Tomato) chemically competent *E. coli* (Invitrogen) by the heat-shock method according to manufacturer's protocol. Bacterial vials were thawed on ice, 20 – 50 ng of plasmid DNA was added, and the vials were incubated for 30 min on ice. The bacterial cells were subjected to heat-shock at 42°C for 45 secs and placed back on ice for 2 min. Next, the vials were incubated on a shaker for 1 hour at 37°C at 225 rpm with 250 µL of S.O.C. medium. 100 µL of the transformation mix was spread onto 1.5% agar plates (including selection pressure), such that a few sequential levels dilution of bacterial suspension were achieved. Plates were inverted and incubated and 37°C o/n.

5.2.1.2 Bacterial Culture

Single bacterial colonies were picked, using a sterile pipette tip, and grown in sterile lysogeny broth (LB) inside a shaking incubator (Innova 4330, New Brunswick Scientific, Cambridge) at 37°C at 180 rpm o/n.

LB broth was prepared by dissolving 25 g of high salt broth mix (Melford Laboratories, Ipswich), which consists of tryptone, NaCl and yeast extract at a 2:2:1 ratio, in 1 L of distilled water sterilised by autoclaving. To prepare agar plates, 15 g/L of agar (Thermo Fisher) was added to the broth then autoclaved. It was cooled down to approximately 60°C, poured into petri dishes and allowed to set for 30 min inside a laminar flow hood. Plates were covered and stored in air-sealed containers at 4°C. When required, ampicillin was used for selection by adding 100 µg/mL to either the growth medium or to the agar solution prior pouring into plates.

5.2.1.3 Plasmid Preps

Plasmids were isolated from bacterial cultures using kits from Qiagen® (Manchester). To generate a Mini prep, 2.5 mL of an o/n bacterial culture was centrifuged at 8000 g for 3 min and the pellet was resuspended in buffer containing RNase A. SDS-based lysis buffer was then added to the pellet, followed by a neutralization buffer, which precipitates SDS-bound cell debris. After

centrifugation at 18’000 g, the supernatant was applied to a plasmid-DNA-binding spin column. The column was then washed with isopropanol- and ethanol-based buffers. Finally, the column was dried by brief centrifugation and plasmid DNA eluted using 30 – 50 µL 10 mM Tris-HCl pH 8.5 buffer.

As recommended by the manufacturer’s protocol, for high-copy plasmids, 25 mL of an o/n bacterial culture was used for a Midi prep and 100 mL for a Maxi prep. The transformed bacteria were spun down at 6000 g at 4°C for 15 min then lysed in the same way as a plasmid mini prep. The lysate was centrifuged at 14’000 g for 45 min. The supernatant was filtered through an equilibrated DNA binding tip, which was washed, and the plasmid DNA was eluted in a pre-warmed buffer containing 1.25 M NaCl, 50mM Tris-Cl pH 8.5 and 15% isopropanol. DNA was precipitated by adding 0.7 volumes of isopropanol and centrifuged. To purify the prep, the precipitation and centrifugation steps were repeated with 70% ethanol. The pellet was dried and resuspended in 200 – 1000 µL of TE buffer (10 mM Tris-HCl pH 8.0, 1 mM EDTA).

Plasmid DNA concentration and quality was determined using a NanoDrop™ 1000 spectrophotometer (Section 4.2.2).

5.2.1.4 Restriction Digests

Restriction enzymes used are listed in **Table 5.1** below. All enzymes and buffers were obtained from New England Biolabs (Hitchin), except buffer D (Promega, Southampton). 0.2 – 1 µg of DNA was digested in the presence of an appropriate buffer for 1 hour at 37°C. The reaction was inactived by heating to 65°C for 15 min or by the addition of 6X gel loading dye (New England Biolabs).

Table 5.1 List of restriction enzymes

Enzyme	cut site	working conc. (U/µL)	buffer	plasmid	catalogue number
HpaI	GTT^_AAC	0.3	CutSmart	pSico, pSicoR	R0105S
XhoI	C^TCGA_G	0.4	CutSmart	pSico, pSicoR	R0146S
SacII	CC_GC^GG	0.8	D	pSico	R0157S
NotI	GC^GGCC_GC	0.2	D	pSico	R0189S
XbaI	T^CTAG_A	0.4	CutSmart	pSicoR	R0145S
KpnI	G_GTAC^C	0.75	2.1	Tomato-Nestin	R0142S
SalI-HF	G^TCGA_C	1	2.1	Tomato-Nestin	R3138S
HindIII	A^AGCT_T	0.5	2.1	Tomato-Nestin	R0104S

"^" indicates the cut site, "_"is the cut site on the complementary strand

5.2.1.5 Sequencing

As recommended by Ventura *et al.,* the pSico sequencing primer used was: 5'-CAAACACAGTGCACACCACGC and the pSicoR primer was: 5'-TGCAGGGGAAAGAATAGTAGAC [463].

The nestin construct sequencing was initiated from within the cDNA insert outwards to confirm if ligations were successful. A forward primer Nes3'seqF (5'-AGCAAGTGAATGGGAGGATG) which bound ~170 bp upstream of the 3' end of the insert and a reverse primer Nes5'seqR (5'-ACCTCAGCCTCGTGCTTCT) ~250 bp downstream of the start codon were used. Primers Nes3'seqF and Nes5'seqR were picked using Primer3Plus online software (Andreas Untergasser and Harm Nijveen).

Sanger sequencing was carried out by Cambridge BioScience (Cambridge) and Eurofins (Ebersberg, Germany). Samples were prepared according to the specific requirements of each company.

5.2.2 Building shRNA Constructs against Nestin, Plectin and Vimentin

5.2.2.1 Oligo Design and Annealing

shRNA oligos were designed using pSicoOligomaker 1.5 [463]. The target sequence was inserted into the "sequence" window and a cut-off value of 6 (on a scale of -2 to 9) was selected. The score was based on criteria according to Reynolds *et al.* [464]. An oligo with a score of 7 or higher has a 90% chance of silencing the target mRNA [464]. Highest scoring 19-mers found by the program were selected and used to generate sense and anti-sense oligos, according to the following formula: sense – 5'-T-19mer-TTCAAGAGA-19merRevComp-TTTTTTC and anti-sense – 5'-TCGAGAAAAAA-19mer-TCTCTTGAA-19merRC-A, where '19merRC' means reverse complement of the 19-mer.

Oligos were annealed as described by Ventura *et al.* [463]. 23 µL of 2X Annealing buffer (200 mM potassium acetate, 60 mM HEPES-KOH pH 7.4 and 4 mM magnesium acetate) was combined with 25 µL nuclease-free water and 1 µL of sense, and 1 µL anti-sense oligos (both 100 µM). The reaction on the thermocycler was as follows: denaturation at 95°C, annealing at 70°C for 10 min and slow cooling to 4°C.

5.2.2.2 Plasmid Generation

Molecular cloning strategy was performed according to Ventura *et al.*'s [463] guidelines. Backbone plasmids pSico and pSicoR, based on the pLL3.7 Lentilox created by Rubinson *et al.* [465], were obtained from (Addgene, Cambridge, US). HpaI-XhoI digested plasmids were ligated with annealed oligos (Section 5.2.2.1) using T4 DNA ligase (New England Biolabs, Hitchin) for 3 hours at RT or 16°C o/n and transformed into One Shot™ Stbl3™ competent bacteria, as described in Section 5.2.1.1. Transformations were plated, with single colonies picked aseptically and expanded in 3 mL ampicillin-containing-LB o/n for plasmid mini preps. Once isolated, plasmids underwent SacII-NotI (pSico) or XhoI-XbaI (pSicoR) test digest. Successful cloning resulted in a 50 bp larger fragment when run a 2% agarose gel (Section 2.9). To verify insertions were correct, Sanger sequencing was performed. Once insertions were verified, cultures were set up for Midi or Maxi plasmid preps as outlined in Section 5.2.1.3.

5.2.2.3 Lentivirus Production

Lentivirus was generated using Invitrogen's ViraPower™ Packaging Mix in HEK293FT cells according to manufacturer's protocol. HEK293FT cells were seeded at a density of 5 x 10^6 into a 10 cm plate and incubated o/n at 37°C. Prior to transfection, cell culture medium was replaced with serum-containing Opti-MEM™ without antibiotics. A lipofection mixture was prepared containing 9 µg ViraPower™ (from where), 3 µg shRNA construct (from where) and 36 µL of Lipofectamine™ 2000 (Invitrogen) in Opti-MEM™, which was added dropwise to the cells, followed by an o/n incubation at 37°C. Medium was replaced with complete culture medium without antibiotics then the cells were incubated for a further 48 – 72 hours. Virus was harvested and filtered through a 0.45 µm syringe filter. Clarified viral suspension was combined with the Lenti-X™ Concentrator (ClonTech, Saint-Germain-en-Laye, France) at a 3:1 ratio and incubated at 4°C o/n. This was followed by a centrifugation at 1500 g for 45 min at 4°C. The supernatant was discarded, and the lentiviral pellet resuspended in 1 mL of Opti-MEM™ and stored at -80°C until required for IF protein depletion.

5.2.2.4 Lentiviral Transfection into Cells

The lentiviral prep as described in Section 5.2.2.3 was pseudo-titrated based on its efficacy of infecting HEK293FT cells, as reported by the presence of GFP positive cells. Cells were seeded at 2 x 10^4 per well in 6-well plates, incubated at 37°C o/n then infected with 2, 4, 8, 16, 32 or 64 µL of concentrated virus in the presence of 8 µg/mL polybrene, to increase transduction efficiency. Wells were photographed 48 hours post-transfection in the FITC channel and the percentage of green cells was calculated.

As described in Section 2.2, MLECs were isolated then grown in tissue culture flask coated with gelatin, collagen I and FN. To positively sort the ECs by MACS, the rat anti-mouse endomucin Ab (clone V.7C7, Santa Cruz Biotechnology, Dallas, US) was used. Cells were cultured in MLEC medium (Section 2.2).

Pdgfb+ primary lung ECs were seeded at 2 x 10^5 cells per well into 6-well plates in 2mL MLEC medium and incubated at 37°C for 24 hours. These were infected with 100 µL of inducible-shRNA lentivirus in the presence of 8 µg/mL polybrene and incubated o/n. Medium was changed back to MLEC and cells were incubated for a further 48 hours. At this point, cells were checked for GFP expression and medium was supplemented with 1 µM 4-hydroxytamoxifen (OHT) to induce Cre recombinase and thus activate shRNA expression, which is reported by the loss of green fluorescence in the Pdgfb+ cells. Cells were lysed 72 hours later in EB buffer for WB analysis, as described in Section 2.4.

5.2.3 Nestin Overexpression Plasmids

5.2.3.1 Primer Design

Primers were picked based on the nestin cDNA sequence Nes-201 (ENSMUST00000090973.11) obtained from the online e!Ensembl (EMBI-EBI, Hinxton) database using Primer3Plus online software. The primers consisted of 6 random nucleotides, followed by a restriction site and a *Nestin* target sequence (6R-RS-NesSeq). The SalI restriction site (GTCGAC) was embedded in the forward primer for the pTom-C-Nes construct (F.C1) and the common reverse primer (R), whereas the forward pNes-N-Tom primer contained a HindIII site (AAGCTT). The forward primers spanned the *Nestin* ATG start codon, while the reverse primer was bound 25 bp upstream of the stop codon. The resulting primers were as follows:

F.C1: 5’-ATCGTA-GTCGAC-AGCGACATGGAGGGTTGC

F.N1: 5’-ATCGTA-AAGCTT-AGCGACATGGAGGGTTGC

R: 5'-ACTGTA-GTCGAC-TCTCCATCTACCCCACTCAGA

5.2.3.2 Nestin PCR

All PCR reagents for the nestin work were obtained from Invitrogen. The PCR and electrophoresis were run according to Section 2.9 however, the reaction mixture for nestin PCR contained 25 µL of Platinum SuperFi Green PCR Master Mix (2X), 9 µL of nuclease-free water, 10 µL of SuperFiGC Enhancer (5X), 1 µL of neat cDNA, primer R and either primer F.C1 or F.N1. All three primers were used at a final concentration of 0.5 µM and both PCRs gave rise to a 5588 bp DNA fragment. The PCR program used was as follows: 98°C for 30 sec; 35 cycles of 98°C for 10 sec, 62°C for 10 sec and 72°C for 3 min; and 72°C for 5 min.

5.2.3.3 Nestin Plasmid generation

The majority of this work was done using the TOPO™ XL-2 PCR Cloning kit (Invitrogen). RNA was isolated from IMMLECs and mRNA was reverse-transcribed into cDNA (Section 4.2.2). Primers were designed (Section 5.2.3.1) then used to amplify nestin cDNA by PCR (Section 5.2.3.2). Nestin DNA was purified from the PCR reaction using the PureLink Clean-up kit (Invitrogen). Backbone plasmids tdTomato-C1 and tdTomato-N1 were obtained from Addgene (Cambridge, US). At this stage, we made use of a naturally occurring KpnI site, which resides 63 bp upstream of the R primer within the nestin sequence. The C1 plasmid and F.C1-amplified nestin cDNA were

digested with SalI-HF and KpnI restriction enzymes (New England Biolabs, Hitchin) and subsequently ligated together using T4 DNA ligase (New England Biolabs). Similarly, the N1 vector and the F.N1-amplified cDNA were cut with HindIII and SalI-HF (New England Biolabs), and ligated. The resulting pTom-C-Nes and pNes-N-Tom plasmids were transformed into One Shot™ OmniMAX™ competent bacteria (Invitrogen). This was followed by plating out on kanamycin-selective agar; and single resistant colonies were picked and expanded for plasmid mini preps (as in Section 5.2.1.3). The latter were HindIII digested then run on a 1% agarose gel (as in Section 2.9), where a doubling in size from 5.5 to 11 kbp reported a successful recombination. Plasmids with insertions were purified from the PCR reaction as the nestin DNA (above) and sequenced, as described above (Section 5.2.1.5). Small cultures were then expanded for maxi preps and used for nestin localisation studies.

5.2.3.4 Immunocytochemistry with Labelled Nestin and Vimentin

We transfected the IMMLECs with 10 µg of plasmid DNA, as described in Section 2.3. For ICC with the pTom-C-Nes and pNes-N-Tom plasmids, transfected cells were fixed 48 hours post-transfection and all other steps were carried out as described in Section 2.8. For ICC using the pmCherry-Vim plasmid, 48 hours post-transfection, cells were treated with 0.5 µM WFA or DMSO for 5 hours and adhered in the presence of WFA or DMSO. All other steps were as in the protocol in Section 2.8.

5.3 Results

5.3.1 Generation of pSico and pSicoR plasmids

As explained in the previous chapters, nestin, plectin and vimentin were our chosen targets to pursue, as potential mediators of the escape mechanism arising due to long-term depletion of β3-integrin. Guided by Ventura *et al.*, we set out to generate pSico shRNA constructs against the three IF proteins (Section 5.2.2) [463]. To increase our chances of successfully depleting expression of the targets, we generated two constructs per target.

All three genes have multiple protein-coding splice variants of different lengths. Mouse Nes gene encodes two of these, Vim encodes 3, while Plec encodes 20 (**Table 5.2**). Every effort was made to ensure the shRNA oligos targeted as many variants as possible. The shRNA oligo pairs Nes1 and Nes2 bind within both Nes gene splice variants (**Table 5.3**). The Plec shRNA oligo pairs (Plec1 and Plec2) target 18 out of 20 variants, while omitting only 2, very short splice variants, i.e. Plec-219 and 220 (**Table 5.3**). The Vim1 oligo pair targets the 5' untranslated region (UTR), whereas the Vim2 pair binds within exon 3. These both bind two of the three variants as shown in **Table 5.3**. In the case of the Vim shRNA target sequences, we had to compromise on the number of variants targeted in exchange for a higher oligo score.

The shRNA oligos were generated using the pSicoOligomaker software and aligned, as described in Section 5.2.2.1. Target sequences chosen for shRNA generation all scored 7 or higher (**Table 5.3**), while the location of the target sequence was also considered, as described above. The full, final oligo sequences used are presented in **Table 5.4**, with the target sequences underlined.

Table 5.2 Summary of protein coding splice variants of the genes of interest

Gene name	Ensembl Gene Ref.	Splice Variant	Number of exons	Length in amino acids
Nes	ENSMUSG00000004891	Nes-201	4	1864
		Nes-203	5	1820
Plec	ENSMUSG00000022565	Plec-201	32	4543
		Plec-202	33	4548
		Plec-203	32	4521
		Plec-204	32	4550
		Plec-205	33	4691
		Plec-206	32	4534
		Plec-207	32	4686
		Plec-208	34	4386
		Plec-209	34	4589
		Plec-212	17	661
		Plec-213	19	676
		Plec-214	19	702
		Plec-215	32	4511
		Plec-216	18	499
		Plec-217	32	4386
		Plec-218	32	4543
		Plec-219	4	43
		Plec-220	4	53
		Plec-221	32	4386
		Plec-222	21	964
Vim	ENSMUSG00000026728	Vim-201	9	466
		Vim-202	1	134
		Vim-206	8	427

Adapted from e!Ensembl © EMBL-EBI

Table 5.3 shRNA oligos for pSico constructs

shRNA	Target sequence	Score	Target region	Targeted splice variants	Omitted splice variants
Nes1	GTCTGGAAGTGGCTACATA	7	Exon 2	Nes-201 and 203	none
Nes2	GGAAGAAGATGCTGATGAA	8	Exon 4	Nes-201 and 203	none
Plec1	GGCCTCATCTGGACAATCA	7	Exon 5	Plec-201-209, 212-218, 221 and 222	Plec-219 and -220
Plec2	GGAGAACCAGCGTCGAATA	7	Exon 14	Plec-201-209, 212-218, 221 and 222	Plec-219 and -220
Vim1	GGATCGCTTTACTCAACTT	7	5'UTR	Vim-201 and -202	Vim-206
Vim2	GAAGAAACTGCACGATGAA	7	Exon 3	Vim-201 and -206	Vim-202

5'UTR – 5' untranslated region. Adapted from e!Ensembl © EMBL-EBI

Table 5.4 Full sequences of shRNA oligos for pSico constructs

oligo	Sequence
Nes1 Fwd	T**GTCTGGAAGTGGCTACATA**TTCAAGAGA**TATGTAGCCACTTCCAGAC**TTTTTTC
Nes1 Rev	TCGAGAAAAAA**GTCTGGAAGTGGCTACATA**TCTCTTGAA**TATGTAGCCACTTCCAGAC**A
Nes2 Fwd	T**GGAAGAAGATGCTGATGAA**TTCAAGAGA**TTCATCAGCATCTTCTTCC**TTTTTTC
Nes2 Rev	TCGAGAAAAAA**GGAAGAAGATGCTGATGAA**TCTCTTGAA**TTCATCAGCATCTTCTTCC**A
Plec1 Fwd	T**GGCCTCATCTGGACAATCA**TTCAAGAGA**TGATTGTCCAGATGAGGCC**TTTTTTC
Plec1 Rev	TCGAGAAAAAA**GGCCTCATCTGGACAATCA**TCTCTTGAA**TGATTGTCCAGATGAGGCC**A
Plec2 Fwd	T**GGAGAACCAGCGTCGAATA**TTCAAGAGA**TATTCGACGCTGGTTCTCC**TTTTTTC
Plec2 Rev	TCGAGAAAAAA**GGAGAACCAGCGTCGAATA**TCTCTTGAA**TATTCGACGCTGGTTCTCC**A
Vim1 Fwd	T**GGATCGCTTTACTCAACTT**TTCAAGAGA**AAGTTGAGTAAAGCGATCC**TTTTTTC
Vim1 Rev	TCGAGAAAAAA**GGATCGCTTTACTCAACTT**TCTCTTGAAAAG**TTGAGTAAAGCGATCC**A
Vim2 Fwd	T**GAAGAAACTGCACGATGAA**TTCAAGAGA**TTCATCGTGCAGTTTCTTC**TTTTTTC
Vim2 Rev	TCGAGAAAAAA**GAAGAAACTGCACGATGAA**TCTCTTGAA**TTCATCGTGCAGTTTCTTC**A

Target sequences and their complementary sequences are in bold and underlined.

Aligned oligo pairs (Nes1, Nes2, Plec1 etc.) were ligated with the pSico (**Fig 5.1A**) and pSicoR backbone plasmids cut with the HpaI and XhoI restriction enzymes (**Fig. 5.1 B** and **C**). In both cases the HpaI site is lost, as this enzyme leaves a blunt end, whereas the XhoI site (the sticky end) is reconstituted after insertion of the oligo. The pSico backbone plasmid contains an ampicillin resistance gene for selection of transformed bacterial colonies and cytomegalovirus (CMV)-promoter-driven enhanced green fluorescent protein (EGFP) gene (**Fig 5.1A**). The CMV-EGFP fragment is flanked by two loxP sites (floxed) followed immediately by the shRNA-insertion site (**Fig. 5.1B**) and a U6 promoter upstream of the first loxP site. The pSicoR plasmid differs from the pSico with respect to the position of the shRNA-insertion site. It resides within the floxed region (**Fig 5.1C**). Induction of Cre activity in the pSico plasmid results in the removal of the floxed region (the EGFP gene) which brings the shRNA insert within reach of the U6 promoter, thus allowing for its expression (**Fig 5.2 A**). Induction of Cre activity in the pSicoR plasmid removes both the EGFP gene and the shRNA. However, we did not plan to use pSicoR in combination with the Cre recombinase, only in its full form (**Fig 5.2 B**), as a means of testing the efficiency of the shRNA constructs, without a need for Cre activity.

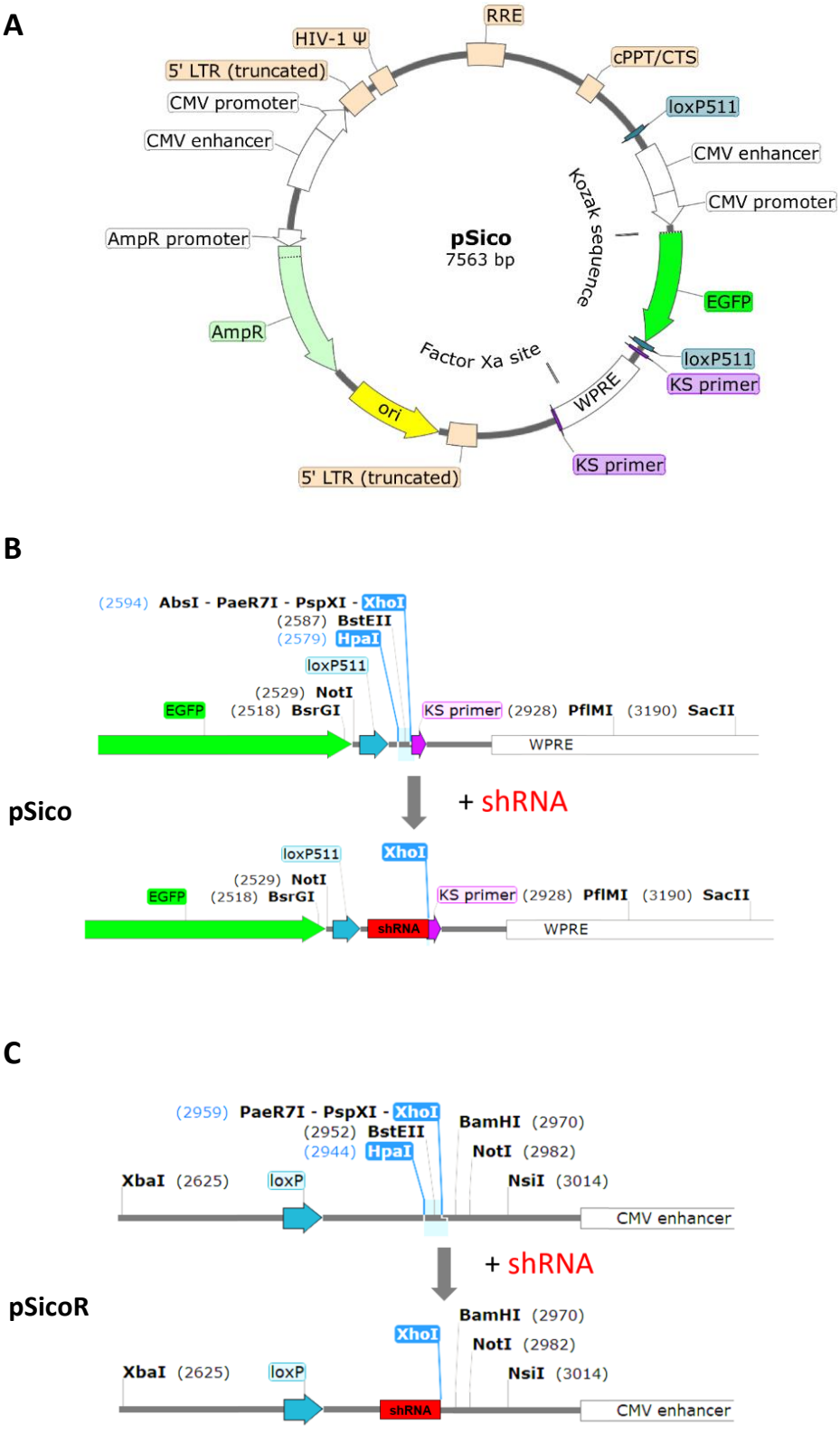

Figure 5.1 Engineering pSico and pSicoR plasmids.

(**A**) pSico backbone contains an ampicillin resistance cassette (AmpR), and a floxed (loxP511) CMV-driven EGFP gene. (**B**) The shRNA sequence was inserted in the pSico and (**C**) pSicoR plasmids using HpaI and XhoI restriction enzymes. Plasmid map in A was downloaded from the Addgene Plasmid Repository (Plasmid #11578) website and adjusted using SnapGene Viewer and used to generate sequence maps in B and C.

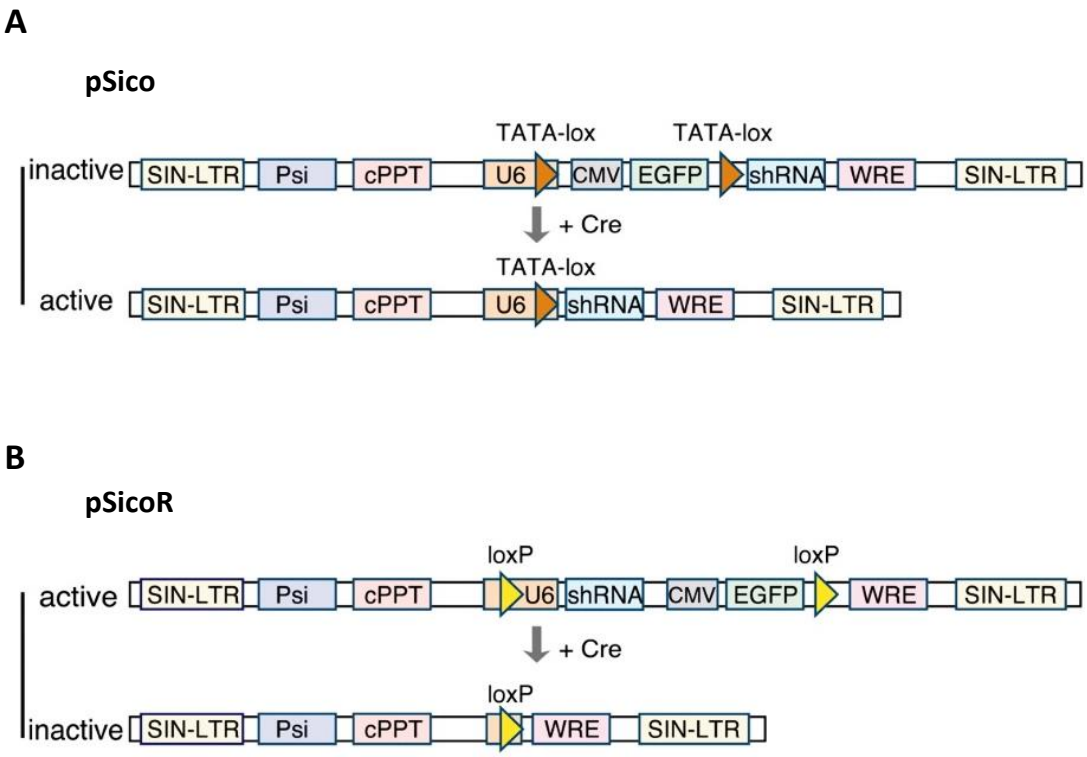

Figure 5.2 Cre activity in the pSico and pSicoR plasmids.

(**A**) The shRNA sequence is inserted into the pSico plasmid outside of the floxed region, while Cre activity removes EGFP and brings shRNA near the U6 promoter, thus activating it. (**B**) In the pSicoR plasmid, the shRNA sequence is inserted into the floxed region with Cre activity removing both EGFP and shRNA. Adapted from Ventura et al [463].

The backbone plasmids were digested with HpaI and XhoI (double digest, DD) in preparation for accepting the insert. Single digests of the pSico plasmid (HpaI only or XhoI only) were conducted alongside, to ensure both enzymes were cutting. Both DD and single digests were run on a 1% agarose gel to confirm cutting (**Fig. 5.3 A**). Linearised (cut) plasmid appears smaller than an open circular (nicked) plasmid, but larger than a supercoiled plasmid in agarose gel electrophoresis.

As a method for screening ampicillin resistant colonies and identifying those colonies producing a plasmid with the correct insertion, we conducted test digests on plasmid Mini preps post-ligation. These were SacII + NotI digests for the pSico plasmids or XhoI + XbaI for the pSicoR plasmids. The correct insertions resulted in a ~40bp-longer DNA fragment, when run on a 2% agarose gel (**Fig. 5.3 B** and **C**). Plasmids containing insertions were sequenced for confirmation. Examples of desired sequencing reads are shown in **Fig. 5.4** (pSico) and **Fig. 5.5** (pSicoR). Approximately eighty pSico colonies were screened with a test digest, fourteen of which contained an insert, resulting in a 20% success rate at this stage. In the process of making of the pSicoR plasmids the accuracy at this stage was 25%. On average, 65% of plasmids seen in the test digest to contain an insertion were shown to be correct by sequencing. In summary, six pSico plasmids were generated, using all the shRNA oligo pairs (Nes1, Nes2, Plec1, Plec2, Vim1 and Vim2), as well as two pSicoR plasmids (Nes1-R and Vim1-R). The corresponding colonies were expanded for Maxi Preps. pSicoR constructs were intended for transfection into cells in the plasmid form. pSico plasmids were taken forward for lentiviral packaging in HEK293FT cells as described in Section 5.2.2.3.

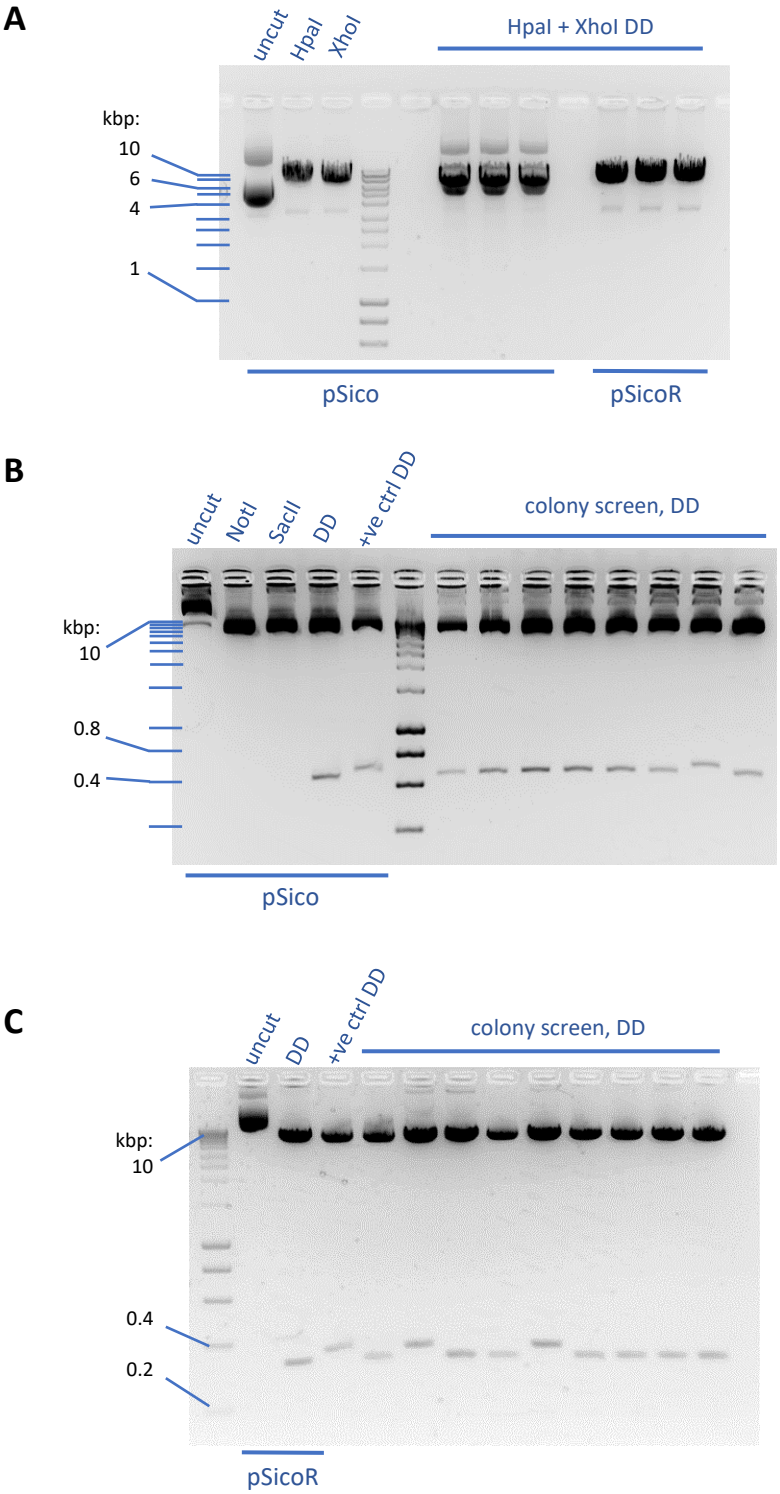

Figure 5.3 Restriction digests in the process of generation of pSico and pSicoR Plasmids.

(**A**) 1% agarose gel of a backbone digest using HpaI and XhoI, in preparation for the insert. (**B**) Example 2% agarose gel of a colony screen using a NotI + SacII test digest of pSico plasmids. Controls are shown on the left of the ladder and 8 putative nestin shRNA pSico plasmid DD's to the right, with an insertion in the 2nd to last lane. (**C**) An example 2% agarose gel showing a test digest of pSicoR plasmids using XhoI and XbaI: 3 control lanes, followed by 9 putative plectin shRNA pSicoR plasmids, with 2nd and 5th colony containing and insertion (higher band). DNA ladder used – HyperLadder™ I, Bioline, London. DD – double digest.

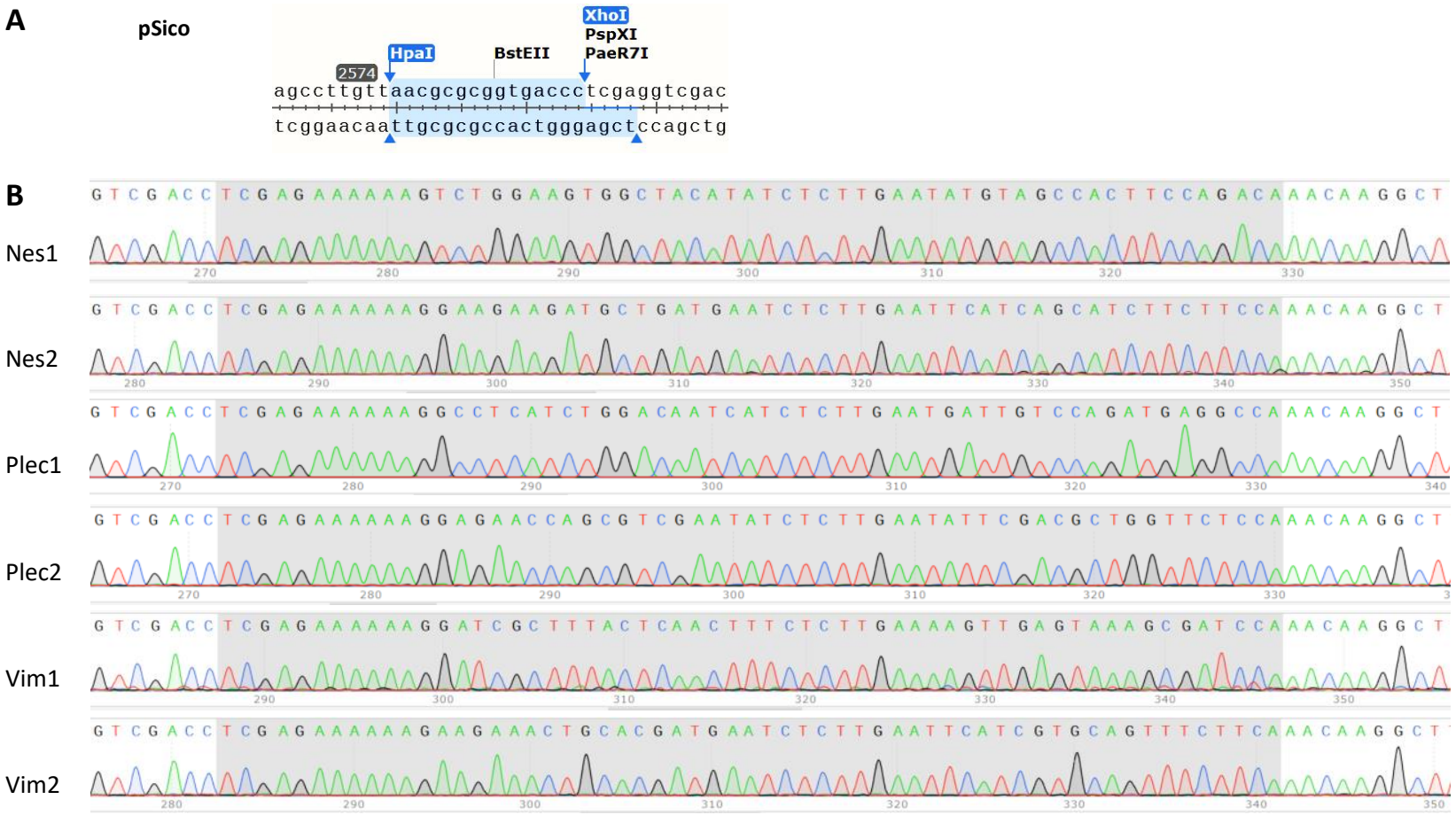

Figure 5.4 Confirmation of shRNA Insertions into pSico Plasmids by Sequencing.

(**A**) pSico backbone sequence near the insertion site, with the fragment removed by HpaI + XhoI digest highlighted. (**B**) pSico plasmid preps were sequenced using a reverse primer that bound downstream of the insertion site. Sequencing reads are showing the anti-sense strand, with shRNA oligos highlighted in grey. Generated using SnapGene Viewer.

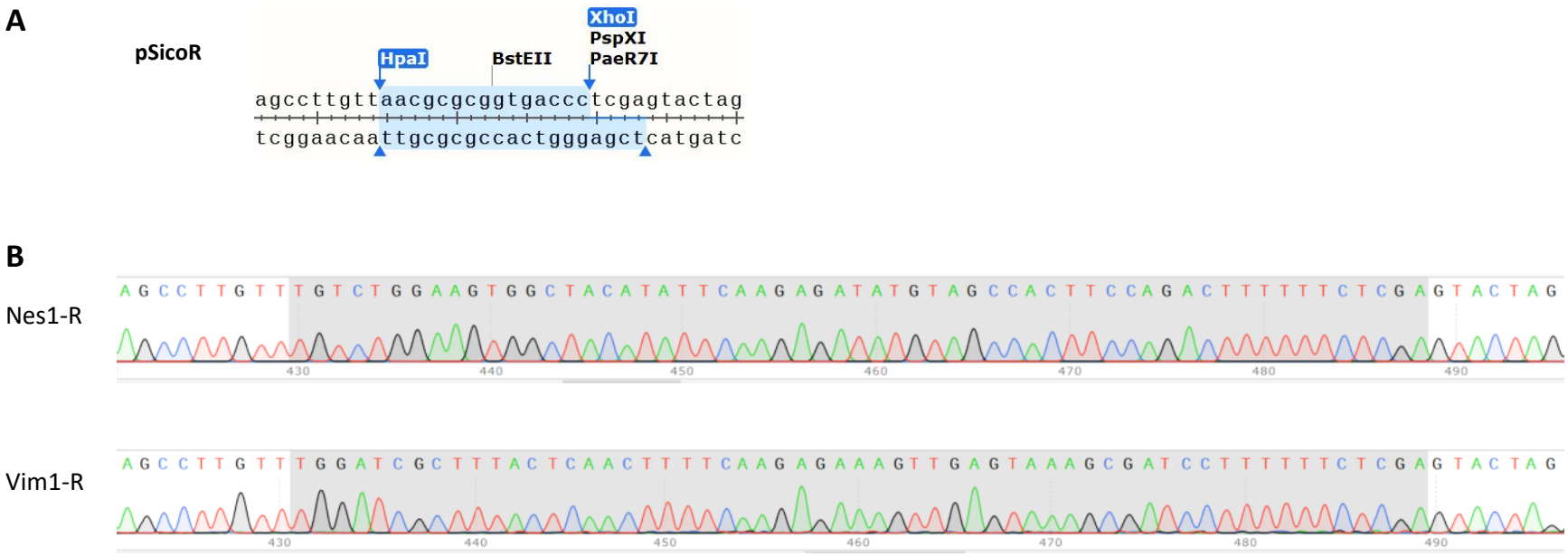

Figure 5.5 Confirmation of shRNA Insertions into pSicoR Plasmids by Sequencing.

(**A**) pSicoR backbone sequence near the insertion site, with the fragment removed by HpaI + XhoI double digest, highlighted in blue. (**B**) pSicoR plasmids were sequenced using a forward primer, thus the sense strand is shown. shRNA oligos are highlighted in grey. Generated using SnapGene Viewer.

5.3.2 Testing shRNA constructs

Upon completion of the pSico lentiviral preps, the next step was to determine the optimal experimental dose. Therefore, a pseudo-titration in HEK293 cells was carried out. We infected HEK cells as described in Section 5.2.2.4. The preps were identical in the amounts of reagents used and we did not observe a significant variation in the percentage of infected (green) HEK293 cells in the pseudo-titration, except for VEGFR2 which had a lower transduction efficiency (55% with 64 µL) compared to the rest of the preps that were tested (70 – 90% with 64 µL) (**Fig 5.6**). At 72 hours post-transfection the majority of HEK cells transfected with 16 µL of any of the virus prep were green, while at 96 hours, 8 µL was enough the turn most of the cells green (data not shown). Primary cells can be expected to be more difficult to infect than HEK cells. Therefore, taking all of the above in to account, we decided that using 100 µL of concentrated virus prep per well in a 6-well plate was an appropriate amount to use in the experiments that were to follow. Although the preps exhibited some variation in transduction efficiency (VEGFR2), they were all deemed equivalent, including the preps that were not pseudo-titrated (Nes2, Plec1 and Vim1).

We went on to assess the efficiency of the lentiviral preps on primary ECs by their ability to turn the cells green and achieve knock-down of the desired targets at the protein level. Primary mouse lung ECs (MLECs) were isolated, as described Section 2.2 from Pdgfb.Cre (OHT inducible Cre) mice and infected with the lentiviral pSico preps, as outlined in Section 5.2.2.4. Images of cells were taken at 48 hours post-infection to observe the EGFP signal, as a confirmation for successful introduction and expression of the pSico constructs. Indeed, many of the primary cells turned green, but many did not (**Fig. 5.7 A**). The isolation protocol includes cell sorting using magnetic beads to sort for ECs. The magnetic beads used for cell sorting were still attached to the EGFP expressing cells at 48 hours post-transfection, which suggests their endothelial identity. At this point, we induced Cre expression by the addition of OHT to activate shRNA expression (**Fig. 5.2 A**). Cells were cultured for a further 72 hours. At the point of lysis (T120), some of the cells were still green. Cells were then lysed, and target depletion was assessed by WB (**Fig. 5.7 B**). Unfortunately, we did not observe Plec, Vim or VEGFR2 depletion in the primary cells by WB. We were unable to assess Nes depletion by WB, as the three Abs we used showed either non-specific bands or no bands at all.

A

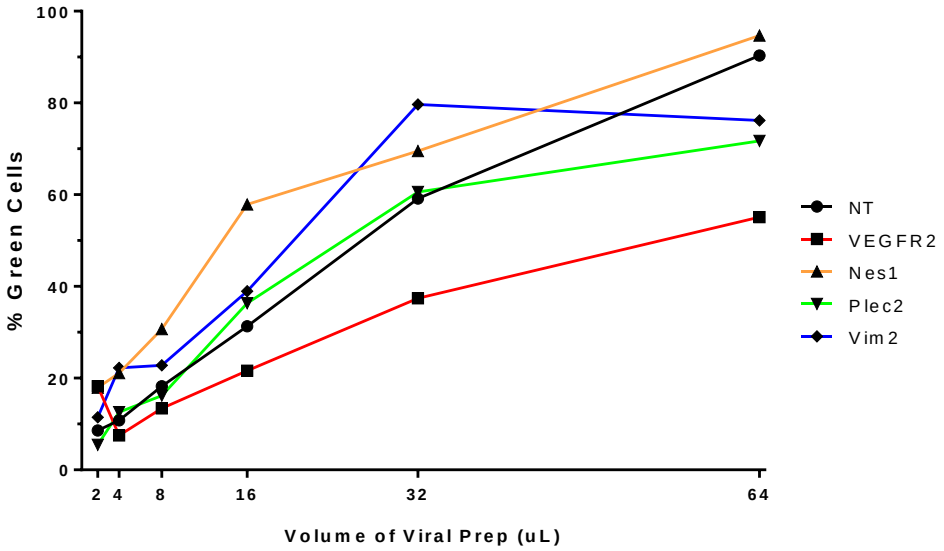

B

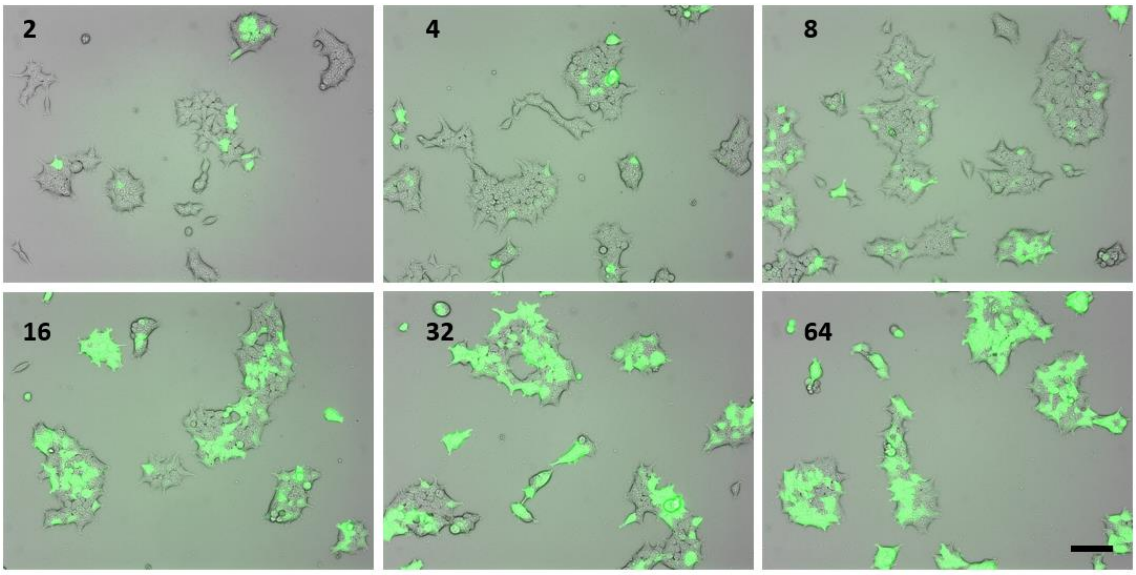

Figure 5.6 Pseudo-titration of pSico Lentiviral Preps in HEK cells.

10^5 HEK293 cells were seeded in 6-well plates and incubated o/n. On day 2, cells were infected with 2, 4, 8, 16, 32 or 64 µL of neat, concentrated virus prep per well. 48 hours later, a representative image of each well was taken in the brightfield and green channel at same coordinates. (**A**) The two channels were subsequently merged, green cells counted and % infected (green) cells was calculated for each condition. (**B**) Representative images of HEK293 cells infected with Nes1 pSico lentivirus. Scale bar = 100 µm.

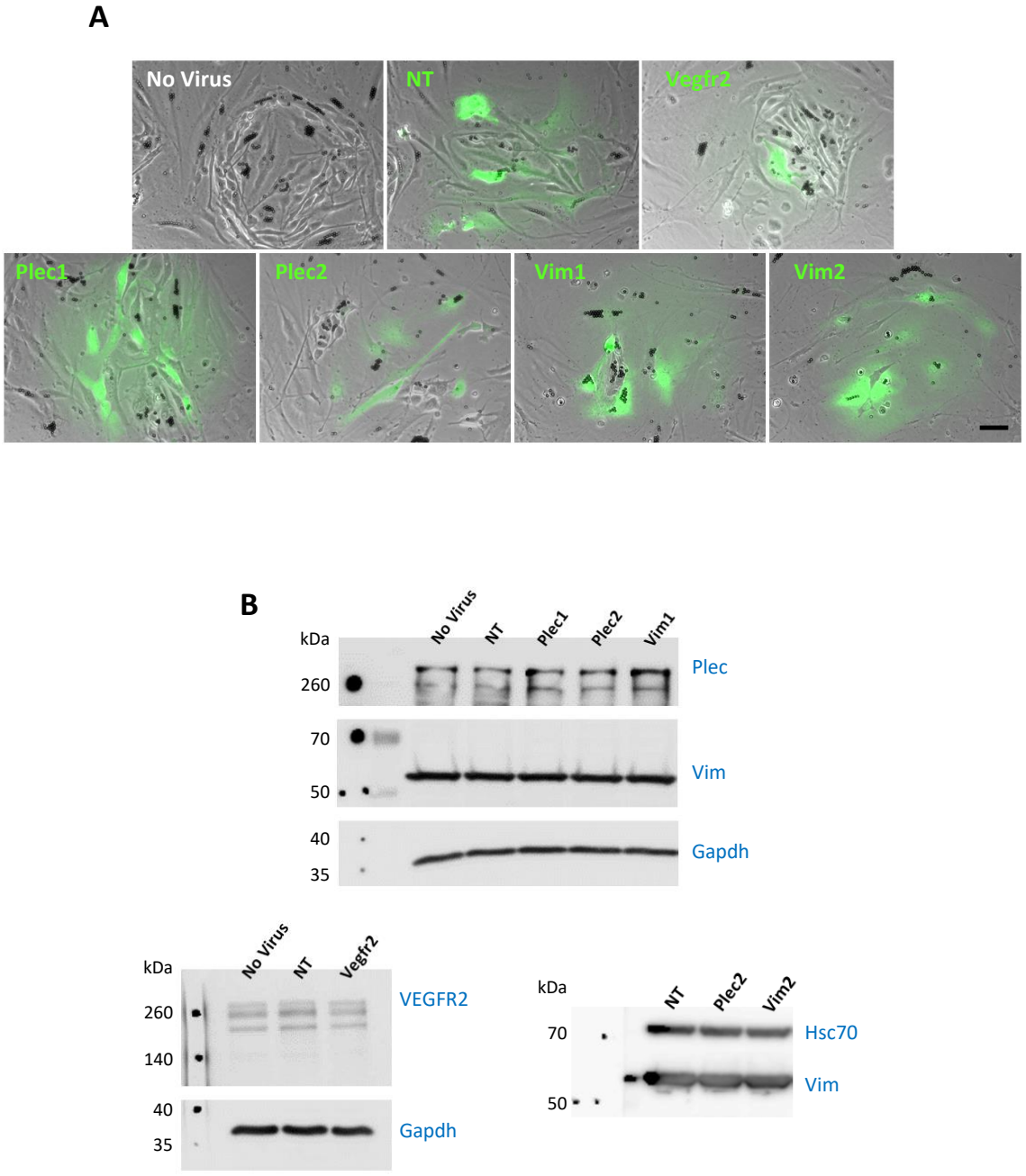

Figure 5.7 Introducing shRNA constructs into Primary ECs.

Primary lung ECs were isolated and infected with lentivirus containing pSico shRNA constructs against VEGFR2, Plec, Vim or non-targeting (NT). (**A**) After 48 hours, images were taken at 20x magnification in both the brightfield and green channel, then merged. Scale bar = 50 µm. (**B**) To induce shRNA expression, OHT was added to the cells, for a further 72 hours post-transfection at which point cells were lysed and the lysate subjected to WB to check for shRNA-mediated target depletion. Gapdh and Hsc70 were used as loading controls.

5.3.3 Building Nestin-Tomato labelled constructs

In order to further investigate nestin's role in angiogenesis-relevant processes, we needed a tool to study it *in vitro*. The three commercially available antibodies against nestin that we attempted to use did not work in our hands. Therefore, we decided to generate a DNA construct that would encode a directly-labelled nestin protein, which could be utilised in ICC to provide us with information regarding the localisation and architecture of nestin in ECs, as well as its presence in and/or interaction with FAs. The fluorescent protein that we chose to work with was the very bright, red and photostable tandem Tomato (tdTomato) [466]. Proper folding and function of nestin could potentially be affected by addition of the tdTomato onto it. Therefore, we decided to build two nestin constructs, one where nestin was joined to the C-terminal end of tdTomato (pTom-C-Nes) and one with nestin attached to the N-terminus of tdTomato (pNes-N-Tom), thus increasing our chances of generating a structurally and functionally normal labelled nestin.

Generation of the pTom-C-Nes and pNes-N-Tom plasmids were performed, as described in Section 5.2.3, using the tdTomato-C1 and tdTomato-N1 plasmids (Addgene) as backbones (**Fig. 5.8).** The tdTomato-C1 plasmid contains a CMV-driven tdTomato coding sequence followed by a multiple cloning site (MCS) (**Fig. 5.8 A**), whereas the MCS in the tdTomato-N1 plasmid is adjacent to the 5' end of the tdTomato sequence (**Fig. 5.8 B**). Both backbones are approximately 5.5 kbp in size and possess a neomycin/kanamycin resistance cassette for selection in culture. The cloning strategy has been outlined in Figure 5.9. Briefly, SalI and KpnI digested tdTomato-C1 and nestin cDNA are ligated to give rise to the pTom-C-Nes construct (**Fig 5.9 A**), while HindIII and SalI digested tdTomato-N1 and nestin cDNA are combined to generate pNes-N-Tom (**Fig 5.9 B**). In these designs, the pTom-C-Nes construct uses the Tomato start codon and the stop codon at the end of the MCS fragment, present immediately downstream of the nestin sequence, as the boundaries of the amplicon (**Fig 5.9 A**). In the pNes-N-Tom plasmid, the nestin start codon and the Tomato stop codon are used (**Fig 5.9 B**).

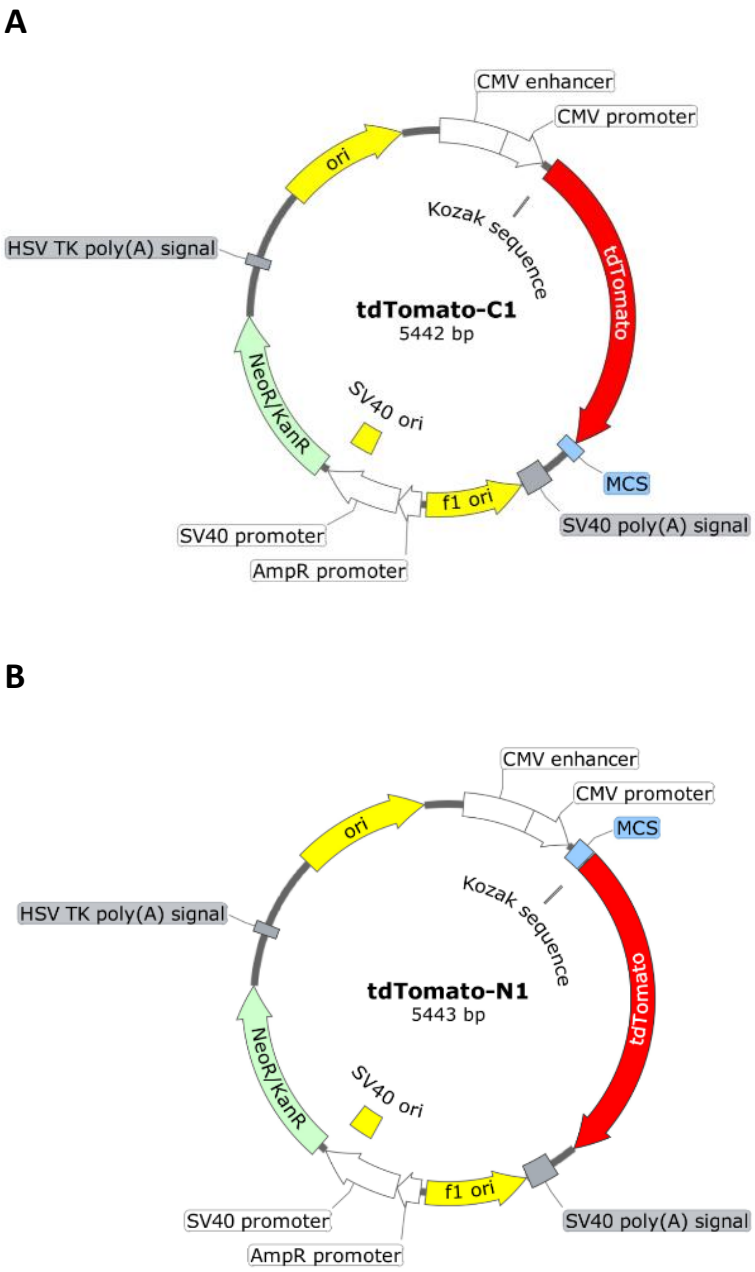

Figure 5.8 tdTomato backbone plasmid maps.

(**A**) tdTomato-C1 plasmid contains the multiple cloning site (MCS) immediately downstream of the Tomato coding sequence driven by the CMV promoter, whereas (**B**) the MCS within the tdTomato-N1 plasmid is downstream of the promoter and immediately upstream of the Tomato sequence. Both plasmids contain the neomycin/kanamycin (NeoR/KanR) resistance cassette for selection of transformed colonies.

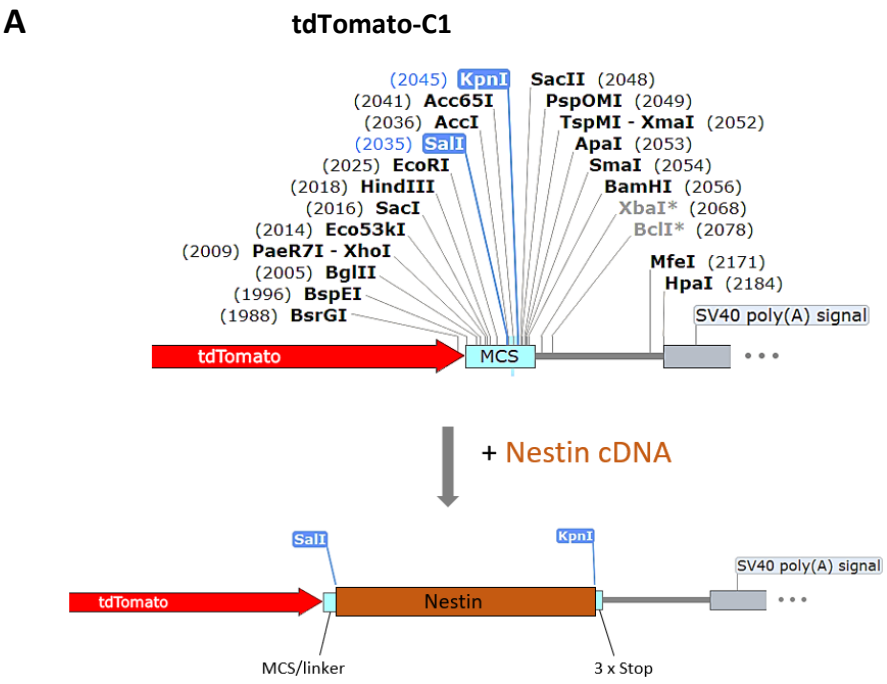

Figure 5.9 Cloning strategy for generating Tomato-labelled nestin constructs.

(**A**) tdTomato-C1 backbone plasmid was cut using SalI + KpnI restriction enzyme pair, while (**B**) tdTomato-N1 by HindIII + SalI. Cut plasmids were then ligated to the nestin cDNA sequence digested with the correspoding enzyme pairs. Thus, pTom-C-Nes and pNes-N-Tom plasmids were generated. MCS – multiple cloning site.

From the start to the stop codon (excluding the latter), the nestin transcript Nes-201 (ENSMUST00000090973.11) is 5592 nucleotides long and translates to 1864 Amino Acids (**Fig. 5.10**). We designed primers to amplify Nestin cDNA, then added restriction sites on both ends (Section 5.2.3.1). These sites were utilised for inserting the nestin sequence into the backbone plasmid. The nestin target sequence for the forward primers (F.C1 and F.N1) was 18 nucleotides (nt) long, starting 6 nt upstream of the start codon, whereas for the reverse (R) primer was 21 nt long, ending 22 nt upstream of the stop codon (**Fig. 5.10**). We used Primer-BLAST (NCBI) to check the parameters of the primers [467]. GC content for the reverse primer (recommended 40-60%) was correct, however it was marginally too high for the forward primer (see **Table 5.5** below). Melting temperatures (T_m) of the primers need to be between 45°C and 65°C, and within 5°C of one another. The optimal primer length to ensure binding specificity and ease of annealing is between 18 to 25 bps. The T_m and length guidelines were met for both primers (**Table 5.5**). Also, the self-complementarity (self-binding) scores were acceptable. These are more qualitative rather than quantitative and there is not a defined cut-off value, but the lower the self-complementary score the better, to minimise the likelihood of the primer forming a secondary structure rather than binding the template DNA. Primer-BLAST also reported how specific the primer pair was against the mouse transcriptome. The only PCR product of less than 15 kbp, identified by Primer-BLAST, using the Refseq mRNA database of Mus musculus (taxid: 10090) was a transcript of the Nes gene (>NM_016701.3).

Table 5.5 Parameters of the Primers Used for the Nestin cDNA Amplicon.

	Sequence (5'->3')	Length	T_m	GC%	Self complement.	Self 3' complement.
Fwd primer	AGCGACATGGAGGGTTGC	18	60.05	61.11	4.00	2.00
Rev primer	TCTCCATCTACCCCACTCAGA	21	59.07	52.38	3.00	3.00

>ENSMUST00000090973 cdna:KNOWN_protein_coding
CGCTGGGTCACTGTCGCCGCTACTCCCTTTCTCCCCCTTAAAAGCTCCAAGGGCCACTCC
CTTCTCTAGTGCTCCACGTCCGCTTGCCCTCGGGGGGCCAGACCAGCGACATGGAGGGTT
GCGTCGGGGAAGAATCTTTTCAGATGTGGGAGCTCAATCGACGCCTGGAGGCCTACCTGA
CCCGGGTCAAGACGCTGGAGGAGCAGAACCAGCTGCTCAGTGCCGAGCTTGGGGGACTCC
GGGCGCAGTCCGGGGACGCCTCCTGGCGAGCCCGAGCCGACGACGAGCTGGCAGCCCTGC
GGGTCCTCGTCGATCAGCGCTGGCGGGAGAAGCACGAGGCTGAGGTGCAGCGCGACAACC
TTGCCGAAGAGCTGGAGAGCGTGGCGGGCCGGTGCCAGCAGGTGCGGCTCGCCCGGGAGC
GGACCATCGAGGAGGCGGCCTGCAGCCGGCGCGCGCTCGAGGCGGAGAAGAATGCGCGGG
GCTGGCTGAGCACCCAGGCTGCCGAGCTGGAGCGCGAGTTAGAGGCTCTGCGAGCGTCGC
ACGAGGAGGAGCGCGCGCACCTGAACGCCCAGGCCGCCTGTACGCCGCGCCGACCCCCCG
CGCCGGCCCACGCATCCCCCATCCGGGCCCCTGAAGTCGAGGAGCTGGCCAGGCGCCTAG
GCGAAGTGTGGCGCGGGGCGGTGCGTGACTACCAGGAGCGCGTGGCTCACATGGAGAGCT
CGCTGGGCCAGGCCCGCGAGCGTCTGGGCCAAGCCGTGCGGGGCGCTCGGGAGAGTCGCT
TAGAGGTGCAGCAGCTGCAGGCTGATCGCGACAGCCTCCAGGAGCGCAGAGAGGCGCTGG
AACAGAGATTGGAAGGCCGCTGGCAGGACCGGCTGCAGGCCACTGAAAAGTTCCAGCTGG
CTGTGGAAGCCCTGGAGCAGGAGAAGCAGGGTCTACAGAGTCAGATCGCTCAGATCCTGG
AAGGTGGGCAGCAACTGGCACACCTCAAGATGTCCCTTAGTCTGGAAGTGGCTACATACA
GGACTCTGCTGGAGGCTGAGAACTCTCGCTTGCAGACACCTGGAAGAAGTTCCCAGGCTT
CTCTTGGCTTTCCTGACCCCAAGCTGAAGCTGCATTTCCTTGGGATACCAGAGGACCAGC
ACCTGGGATCTGTGCTCCCTGTCCTCAGCCCAACATCCTTCTCTTCCCCCTTGCCTAATA
CCCTTGAGACTCCTGTGACAGCCTTTCTGAAGACACAGGAATTCCTTAAGGCCAGAACCC
CCACCTTGGCCAGCACTCCCATCCCACCTATGTCTGAGGCTCCCTATCCTAAAAATGCAG
AGGTCAGAGCCCAGGATGTCCCCCATTCCCTGCTCCAGGGTGGGAGGCAACAGGCTCCAG
AGCCTCTTTGGGCTGAGGCCACAGTGCCCAGTTCTACTGGTGTCCTCCCAGAGCTGGAGG
AGCCTGGGGGCGAGCAGCCGGACCACTTCCCTGATGATCCAACCTCCTTAGCCCCACCCC
TCAACCCTCACCACTCTATTTTAGAGGCTAAAGATAGAGAATCCAGTGAGTCTAGAGTTT
CTAGCATATTCCAGGAAGAAGAAGGGCAAATCTGGGAACTTGTAAAGAAAGAAGCAGCCA
CAGAGGTAAAAGTAGAAAACAGCTTAGCACAGGAAATACAAGAAAGTGGTCTGGACACAG
AAGAAATCCAGGATTCCCAGGGACCTTTGCAGATGGAAACCCTGGAGGCTCTAGGAGATG
AGCCACTGATGTCTCTGAAAACCCAGAACCATGAGACCCCAGGAAAGGAGAATTGCAATT
CATCTATAGAAGAGAACTCGGGGACAGTAAAAAGCCCAGAAAAAGAAAAACAAACACCAC
TGAAGTCTTTAGAAGAAAAGAATGTAGAGGCAGAGAAAACTCTAGAAAATGGGGTTCTTG
AACTATCTAAACCTTTAGGAGAAGAAGAACCAAGAATGGAGGATCAAGAATTAATGTCTC
CTGAACACACACTAGAGACAGTTTCATTTCTAGGAAAGGAAAATCAGGAAGTAGTGAGGT
CTTCAGAAGAACAGAACTTAGAATCATTGATAACTTTTAAAGAGGAGAGCCAATACCCAC
TGGGAGGTCCAGAAGCCGAGGACCAGATGCTTGAAAGACTGGTAGAGAAAGAGGATCAGA
GGTTCCCAAGGTCTCCAGAAGAAGACCAGCAGGCGTTTAGACCTCTGGAGAAAGAGAATC
AGGAGCCACTAAGATTTGAAGAAGCAGAGGACCAGGTGCTTGAGAGACTGATAGAAAAGG
AAAGGCAGGAGTCCCTGAAGTCTCCAGAAGAAGAGGACCAGCAGGCATTTAGACTTCTGG
AGAAAGAGAATCAAGAACCACTAAGGTTTGAAGACGCAGAGGACCAGGTGCTTGAGAGAC
TGATAGAAAAGGAAAGACAGGAGTCCCTGAAGTCTCCAGAAGAAGAGGACCAGCAGGCAT
TTAGACTTCTGGAGAAAGAGAATCAAGAACCACTAAGGTTTGAAGAAGCAGAGGACCAGG
TGCTTGAGAGACTGGTAGAAAAGGAAAGTCAGGAGTCCCTGAAGTCTCCAGAAGAGGAGG
ACCAGAGGACTGGGAAGCCTCTAGAAAAAGAAAATCAGGAATCTCTGAGGTCTCTTGATG
AAAACCAGGAGACAATTGTACTGCTAGAAAGCAAGAACCAGAGGCCACTGAGATCTCTAG
AAGTAGAAGAGGAGGAGCAGAGAATTGTGAAACCTCTAGAAAAAGTGAGCCAGGTCTCCC
TCGAATCTCTCGAAAAAGAGAATGTGCAGTCACCAAGGTATCTGGAAGAAGATGACCACA
TGATTAAGAGCCTGCTAGAAGACAAGACTCATGAGATCCTGGGATCTCTTGAAGATAGAA
ATGGGGAGAACTTTATACCACCTGAAAATGAGACCCAGGGTTCATTGAGGCCTCCAGAAG
AAGAGGACCAGAGGATTGTGAACCATCTAGAAAAAGAAAGCCAGGAGTTCCTGAGGTCTC
CAGAAGCAGAGGAAGAAGAAGAGCAGGTGATGGTGAGATCTCTAGAAGGAGAGAACCACG
ACCCACTGAGCTCTGTGGTGAAAGAGGAGCAGATGGCTGAGAGCAAGCTAGAGAACGAGA
GTCAGGACTCCAGGAAGTCTCTTGAAGATGAGAGCCAGGAGACCTTTGGGTCTCTGGAAA
AAGAGAATCTAGAGTCCCTGAGGTCTCTAGCAGGACAGGACCAAGAGGAACAGAAACTCG
AACAAGAGACCCAGCAGCCACTGAGGGCTGTAGAAGATGAGCAGATGACAGTGAACCCTC
CAGAAAAGGTGGATCCAGAGTTACCAAAGCCTCTTAGAAATGACCAGGAAGTAGTCAGAT
CTCTTGACAAGGAGAATCAAGAGTCACTAGTGTCACTGAATGAAGGAGGTATGGAGACAG
TGAAGTCTTCAGAAACAGAGAACATAGAATCACTGGAGACTGTGGGAGAGTGCCTGGGAA
GAAGGAAGTCTGTAGATACTCAAGAGCCATTGTGGTCTACGGAAGTGACTAGTGAGACAA
TAGAACCTCTAGAAGATGAGACCCAAGAACCACTGGGGTGTGTGGATGAGAACCAAGAGG
TGCTGACACCCCTTGAAAGGGAGAGTCAAGAACTGAGATCTCTGGGCAAGTGGAACCCAG
AGACTGTGGAATCACCAGGAGGGGTGGAGGACAGTCAGCAGTGCCTGGAAGTGGAAGAGG

GCCCGGAGAGGGAGCAGCACCAAGAGTCTCTGAGGTCTCTGGGAGAGGTGGAATGGGAGC
TGCCTGGATCTGGAAGTCAACAGAGGTGGGAGGATGTGGTGGAGGATGGAGAAGGTCAGG
AAGCATCCCTGGGGGCTACAGGAGTGGAAACTGAGGATAAGGCAGAGTTGCATCTGAGGG
GCCAAGGTGGGGAGGAGAAAGCTGTAGAGGAGGGAGAGCTGCTGCAGGATGCTGTGGGGG
AGGCCTGGAGTCTGGGGAGCTCGGAGCCCAAGGAGCAGAGGGTCCCTGCTGAGCCCCTCG
ATGACCTGGAGGGACAACCAGAGCAGACGGGAACCCTAGAGGTCCCAGTTGCTCAGGGAA
TGCCAGAGGCAACAGAGCAAGATGAGGACAGAGCCCAAGCAGGTGAACAAGACTCCGTAG
AGGTGACCCTTGGGTTAGAGGCTGCCAGAGCTGGACTGGAACTCGAGCAGGAAGTGGTAG
GGCTAGAGGACCCAAGGCATTTCGCCAGGGAGGAGGCCATTCACCCATCCCTGGGGGAGG
AAAGTGTGAAGGCAAAGATAGATCAGGGCTTGGAAGAGCCTGGAAAGGAACCAAAAGAGG
CAGGTGCTCTGGACTCAGGCATCCCTGAATTACCCAAGACTAGCAGTGAGACTCTGGAAT
GCAAGGGCTGGGAAGAGTCTGGGGAGGGCTGGGGAGAAGAGGAGGCCTCGCTGGAGACCT
CAGACCATGAGGGCAGCCATGCCCCTCAGCCCAGGCCCCCTAAGACAGAGGAAGATGAGG
GTCTACAGGCAGCGCTAACAGTCCCTGGTCCCAAGCTCCTGGAACCCTGTTCACCCATCC
CGATCTTGACAGATGCCCATGAGCTGCAGCCCCAAGCTGAGGGGATCCAGGAGGCTGGGT
GGCAGCCGGAAGCTGGGACTGAAGCACTGGGAAGAGTAGAAGATGAGCCAGAGTTTGGTC
GTGGGGAGATTCCTGAGGGCCTCCAGGATTGGGAGGAGGGCAGAGAAGACAGTGAGGCAG
ATGAGTTAGGGGAAACTCTCCCTGACTCTACTCCCTTGGGCCTCTACCTGAAGTCTCCTG
CCTCCCCAAAGTGGGAGCAAGCTGGAGAACAGAGGCTTTTCCCTCAAGGGGAGGCCAGGA
AGGAAGGCTGGAGTCCTGCTGCCCTGGCTGCCCAGGGTCTCAGTGACCCACCAGAGGAAG
AGCAGCAAGGCCATGACTCTGACCTCTCATCTGAGGAATTTGAGGACCTAGGGACTGAGG
CCTCTCTTCTTCCAGGGGTTCCCAAAGAGGTGTCCGATCATCTGGGCCAAGAGCCCCCCG
TACTGCAGCCTGCATGCTGGGATCAGGGTGGGGAGTCTGATGGGTTTGCTGATGAGGAAG
AGAGTGGGGAAGAGGGAGAGGAAGAAGATGCTGATGAAGAAGAAGGAGCAGAGTCAGGGA
CTCAGTGGTGGGGGCCAGGGCCCTCTGGTGGAGGTGTCAAGGTCCAGGATGTCACCCAGA
GAGGGGACCTGGAACATGAATCTGTGGGTGACAGTGGCCTCTGGGATGATGGCTTGAGTG
GGGCTGCAGCTAATGTTCTTGTAACTGCCCTAGAGACGGTGTCTCAGGACAGTGCTGAGC
CTTCCGGGTCAGAGGGGTCTGAGTCTGCTTCCTTGGAGGGGGAGGAAGGTCAAGCGATTG
ACCATTTAGATGCCCCCCAAGAGGTGACTAGCGTGGTCCCAGGGGCAGGAGACACCTTTG
ATATCAGTGGCCAGGGCCCCAACCTGGAGTCAGAGCAAGTGAATGGGAGGATGGAGAATG
GACTAGAGCAGGCTGAGGGTCAGGTGGTTCTGCATGGGGACGAGGATCAAGGCATCCCTT
TACAGGAACAGGGTACCCTCAAGGCCCCTTTAGTAGGGTCTCCTGTGCATCTAGGCCCAA
GCCAGCCGCTGAAGTTCACTCTGAGTGGGGTAGATGGAGACTCCTGGTCCTCAGGGGAAG
ATTAGAAACTGCCCCTCTGGCACTGAGGACTTAGTGGGGGGTGGGGGGAATGTCCCTCCC
TGCTCTGGGCCAGCACTCTTAGCTTTGATAACTTGACCTGTGGTATCTCTCGTGGAGAGG
TGTGGCTGGCTGAGACAGGTGAGATCCTGCCTGGATCACCCTGAAGGCTCAGGTCAGCTG
AGCCTATAGTTCAACGCCCCCTTTCTTCTGTGGCTCACCTGCTGGAAGAGGCTTGGGCCC
AGAGCTTTCCCACGAGACTGCTCTGGCCAGAGCTTGCTAGCCCTGCCTGTCTACAGTAGC
ACCACCTGCACAGGGTCTGGTGCATGCCCAGAGGAGCAGCAATGATGAGTGACTCTCATC
ATCTCAGCCTGCTGAGATCTTGTTTCTCTCTTCCTCCCTTGAATAAAGCTGTATCCCTAC

F.C1 / F.N1 primer | start codon | Nes5'seqR | Nes3'seqF

KpnI site | R primer | stop codon

Figure 5.10 Nestin cDNA sequence.

Nestin transcript Nes-201 (ENSMUST00000090973.11) of the nestin mouse gene (ENSMUSG00000004891) results in the cDNA sequence presented above. It has been obtained from the Ensembl online database. From the start to the stop codon (excluding the stop), the sequence is 5592 nucleotides long and translates to 1864 Amino Acids. Features relevant in the generation of our nestin constructs have been highlighted in various colours here.

We attempted a series of PCR reactions to amplify the Nes cDNA from total mouse cDNA and analysed those by agarose gel electrophoresis (Section 2.9). **Fig. 5.11 A** shows four of the unsuccessful PCR attempts with a number of unspecific bands in lanes 2 to 5, as well as two successful reactions resulting in one band, at the correct size of approximately 5.5 kbp, in lanes 6 and 7. These two positive reactions were carried out using F.C1 + R and F.N1 + R primer pairs, while the annealing temperature in the PCR was 62°C.

Next, the backbone plasmids and the PCR-amplified, purified nestin cDNA were digested using matching pairs of restriction enzymes. We utilised a naturally occurring KpnI site 62 nt upstream of the R primer target sequence (**Fig. 5.10**) in the making of the pTom-C-Nes. Therefore, the tdTomato-C1 backbone and nestin cDNA were cut using SalI and KpnI enzymes then ligated to result in the plasmid pTom-C-Nes, while pNes-N-Tom was generated by digesting the tdTomato-N1 backbone and nestin cDNA, using Hind III and SalI (**Fig. 5.9**).

After ligation, transformation into *E. coli* and a MiniPrep we conducted a test digest of pTom-C-Nes and pNes-N-Tom using the HindIII restriction enzyme (for protocols, see Section 5.2.3). The digest confirmed an insertion of approximately 5.5 kbp in both constructs (**Fig. 5.11 B**).

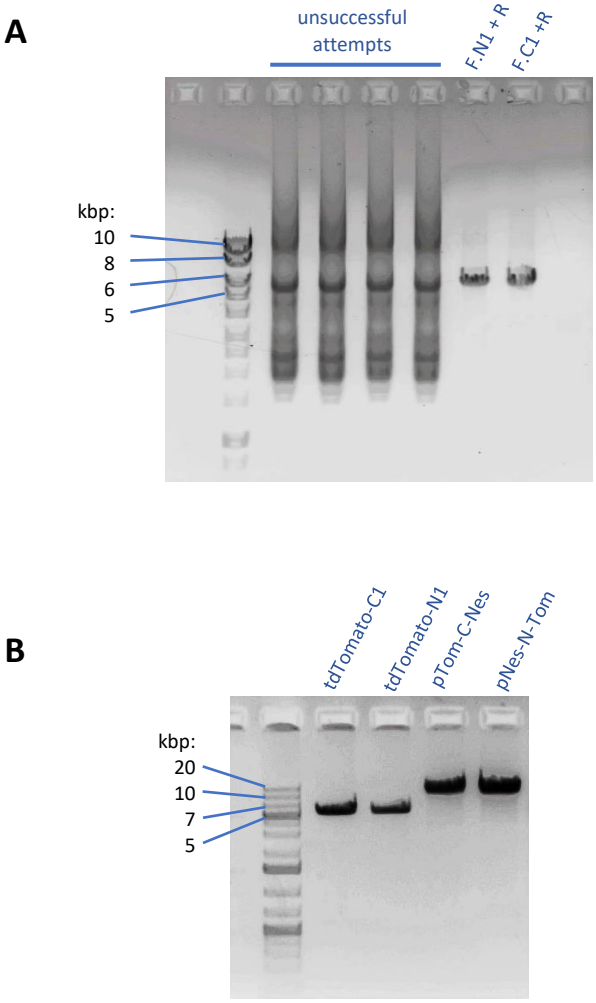

Figure 5.11 Generating Tomato-Nestin DNA constructs.

(**A**) Several primer pairs were tested for amplification of nestin cDNA by PCR. 1uL of neat mouse cDNA (100 ng) was subjected to PCR using a number of combinations of primer pairs and run on a 1% agarose gel: 4 unsuccessful nestin PCR attempts, then cDNA amplified using primer pair F.N1 + R and F.C1 +R. Ladder – HyperLadder™ I (Bioline). (**B**) Also, ~250 ng of plasmid preps (0.5 µL) were digested with HindIII and run on a 1 % agarose gel to verify insertion of the nestin sequence. Ladder – GeneRuler™ 1 kb Plus DNA ladder (Thermo).

Finally, we sequenced pTom-C-Nes and pNes-N-Tom using primers binding within the nestin cDNA sequence, near the ends and initiating sequence reads outwards, i.e. primer Nes5'seqR – a reverse primer which binds near the 5' end, and Nes3'seqF – a forward primer near the 3' end (**Fig. 5.10**). **Figure 5.12** contains the sequences of the backbones and nestin cDNA near the ends. It can be used for reference when looking at the sequencing results in **Fig. 5.13**, which demonstrates that the recombination events occurred. Thus, we successfully generated the pTom-C-Nes and the pNes-N-Tom constructs as planned (**Fig. 5.9**).

A

tdTomato-C1

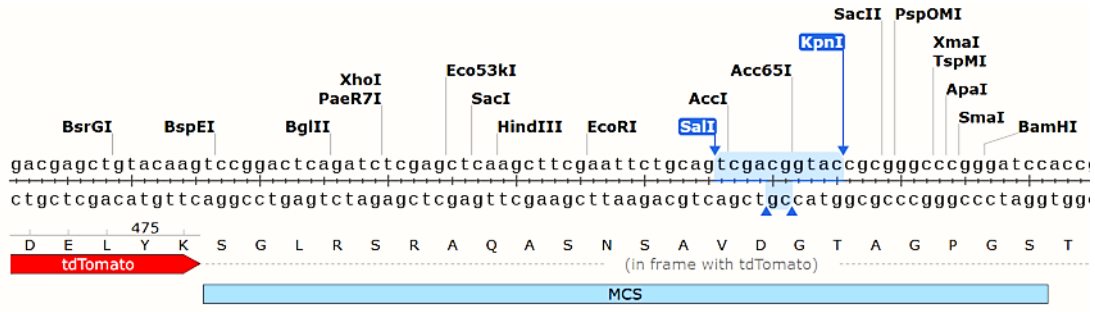

B

tdTomato-N1

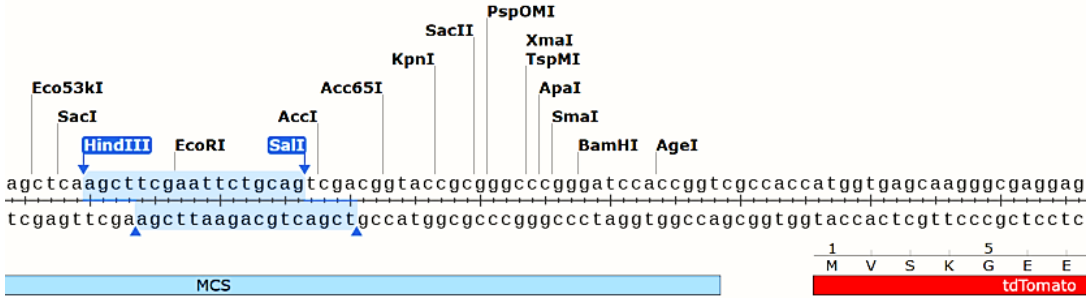

C

C-Nes

5’-GTCGACAGCGACATGGAGGGTTGC…(nestin)…TTACAGGAACAGGGTACC

Nes-N

5’-AAGCTTAGCGACATGGAGGGTTGC…(nestin)…TCTGAGTGGGGTAGATGGAGAGTCGAC

SalI, KpnI, HindIII, start codon, F.C1, F.N1 and R primers

Figure 5.12 Reference sequence near the recombination site.

(**A**) and (**B**) tdTomato backbone plasmids were ligated with nestin cDNA, following matching restriction digests. (**C**) Nestin cDNA was inserted into tdTomato-C1 using SalI and KpnI enzymes, whereas the insertion into tdTomato-N1 was done using HindIII and SalI. The KpnI site naturally occurrs near the 3’ end of the Nes gene, while SalI and HindIII restriction sites were added onto the ends of the cDNA using primers F.C1, F.N1 and R.

pTom-C-Nes, primer Nes5'seqR

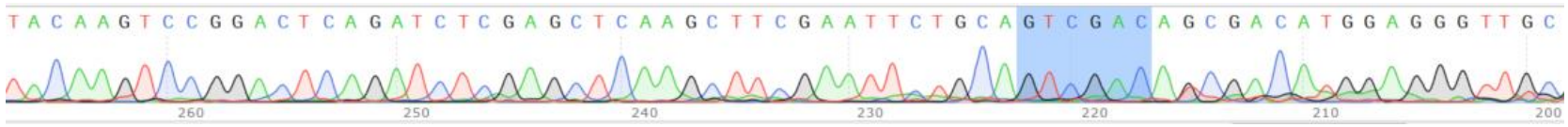

pTom-C-Nes, primer Nes3'seqF

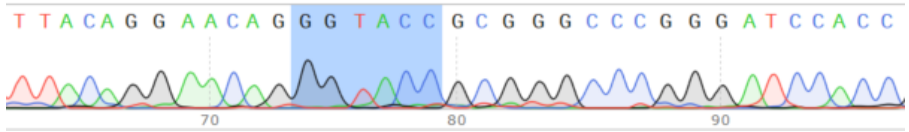

pNes-N-Tom, primer Nes5'seqR

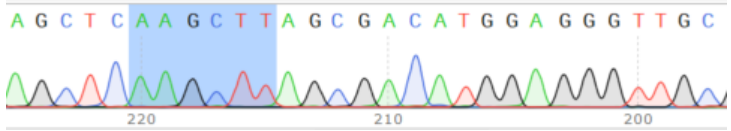

pNes-N-Tom, primer Nes3'seqF

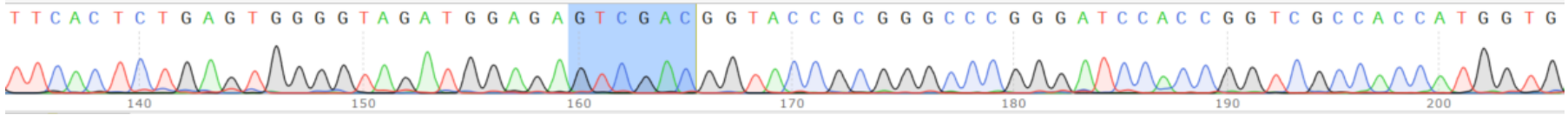

Figure 5.13 Confirmation of Nestin Constructs by Sequencing.

pTom-C-Nes and pNes-N-Tom plasmid DNA were sequenced using primers Nes3'seqF and Nes5'seqR over the recombination sites. For the latter primer, the reverse complement of the sequencing read is shown. Restriction sites are highlighted in blue: GTCGAC – SalI, GGTACC – KpnI and AAGCTT – HindIII.

5.3.3 ICC using Nestin-Tomato and Vim-Cherry

We wanted to investigate nestin localisation in ECs, to determine whether nestin is associated with FAs and if this association changes between different IMMLEC β3-genotypes. We were able to transfect our IMMLEC cells with the Tomato-labelled nestin constructs made in-house and use ICC to assess localization of nestin. With the protocol used (Section 5.2.3.4) we exhibited a problem with the tdTomato signal bleaching quite readily and the images obtained do not reflect the full intensity of the red signal as observed down the microscope. However, examples of ICC images are shown in **Figure 5.14 A**. We saw filament-like structures with both constructs, most likely type VI IFs [468]. The interaction between nestin and FA complexes is likely, given the extension of nestin structures to the periphery of the cell and the overlap of the nestin (red) and paxillin (green) signals (**Fig. 5.14 A**). We did not observe any changes in nestin-FAs interactions between WT, β3-HET and β3-KO cells, although this remains to be concluded with more in-depth analysis.

In Chapter 4 (Section 4.3.2), we discussed disrupting Vim using WFA in ECs and presented ICC images of WFA-treated cells (**Fig. 4.11**). We also attempted to determine how WFA affects Vim interactions with FAs by ICC in WT IMMLECs. To do this, we transfected the cells with a Vim construct directly-labelled with a C-terminal mCherry (red fluorescent) protein. We achieved a transfection efficiency of approximately 20% with 10 µg of plasmid per 1 million cells (protocol in Section 5.2.3.4). We conducted a limited ICC analysis of ~10 cells per condition. There appeared to be fewer Vim-FA associations in the WFA-treated cells then in the DMSO-treated cells (**Fig 5.14 B**), although we did not carry out a detailed analysis or quantification. Also, we observed that the Vim filaments were less spread-out within the WFA-treated ECs than in the DMSO-treated, but to a lesser degree than previously, when we performed ICC with the anti-Vim Ab, rather than using a labelled Vim construct (**Fig 4.11**). The Vim-FA interaction was closer to the centre of the cell in the WFA-treated condition, as the filament network was retracted (**Fig 5.14 B**). When using the Vim-Cherry plasmid we encountered a technical problem in ICC. The red (Vim) signal was bleaching rapidly, similar to that of tdTomato-Nestin.

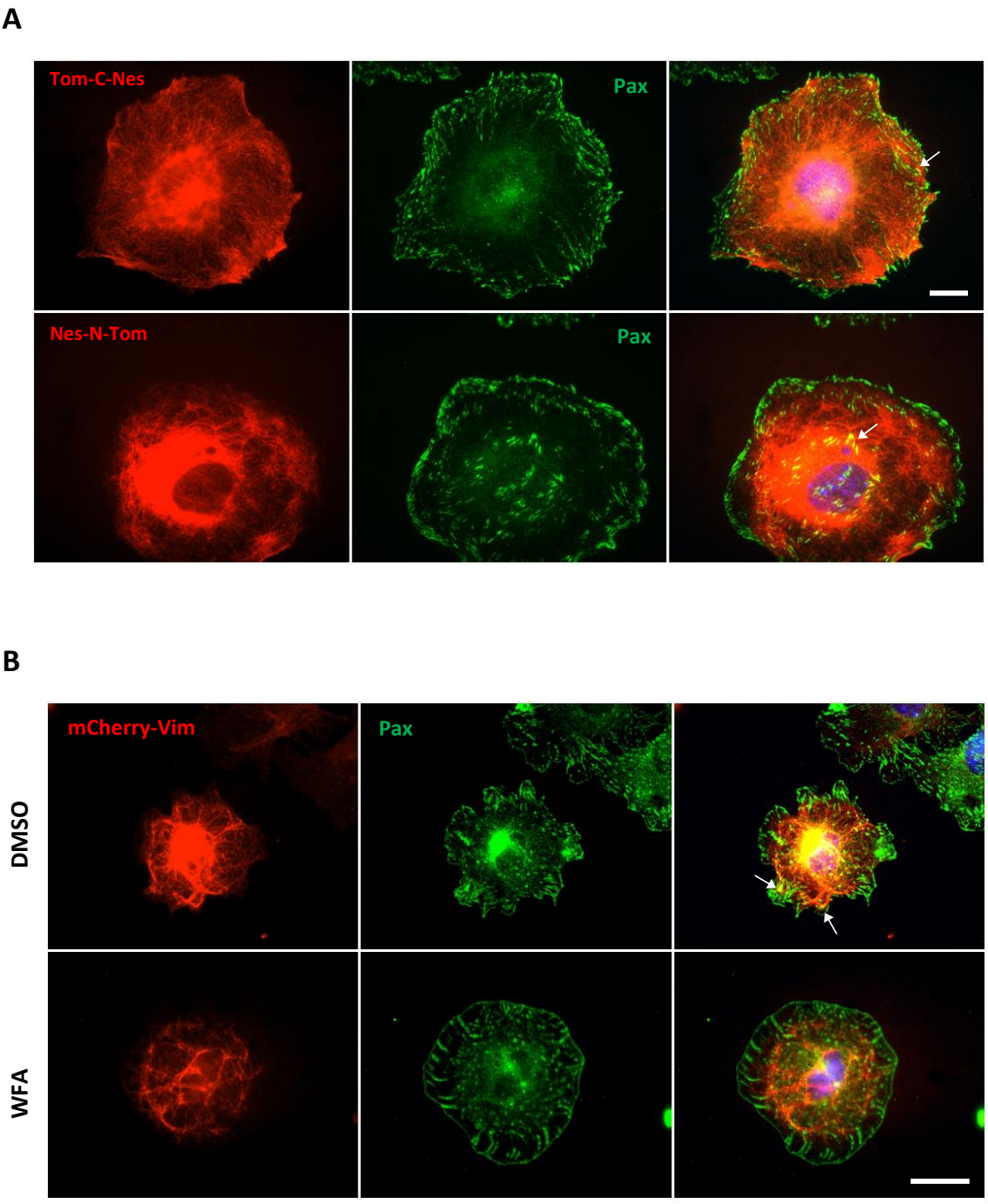

Figure 5.14 Investigation of the IF and FA association in WT IMMLECs by ICC.

(**A**) To investigate Nes-FA interaction, cells were transfected with pNes-N-Tom or pTom-C-Nes construct, then adhered for 90 min on FN, fixed, stained for paxillin (Pax) and imaged at 100x. Scale bar = 20 µm. (**B**) ECs were transfected with pmCherry-Vim, then pre-treated with 0.5 µM Withaferin A (WFA) or DMSO and adhered for 90 min on FN in the presence of DMSO or WFA. Next, they were fixed and stained for Pax and imaged at 63x to investigate Vim-FA associations. Scale bar = 50 µm. White arrows point out the likely IF-FA associations.

5.4 Discussion

We generated six pSico constructs (two per target) encapsulated by lentivirus, an shRNA delivery technology designed by Ventura [463]. We pseudo-titrated the viral preps and tested them in primary cells. Unfortunately, we do not possess clear proof of target depletion by these pSico shRNA constructs made in-house. The shRNA oligo insertion was confirmed by a test digest and sequencing that span the insertion. The EGFP signal, originating from the backbone, was present in both tests, in HEK293 and primary cells. EGFP in these constructs is CMV-driven, which is a strong mammalian expression promoter from the human cytomegalovirus [469]. We successfully achieved all the steps until this point. Unfortunately, we were unable to demonstrate target depletion by WB. Our lab has previously been successful with this technology, therefore we were disappointed about potentially failing to achieve the main aim of generating the constructs – stable target knockdown.

One explanation for the lack of success, is that Cre expression was insufficient in the cells transfected with the constructs. The Cre recombinase is driven by a Pdgfb promoter in the animals from which we isolated the cells. An insufficient Cre expression could be due a mixed cell population or cells reaching senescence. An impure cell prep could have resulted in a mixed cell population, including those that do not express Pdgfb and thus Cre as well. This would impact what we see by WB and any changes in protein levels could be overshadowed. Also, senescent cells have an altered gene expression profile and it this case they may have stopped expressing Pdgfb and thus Cre [470], [471]. Since we are confident in our cell isolation protocol, involving two rounds of a positive cell sort, senescence is the more likely explanation. Cells could be tested by β-galactosidase staining, a biomarker of senescent cells [472]. This could be done in a number of ways using commercially available kits, if we had more time [473].

Another possibility could be an insufficient transfection efficiency. Once again, this would affect what we observed by WB, as our analysis would be of a lysate from a mixed population. We demonstrated that the virus preps transfect nearly all of the HEK293 cells exposed to it, but it can be expected that the transfection efficiency of primary ECs was lower.

One way to investigate this further would be by qRT-PCR, using RNA from additional lentivirus-transfected primary cells, although the problems mentioned above would still apply. We also generated pSicoR plasmids (pSicoR_Nes1 and pSicoR_Vim1) corresponding to the pSico_Nes1 and pSico_Vim1. Another, more straightforward way of testing the shRNA constructs, as it does not require isolating primary cells, would be to transfect the pSicoR into a mouse cell line, e.g. Mouse Embryonic Fibroblasts (MEFs) and check target depletion by WB or qRT-PCR. This is something that we planned and would attempt, if we had more time.

In the case of the Vim shRNA target sequences, we were forced to compromise on the number of variants targeted in exchange for a higher oligo score. Having one of the splice variants unaffected by the shRNA could be a potential lack of depletion. However, the main splice variant Vim-201 (UniProt – P20152) is targeted by both Vim shRNA oligo pairs. In addition, there is very little evidence of the existence of splice variants Vim-202 (UniProt – A2AKJ2) and 206 (UniProt – A0A0A6YWC8), while the former splice variant encodes a considerably truncated form of the Vim protein. We were confident that the location of the target sequences of the Nes and Plec is optimal. Both protein-coding Nes splice variants are targeted with both of our oligo pairs. Also, most of the Plec splice variants are targeted. Only two very short Plec fragments (~50aa) did not contain shRNA target sequence, i.e. Plec-219 (UniProt – A0A0B4J1M7) and 220 (UniProt – A0A0B4J1M3) with very little evidence of existence, while the full plectin protein is 4691 aa long (UniProt – Q9QXS1). In summary, we have confidence in the shRNA oligo design.

There are more accurate methods of titrating viral preps than we have done, such as the Lenti-X™ qRT-PCR Titration Kit (Takara Bio Group). However, we believe that the pseudo-titration we conducted was the most time and cost efficient, and sufficient for our application. It provided us with a dose of virus which delivers the shRNA construct to the majority of transfected cells (HEK293). Although, we do not possess a definite proof of target depletion, we attempted to use our pSico lentiviruses in the *ex vivo* aortic ring assay, for which we intended them from the beginning. This work will be discussed in the next chapter.

We successfully generated two plasmids of 11 kbp in size, containing an insert of 5.6 kbp, which encode a construct for expression of a directly-labelled Nes gene, where the Nes protein is merged with tdTomato via either the N-terminal (pTom-C-Nes) or C-terminal end (pNes-N-Tom). It is possible that extending the protein structure of Nes, through the addition of tdTomato onto it could affect its folding and function. Fortunately, we did not observe any interference of this kind, when we carried out proof-of-concept ICC in WT IMMMLECs. Red-labelled nestin arranged into filament-like structures, as seen previously in ECs [474]. Moreover, these filaments reached FAs, including those at the cell periphery.

Also, we investigated how WFA affected Vim filaments in IMMLECs, using a mCherry-labelled Vim construct and ICC. We saw a similar phenotype as previously when we stained Vim using an Ab, a restricted extension of the Vim filaments in the WFA-treated cells. There was an indication of less Vim-FA association in the WFA-treated cells. This interaction promotes integrin adhesiveness, a pro-angiogenic phenotype [475]. Therefore, inhibition of Vim-FA interaction is a way forward for anti-angiogenic strategy.

tdTomato and mCherry compare well with other fluorophore-containing proteins. Due to being a tandem dimer, tdTomato is not small in size (54 kDa), but possesses two fluorophore sequences, thus making it very bright [476]. The advantages of using the mCherry in comparison to other fluorophore-containing protein, is its small size (29 kDa) and bright signal [466]. The mCherry has been reported to be more photo-stable than RedStar, RFP and tdTomato [477]. However, in our hands tdTomato and mCherry were subject to a similar level of photo-bleaching, starting seconds after illuminating the slides with the excitation laser.

This chapter's focus was on describing our efforts to build and test tools that we could utilise in the investigation of nestin, plectin and vimentin in angiogenesis. Next, we will move on to describing our work with pSico constructs and WFA in the *ex vivo* aortic ring assay, as well as the use of WFA *in vivo* in tumour growth experiments.

6 Co-targeting β3-Integrin and Vimentin Intermediate Filaments *Ex Vivo* and *In Vivo*

6.1 Introduction

Previous work in the Robinson lab (as discussed in the introduction chapter), has employed two endothelial-specific models of β3-integrin depletion, the Pdgfb.CreER inducible model and the Tie1.Cre constitutive model where the integrin is missing from birth [180]. We have observed that acute depletion of β3-integrin impairs pathological angiogenesis and tumour growth (Pdgfb.CreER model), whereas long-term depletion of the molecule (Tie1.Cre model) results in similar sized tumours between Cre -ve and +ve animals with enhanced microvascular sprouting. Importantly, inducing β3-integrin depletion for an extended period of time in the Pdgfb.CreER model results in a loss of tumour growth inhibition, turning this into a long-term depletion mode, similar to the Tie1.Cre phenotype. The work described in this chapter utilises both of these Cre models.

Firstly, I combined the inducible Pdgfb.CreER model with the pSico technology (described in the previous chapter) to target Nes, Plec and Vim in the *ex vivo* aortic ring assay to further investigate their involvement in angiogenesis. My endeavours of generating and testing pSico constructs has already been described in the first part of Chapter 5.

Secondly, I employed the β3-integrin/Tie1.Cre model both *in vivo* and *ex vivo*, in combination with the use of Withaferin A (WFA), as a dual-targeting strategy directed against both endothelial β3-integrin and Vim. Since we had interesting findings with WFA *in vitro*, a dramatic effect of WFA on migration and disassembly of Vim IFs in β3-HET cells compared to WT cells (Chapter 4), we were eager to test WFA in an *in vivo* tumour growth experiment in combination with the endothelial-specific depletion of β3-integrin. For this purpose, we chose the β3-floxed Tie1.Cre model, as we felt it is a better reflection of the adhesome changes occurring in β3-HET cells, where β3-integrin is constitutively depleted. We hypothesised that the upregulation of Nes, Plec and Vim in the β3-HET endothelial adhesome occurs in compensation for the loss of β3-integrin, and that a similar mechanism would be operating in ECs *in vivo* in the β3-integrin floxed Tie1.Cre mice.

A significant decrease in tumour growth in WFA-treated mouse models was observed [418]. Stan *et al*. have seen this using a dose of 4 mg/kg [419]. Thaiparambil *et al*. have used a range of doses from 0.1 to 4 mg/kg [444]. A dose as low as 0.1 mg/kg inhibited metastasis, but significant reduction in primary tumour burden was achieved only at 4 mg/kg. Guided by these studies, we also used the dose of 4 mg/kg for our tumour growth experiment. Before moving on to the next section, it is important to summarise *in vivo* and clinical studies to date which involved the use of WFA.

6.1.1 WFA dosage, toxicity and clinical studies

An important aspect of WFA as an anti-angiogenic strategy is its toxicity. A dose of 4 mg/kg in mice is equivalent to approximately 0.325 mg/kg in humans (12.3 fold less per kg) using a scale factor calculation, taking into account body surface area and metabolic rate [478]. It is difficult to determine how this amount compares to that present in health supplements or used in studies in humans. This is because, to our knowledge, there have been no documented studies in humans using pure WFA from which we could draw conclusions about its toxicity.

WFA is a steroidal lactone, most commonly isolated from the root of the *Withania somnifera* plant [479], [480]. A number of studies involving arthritis patients and healthy participants investigated the effects of the *Withania somnifera* extract (WSE), containing WFA and other bioactive compounds [414]. The amount administered to human volunteers in these studies was between 1.5 and 3 g of WSE per day, which is equivalent to 25 – 50 mg/kg for a 60 kg person [481]–[483]. Some mild adverse effects were seen, namely nausea, dermatitis, sleepiness and pain in the abdomen, but they did not necessitate withdrawal from the study. However, WFA is only a fraction of the content of the WSE, which can vary from 0.003 to 0.066%, on average 0.04% [484], [485]. Similarly, the specifications of WSE available for purchase as a health supplement state that WFA constitutes less than 0.1% of the content. Therefore, the amount of WFA administered to volunteers in these studies, as part of the WSE, was 0.01 – 0.02 mg/kg, i.e. at least 10-fold lower than (0.325 mg/kg) the equivalent dose of that used in mice *in vivo* (4 mg/kg). At the same time, there are other bio-actives present in the WSE, alkaloids and other steroidal lactones, adding to the difficulty of drawing conclusions about the toxicity of WFA specifically. More recently, several other clinical studies in India and the USA showed positive effects of 0.3 – 1 g of WSE per day in periodontitis, athletic performance, vascular disease, as well as bipolar disorder and schizophrenia [486]–[489]. Those who ingested WSE exhibited improved cognition, cardiorespiratory endurance, and a reduction in stress and anxiety, compared to the individuals in the placebo control groups [487]–[489]. In addition, WSE improved sexual function in women (600 mg per day) and caused spermatogenic activity (675 mg per day) in men with deficient sperm counts [490], [491]. WFA induces apoptosis of cancer

cells *in vitro* at 1 µM or higher [418], [444]. We have observed that this dose also inhibits growth of our IMMLEC cells (**Fig. 4.6 A and B**). Others have seen that WFA shows signs of cytotoxicity in HUVECs at 12 nM [417]. An IP injection of 4 mg/kg in mice results in a peak concentration of 2 µM of WFA in the blood plasma, which has a half-life of 1.4 hours [444]. Studies in mice reported minimal toxicity (negligible weight loss) with WFA even at 6 mg/kg [418], [444]. Toxicity studies in rats involved oral gavage of 500, 1000 and 2000 mg/kg of WSE for up to 28 days and no adverse effects were observed [485], [492]. 2000 mg of WSE contains approximately 0.8 mg of WFA [485]. Using 2000 mg/kg of WSE in rats corresponds to approximately 1.6 mg/kg of WFA in mice, accompanied by other bio-actives [478].

In summary, the highest safe and active dose of WFA in humans is not yet known and we would need to administer pure WFA in a clinical trial to be fully clear about this. In a hypothetical clinical trial in cancer patients a recommended, active dose would likely be approximately 0.2 mg/kg/day, an equivalent of 2.5 mg/kg/day in mice. This dose could be delivered as 500 mg/kg/day of WSE, as WFA typically constitutes 0.04%, and this has been the only documented way in clinical studies [485].

6.2 Materials and Methods

6.2.1 Animals

All animals were on a mixed C57BL6/129 background. Littermate controls were used for all *in vivo* experiments. All animal experiments were performed in accordance with UK Home Office regulations and the European Legal Framework for the Protection of animals used for Scientific Purposes (European Directive 86/609/EEC) under Project Licence SDR70/8722 and Personal Licence I44412839.

6.2.2 Genotyping

Ear snips of recently weaned animals (3 weeks old) or post-mortem tail snips from experimental animals were placed in individual wells of a 96-well plate. These were digested in 100 µL of ear/tail snip lysis buffer (50 mM Tris-HCl pH 8.5, 10 mM EDTA pH 8.0, 100 mM NaCl, 0.2% SDS), containing 100 µg/mL proteinase K (Thermo Fisher), at 56°C o/n. 100 µL of isopropanol was added to each well to precipitate DNA, which was pelleted by centrifugation at 1400 g for 30 min. Supernatant was decanted gently and the pellet dried at 37°C for 1 hour. DNA was resuspended in 200 µL TE buffer (10 mM Tris-HCl pH 7.5, 1 mM EDTA) and incubated at 37°C o/n to aid this process.

The genotyping PCR and electrophoresis were run according to Section 2.9. The unique details are described below.

6.2.2.1 β3-Integrin-floxed PCR

The β3-Integrin-floxed allele was generated with exon 1 and PGK-neo cassette flanked by 2 *loxP* sites by Morgan *et al.* [176]. The sequence of the forward genotyping primer was 5'-TTGTTGGAGGTGAGCGAGTC and the reverse: 5'-CCCAGCGGATCTCCATCT. The PCR program used was: 95°C for 2 min; followed by 35 cycles of 95°C for 30 sec, 56°C for 30 sec and 72°C for 30 sec; and 72°C for 8 min. The β3-WT allele resulted in a 182-bp DNA fragment, while the floxed allele gave rise to a 272-bp fragment.

6.2.2.2 Pdgfb.CreER PCR

The tamoxifen-inducible Pdgfb-iCreER^{T2} allele was generated by Claxton *et al.* [461]. Exon I of the *Pdgfb* gene was replaced with the iCreER^{T2}-IRES-EGFP-pA sequence. Primers used for the Pdgfb.CreER genotyping reaction were: forward 5'-GCCGCCGGGATCACTCTC and reverse 5'-CCAGCCGCCGTCGCAACT. The PCR program used to detect this allele: 94°C for 4 min; then 34 cycles of 94°C for 30 sec, 57.5°C for 45 sec and 72°C for 1 min; and a final elongation step at 72°C for 10 min. This PCR reaction amplified a 443-bp DNA fragment unique to the Pdgfb.CreER allele.

6.2.2.3 Tie1.Cre PCR

The Tie1.Cre allele was generated by Gustafsson *et al*. by insertion of a Cre construct including a nuclear localisation signal behind the *Tie1* promoter [493]. Primers used for the genotyping PCR: forward 5'-GCCTGCATTACCGGTCGATGCAACGA, reverse 5'-GTGGCAGATGGCGCGGCAACACCATT. The PCR program: 95°C for 4 min; then 34 cycles of 95°C for 1 min, 67°C for 90 sec and 72°C for 1 min; followed by 72°C for 10 min. The Tie1.Cre allele resulted in a 770-bp DNA fragment.

6.2.3 Lentiviral Transfection of Aortic Rings

Similar to Robinson *et al*.'s methodology, Pdgfb.CreER +ve aortic rings were incubated in Opti-MEM with 100µL of lentiviral prep and polybrene (8 µg/mL) o/n which constituted day 0 [181]. From day 1 of the assay onwards, growth medium was supplemented with OHT to induce Cre recombinase and thus activate the constructs to express shRNA.

6.2.4 *Ex Vivo* Aortic Ring Assay

This assay was performed using the protocol by Baker *et al.* [462]. Aortas were dissected from of 6-8-week-old mice (young age of the mice ensures higher likelihood of sprouting) inside a sterile culture hood (day 0). Aortas were then stripped of the surrounding fat and connective tissue then cut with a scalpel into rings of about 0.5mm in width, under a dissection microscope inside a laminar flow hood. Approximately 20-30 rings were serum starved in 12-well plates (Corning®, Flintshire) in 1 mL serum-free Opti-MEM™ + P/S per well at 37°C o/n. Lentiviral transfection of Pdgfb.CreER +ve rings or Withaferin A (WFA - Enzo, Exeter) treatment at 0.2 µg/mL (made up in DMSO, the final concentration of DMSO was 0.005%) of β3 fl/fl Tie1+/- rings occurred at this stage. On day 1, the rings were embedded in 1.1 mg/mL cold collagen with 1

ring per well in 96-well plates. Collagen was set at 37°C for 1h and then the rings were fed with Opti-MEM™ 2.5% FBS + P/S, supplemented with 30 ng/mL VEGF to induce sprouting, with the addition of OHT or continued WFA/DMSO treatment. Medium containing FBS, VEGF + OHT or WFA/DMSO was refreshed on day 4 and the rings were fixed in 4% paraformaldehyde (PFA) on day 7. Aortic rings were permeabilised with 0.25% Triton and stained with FITC-conjugated BS-1 lectin for enhanced visualization of the endothelial sprouts. The FITC-labelled microvascular branches (not the stalks) were counted to quantify angiogenic sprouting.

6.2.5 Tumour Growth Assay In Vivo

A mouse lung carcinoma cell line CMT19T, syngenic to the mice used (C57BL6/129), was trypsinised and resuspended in PBS at 10^7 cells per mL. 8 – 10-week-old β3 fl/fl Tie1+ mice, and their Cre -ve littermate controls, were subcutaneously injected in the flank (1 injection per animal) with 100 µL (10^6 cells) of the cell suspension using a sterile syringe and a 26-gauge hypodermic needle (BD Biosciences, Wokingham). On day 7 post-injection, tumours were palpable and the intraperitoneal (IP) drug administration begun. Withaferin A (WFA – ENZO Life Sciences, Exeter) powder was reconstituted in DMSO at 5 mg/mL. A 10% WFA/DMSO, 40% vehicle (Kolliphor® EL), 50% PBS solution was injected at 4 mg/kg according to the individual weight of the animal, as previously done by Thaiparambil *et al*. [444]. Thus, 200 µL of WFA/vehicle/PBS was injected into a 25 g mouse on day 7, 9, 11, 14 and 16. On day 18, mice were sacrificed, tumours were excised, photographed, measured using a digital calliper and weighed. They were then bisected along the midline with a scalpel (Swann-Morton, Sheffield) and fixed in 4% PFA o/n at 4°C.

6.2.6 Immunohistochemistry

Tumours were removed from fixative into a solution of PBS, 20% sucrose, 2% PVP (polyvinylpyrrolidone) for 24 – 72 hours. Next, they were embedded in 8% gelatin and snap-frozen in -40 to -50°C isopentane and stored at -80°C until cryosectioned. Using a MICROM HM 550 cryostat (Thermo Fisher) at -20°C, 6 µm sections were cut from the sliced end of the tumour i.e. centre and mounted onto positively charged ColorFrost™ glass slides (Thermo Fisher). Slides were air-dried at RT for 10 min then the gelatin was melted in PBS at 37°C for 10 min. A hydrophobic circle was then drawn around the tumour sections using a PAP pen (ImmEdge™ - Vector Laboratories, Peterborough). Slides were placed into coplin jars and washed twice with in PBS 0.25% Triton-X-100 and twice with PBLEC (PBS 1% Tween-20, 1 mM $MgCl_2$, 1 mM$CaCl_2$, 100 µM $MnCl_2$). Tumour sections were then blocked with PBLEC 1% BSA, 2% goat serum for 1

hour at RT, incubated with a rat primary Ab against endomucin (**Table 2.1**) at 1 in 500 in PBLEC at 4°C o/n, washed in PBS 0.1% Triton three times for 15 min and incubated with secondary Alexa-594-conjugated anti-rat Ab (**Table 2.2**) in PBLEC for 2 hours at RT. This was followed by another two washes in PBS 0.1% Triton, a dip in PBS, then immersion in 0.1% Sudan Black for 10 min to reduce auto-fluorescence [494] and a rinse under tap water for 3 min to wash off excess Sudan Black. Slides were dried briefly, mounted with Fluroromount-G™ with DAPI (Thermo Fisher) and the edges sealed with nail polish.

6.2.7 Imaging and Blood Vessel Density

Images of the labelled blood vessels (Section 6.2.6) were taken at 10x magnification using the Axioplan Epifluorescent microscope (Zeiss, Cambridge) and the AxioCam MRm camera (Zeiss). The software used for fluorescence microscopy and imaging was Axiovision, specifically the Multidimensional Acquisition tool. Images of different colour channels were merged using the Image J™ software. Vessel density was determined by manually counting vessels in 3 hot-spots per section, adjacent to and excluding the tumour border, avoiding the necrotic centre of the tumour. The Cell Counter Plug-in for ImageJ™ was used to aid the counting and to measure the area of the hot-spots.

6.2.8 Hematoxylin and Eosin (H&E) staining

Tumour sections were prepared and gelatin melted away, as described above in Section 6.2.6. Slides were then submerged in tap water for 30 sec, stained with Mayer's Haematoxylin for 5 min, rinsed in running tap water for 2 min until blue, eosin was applied to the slides for 15-20 sec, then blotted off then very quickly rinsed in running tap water, so as not to lose excess eosin. Next, sections (slides) were dehydrated by agitation (approximately 20 times) in ethanol solutions of increasing concentration, from 50%, through 70%, 80% and 95% to 100%, followed by Histoclear (Thermo Fisher) #2 and Histoclear #1. Finally, slides were mounted using DPX. Hematoxylin stains acidic structures, such as nucleic acids, nucleus and ER, while eosin adheres to basic structures (proteins and cell membranes).

6.3 Results

6.3.1 Nestin is Pro-Angiogenic in an *Ex Vivo* Model of Angiogenesis.

Using the pSico constructs described in Chapter 5, we conducted aortic ring assays to investigate the effect of depleting endothelial Nes, Plec and Vim on angiogenesis *ex vivo*. Using the PCR protocol outlined in section 6.2.2.2, mouse litters were genotyped for the presence of the Pdgfb.CreER allele (**Fig. 6.1 A**) and the Cre +ve mice were taken forward for the assay. We observed a significant decrease in microvascular sprouting when using one of the two anti-Nes shRNA constructs (N1, 2.8 ± 0.6) compared to the negative, non-targeting control (nt, 6.4 ± 1.1), which achieved the same level of inhibition as the positive control, anti-VEGFR2 shRNA (VR2, 3.0 ± 0.6), expected to inhibit VEGF-dependent angiogenic sprouting of aortic rings [181]. In addition, all the other anti-IF constructs (N2, P1, P2, V1 and V2) showed a similar trend to N1 – N2, P2 and V2, more so than P1 and V1 (**Fig. 6.1 B and C**). Overall, the number of sprouts were slightly lower than expected, as in the non-targeting shRNA (nt) condition there were on average 6.4 ± 1.1 sprouts per ring, compared to 8 ± 2 seen previously in the Pdgfb.CreER control rings [180]. It could be that adding the lentivirus has a detrimental effect on sprouting or proliferation in general. An additional negative control condition, where no virus is added to the rings, could help clarify this.

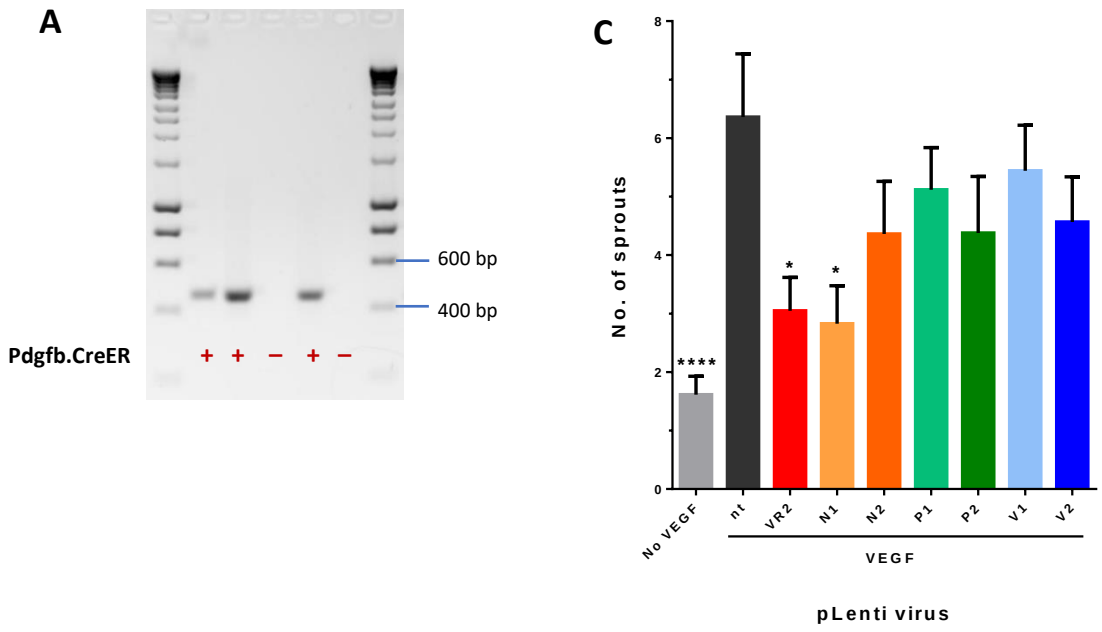

B

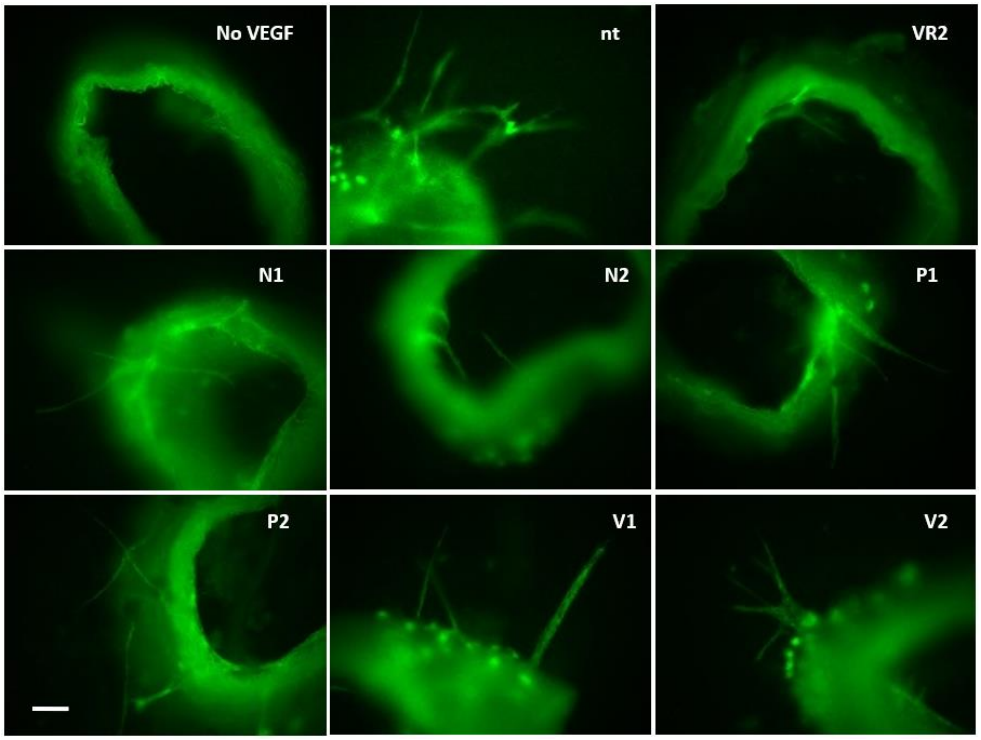

Figure 6.1 Nestin KD impairs angiogenesis *ex vivo*.

(**A**) Ear-snip DNA of mouse litters was subjected to a Pdgfb.CreER genotyping PCR, where a 440 bp band indicated the presence (+) of the CreER allele. Aortas from Pdgfb.CreER +ve mice were infected with pSico shRNA lentivirus against VEGFR2 (VR2, +ve control), Nes (N1, N2), Plec (P1, P2), Vim (V1, V2) or with a non-targeting (nt) control and subjected to a VEGF-dependent aortic ring assay. (**B**) In the final stage, the rings were stained with FITC-laveled IB4, a green-fluorescently-labelled EC marker and imaged at 10x, scale bar = 50 µm. Microvascular sprouts were counted over 3 independent experiments (30+ technical repeats per condition) to determine the effects of shRNA-induced depletion of Nes, Plec or Vim on angiogenesis *ex vivo* and graphed in **C.** * indicates P<0.05 and **** P<0.0001, as determined by an unpaired student's *t*-test.

6.3.2 Withaferin A Inhibits Angiogenesis in the Absence of β3-Integrin

Work by Stan *et al*. and others has shown a significant WFA-induced inhibition of tumour growth in mouse models [418], [419], [444]. As described in Chapter 4, we observed that WFA has a more pronounced anti-angiogenic effect in β3-HET cells than in WTs (e.g. a dramatic disruption of the Vim IFs and migration inhibition). Therefore, we wanted to investigate the effects of combining WFA and β3-integrin depletion on angiogenesis and tumour growth *in vivo*. To do this, we used our in-house mouse model of long-term endothelial-specific deletion of β3-integrin, the Tie1.Cre, β3-floxed line. In this background, endothelial β3 integrin is missing from birth and any potential compensatory mechanisms arising from the loss of β3-integrin expression have taken place.

Adolescent mice (3 – 4 weeks old) were genotyped according to Section 6.2.2.1 and 6.2.2.3 to ensure β3-floxing and to determine Tie1.Cre status. As well, a tail snip for DNA extraction at the time of tumour harvest was obtained, to re-genotype the mice used in the experiments (**Fig. 6.2 A and B**), as confirmation of their Cre and floxing status. The protocol of the tumour growth experiment can be found in Section 6.2.5. Briefly, 8 – 10-week-old mice were subcutaneously injected with 10^6 CMT19T mouse lung carcinoma cells (Day 0) and then IP injected 5 times (every 2 to 3 days) between Day 7 and 18, with vehicle or WFA at 4 mg/kg, as outlined in the experiment schedule in **Figure 6.2 C**. Following our experimental design, we observed no significant difference between control and WFA-treated animals, either by measuring tumour volume or weight, though there was a trend toward WFA-treated tumours being smaller (**Fig. 6.2 D and E**). The mice were weighed at the time of every injection and there were no signs weight loss throughout the experiment in any of them. We also took measurements of the tumours at all the time-points of IP injections, except for Day 7, as the tumours were too small to measure accurately with a calliper. Therefore, we were able to track and assess any differences in tumour volume between groups at earlier stages, unfortunately there was no significant differences observed at any time-point (**Fig.6.2 F**).

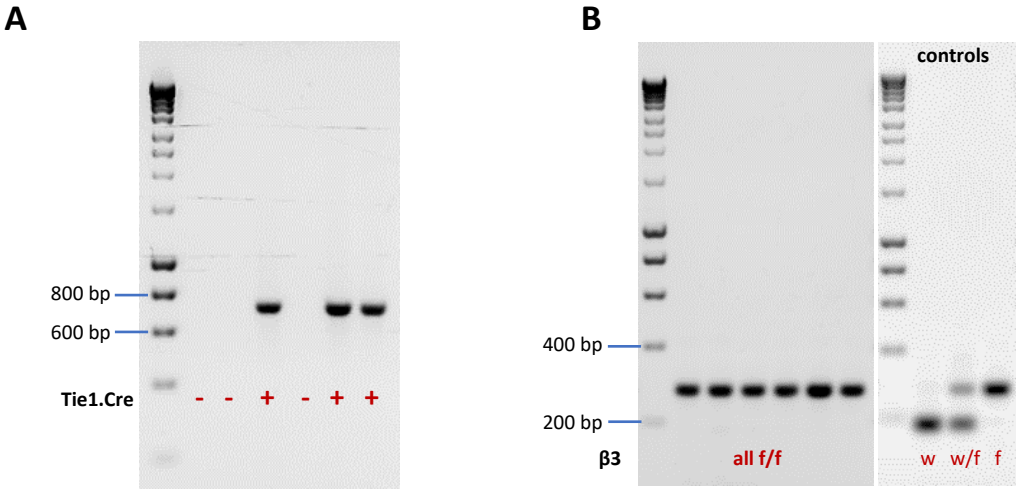
A
800 bp
600 bp
Tie1.Cre
- - + - + +
B
controls
400 bp
200 bp
β3
all f/f
w w/f f

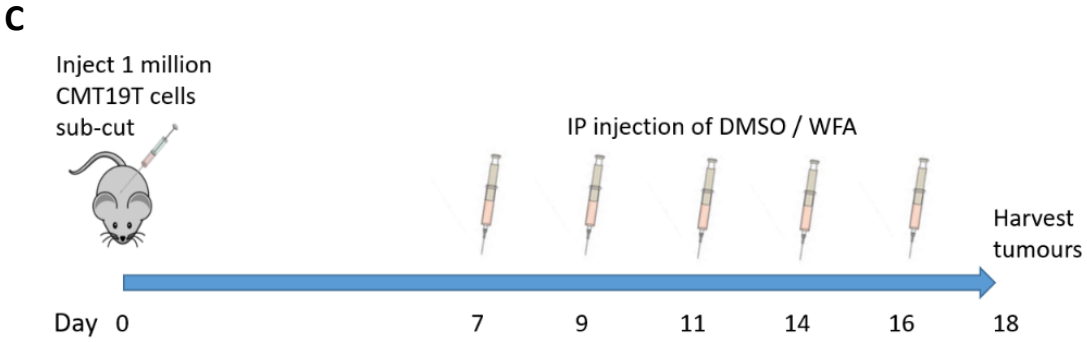
C
Inject 1 million
CMT19T cells
sub-cut
IP injection of DMSO / WFA
Harvest
tumours
Day 0 7 9 11 14 16 18

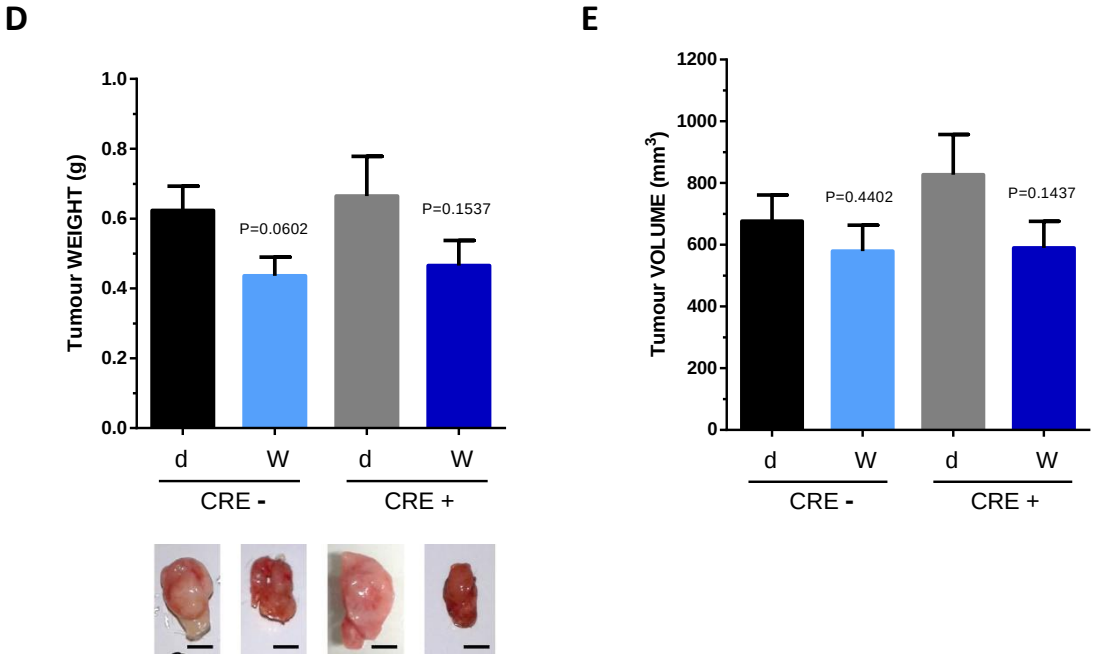
D
Tumour WEIGHT (g)
1.0
0.8
0.6
0.4
0.2
0.0
P=0.0602
P=0.1537
d W d W
CRE - CRE +
E
Tumour VOLUME (mm3)
1200
1000
800
600
400
200
0
P=0.4402
P=0.1437
d W d W
CRE - CRE +

F

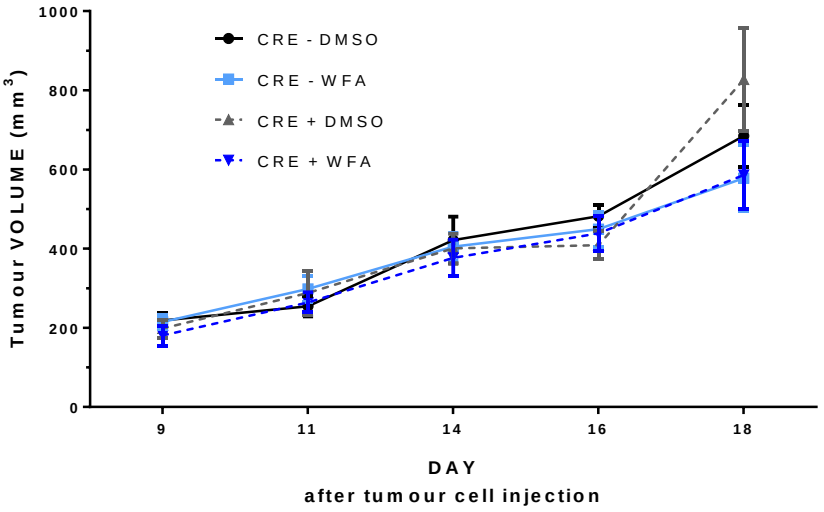

Figure 6.2 The effect of Withaferin A on tumour growth *in vivo*.

Ear-snip DNA of mouse litters was subjected to genotyping PCR. (**A**) 770 bp band indicates the presence (+) of the Tie1.Cre allele. (**B**) In the β3-floxed PCR a 180 bp band reports a β3-WT (w) allele, while a 270 bp band indicated β3-floxing (f). (**C**) Experimental schedule of the tumour growth experiment. (**D**) The average tumour weight and (**E**) tumour volume at Day 18 was determined for Cre -ve and Cre +ve animals treated with DMSO (d) or WFA (W) (4mg/kg) (pooled data from 6-independent experiments; 11+ animals per group). P values from the comparison between the d and W groups appear in D and E (unpaired student's *t*-test). Representative images of a tumour from each group were included in D, scale bar = 5 mm. (**F**) Also, tumour volume was measured at the time of IP injections, average volumes were graphed to assess tumour growth at earlier time points. Error bars in D, E and F represent SEM.

Given the observed trend of WFA-induced reduction in tumour growth, I was interested in determining the numbers required to achieve significant difference between DMSO- and WFA-treated groups, especially in the Cre +ve background. The power calculations reported that the differences would reach statistical significance, when the n number is extrapolated to approximately 40 animals per group for tumour weight comparison and 60 animals per group for tumour volume comparison. I felt the numbers required to produce a potential significance went against "The Principles of Humane Experimental Technique" of replacement, reduction and refinement (the 3Rs) of *in vivo* experiments, so decided not to pursue this finding further [495].

However, the tumours from the *in vivo* experiment described above were sectioned and an H & E staining (protocol in Section 6.2.8) was performed to examine tumour architecture, and endomucin immunostaining was performed to investigate blood vessel density between the four experimental groups (protocol in Section 6.2.6 and 6.2.7). There were no apparent differences in tumour morphology between the groups (**Fig 6.4 A**). Tumours in all four groups exhibited a similar level of and variation in: density, fibrosis, necrosis and infiltration of immune cells. Perhaps a more detailed analysis, would identify differences, but we did not observe anything striking to report. Interestingly, tumours from the WFA-treated Cre +ve mice exhibited a significant reduction in blood vessel density (91 ± 5 vessels per mm^2) compared to the other experimental groups: vehicle-treated Cre -ve group (114 ± 4 vessels per mm^2), the WFA-treated Cre -ve group (106 ± 4 vessels per mm^2) and Cre +ve vehicle-treated tumours (125 ± 5 vessels per mm^2) (**Fig. 6.3 B and C**). The greatest significant reduction was between the Cre +ve vehicle- and WFA-treated mice ($P < 0.0001$), suggesting WFA inhibited pathological angiogenesis only in the absence of β3-integrin.

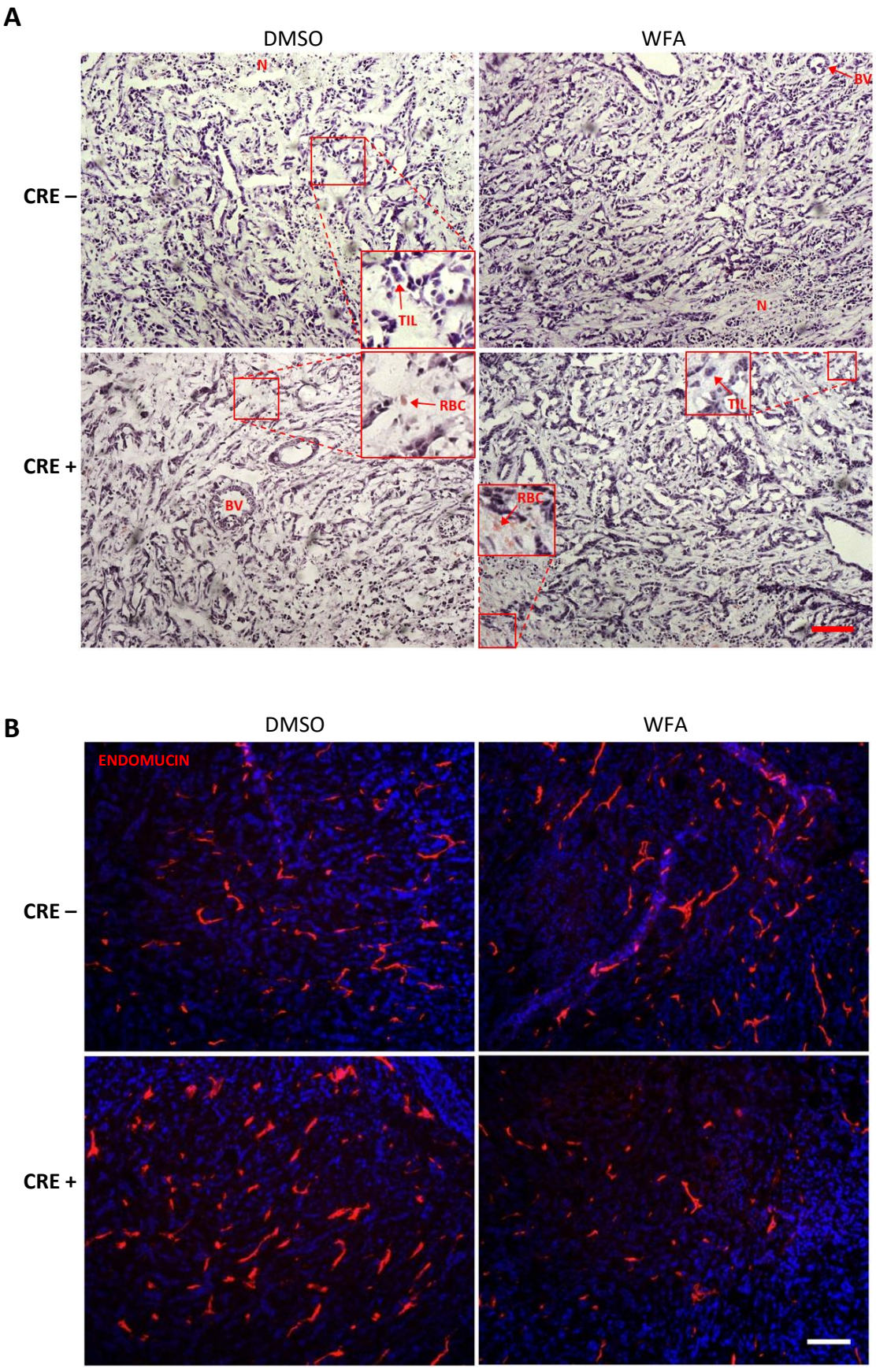
A
DMSO
WFA
CRE –
CRE +
N
TIL
RBC
BV
B
DMSO
WFA
CRE –
CRE +
ENDOMUCIN

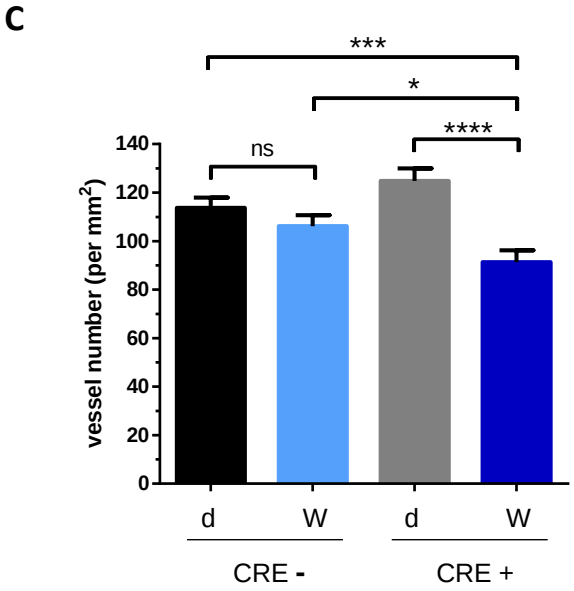

Figure 6.3 Withaferin A reduces pathological angiogenesis *in vivo*.

(**A**) Tumour H&E sections from *in vivo* experiment in Fig 6.2 demonstrating tumour morphology of tumours implanted into Tie1.Cre -ve and Cre +ve animals, treated with DMSO or WFA, BV – blood vessel, N – necrotic area, RBC – red blood cell, TIL – tumour-infiltrating lymphocyte. (**B**) Endomucin staining on tumour sections comparing blood vessel density. Scale bars in A and B = 100 µm (10x). (**C**) Blood vessel counts in 3 representative fields per section in all tumours from the *in vivo* experiment (11+ per group) to determine vessel density, d = DMSO, W = WFA. * indicates P<0.05, *** P<0.001 and ****P<0.0001, as determined by an unpaired student's *t*-test.

We noticed that WFA reduced pathological angiogenesis in the *in vivo* tumour growth experiment, in the Tie1.Cre model of β3-integrin depletion. We wanted to complement these findings using the aortic ring assay (for protocol see Section 6.2.4), an *ex vivo* assay of angiogenesis. Firstly, we performed a dose response curve with WFA in WT aortic rings to identify the optimal dose, using a similar range as in ECs in Chapter 4 (**Fig. 6.4 A**). For the dual-targeting experiment, we opted for the lowest dose that significantly inhibited VEGF-dependent microvascular sprouting in the test assay, 0.2 μM. As expected from previous findings in the lab, we saw an increase in sprouting between the Cre -ve (β3-integrin present, on average 3 ± 1 microvascular branches per ring) and Cre +ve (β3-integrin missing, 11 ± 2) untreated (ut) aortic rings (**Fig. 6.4 B and C**) [180]. Interestingly, WFA reduced aortic ring VEGF-dependent sprouting in the Cre +ve background (4 ± 1), whereas it stimulated sprouting of the Cre -ve rings (5 ± 1), compared to their respective ut controls. This differential outcome may have occurred due to the proliferative effect of WFA on cells, described in the previous chapter, particularly at 0.2 μM (**Fig. 4.7 B**) and we also observed a similar pattern in the scratch migration assay with WFA in WT and β3-HET cells (**Fig. 4.8**). DMSO alone appeared to reduce sprouting of the Cre +ve rings (5 ± 1) although, there was no significant difference in sprouting between DMSO-treated and WFA-treated Cre +ve rings (**Fig. 6.4 B and C**). Overall, number of sprouts were lower than we have seen previously in the ut rings, i.e. 6 ± 1 in the Cre -ve rings and 16 ± 2 in the Cre +ve [180].

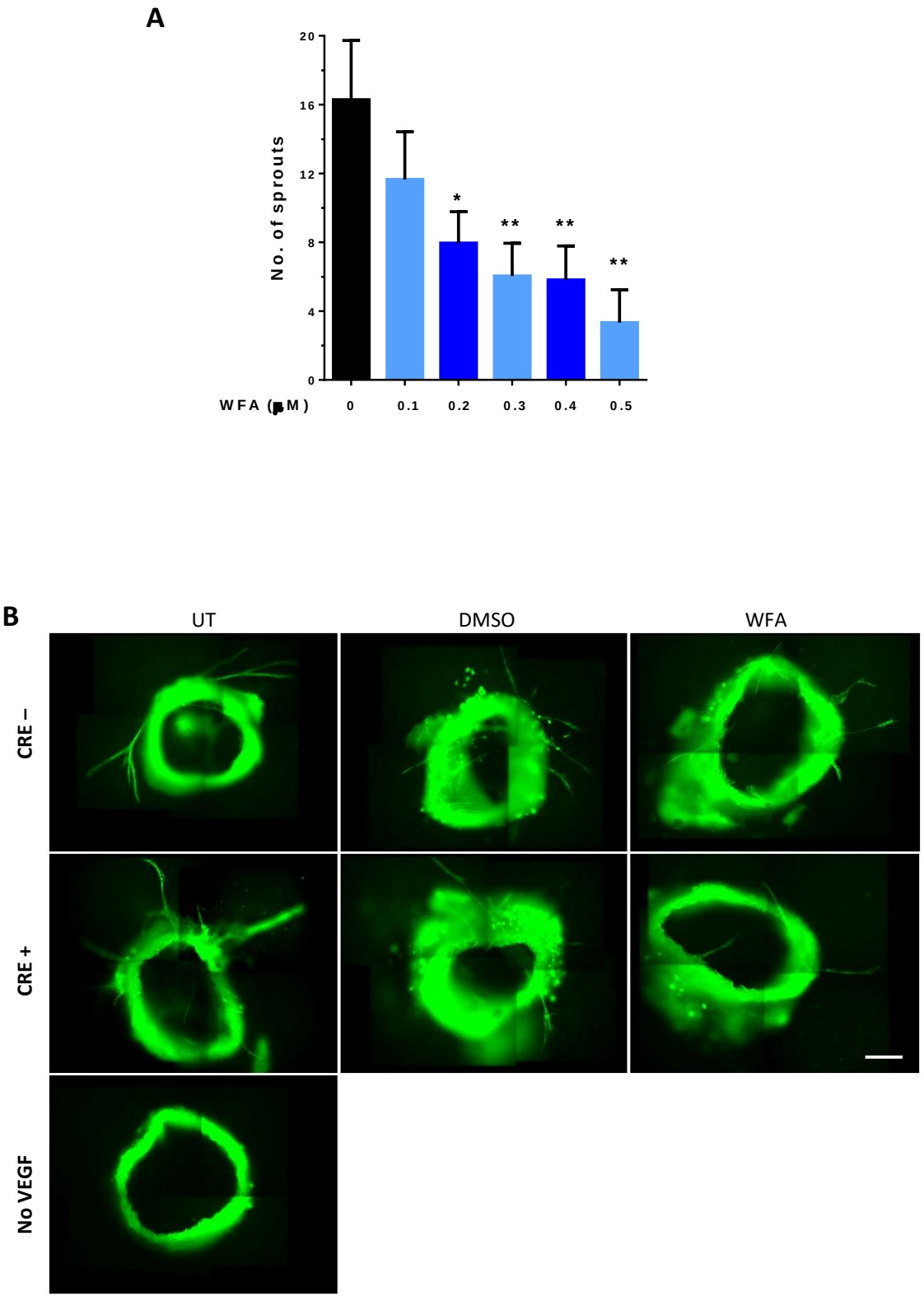
A
No. of sprouts
20
16
12
8
4
0
*
**
**
**
WFA (μM)
0
0.1
0.2
0.3
0.4
0.5
B
UT
DMSO
WFA
CRE –
CRE +
No VEGF

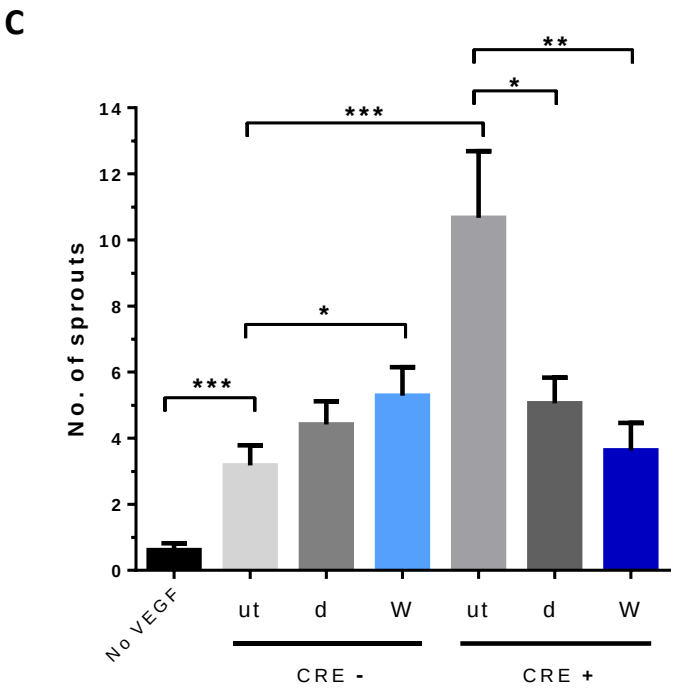

Figure 6.4 The effect of Withaferin A on angiogenesis *ex vivo*.

(**A**) An optimal dose of Withaferin A (WFA) for use in the aortic ring assay was determined by a dose response curve in WT aortas (14+ technical repeats per dose). (**B**) Aortas from β3-floxed Tie1.Cre -ve/+ve mice were used in the aortic ring assay with DMSO (d) / 0.2 µM WFA (W) treatment or untreated (ut) (scale bar = 100 µm). (**C**) Microvascular sprouts were counted (n = 5 independent experiments, 49 technical repeats per condition), to quantify the effect of WFA on angiogenesis *ex vivo*. * indicates P<0.05, ** P<0.01 and *** P<0.001, as determined by an unpaired student's *t*-test.

6.4 Discussion

We attempted to deplete endothelial Nes, Plec and Vim using shRNA containing lentiviruses, to see what effect this could have on angiogenesis *ex vivo*, in the aortic ring experiment. One of the anti-Nes shRNAs (N1) decreased aortic ring sprouting, while the other shRNAs used against Nes, Plec or Vim showed little or no effect. We were unable to confirm the depletion of these targets using the shRNA constructs that we generated (Chapter 5), therefore we cannot make firm conclusions based on the results of this aortic ring assay. In summary, endothelial Nes appears to be pro-angiogenic, whereas we do not know if depleting Vim and Plec has little or no effect here, or whether the shRNAs are achieving a little or no depletion. Nes has been shown to promote both proliferation and invasion in cancer cells [394], [398]. At the same time, it has been suggested as a new marker of neovasculature [460], [496]. Plec is a versatile cytolinker, shown to interact with Actin, Vim and β3-integrin, among other proteins [408], [475], [497]. It is required for vascular integrity and normal function of FAs and tight junctions [410]. Vim interacts with β3-integrin in ECs, most likely via Plec, and regulates FAs [222], [293]. In general, Vim-IF network serves to provide support in cells against shear stress and promotes greater adhesion strength [385]. Thus, the literature suggests all three IF proteins play a pro-angiogenic role and we would expect their absence to impair EC function and therefore sprouting in the aortic ring experiment. Perhaps their involvement in angiogenesis becomes more apparent when β3-integrin is depleted. To our knowledge, using the aortic ring assay in the Pdgfb.CreER background is a unique attempt at investigating the role of endothelial Nes, Plec and Vim. Initially, we considered using the pSico lentiviral preps for an *in vivo* experiment. Theoretically, they could be a tool for endothelial specific depletion of candidate genes in mice in e.g. tumour growth experiments, when used in Cre-expressing mouse models [498], [499]. However, the lack of proof of achieving target depletion in primary cells (Chapter 5) and the limited effects in the aortic ring assay steered us away from the idea of using them *in vivo*.

We were determined to take at least one of the IF proteins forward to an *in vivo* experiment, to address the hypothesis more fully. Therefore, we conducted a tumour growth assay in β3-floxed Tie1.Cre mice and treated them with WFA (or vehicle), as a strategy of modelling a dual-targeting of β3-integrin and Vim. We have previously compared the difference in tumour growth between β3-floxed Tie1.Cre -ve and +ve animals, while others have looked at the effect of WFA alone [419], [444]. The novelty of this experiment was to simultaneously look at β3-integrin endothelial depletion and Vim inhibition (WFA), i.e. comparing the rate of tumour growth of the β3-flox Tie1.Cre +ve mice when treated with WFA or vehicle alone.

We observed a trend in a reduction of tumour growth with WFA treatment at 4 mg/kg, while others saw this to a statistically significant degree [418], [419], [444]. This difference may be explained by two major factors – the type of cells used and the WFA treatment regime. Stan *et al*. set up human breast cancer cell (MDA-MB-231) subcutaneous xenografts in immunocompromised nude mice and injected WFA 5 times a week for two weeks [419]. Thaiparambil *et al*. used a mouse breast cancer cell line (4T1) implanted into the mammary fat pad and injected WFA daily for a month, also in immunocompromised animals [444]. We used subcutaneous allografts of mouse lung carcinoma cells (CMT19T), followed by less frequent IP injections of WFA over a shorter period, every 2 – 3 days over an 11-day time course. We were required to stop here, as the tumours were approaching the legal limit, stipulated by our Home Office Project licence (1000 mm^3). Moreover, the half-life of WFA in the blood plasma is approximately 1.5 hours, its clearance from the blood occurs at a relatively high rate whereby it becomes undetectable 24 hours post-injection [444]. In our study design, there was more time between injections for 'recovery' from the effect of WFA, compared to some of the other studies. Therefore, if we were to inject WFA more frequently, the trend for smaller tumours in WFA-treated animals could become significant, especially in the Cre +ve mice. On the other hand, Yu *et al*. used an entirely different regime of treatment, initial IP injection of WFA on two consecutive days, then twice a week, and still observed a WFA-induced significant decrease in tumour volume even at 3 mg/kg, but in a long-term treatment scenario (30 days) [418].

Interestingly, we saw a significant decrease in blood vessel density upon WFA treatment in β3-floxed Tie1.Cre +ve, but not in the Cre -ve, mice in the *in vivo* tumour growth experiment using our treatment schedule. Similarly, a low dose of WFA impaired microvascular sprouting in the β3-floxed Tie1.Cre +ve but not in the Cre -ve background. These observations imply that the absence of endothelial β3-integrin sensitises the vasculature to WFA-induced inhibition of pathological angiogenesis – an exciting finding in the context of anti-angiogenic treatment.

We did not observe any apparent signs of weight loss, while Yu *et al*. observed some, but negligible weight loss (<10%) in the first week of treatment, which was regained in the second week [418]. Thaiparambil *et al*. also assessed necrosis and fibrosis of the lungs and livers of the mice used in their 30-day tumour growth experiment and did not observe any [444]. The WFA- and vehicle-treated mice displayed similar profiles of fibrosis and necrosis. The dose used in these *in vivo* studies in mice was much higher than the dosage used in clinical trials, yet positive effects are seen in both [414], [418], [444], [487], [500]. All the documented studies in humans involving ingestion of WFA have used WFA-containing *Withania somnifera* plant extract, rather than pure WFA. Overall, research suggests that WFA is a relatively safe substance and it may be possible to define an active dose, safely below toxic levels.

To complement the *in vivo* experiment, we conducted an aortic ring assay using WFA in the same genetic background. We observed that WFA inhibited microvascular sprouting upon β3-integrin depletion (Cre +ve), compared to the untreated control, which corroborates with the vessel density result from the *in vivo* work. However, we also observed sprouting inhibition using DMSO alone in the Cre +ve background. DMSO appears to be having an effect almost as strong as WFA. This was very surprising, as the content of DMSO in the media used was only 0.01%, too low to cause any toxicity, while it did not have any effect on the Cre -ve rings or wild-type rings in the dose finding experiment. Generally, it is accepted as non-toxic, when used at less than 0.1% (v/v) *in vitro*, while high doses induce apoptosis [501]. On the other hand, 0.1% DMSO caused genome-wide changes in DNA methylation of cardiac and hepatic cells in culture, with a range of implications on biological processes [501]. Others have shown substantial sprouting, in the presence of DMSO, in the rat aortic rings (0.5%) and in mouse spheroids (0.1%) [502], [503]. However, to our knowledge, a detailed analysis of the effect of DMSO on mouse aortic ring sprouting has not been published. In conclusion, it is unlikely that 0.01% DMSO has such a dramatic effect on microvascular sprouting. We believe that increasing the n numbers in this experiment would abolish the difference between the Cre +ve untreated and Cre +ve DMSO-treated conditions.

There appeared to be a marginal increase in sprouting in the presence of β3-integrin (Cre -ve) upon WFA treatment. The stimulation of sprouting in WFA-treated aortic rings could be explained by the increase in proliferation described in Chapter 4, most pronounced at 0.2 μM. However, it is interesting that we did not see the same effect in the dose-response test with WFA, perhaps due to the difference in the genetic background of the mice used. The dose-finding experiment (**Fig 6.4 A**) was conducted on aortic rings isolated from wild-type pure C57 mice, whereas the ones used in the dual-targeting experiment (**Fig 6.4 B and C**) were on a mixed C57/129 background.

Here, we used the Tie1.Cre model of endothelial depletion of β3-integrin in the *ex vivo* and the *in vivo* experiments. In the Pdgfb.CreER model, when Cre activity is induced shortly before implantation of tumour cells (short OHT), the depletion of β3-integrin causes a significant decrease in tumour growth and microvascular sprouting [180]. When the induction of Cre occurs 21 days before tumour implantation (long OHT), tumour growth and aortic sprouting are no longer inhibited by the loss of β3-integrin [180]. It would be interesting to see whether WFA leads to an additional effect of tumour growth inhibition in the short OHT model and even more interestingly, if WFA could restore tumour growth inhibition in the long OHT model of β3-integrin depletion.

WFA treatment is a systemic method of Vim inhibition. We would need to generate Vim-floxed β3-floxed Pdgfb.CreER / Tie1.Cre mice in order to fully focus on the endothelial proteins. Both β3-KO and Vim-KO mice can reach adulthood and are fertile [175], [305]. Therefore, a double floxed Cre mouse of this sort would most likely be viable and could be used to expand the analysis done here, providing information about endothelial-specific dual-targeting of Vim and β3-integrin.

In summary, we were surprised that only one of the shRNA constructs against Nes had a significant effect on aortic ring sprouting and disappointed that we could not confirm target depletion. We were excited to see a decreased blood vessel density in the Cre +ve WFA-treated tumours, suggesting that co-targeting Vim and β3-integrin is beneficial in the context of pathological angiogenesis. In the context of cancer, it is interesting to see the trend for smaller tumours in the β3-floxed Cre +ve mice treated with WFA, but we are slightly disappointed that this is not a statistically significant difference, as others have seen in different models using WFA.

7 Final Discussion and Future Work

Anti-angiogenic agents used in the clinic all target the VEGF-pathway [247]. Unfortunately, they often cause significant side effects [249]. In comparison, inhibition of αVβ3 integrin, expression of which is turned on in angiogenic vasculature, is much less toxic, thanks to the specificity of the target [251], [274]. This has led to a substantial focus from the research community to evaluate it as an anti-angiogenic target. A prominent αVβ3 inhibitor, Cilengitide, was shown to effectively inhibit angiogenesis, tumour growth and metastasis *in vivo* and made it all the way to late stage clinical trials [168], [504]. Unfortunately, it failed to provide a meaningful survival benefit to the cancer patients participating in the trials [504], [505]. Surprisingly, β3-KO mice exhibit enhanced tumour growth and angiogenesis [275]. We previously investigated the endothelial-specific contribution of β3-integrin to angiogenesis in mice, using an inducible/acute model of depletion (β3-floxed Pdgfb.CreER) and a deletion from birth (β3-floxed Tie1.Cre). We observed impaired angiogenesis and tumour growth in the acute model but no change in tumour growth and enhanced VEGF-dependent angiogenesis in the long-term model, when β3-integrin was depleted [180]. Acquired resistance to drug treatment, as well as the observations made using genetic models, is indicative of an escape mechanism upon long-term inhibition and depletion of β3-integrin. Recently, we investigated this escape mechanism by analysis and comparison of the normal and β3-depleted endothelial adhesomes, through which EC adhesion and migration, and thus angiogenesis, are regulated. Mass spectrometry identified increased presence of tubulins in the β3-depleted EC adhesome compared to the control [232]. We followed this up with a series of experiments and identified a Rac1-dependent stabilisation of MTs in β3-depleted ECs [232]. Moreover, EC migration became more MT-dependent in β3-depleted cells, while tumour growth and angiogenesis were more susceptible to MT inhibitors in mice depleted in β3 integrin in the endothelium [232]. The mass spectrometry identified other potential pathways of compensation that accompany β3-integrin depletion/inhibition. This thesis re-visited this dataset to investigate potential escape targets beyond MTs.

We focused on the candidates which were upregulated in the β3-depleted EC adhesome, then narrowed down the candidate list to those that did so in at least two of the three β3-depletion models (β3-HET, β3-KO and cRGD-treated). From this list of 104 proteins, based on GO and KEGG annotations, with aid of publication search engines, we chose 12 candidates known to be involved in angiogenesis or EC biology. We investigated how their siRNA KD affects adhesion and migration of WT and β3-HET ECs. Interestingly, siRNA KD of Nes, Plec and Vim impaired migration in both WT and β3-HET cells. Adhesion was impaired only in the β3-HET cells,

suggesting a differential role for these proteins upon β3-depletion. These findings led us to focus on these three IF-type proteins and evaluate them as potential mediators of compensation upon β3-integrin depletion. STRING, a protein interaction search tool, highlighted previously identified interactions of Vim with β3-integrin and Src, as well as Plec with a number of canonical FA players, namely β3-integrin, FAK, paxillin and vinculin [475], [506].

Mass spectrometry of the adhesomes also identified numerous angiogenesis-relevant players that were downregulated upon β3-integrin depletion, such as Adam10, Adamts1, Adamts4 and the whole ERM family of FA adaptors: ezrin, moesin and radixin. Two known anti-angiogenic players, vWF and Thbs1, were differentially altered in the β3-HET and β3-KO adhesomes. In the future, it would be interesting to follow these up, as well as other proteins seen upregulated in the β3-depleted EC adhesome, such as Naa15 and Slit3.

We begun testing our hypothesis that Nes, Plec and Vim were mediators of the compensation mechanism by further *in vitro* experiments using siRNA and WFA, an inhibitor of Vim. Nes KD impaired random migration in WT cells, but not in β3-depleted cells. However, we were unable to assess Nes KD. We decided to generate labelled Nes constructs that could be used to investigate Nes-FA interaction. We were successful in generating the constructs but were only able to conduct proof-of-concept ICC using these constructs, before running out of time. We also generated shRNA constructs, using the pSico technology, that could be used in Cre-expressing cells/tissue for targeting endothelial Nes, Plec and Vim [463]. These were utilised in the aortic ring assay using aortas from Pdfb.CreER mice. In this experiment, one of the constructs targeting Nes led to an inhibition of microvascular sprouting. Nes has been shown to be upregulated in tumour vasculature, and to promote invasion and metastasis of cancer cells [398], [496]. On the other hand, Nes has been shown to inhibit FAK and FA turnover, so it would be interesting to elucidate its role in FAs and angiogenesis further [400]. Interestingly, synemin, structurally very similar to Nes, has been shown to bind some of the canonical members of FAs, α-actinin and vinculin [291]. We confirmed an upregulation of Plec in β3-HET adhesome compared to WT by WB of FA enrichment samples, as seen by mass spectrometry. However, in our hands, Plec KD had no significant effect on random migration or ERK1/2 phosphorylation of ECs. This is surprising, since Plec has been shown to recruit Vim IFs to FAs in ECs [293]. Others have concluded that it is required for vascular integrity due to its role in FAs and tight junctions [410]. Vim binds β3-integrin in FAs, directly and via Plec [222], [475]. This interaction serves to stabilise FAs and promote cell adhesion [222], [475]. Unfortunately, like Plec KD, Vim KD did not significantly affect EC migration or ERK1/2 phosphorylation in our hands, although it may be that this protein is very abundant and its turnover is rapid, resulting in an inefficient KD. Overall, we did not obtain any striking results in our attempts to co-target β3-integrin (β3-HET cells) and IF

proteins (siRNA) in angiogenesis-relevant assays. We obtained different results using the wound-closure and the random migration assay, likely due to the different nature of these assays. In the former ECs were more closely interacting with one another, which makes this assay more relevant to angiogenesis, while in the latter we assessed migration speed of individual cells. It would be interesting to attempt a triple KD (Nes, Plec and Vim) in β3-HET ECs. It is likely that we would see a synergistic, pro-angiogenic contribution of these three proteins, or redundancy, especially between Vim and Nes, which are both IF monomers.

However, our luck changed, when we came across WFA, an inhibitor of Vim. There was a differential response to WFA in WT and β3-HET ECs in terms of migration and proliferation. WFA had an inhibitory effect on proliferation of β3-HET compared to WT ECs, and stimulated WT but inhibited β3-HET EC migration in the wound-closure assay. From ICC, it was evident that WFA disrupts the Vim IFs, especially in the periphery of ECs. We quantified the amount of Vim fragments with and without WFA treatment in WT and β3-HET ECs, and there appeared to be more of these in the WFA-treated β3-HET cells than in the WFA-treated WT cells. We utilised an mCherry-labelled Vim construct in ICC to look at Vim-FA associations in WT ECs. There appeared to be less of these associations in the WFA treated ECs compared to DMSO-control cells. This is a logical conclusion, given the collapsed Vim IFs around the nucleus in WFA-treated cells but unfortunately, we have not done extensive analysis of this, to state this with confidence. We followed this up with a WB of WT ECs treated with a range of concentrations of WFA. It was observed that the more of WFA was added to the cells the more P-Vim was detected. Dave *et al*. observed that the loss of Vim (shRNA) in ECs decreased both total and phosphorylated FAK [446]. This prompted us to check if WFA is influencing FAK expression and phosphorylation in our cells. WFA treatment is expected to disrupt Vim-FA interaction, which would imply that Vim would not complex with FAK to the same extent, similar to the Vim shRNA transfected cells. There appeared to be a decrease in both total and phosphorylated FAK in our WFA-treated WT ECs but densitometry from two WBs revealed no significant difference. If we had more time, we would further investigate FAK expression and activation in relation to WFA-treatment. Others have shown that WFA inhibits angiogenesis and tumour growth [417], [444]. We used an endothelial-specific β3-deletion model (β3-floxed Tie1.Cre) in combination with WFA treatment to assess co-targeting of β3-integrin and Vim in the context of tumour growth and angiogenesis. Whilst there was no statistically significant change in tumour growth in the WFA-treated animals, there was a trend for tumour growth inhibition. However, WFA treatment did inhibit pathological (tumour) angiogenesis and microvascular sprouting (aortic ring assay) in the Cre +ve (β3-depleted), but not in the Cre -ve (β3-WT) background. This is an exciting finding, supporting a potential benefit of co-targeting β3-integrin and Vim as an anti-angiogenic strategy.

Many questions remain unanswered. How does β3-depletion or inhibition lead to an upregulation of Nes, Plec and Vim in the FAs? Via what molecular mechanism? What other FA and non-FA players are involved? Is WFA definitely disrupting Vim-FA interactions? Is fragmented/soluble Vim able to bind and regulate FAs? How effectively? What other FA proteins does Vim bind in FAs? Are these contributing to the escape mechanism upon β3-integrin depletion or inhibition? These questions could be addressed with further experiments using analytical methods such as immunoprecipitation, fluorescence and FRET microscopy, if we had more time.

Overall, all three IF proteins appear to play pro-angiogenic roles in ECs [385], [410], [496]. Vim KO mice experience much less severe consequences compared to Nes KO and Plec KO mice, both of which result in prenatal death [390], [403]. Vim KO mice develop into fertile adulthood, but exhibit a wound healing impairment [305]. This suggests that from these three, Vim targeting would be associated with the least severe side effects. Indeed, WFA, as part of the *W. somnifera* plant extract, is in extensive use as a food supplement and as part of clinical trials for a variety of conditions [486]–[489].

Additional work could be conducted to further investigate Nes, Plec and Vim as mediators of compensation which accompanies β3-integrin depletion and inhibition. Further study would benefit from a conclusive assessment of co-targeting β3-integrin and Nes/Plec/Vim with respect to EC adhesion. Certainly, the molecular mechanism of interaction of β3-integrin and Nes/Plec/Vim in FAs requires further investigation. Also, we could expand this study with additional cell models, such as β3-HET Vim-HET ECs; and additional mouse models such as β3-floxed Vim-floxed Tie1.Cre animals. Nevertheless, our findings suggest that dual targeting of Vim and β3-integrin may hold promise as a novel anti-angiogenic strategy.

Appendix

1. Supplementary figures and tables

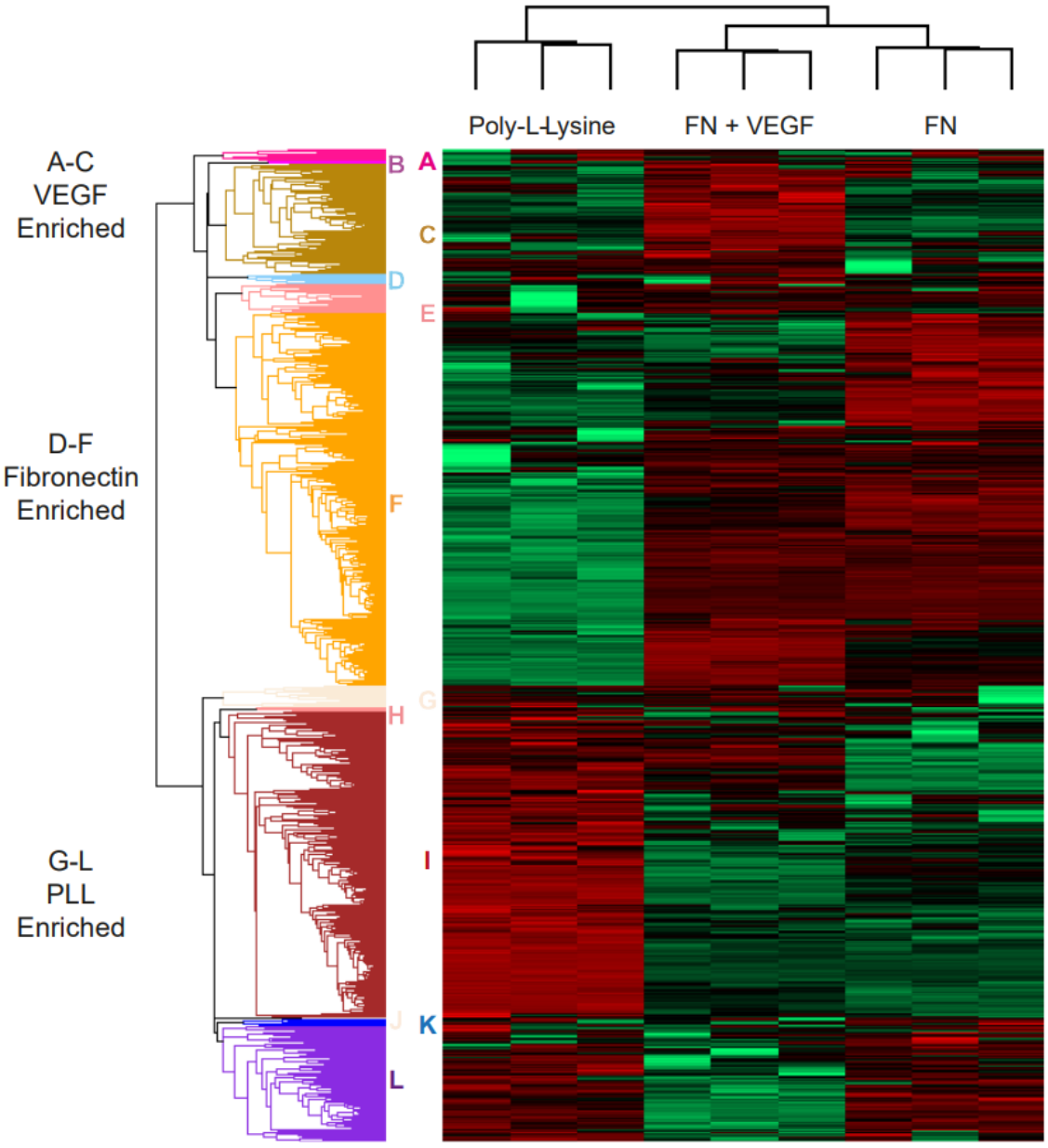

Supplementary Figure 1 Hierarchical clustering of the endothelial adhesome

Unsupervised hierarchical clustering based on Euclidian distance (threshold of 3.34) of 3 FN, 3 FN with VEGF and 3 poly-l-lysine β3+/+ EC adhesome samples. A - L are cluster labels, red indicated high and green indicates low expression. Taken from [232].

Supplementary Table 1 List of proteins upregulated in the β3-KO vs WT endothelial adhesome.

				LFQ NORMALISED TO WT β3			
GENE NAME	**PROTEIN ID**	**PROTEIN NAME**	**CLUSTER**	**WT**	**β3-KO**	**-LOG P VALUE**	**DIFFERENCE**
Itgb3	**O54890**	**Integrin beta-3**	**F**	**100.000**	**0.000**	**4.413**	**-4.052**
…							…
Slit3	**Q3UHN1**	**Slit Guidance Ligand 3**		**0.000**	**136.457**	**3.271**	**3.871**
H3f3a	P84244	Histone H3.3	I	0.000	161.008	1.559	3.709
Nos3	P70313	Nitric oxide synthase, endothelial	F	21.839	241.674	3.616	3.512
Cd55	Q61475	CD antigen CD55	C	0.000	53.787	3.619	3.301
Htra1	Q9R118	Serine protease HTRA1	F	0.000	60.743	3.011	3.073
Ifrd2	Q9D8U0	Interferon-related developmental reg. 2		0.000	57.353	3.835	2.966
Top2a	Q01320	DNA topoisomerase 2-alpha		0.000	56.941	3.538	2.95
Actg1	Q9QZ83	Gamma actin-like protein	F	36.251	166.814	1.218	2.679
Oasl1	Q8VI94	2'-5'-oligoadenylate synthase-like prote		0.000	39.198	2.579	2.531
Trmt1l	A2RSY6	TRMT1-like protein	C	0.000	44.061	3.495	2.531
Vwf	Q2I0J8	Von Willebrand factor	F	44.297	241.379	4.981	2.452
Cars	Q3U716	Cysteinyl-TRNA Synthetase		4.716	43.943	2.331	2.416
Cdc37	Q61081	Hsp90 co-chaperone Cdc37	C	0.000	32.567	4.004	2.403
Impdh2	A0A0A6YY72	Inosine-5'-monophosphate dehydrogenase 2	I	12.555	65.606	1.88	2.353
Col4a2	**B2RQQ8**	**Collagen, type IV, alpha 2**	**F**	**11.833**	**52.608**	**1.855**	**2.303**
Vat1	Q5RKP0	Vat1 protein	L	0.000	27.409	3.071	2.239
Prr11	Q8BHE0	Proline-rich protein 11	E	22.841	113.999	2.258	2.226
Apobec3	H3BJQ3	Apolipoprotein B MRNA Editing Enzyme 3		0.000	39.876	3.018	2.218
Dnaja1	Q5NTY0	DnaJ (Hsp40) homolog	I	7.692	69.850	2.89	2.113
Slc25a3	Q3THU8	Solute Carrier Family 25 Member 3	C	19.599	61.214	0.987	2.084
Ctps1	P70698	CTP synthase 1	I	20.483	84.792	3.305	2.077

				LFQ NORMALISED TO WT β3			
GENE NAME	**PROTEIN ID**	**PROTEIN NAME**	**CLUSTER**	**WT**	**β3-KO**	**-LOG P VALUE**	**DIFFERENCE**
Isg15	Q4FJR9	G1p2 protein (ubiquitin-like modifier)	C	8.806	37.106	2.601	2.023
Surf4	Q545Q2	Surfeit gene 4, isoform CRA_a	F	2.735	31.064	2.744	1.955
Hspa9	P38647	Stress-70 protein, mitochondrial		0.000	35.102	1.291	1.954
Mndal	D0QMC3	Myeloid cell nuclear diff. antigen-like		6.897	48.364	1.827	1.915
Dnm2	Q3T9X3	Dynamin-2	C	0.000	23.961	1.716	1.901
Bmp1	Q570Z4	Bone Morphogenetic Protein 1	K	35.131	127.910	3.864	1.861
Lbr	Q3U9G9	Lamin-B receptor	F	816.387	2932.508	6.344	1.844
Smc3	Q6P5E5	Structural maintenance of chromosomes 3		9.402	43.884	0.878	1.816
Hspd1	P63038	60 kDa heat shock protein, mitochondrial	G	4.804	45.122	2.461	1.784
Rrp9	Q91WM3	U3 small nucleolar RNA-interacting		0.000	19.216	2.246	1.779
Gcn1l1	Q3UHQ5	EIF2 Alpha Kinase Activator Homolog	G	0.000	25.052	3.046	1.764
Znf22	Q9ERU3	Zinc finger protein 22		0.000	30.091	1.454	1.732
Phgdh	Q61753	D-3-phosphoglycerate dehydrogenase	C	9.078	31.594	1.514	1.729
Rnf213	F7A6H4	E3 ubiquitin-protein ligase RNF213	I	65.075	213.970	3.538	1.712
Ehd4	Q3TM70	EH-domain containing 4	C	80.253	262.305	4.508	1.712
Smc2	Q3ULS2	Structural maintenance of chromosomes 2	I	28.559	93.369	3.081	1.69
Serpine1	D0ESZ6	Ser or Cys peptidase inhibitor cl E member 1	F	65.488	208.960	2.941	1.685
Psmd3	Q8BK46	Proteasome 26S Subunit, Non-ATPase 3	I	14.235	45.299	4.621	1.672
Psmc4	Q3UBF0	Proteasome 26S Subunit, ATPase 4		0.000	25.258	2.135	1.671
Fbxl6	Q9QXW0	F-box/LRR-repeat protein 6		0.000	22.370	1.996	1.656
Pdia4	P08003	Protein disulfide-isomerase A4	I	0.000	25.700	1.413	1.637
Abcf2	Q3UVI9	ATP Binding Cassette Subfamily F Member 2	C	21.515	64.132	1.2	1.62
Cct7	Q3UIJ0	Chaperonin Containing TCP1 Subunit 7	I	49.190	141.173	2.38	1.559
Oas1a	P11928	2'-5'-oligoadenylate synthase 1A	F	29.089	89.861	1.772	1.541
Mdh2	P08249	Malate dehydrogenase, mitochondrial	C	5.836	27.645	1.149	1.532

				LFQ NORMALISED TO WT β3			
GENE NAME	PROTEIN ID	PROTEIN NAME	CLUSTER	WT	β3-KO	-LOG P VALUE	DIFFERENCE
Fscn1	Q61553	Fascin (Singed-like protein)	F	54.937	156.499	3.735	1.523
Ncbp1	Q3UYV9	Nuclear cap-binding protein subunit 1	E	0.000	35.838	3.874	1.511
Ncapg	E9PWG6	Non-SMC condensin I complex, subunit G	L	17.035	47.952	4.054	1.493
Rpn2	Q61833	Ribophorin	I	3.979	24.138	1.195	1.476
Mina	Q8CD15	Ribosomal oxygenase 2	F	129.089	357.795	3.238	1.471
Gfpt1	P47856	Glutamine-fructose-6-P aminotransferase		0.000	18.715	4.498	1.462
Paics	Q9DCL9	Multifunctional protein ADE2	I	26.820	73.475	3.273	1.458
Tagln2	Q9WVA4	Transgelin-2 (SM22-beta)	E	31.300	85.470	3.785	1.452
Iars	Q8BU30	Isoleucine--tRNA ligase, cytoplasmic	I	250.516	669.319	3.534	1.419
Gvin1	**L7N451**	**Interferon-induced very large GTPase 1**	**I**	**134.394**	**354.553**	**5.458**	**1.397**
Atp5a1	**D3Z6F5**	**ATP synthase subunit alpha**	**G**	**61.627**	**161.214**	**3.906**	**1.392**
Chd3	F7C528	Chromodomain helicase DNA-binding 3		0.000	38.432	1.361	1.388
Dimt1	Q3UK38	rRNA adenine N(6)-methyltransferase	L	20.631	53.375	3.155	1.382
Tgm2	P21981	Protein-glutamine γ-glutamyltransferase 2	F	73.504	189.508	3.193	1.367
Serpinh1	**Q3TWG9**	**Serpin Family H Member 1**	**F**	**365.753**	**940.171**	**4.526**	**1.36**
Ncapd2	Q8K2Z4	Condensin complex subunit 1		0.000	13.027	1.369	1.353
Atp2a2	J3KMM5	ATPase Reticulum Ca2+ Transporting 2		0.000	21.751	1.398	1.341
Sntb2	Q542S9	Syntrophin, basic 2	F	0.000	18.096	1.759	1.325
Canx	Q5SUC3	Calnexin, isoform CRA_a	I	21.220	52.431	2.371	1.312
Smc1a	A0JLM6	Smc1a protein		5.305	22.812	1.509	1.311
Eif3e	Q3UIG0	Eukaryotic translation initiation factor	I	89.891	217.212	4.208	1.275
Kpna2	Q52L97	Importin subunit alpha	L	25.081	55.791	2.004	1.186
Ddx47	Q4VBG1	Asp-Glu-Ala-Asp box polypeptide 4	F	136.752	311.229	2.947	1.174
Sp110	Q8BVK9	Sp110 nuclear body protein	F	105.217	234.895	3.338	1.163
Tars	Q99KJ4	Tars protein	E	11.583	25.936	3.276	1.163

				LFQ NORMALISED TO WT β3			
GENE NAME	**PROTEIN ID**	**PROTEIN NAME**	**CLUSTER**	**WT**	**β3-KO**	**-LOG P VALUE**	**DIFFERENCE**
Naa15	**Q80UM3**	**N-alpha-acetyltransferase 15**	**I**	**113.174**	**252.579**	**3.178**	**1.158**
H2afv	B2RVP5	Histone H2A	I	37.430	82.641	2.688	1.136
Cct3	Q3U4U6	T-complex protein 1 subunit gamma	I	110.816	241.379	3.688	1.124
Drg2	Q9QXB9	Developmentally-regulated GTP-binding 2	C	11.052	23.873	3.204	1.116
Cct4	Q564F4	T-complex protein 1 subunit delta	I	108.164	233.422	3.236	1.114
Gsn	Q6PAC1	Gelsolin, isoform CRA_c	F	35.102	75.950	3.07	1.112
Wdr5	P61965	WD repeat-containing protein 5	F	62.629	133.215	4.025	1.09
Cct6a	Q52KG9	Chaperonin containing Tcp1, subunit 6a	I	91.482	192.455	4.62	1.077
Cct8	Q3UL22	Chaperonin subunit 8 (Theta)	I	79.310	167.403	3.38	1.076
Sdpr	Q63918	Caveolae-associated protein 2 (Cavin-2)	I	33.068	68.553	2.839	1.062
Cct5	P80316	T-complex protein 1 subunit epsilon	I	91.954	192.455	3.387	1.059
Snx9	Q9CZK0	Sorting Nexin 9	I	24.433	50.280	4.45	1.041
Hsp90ab1	Q71LX8	Heat shock protein 84b	C	1093.428	2216.328	5.163	1.019
EG433182	Q5FW97	Enolase 1, alpha non-neuron	L	274.388	553.198	5.115	1.011
Eif3f	Q6IRT4	Eukaryotic translation initiation factor	I	65.105	130.563	3.681	1.01
Ddx58	A1L0V6	Ddx58 protein	I	37.047	73.976	4.155	0.996
Tcp1	**P11983**	**T-complex protein 1 subunit alpha**	**I**	**191.276**	**376.953**	**4.767**	**0.979**

Second column contains one of the corresponding peptide IDs identified for each gene using the Andromeda database. The 4th column informs on inclusion to a particular cluster, as identified by unsupervised hierarchical clustering: A, B, C – VEGF-enriched; D, E, F – fibronectin-enriched and clusters G, H, I, J, K, L – poly-L-lysine enriched. LFQ – label free quantification value obtained from the mass spectrometer. The LFQ values presented here are averages from 3 runs of FA enrichment samples expressed relative to the average LFQ detected for β3-integrin in WT condition. The last 2 columns report the -log P value and the *t*-test difference from the Significance Analysis of Microarrays (SAM) carried out in Perseus. The table was sorted in descending order based on the last column. Chosen candidate genes taken forward for further analysis are highlighted and in bold. Adapted from Atkinson et al (2018) [232].

Supplementary Table 2 List of proteins upregulated in the cRGD-treated vs WT endothelial adhesome.

				LFQ NORMALISED TO DMSO β3		
GENE NAME	**PROTEIN ID**	**PROTEIN NAME**	**CLUSTER**	**DMSO**	**cRGD**	**FOLD CHANGE**
Itgb3	**O54890**	**Integrin beta-3**	**F**	**100.000**	**47.844**	**0.478**
…						…
Fgb	Q3TGR2	Fibrinogen beta chain	F	1.000	33.793	33.793
Nes	**Q6P5H2**	**Nestin**		**1.000**	**33.564**	**33.564**
Ncbp1	Q3UYV9	Nuclear cap-binding protein subunit 1	E	1.000	24.342	24.342
Cd55	Q61475	Complement decay-accelerating factor, GPI-anchored	C	1.000	19.898	19.898
Cs	Q0QEL9	Citrate synthase;Citrate synthase, mitochondrial	F	1.000	14.525	14.525
Aldh2	Q544B1	Aldehyde dehydrogenase, mitochondrial		1.000	14.523	14.523
Col4a1	P02463	Collagen alpha-1(IV) chain;Arresten	F	1.742	13.854	7.955
Surf4	Q545Q2	Surfeit locus protein 4	F	2.739	21.190	7.737
Rpl36;Gm8973	Q6ZWZ4	60S ribosomal protein L36	I	28.703	154.452	5.381
Actg1	Q9QZ83	Actin, cytoplasmic 2	F	36.384	195.195	5.365
Mest	Q07646	Mesoderm-specific transcript protein	F	3.752	19.663	5.240
Ptk2	K7Q751	Focal adhesion kinase 1	F	5.110	24.695	4.833
Hspd1	P63038	60 kDa heat shock protein, mitochondrial	G	4.807	22.107	4.599
Fgg	Q3UEM7	Fibrinogen gamma chain	F	6.082	27.561	4.531
Phb;1700071K01Rik	P67778	Prohibitin	D	2.075	8.850	4.265
Dnaja1	Q5NTY0	DnaJ homolog subfamily A member 1	I	7.699	30.152	3.916
Cttn	Q921L6	Src substrate cortactin	F	6.851	25.900	3.780
Pdlim1	Q3TZ17	PDZ and LIM domain protein 1	C	5.971	21.939	3.674
Sec23a	E9Q1S3	Protein transport protein Sec23A	F	6.858	25.105	3.661
Cars	Q3U716	Cysteine--tRNA ligase, cytoplasmic		4.737	17.249	3.641
Mdh2	P08249	Malate dehydrogenase, mitochondrial	C	5.849	20.699	3.539

				LFQ NORMALISED TO DMSO β3		
GENE NAME	**PROTEIN ID**	**PROTEIN NAME**	**CLUSTER**	**DMSO**	**cRGD**	**FOLD CHANGE**
Slc25a3	Q3THU8	Phosphate carrier protein, mitochondrial	C	19.629	62.219	3.170
Srsf7	Q3THA6	Serine/arginine-rich splicing factor 7	E	10.999	34.260	3.115
Sept10	Q8C650	Septin-10	I	14.945	45.340	3.034
Ppp2r2a	Q9CWU3	Ser/Thr-protein P-ase 2A 55 kDa regulatory subunit B α isoform		16.654	50.383	3.025
Lamb1	Q3UHL7	Laminin subunit beta-1	F	6.387	17.250	2.701
Anxa6	Q99JX6	Annexin;Annexin A6	C	5.892	15.876	2.695
Cpsf7	Q8BTV2	Cleavage and polyadenylation specificity factor subunit 7		4.710	12.323	2.616
Eps15l1	Q60902	Epidermal growth factor receptor substrate 15-like 1	I	5.935	13.867	2.336
Pdlim5	D9J2Z9	PDZ and LIM domain protein 5	F	7.362	16.647	2.261
Cnbp	Q3U935	Cellular nucleic acid-binding protein	I	10.331	22.938	2.220
Rpl28	Q5M9N5	60S ribosomal protein L28	L	67.736	148.682	2.195
Ybx1	Q60950	Y-Box Binding Protein 1	E	1246.128	2669.949	2.143
Rpn1	Q5RKP4	Dolichyl-di(P)oligosaccharide protein glycosyltransferase 1	I	18.924	38.905	2.056
Trip10	Q8CJ53	Cdc42-interacting protein 4	A	11.108	22.206	1.999
Rpl36a	Q5M9P1	60S ribosomal protein L36a	F	730.369	1448.200	1.983
Vim	**Q5FWJ3**	**Vimentin**	**F**	**1236.307**	**2409.453**	**1.949**
Gar1	D3YZ09	H/ACA ribonucleoprotein complex subunit 1	L	9.357	18.127	1.937
Eprs	B9EIU1	Glutamyl-Prolyl-TRNA Synthetase	I	184.771	353.060	1.911
Rpl18	Q642K1	60S ribosomal protein L18	F	940.142	1773.480	1.886
Hist1h3b/1h3e/2h3b	A1L0U3	Histone H3;Histone H3.2	C	1981.771	3665.219	1.849
Purb	O35295	Transcriptional activator protein Pur-beta	I	17.168	31.651	1.844
Sptan1	P16546	Spectrin alpha chain, non-erythrocytic 1	I	424.896	779.069	1.834
Ctps1	P70698	CTP synthase 1	I	20.526	37.550	1.829
Atp5a1	**D3Z6F5**	**ATP synthase subunit alpha**	**G**	**61.739**	**112.378**	**1.820**
Mars	E9QB02	Methionine--tRNA ligase, cytoplasmic	C	20.858	37.786	1.812

				LFQ NORMALISED TO DMSO β3		
GENE NAME	PROTEIN ID	PROTEIN NAME	CLUSTER	DMSO	cRGD	FOLD CHANGE
Macf1	B1ARU1	Microtubule-actin cross-linking factor 1	G	22.221	40.206	1.809
Elavl1	Q8BTQ1	ELAV-like protein 1	I	17.393	31.128	1.790
Myh10	Q5SV64	Myosin-10	I	65.495	116.343	1.776
Rpl6;Gm5428	Q3UCH0	60S ribosomal protein L6	C	2410.103	4265.228	1.770
Sept11	Q8C1B7	Septin-11	L	162.008	286.091	1.766
Rpl15;Gm10020	Q5M8Q0	Ribosomal protein L15;60S ribosomal protein L15	F	1545.081	2726.111	1.764
Phb2	Q3V235	Prohibitin-2	C	9.377	16.504	1.760
Vps35	Q3TRJ1	Vacuolar protein sorting-associated protein 35	I	14.645	25.762	1.759
Rpl32	P62911	60S ribosomal protein L32	F	323.647	568.780	1.757
Tpm3;Tpm3-rs7	Q58E70	Tropomyosin 3	C	91.059	159.909	1.756
Rrs1	Q80U76	Ribosome biogenesis regulatory protein homolog	C	626.418	1086.984	1.735
Sptbn1	Q62261	Spectrin beta chain, non-erythrocytic 1	I	365.063	632.876	1.734
Drg2	Q9QXB9	Developmentally-regulated GTP-binding protein 2	C	11.085	19.044	1.718
Rpl34	Q9D1R9	60S ribosomal protein L34	C	75.270	128.993	1.714
Plec	**Q6S390**	**Plectin**	**F**	**410.043**	**696.612**	**1.699**
Atp5b	P56480	ATP synthase subunit beta, mitochondrial	C	52.870	89.123	1.686
Flnc	D3YW87	Filamin-C	F	35.369	59.300	1.677
Ahnak	E9Q616	AHNAK Nucleoprotein	F	541.856	906.497	1.673
Sept2	P42208	Septin-2	C	203.338	340.047	1.672
Coro1c	Q5PPQ7	Coronin;Coronin-1C	I	240.966	401.208	1.665
Psmd3	Q8BK46	26S proteasome non-ATPase regulatory subunit 3	I	14.259	23.555	1.652
Ywhag	A8IP69	14-3-3 protein gamma, N-terminally processed	I	30.305	49.878	1.646
Dars	Q8BK18	Aspartate--tRNA ligase, cytoplasmic	I	143.798	233.501	1.624
Ola1	Q3TW21	Obg-like ATPase 1	F	10.645	17.268	1.622
Abcf2	Q3UVI9	ATP-binding cassette sub-family F member 2	C	21.561	34.862	1.617

				LFQ NORMALISED TO DMSO β3		
GENE NAME	**PROTEIN ID**	**PROTEIN NAME**	**CLUSTER**	**DMSO**	**cRGD**	**FOLD CHANGE**
Rpl29;Gm17669	Q5M8M8	60S ribosomal protein L29	C	670.448	1083.411	1.616
Sdpr	Q63918	Serum deprivation-response protein	I	33.137	53.405	1.612
Lmnb1	P14733	Lamin-B1	C	26.564	42.368	1.595
Rpl35;Gm10269	Q6ZWV7	60S ribosomal protein L35	F	714.432	1135.764	1.590
St13	F8WJK8	Hsc70-interacting protein	L	9.701	15.409	1.588
Sept7	E9Q1G8	Septin-7	F	260.605	412.479	1.583
Eif3i	Q9QZD9	Eukaryotic translation initiation factor 3 subunit I	I	71.146	112.159	1.576
Impdh2	A0A0A6	Inosine-5-mono(P) dehydrogenase 2	I	12.587	19.784	1.572
Actr1a	P61164	Alpha-centractin	I	40.140	62.947	1.568
Eif3e	Q3UIG0	Eukaryotic translation initiation factor 3 subunit E	I	89.866	140.314	1.561
Nckap1	A1L0U6	Nck-associated protein 1	I	27.976	43.551	1.557
Mta2	Q3UDZ8	Metastasis-associated protein MTA2	G	21.786	33.844	1.554
Dync1h1	Q9JHU4	Cytoplasmic dynein 1 heavy chain 1	I	319.053	493.495	1.547
Fn1	Q3UGY5	Fibronectin;Anastellin	F	11450.947	17597.494	1.537
Snx9	Q9CZK0	Sorting nexin;Sorting nexin-9	I	24.512	37.604	1.534
Rpl13a	Q5M9M0	60S ribosomal protein L13a	I	310.646	476.428	1.534
Ptrf	O54724	Polymerase I and transcript release factor	I	128.916	197.256	1.530
Pura	Q8C6E9	Transcriptional activator protein Pur-alpha	I	9.971	15.225	1.527
Rpl18a	Q3THJ0	60S ribosomal protein L18a	F	1095.192	1666.737	1.522
Naa25	B2RQV1	N-alpha-acetyltransferase 25, NatB auxiliary subunit	F	7.835	11.842	1.511
Brix1	Q9DCA5	Ribosome biogenesis protein BRX1 homolog	F	678.269	1015.231	1.497
Rps25	Q58EA6	40S ribosomal protein S25	I	109.445	163.307	1.492
Actg1	Q4KL81	Actin Gamma 1	F	3656.155	5406.277	1.479
Canx	Q5SUC3	Calnexin	I	21.260	31.335	1.474
Cnp	Q3TYL9	2,3-cyclic-nucleotide 3-phosphodiesterase	C	12.829	18.880	1.472

				LFQ NORMALISED TO DMSO β3		
GENE NAME	**PROTEIN ID**	**PROTEIN NAME**	**CLUSTER**	**DMSO**	**cRGD**	**FOLD CHANGE**
Myh9	Q8VDD5	Myosin-9	C	1953.778	2872.659	1.470
Kif5b	Q61768	Kinesin-1 heavy chain	I	87.825	129.085	1.470
Tubb6	Q3UMM1	Tubulin beta-6 chain	F	27.681	40.573	1.466
Ehd4	Q3TM70	EH domain-containing protein 4	C	80.378	117.362	1.460
Rock2	F8VPK5	Rho-associated protein kinase;Rho-associated protein kinase 2	E	86.436	125.529	1.452
Eif3h	Q8BTX5	Eukaryotic translation initiation factor 3 subunit H	I	39.924	57.709	1.445
Rpl14;Rpl14-ps1	Q9CR57	60S ribosomal protein L14	I	471.751	681.305	1.444
Trim25	Q5SU72	E3 ubiquitin/ISG15 ligase TRIM25	I	15.689	22.492	1.434
Dsp	E9Q557	Desmoplakin	F	21.966	31.351	1.427
Myl12a;Myl12b	Q922W7	Myosin regulatory light chain 12B	F	74.266	105.979	1.427
Cltc;mKIAA0034	**Q5SXR6**	**Clathrin heavy chain;Clathrin heavy chain 1**	**I**	**665.215**	**948.350**	**1.426**
Naa15	**Q80UM3**	**N-alpha-acetyltransferase 15, NatA auxiliary subunit**	**I**	**113.361**	**161.223**	**1.422**
Tubb2a	Q7TMM9	Tubulin beta-2A chain	C	21.982	31.205	1.420
Rpl3	Q3UB15	60S ribosomal protein L3	C	7740.581	10969.349	1.417
Tubb4b;Tubb4a	P68372	Tubulin beta-4B chain;Tubulin beta-4A chain	C	701.850	994.532	1.417
Jup	Q02257	Junction plakoglobin	I	68.537	96.987	1.415
Cul1	Q3UIA5	Cullin-1	C	18.940	26.784	1.414
Serpinb6a;Serpinb6	E9Q108	Serpin B6	I	28.965	40.929	1.413
Dnaja2	Q9QYJ0	DnaJ homolog subfamily A member 2	L	48.569	68.586	1.412
Dab2	E9QL31	Disabled homolog 2	L	12.232	17.269	1.412
Myl6	Q642K0	Myosin light polypeptide 6	F	99.707	140.606	1.410
Etf1	Q3U6V5	Eukaryotic peptide chain release factor subunit 1	B	21.559	30.309	1.406
Abce1	Q6NXX7	ATP-binding cassette sub-family E member 1	C	146.515	205.577	1.403
Fam98b	Q80VD1	Protein FAM98B	I	14.527	20.374	1.402
Serpinh1	**Q3TWG9**	**Serpin H1**	**F**	**366.454**	**513.784**	**1.402**

				LFQ NORMALISED TO DMSO β3		
GENE NAME	PROTEIN ID	PROTEIN NAME	CLUSTER	DMSO	cRGD	FOLD CHANGE
Qars	Q8BU21	Glutaminyl-TRNA Synthetase	I	64.888	90.913	1.401
Itga3	Q62470	Integrin alpha-3; heavy and light chain	F	9.687	13.566	1.400
Arl6ip4	D3YWC2	ADP-ribosylation factor-like protein 6-interacting protein 4	C	33.239	46.412	1.396
Eef1a1	Q58E64	Elongation factor 1-alpha;Elongation factor 1-alpha 1	I	3473.730	4846.573	1.395
Ddx58	A1L0V6	Probable ATP-dependent RNA helicase DDX58	I	37.133	51.770	1.394
Son	H9KV01	Protein SON	C	10.818	15.019	1.388
Capza2	Q5DQJ3	F-actin-capping protein subunit alpha-2	I	18.498	25.624	1.385
Rsu1	A2AUR7	Ras suppressor protein 1	A	31.929	44.141	1.382
Hspa12b	**Q9CZJ2**	**Heat shock 70 kDa protein 12B**	**C**	**86.551**	**119.514**	**1.381**
Tuba1a;Tuba3a	P68369	Tubulin alpha-1A chain;Tubulin alpha-3 chain	C	40.803	56.070	1.374
Gtf2i	G3UYD0	General transcription factor II-I	F	20.671	28.382	1.373
Psmc1	Q542I9	26S protease regulatory subunit 4	L	31.692	43.473	1.372
Eif3f	Q6IRT4	Eukaryotic translation initiation factor 3 subunit F	I	65.217	89.426	1.371
Eef1g	Q4FZK2	Elongation factor 1-gamma	I	337.827	463.143	1.371
n/a	A0A097PUG1	Beta thymosin-like protein 2	F	89.386	122.308	1.368
Tinagl1	Q4FJX7	Tubulointerstitial nephritis antigen-like	L	8.880	12.142	1.367
Arf3;Arf1;Arf2	Q3U344	ADP-ribosylation factor 1, 2 and 3	F	76.155	103.980	1.365
Copb1	Q9JIF7	Coatomer subunit beta	I	15.219	20.774	1.365
Cdc42	P60766	Cell division control protein 42 homolog	C	88.744	120.876	1.362
Aimp2	Q8R010	Aminoacyl tRNA synthase complex-inter. multif. protein 2	I	18.629	25.355	1.361
Rpl12	Q5BLK0	60S ribosomal protein L12	I	42.798	58.203	1.360
Myo1b	E9QNH6	Unconventional myosin-Ib	F	29.837	40.576	1.360
Sept9	A2A6U3	Septin-9	C	107.736	146.479	1.360

				LFQ NORMALISED TO DMSO β3		
GENE NAME	**PROTEIN ID**	**PROTEIN NAME**	**CLUSTER**	**DMSO**	**cRGD**	**FOLD CHANGE**
Pds5b	F8WHU5	Sister chromatid cohesion protein PDS5 homolog B		21.152	28.753	1.359
Rps24	Q9CY61	40S ribosomal protein S24	F	1332.362	1809.562	1.358
Cyfip1	Q7TMB8	Cytoplasmic FMR1-interacting protein 1	I	141.495	192.124	1.358
Cald1	Q8VCQ8	Caldesmon 1	F	64.055	86.656	1.353
Gvin1	**L7N451**	**Interferon-induced very large GTPase 1**	**I**	**134.695**	**182.072**	**1.352**
…						…
Tcp1	**P11983**	**T-complex protein 1 subunit alpha**	**I**	**191.811**	**217.234**	**1.133**

Second column contains one of the corresponding peptide IDs identified for each gene using the Andromeda database. The 4th column informs on inclusion to a particular cluster, as identified by unsupervised hierarchical clustering: A, B, C – VEGF-enriched; D, E, F – fibronectin-enriched and clusters G, H, I, J, K, L – poly-L-lysine enriched. LFQ – label free quantification value obtained from the mass spectrometer. The LFQ values presented here are averages from 3 runs of FA enrichment samples expressed relative to the average LFQ detected for β3-integrin in DMSO condition. The last column reports the average fold change in the cRGD condition vs the DMSO control. Chosen candidate genes taken forward for further analysis are highlighted and in bold. Adapted from Atkinson et al (2018) [232].

2. Publications

2018 Samuel J Atkinson, **Aleksander M Gontarczyk**, Abdullah A A Alghamdi, Tim S Ellison, Robert T Johnson, Wesley J Fowler, Benjamin M Kirkup, Bernardo C Silva, Bronwen E Harry, Jochen G Schneider, Katherine N Weilbaecher, Mette M Mogensen, Mark D Bass, Maddy Parsons, Dylan R Edwards and Stephen D Robinson

"*The β3-integrin endothelial adhesome regulates microtubule dependent cell migration*"

(2018) EMBO reports, e44578

Abstract

Integrin β3 is seen as a key anti-angiogenic target for cancer treatment due to its expression on neovasculature, but the role it plays in the process is complex; whether it is pro- or anti-angiogenic depends on the context in which it is expressed. To understand precisely β3's role in regulating integrin adhesion complexes in endothelial cells, we characterised, by mass spectrometry, the β3-dependent adhesome. We show that depletion of β3-integrin in this cell type leads to changes in microtubule behaviour that control cell migration. β3-integrin regulates microtubule stability in endothelial cells through Rcc2/Anxa2-driven control of active Rac1 localisation. Our findings reveal that angiogenic processes, both in vitro and in vivo, are more sensitive to microtubule targeting agents when β3-integrin levels are reduced.

Synopsis

Engagement of αvβ3-integrin with fibronectin at mature focal adhesions localises an Rcc2/Anxa2/Rac1 containing complex to these sites, preventing Rac1 from stabilising microtubules. When αvβ3 is not present, the complex associates with α5β1-integrin instead, resulting in increased microtubule stability.

- β3-integrin regulates localisation of tubulin subunits to the endothelial adhesome.
- Angiogenic processes both in vitro and in vivo, are more sensitive to microtubule targeting agents when β3-integrin levels are reduced.
- Active Rac1 cellular associations change with depletion of β3-integrin.

2014 Veronica Steri, Tim S Ellison, **Aleksander M Gontarczyk**, Katherine Weilbaecher, Jochen G Schneider, Dylan R Edwards, Marcus Fruttiger, Kairbaan M Hodivala-Dilke and Stephen D Robinson

"*Acute Depletion of Endothelial β3-Integrin Transiently Inhibits Tumor Growth and Angiogenesis in Mice*"

(2014) Circulation Research, 114:79-91

Rationale:

The dramatic upregulation of αvβ3-integrin that occurs in the vasculature during tumor growth has long suggested that the endothelial expression of this molecule is an ideal target for antiangiogenic therapy to treat cancer. This discovery led to the development of small-molecule inhibitors directed against αvβ3-integrin that are currently in clinical trials. In 2002, we reported that β3-integrin−knockout mice exhibit enhanced tumor growth and angiogenesis. However, as β3-integrin is expressed by a wide variety of cells, endothelial cell–specific contributions to tumor angiogenesis are muddied by the use of a global knockout of β3-integrin function.

Objective:

Our aim was to examine the endothelial-specific contribution β3-integrin makes to tumor growth and angiogenesis.

Methods and Results:

We have crossed β3-integrin–floxed (β3-floxed) mice to 2 endothelial-specific Cre models and examined angiogenic responses in vivo, ex vivo, and in vitro. We show that acute depletion of endothelial β3-integrin inhibits tumor growth and angiogenesis preventatively, but not in already established tumors. However, the effects are transient, and long-term depletion of the molecule is ineffective. Furthermore, long-term depletion of the molecule correlates with many molecular changes, such as reduced levels of focal adhesion kinase expression and a misbalance in focal adhesion kinase phosphorylation, which may lead to a release from the inhibitory effects of decreased endothelial β3-integrin expression.

Conclusions:

Our findings imply that timing and length of inhibition are critical factors that need to be considered when targeting the endothelial expression of β3-integrin to inhibit tumor growth and angiogenesis.

Abbreviations

Ab – antibody
Acta2 – actin (mouse)
Actn1 – α-actinin
Akt – serine/threonine-specific protein kinase B
Amp – ampicillin
Ang1 – angiopoietin 1
Ang2 – angiopoietin 2
Anxa2 – annexin A2
Atp5a1 – ATP synthase α
αVβ3 – αVβ3 integrin
β3 – β3 integrin
BLAST – Basic Local Alignment Search Tool
BM – basement membrane
bp – base pair
BSA – bovine serum albumin
CD – cluster of differentiation / classification determinant, e.g. CD31
CD31 – PECAM-1, Platelet EC adhesion molecule
Cdc42 – cell division cycle 42
cDNA – complementary DNA
Cltc – clathrin heavy chain 1
CMT19T – a mouse lung carcinoma cell line
CMV – cytomegalovirus promoter
Col4a2 – Collagen type IV α 2
Cre-Lox – DNA engineering method based on the Cre recombinase enzyme and loxP sites
cRGD – cyclic arginine-glycine-aspartate motif mimetic, EMD66203
DAPI – 4',6-Diamidino-2-phenylindole
Des – desmin
DMEM – Dulbecco's modified eagle medium
DMSO – dimethyl sulphoxide, cryopreservant
dNTP – deoxy-nucleotide triphosphate
EC – endothelial cell
ECL – peroxidase substrate for enhanced chemiluminescence
ECM – extra-cellular matrix
EDTA – ethylenediaminetetraacetic acid
EGF – epidermal growth factor
EGFP – enhanced GFP
EMBL – European Molecular Biology Laboratory
EMEA – European Medicines Agency
EMT – epithelial to mesenchymal transition
eNOS – endothelial nitric oxide synthase
ESC – embryonic stem cell
***et al*.** – and others
FA – focal adhesion
FAK – focal adhesion kinase

FBS – foetal bovine serum
FGF – fibroblast growth factor
FITC – fluorescein isothiocyanate
fl – floxed
FN – fibronectin
Fwd – forward
Gapdh – glyceraldehyde-3-phosphate dehydrogenase
GEF – guanine nucleotide exchange factor
Gfap – glial fibrillary acidic protein
GFP – green fluorescent protein
GgP+E – mouse embryonic fibroblast cell line used for virus production
GlutaMAX™ – a more stable L-glutamine formulation for tissue culture (Thermo)
GO – Gene Ontology
GTPase – guanosine triphosphatase
Gvin1 – interferon-induced very large GTPase 1
H & E – hematoxylin and eosin stain
HEK293 – human embryonic kidney cell line
HET – heterozygous
HIF – hypoxia-inducible factor, e.g. HIF-1α
HRP – Horseradish peroxidase
Hsc70 – heat shock 70kDa protein 8
Hspa12b – heat-shock 70kD 12b
HUVEC – human umbilical vein EC
ICAM – intercellular adhesion molecule
ICC – Immunocytochemistry
IF – intermediate filament
IFAP – IF-associated protein, e.g. plectin
IHC – immunohistochemistry
IκBα – NF-κB inhibitor α
IKKB – NF-κB inhibitor kinase β
IMMLEC – immortalised lung EC
IP – intraperitoneal
Kan – kanamycin
KEGG – Kyoto Encyclopedia of Genes and Genomes
KD – siRNA knockdown
KO – knockout
LC-MS/MS – liquid chromatography tandem mass spectrometry
LFQ – label-free quantification
Lmna – lamin
loxP – floxing / target sites for the Cre recombinase
MACS – magnetic activated cell sorting
MaxQuant – mass spectrometry analysis software
MCAM – melanoma cell adhesion molecule
MCS – multiple cloning site
MF – actin microfilament
MLEC medium – medium used for primary lung EC culture

MMP – matrix metalloproteinase
mRNA – messenger RNA
MT – microtubule
Naa15 – N-α-acetyltransferase 15
NCBI – National Center for Biotechnology Information
Neo – neomycin
Nes – nestin
NF-κB – nuclear factor kappa B
NO – nitric oxide
Nrp-1 – neuropilin-1
nt – non-targeting / nucleotide
o/n – overnight
OHT – 4-hydroxy-tamoxifen
Opti-MEM™ - Minimum Essential Media
P – phospho(rylated) / P value
PBLEC – PBS, 1% Tween-20, 1 mM MgCl2, 1 mMCaCl2, 100 µM MnCl2
PBS – phosphate buffered saline
PBS/T – PBS 0.1% Tween-20
PCR – polymerase chain reaction
Pdgfb – platelet-derived growth factor B
PFA – paraformaldehyde
PGF – placenta growth factor
PI3K – phosphoinositide 3-kinase
Plec – plectin
PLL – poly-L-lysine
pNes-N-Tom – plasmid expressing a Nes-tdTomato construct
pSico – conditional (Cre-Lox), stable shRNA expression system, Cre turns on shRNA
pSicoR – conditional (Cre-Lox), stable shRNA expression system, Cre turns off shRNA
pTom-C-Nes – plasmid expressing a tdTomato-Nes construct
Ptk2 – gene name for FAK, focal adhesion kinase
Pxn – paxilin
PyMT – polyoma middle T antigen
P/S – Pen/Strep, Penicillin/Streptomycin
qRT-PCR – real-time PCR
Rac1 – Rac Family Small GTPase 1
Rcc2 – regulator of chromosome condensation 2
Rev – reverse
RGD – arginine-glycine-aspartate motif
RIPA – Radioimmunoprecipitation assay (lysis) buffer
RT – Room temperature
SAM – significance analysis of microarrays
SD – standard deviation
SDS – Sodium dodecyl sulphate
SDS-PAGE – Sodium dodecyl sulphate polyacrylamide gel electrophoresis
SEM – standard error of the mean
Serpinh1 – Serpin Family H Member 1

siRNA – small/short interfering RNA
shRNA – short hairpin RNA
Slit3 – Slit Homolog 3
STRING – Search Tool for the Retrieval of Interacting Genes/Proteins
Src – tyrosine-protein kinase, proto oncogene
Sync – syncoilin
Synm – synemin
Tcp1 – T-complex 1 (protein)
tdTomato – tandem Tomato red fluorescent protein
TE – Tris-EDTA buffer
TGF-β – transforming growth factor β
Tie1 – Tyrosine kinase with immunoglobulin-like and EGF-like domains 1
TIMP – tissue inhibitor of metalloproteinases
Thbs1 – Thrombospondin 1
Tln1 – talin
Tns1 – tensin
Tyr – Y / tyrosine
UT – untreated
UTR – untranslated region
Vcl – vinculin
VECAD – VE Cadherin / CD144
VEGF – vascular endothelial growth factor
WB – Western blot
WFA – withaferin A
WSE – *Withania somnifera* extract
WT – wild-type
Vcl – vinculin
VEGF – vascular endothelial growth factor
VEGFR1/2/3– vascular endothelial growth factor receptor 1 / 2 / 3
Vim – vimentin
vWF – von Willebrand factor
Y – Tyr / tyrosine

References

[1] J. W. Baish *et al.*, 'Scaling rules for diffusive drug delivery in tumor and normal tissues', *PNAS*, Jan. 2011.

[2] W. Risau, 'Mechanisms of angiogenesis', *Nature*, vol. 386, no. 6626, pp. 671–674, Apr. 1997.

[3] W. Risau and I. Flamme, 'Vasculogenesis', *Annual Review of Cell and Developmental Biology*, vol. 11, no. 1, pp. 73–91, 1995.

[4] K. Krah, V. Mironov, W. Risau, and I. Flamme, 'Induction of Vasculogenesis in Quail Blastodisc-Derived Embryoid Bodies', *Developmental Biology*, vol. 164, no. 1, pp. 123–132, Jul. 1994.

[5] O. Cleaver and P. A. Krieg, 'VEGF mediates angioblast migration during development of the dorsal aorta in Xenopus', *Development*, vol. 125, no. 19, pp. 3905–3914, Oct. 1998.

[6] T. P. Yamaguchi, D. J. Dumont, R. A. Conlon, M. L. Breitman, and J. Rossant, 'flk-1, an flt-related receptor tyrosine kinase is an early marker for endothelial cell precursors', *Development*, vol. 118, no. 2, pp. 489–498, Jun. 1993.

[7] B. Millauer *et al.*, 'High affinity VEGF binding and developmental expression suggest Flk-1 as a major regulator of vasculogenesis and angiogenesis', *Cell*, vol. 72, no. 6, pp. 835–846, Mar. 1993.

[8] A. Eichmann, C. Marcelle, C. Bréant, and N. M. Le Douarin, 'Two molecules related to the VEGF receptor are expressed in early endothelial cells during avian embryonic development', *Mechanisms of Development*, vol. 42, no. 1, pp. 33–48, Jul. 1993.

[9] P. Carmeliet *et al.*, 'Abnormal blood vessel development and lethality in embryos lacking a single VEGF allele', *Nature*, vol. 380, no. 6573, pp. 435–439, Apr. 1996.

[10] N. Ferrara *et al.*, 'Heterozygous embryonic lethality induced by targeted inactivation of the VEGF gene', *Nature*, vol. 380, no. 6573, pp. 439–442, Apr. 1996.

[11] G.-H. Fong, J. Rossant, M. Gertsenstein, and M. L. Breitman, 'Role of the Flt-1 receptor tyrosine kinase in regulating the assembly of vascular endothelium', *Nature*, vol. 376, no. 6535, pp. 66–70, Jul. 1995.

[12] F. Shalaby *et al.*, 'Failure of blood-island formation and vasculogenesis in Flk-1-deficient mice', *Nature*, vol. 376, no. 6535, pp. 62–66, Jul. 1995.

[13] H.-P. Gerber *et al.*, 'Vascular Endothelial Growth Factor Regulates Endothelial Cell Survival through the Phosphatidylinositol 3'-Kinase/Akt Signal Transduction Pathway REQUIREMENT FOR Flk-1/KDR ACTIVATION', *J. Biol. Chem.*, vol. 273, no. 46, pp. 30336–30343, Nov. 1998.

[14] T. Takahashi, H. Ueno, and M. Shibuya, 'VEGF activates protein kinase C-dependent, but Ras-independent Raf-MEK-MAP kinase pathway for DNA synthesis in primary endothelial cells', *Oncogene*, vol. 18, no. 13, pp. 2221–2230, Apr. 1999.

[15] P. N. Bernatchez, S. Soker, and M. G. Sirois, 'Vascular Endothelial Growth Factor Effect on Endothelial Cell Proliferation, Migration, and Platelet-activating Factor Synthesis Is Flk-1-dependent', *J. Biol. Chem.*, vol. 274, no. 43, pp. 31047–31054, Oct. 1999.

[16] G. H. Fong, L. Zhang, D. M. Bryce, and J. Peng, 'Increased hemangioblast commitment, not vascular disorganization, is the primary defect in flt-1 knock-out mice', *Development*, vol. 126, no. 13, pp. 3015–3025, Jul. 1999.

[17] J. E. Park, H. H. Chen, J. Winer, K. A. Houck, and N. Ferrara, 'Placenta growth factor. Potentiation of vascular endothelial growth factor bioactivity, in vitro and in vivo, and high affinity binding to Flt-1 but not to Flk-1/KDR.', *J. Biol. Chem.*, vol. 269, no. 41, pp. 25646–25654, Oct. 1994.

[18] P. Carmeliet and R. K. Jain, 'Molecular mechanisms and clinical applications of angiogenesis', *Nature*, vol. 473, no. 7347, pp. 298–307, May 2011.

[19] S. Patan, B. Haenni, and P. H. Burri, 'Implementation of Intussusceptive Microvascular Growth in the Chicken Chorioallantoic Membrane (CAM):: 1. Pillar Formation by Folding of the Capillary Wall', *Microvascular Research*, vol. 51, no. 1, pp. 80–98, Jan. 1996.

[20] R. H. D. Short, 'Alveolar epithelium in relation to growth of the lung', *Phil. Trans. R. Soc. Lond. B*, vol. 235, no. 622, pp. 35–86, Nov. 1950.

[21] A. Plein, A. Fantin, and C. Ruhrberg, 'Neuropilin regulation of angiogenesis, arteriogenesis, and vascular permeability', *Microcirculation*, vol. 21, no. 4, pp. 315–323, 2014.

[22] K. Guillemin and M. A. Krasnow, 'The Hypoxic Response: Huffing and HIFing', *Cell*, vol. 89, no. 1, pp. 9–12, Apr. 1997.

[23] P. Carmeliet, 'Mechanisms of angiogenesis and arteriogenesis', *Nature medicine*, vol. 6, no. 4, pp. 389–396, 2000.

[24] P. Carmeliet, 'Angiogenesis in health and disease', *Nature Medicine*, vol. 9, no. 6, pp. 653–660, Jun. 2003.

[25] G. Struhl and A. Adachi, 'Nuclear Access and Action of Notch In Vivo', *Cell*, vol. 93, no. 4, pp. 649–660, May 1998.

[26] S. Weijzen *et al.*, 'Activation of Notch-1 signaling maintains the neoplastic phenotype in human Ras-transformed cells', *Nature Medicine*, vol. 8, no. 9, pp. 979–986, Sep. 2002.

[27] J. K. Park, T. W. Lee, E. K. Do, H. J. Moon, and J. H. Kim, 'Role of Notch1 in the arterial specification and angiogenic potential of mouse embryonic stem cell-derived endothelial cells', *Stem Cell Research & Therapy*, vol. 9, no. 1, p. 197, Jul. 2018.

[28] J. Gavard and J. S. Gutkind, 'VEGF controls endothelial-cell permeability by promoting the β-arrestin-dependent endocytosis of VE-cadherin', *Nature Cell Biology*, vol. 8, no. 11, pp. 1223–1234, Nov. 2006.

[29] J. Kroll and J. Waltenberger, 'A Novel Function of VEGF Receptor-2 (KDR): Rapid Release of Nitric Oxide in Response to VEGF-A Stimulation in Endothelial Cells', *Biochemical and Biophysical Research Communications*, vol. 265, no. 3, pp. 636–639, Nov. 1999.

[30] P. Carmeliet and R. K. Jain, 'Molecular mechanisms and clinical applications of angiogenesis', *Nature*, vol. 473, no. 7347, pp. 298–307, May 2011.

[31] L.-K. Phng and H. Gerhardt, 'Angiogenesis: A Team Effort Coordinated by Notch', *Developmental Cell*, vol. 16, no. 2, pp. 196–208, Feb. 2009.

[32] B. Strilić *et al.*, 'The Molecular Basis of Vascular Lumen Formation in the Developing Mouse Aorta', *Developmental Cell*, vol. 17, no. 4, pp. 505–515, Oct. 2009.

[33] E. I. Deryugina and J. P. Quigley, ‘Pleiotropic roles of matrix metalloproteinases in tumor angiogenesis: Contrasting, overlapping and compensatory functions’, *Biochimica et Biophysica Acta (BBA) - Molecular Cell Research*, vol. 1803, no. 1, pp. 103–120, Jan. 2010.

[34] M. Potente, H. Gerhardt, and P. Carmeliet, ‘Basic and Therapeutic Aspects of Angiogenesis’, *Cell*, vol. 146, no. 6, pp. 873–887, Sep. 2011.

[35] M. Franco, P. Roswall, E. Cortez, D. Hanahan, and K. Pietras, ‘Pericytes promote endothelial cell survival through induction of autocrine VEGF-A signaling and Bcl-w expression’, *Blood*, vol. 118, no. 10, pp. 2906–2917, Sep. 2011.

[36] R. K. Jain, ‘Molecular regulation of vessel maturation’, *Nature Medicine*, vol. 9, no. 6, pp. 685–693, Jun. 2003.

[37] M. C. Dickson, J. S. Martin, F. M. Cousins, A. B. Kulkarni, S. Karlsson, and R. J. Akhurst, ‘Defective haematopoiesis and vasculogenesis in transforming growth factor-beta 1 knock out mice’, *Development*, vol. 121, no. 6, pp. 1845–1854, Jun. 1995.

[38] M.-J. Goumans, F. Lebrin, and G. Valdimarsdottir, ‘Controlling the Angiogenic Switch: A Balance between Two Distinct TGF-b Receptor Signaling Pathways’, *Trends in Cardiovascular Medicine*, vol. 13, no. 7, pp. 301–307, Oct. 2003.

[39] A. B. Roberts *et al.*, ‘Transforming growth factor type beta: rapid induction of fibrosis and angiogenesis in vivo and stimulation of collagen formation in vitro’, *PNAS*, vol. 83, no. 12, pp. 4167–4171, Jun. 1986.

[40] M. Klagsbrun and M. A. Moses, ‘Molecular angiogenesis’, *Chemistry & Biology*, vol. 6, no. 8, pp. R217–R224, Aug. 1999.

[41] S. Artavanis-Tsakonas, M. D. Rand, and R. J. Lake, ‘Notch Signaling: Cell Fate Control and Signal Integration in Development’, *Science*, vol. 284, no. 5415, pp. 770–776, Apr. 1999.

[42] M. A. T. Muskavitch, ‘Delta-Notch Signaling and Drosophila Cell Fate Choice’, *Developmental Biology*, vol. 166, no. 2, pp. 415–430, Dec. 1994.

[43] T. Gridley, ‘Notch Signaling in Vertebrate Development and Disease’, *Molecular and Cellular Neuroscience*, vol. 9, no. 2, pp. 103–108, Jan. 1997.

[44] N. Ferrara, ‘VEGF and the quest for tumour angiogenesis factors’, *Nature Reviews Cancer*, vol. 2, no. 10, pp. 795–803, 2002.

[45] Lewis, W. H, ‘The vascular pattern of tumors.’, *Bulletin of Johns Hopkins Hospital*, no. 41, pp. 156–162, 1927.

[46] L. M. Sherwood, E. E. Parris, and J. Folkman, ‘Tumor Angiogenesis: Therapeutic Implications’, *New England Journal of Medicine*, vol. 285, no. 21, pp. 1182–1186, Nov. 1971.

[47] ‘Tumors: Wounds That Do Not Heal | NEJM’, *New England Journal of Medicine*. [Online]. Available: https://www.nejm.org/doi/pdf/10.1056/NEJM198612253152606. [Accessed: 26-Nov-2018].

[48] J. S. Desgrosellier and D. A. Cheresh, ‘Integrins in cancer: biological implications and therapeutic opportunities’, *Nature Reviews Cancer*, vol. 10, no. 1, pp. 9–22, Jan. 2010.

[49] P. Carmeliet and R. K. Jain, ‘Principles and mechanisms of vessel normalization for cancer and other angiogenic diseases’, *Nature Reviews Drug Discovery*, vol. 10, no. 6, pp. 417–427, Jun. 2011.

[50] J. J. Salk, E. J. Fox, and L. A. Loeb, 'Mutational Heterogeneity in Human Cancers: Origin and Consequences', *Annual Review of Pathology: Mechanisms of Disease*, vol. 5, no. 1, pp. 51–75, 2010.

[51] S. Negrini, V. G. Gorgoulis, and T. D. Halazonetis, 'Genomic instability — an evolving hallmark of cancer', *Nature Reviews Molecular Cell Biology*, vol. 11, no. 3, pp. 220–228, Mar. 2010.

[52] S. M. Weis and D. A. Cheresh, 'Pathophysiological consequences of VEGF-induced vascular permeability', *Nature*, vol. 437, no. 7058, pp. 497–504, Sep. 2005.

[53] M. Toi *et al.*, 'Quantitative analysis of vascular endothelial growth factor in primary breast cancer', *Cancer*, vol. 77, no. 6, pp. 1101–1106, 1996.

[54] M. P. Wong, N. Cheung, S. T. Yuen, S. Y. Leung, and L. P. Chung, 'Vascular endothelial growth factor is up-regulated in the early pre-malignant stage of colorectal tumour progression', *International Journal of Cancer*, vol. 81, no. 6, pp. 845–850, 1999.

[55] J. Goveia, P. Stapor, and P. Carmeliet, 'Principles of targeting endothelial cell metabolism to treat angiogenesis and endothelial cell dysfunction in disease', *EMBO Molecular Medicine*, vol. 6, no. 9, pp. 1105–1120, Sep. 2014.

[56] S. M. Weis and D. A. Cheresh, 'Tumor angiogenesis: molecular pathways and therapeutic targets', *Nature Medicine*, vol. 17, no. 11, pp. 1359–1370, Nov. 2011.

[57] J. W. Baish and R. K. Jain, 'Fractals and cancer', *Cancer Res.*, vol. 60, no. 14, pp. 3683–3688, Jul. 2000.

[58] R. K. Jain, 'Normalizing tumor vasculature with anti-angiogenic therapy: a new paradigm for combination therapy', *Nat. Med.*, vol. 7, no. 9, pp. 987–989, Sep. 2001.

[59] S. Demaria *et al.*, 'Cancer and Inflammation: Promise for Biological Therapy', *J Immunother*, vol. 33, no. 4, pp. 335–351, May 2010.

[60] W. Zou, 'Regulatory T cells, tumour immunity and immunotherapy', *Nature Reviews Immunology*, vol. 6, no. 4, pp. 295–307, Apr. 2006.

[61] V. Plaks *et al.*, 'Uterine DCs are crucial for decidua formation during embryo implantation in mice', *J Clin Invest*, vol. 118, no. 12, pp. 3954–3965, Dec. 2008.

[62] E. Y. Lin *et al.*, 'Macrophages Regulate the Angiogenic Switch in a Mouse Model of Breast Cancer', *Cancer Res*, vol. 66, no. 23, pp. 11238–11246, Dec. 2006.

[63] J. Galon *et al.*, 'Type, Density, and Location of Immune Cells Within Human Colorectal Tumors Predict Clinical Outcome', *Science*, vol. 313, no. 5795, pp. 1960–1964, Sep. 2006.

[64] F. Pagès *et al.*, 'Effector Memory T Cells, Early Metastasis, and Survival in Colorectal Cancer', *New England Journal of Medicine*, vol. 353, no. 25, pp. 2654–2666, Dec. 2005.

[65] P. Carmeliet and R. K. Jain, 'Principles and mechanisms of vessel normalization for cancer and other angiogenic diseases', *Nature Reviews Drug Discovery*, vol. 10, no. 6, pp. 417–427, Jun. 2011.

[66] N. Jetten, S. Verbruggen, M. J. Gijbels, M. J. Post, M. P. J. De Winther, and M. M. P. C. Donners, 'Anti-inflammatory M2, but not pro-inflammatory M1 macrophages promote angiogenesis in vivo', *Angiogenesis*, vol. 17, no. 1, pp. 109–118, Jan. 2014.

[67] J. Ma, L. Liu, G. Che, N. Yu, F. Dai, and Z. You, 'The M1 form of tumor-associated macrophages in non-small cell lung cancer is positively associated with survival time', *BMC Cancer*, vol. 10, no. 1, p. 112, Mar. 2010.

[68] D. M. Mosser and J. P. Edwards, 'Exploring the full spectrum of macrophage activation', *Nature Reviews Immunology*, vol. 8, no. 12, pp. 958–969, Dec. 2008.

[69] T. Asahara *et al.*, 'Isolation of Putative Progenitor Endothelial Cells for Angiogenesis', *Science*, vol. 275, no. 5302, pp. 964–966, Feb. 1997.

[70] D. Lyden *et al.*, 'Impaired recruitment of bone-marrow–derived endothelial and hematopoietic precursor cells blocks tumor angiogenesis and growth', *Nature Medicine*, vol. 7, no. 11, pp. 1194–1201, Nov. 2001.

[71] P. S. Steeg, 'Tumor metastasis: mechanistic insights and clinical challenges', *Nature Medicine*, vol. 12, no. 8, pp. 895–904, Aug. 2006.

[72] A. B. Al-Mehdi, K. Tozawa, A. B. Fisher, L. Shientag, A. Lee, and R. J. Muschel, 'Intravascular origin of metastasis from the proliferation of endothelium-attached tumor cells: a new model for metastasis', *Nature Medicine*, vol. 6, no. 1, pp. 100–102, Jan. 2000.

[73] D. Hanahan and R. A. Weinberg, 'The Hallmarks of Cancer', *Cell*, vol. 100, no. 1, pp. 57–70, Jan. 2000.

[74] D. Hanahan and R. A. Weinberg, 'Hallmarks of Cancer: The Next Generation', *Cell*, vol. 144, no. 5, pp. 646–674, Mar. 2011.

[75] D. T. Connolly *et al.*, 'Tumor vascular permeability factor stimulates endothelial cell growth and angiogenesis.', *J Clin Invest*, vol. 84, no. 5, pp. 1470–1478, Nov. 1989.

[76] D. W. Leung, G. Cachianes, W. J. Kuang, D. V. Goeddel, and N. Ferrara, 'Vascular endothelial growth factor is a secreted angiogenic mitogen', *Science*, vol. 246, no. 4935, pp. 1306–1309, Dec. 1989.

[77] P. J. Keck *et al.*, 'Vascular permeability factor, an endothelial cell mitogen related to PDGF', *Science*, vol. 246, no. 4935, pp. 1309–1312, Dec. 1989.

[78] N. Ferrara, H.-P. Gerber, and J. LeCouter, 'The biology of VEGF and its receptors', *Nature Medicine*, vol. 9, no. 6, pp. 669–676, Jun. 2003.

[79] C. J. Robinson and S. E. Stringer, 'The splice variants of vascular endothelial growth factor (VEGF) and their receptors', *Journal of Cell Science*, vol. 114, no. 5, pp. 853–865, Mar. 2001.

[80] K. A. Houck, N. Ferrara, J. Winer, G. Cachianes, B. Li, and D. W. Leung, 'The Vascular Endothelial Growth Factor Family: Identification of a Fourth Molecular Species and Characterization of Alternative Splicing of RNA', *Mol Endocrinol*, vol. 5, no. 12, pp. 1806–1814, Dec. 1991.

[81] H. Roy, S. Bhardwaj, and S. Ylä-Herttuala, 'Biology of vascular endothelial growth factors', *FEBS Letters*, vol. 580, no. 12, pp. 2879–2887, 2006.

[82] D. Shweiki, A. Itin, D. Soffer, and E. Keshet, 'Vascular endothelial growth factor induced by hypoxia may mediate hypoxia-initiated angiogenesis', *Nature*, vol. 359, no. 6398, pp. 843–845, 1992.

[83] A. P. Levy, N. S. Levy, S. Wegner, and M. A. Goldberg, 'Transcriptional Regulation of the Rat Vascular Endothelial Growth Factor Gene by Hypoxia', *Journal of Biological Chemistry*, vol. 270, no. 22, pp. 13333–13340, Jun. 1995.

[84] Y. Liu, S. R. Cox, T. Morita, and S. Kourembanas, 'Hypoxia Regulates Vascular Endothelial Growth Factor Gene Expression in Endothelial Cells : Identification of a 5' Enhancer', *Circulation Research*, vol. 77, no. 3, pp. 638–643, Sep. 1995.

[85] R. R. Lonser *et al.*, 'von Hippel-Lindau disease', *The Lancet*, vol. 361, no. 9374, pp. 2059–2067, Jun. 2003.

[86] M. Los, J. M. L. Roodhart, and E. E. Voest, 'Target Practice: Lessons from Phase III Trials with Bevacizumab and Vatalanib in the Treatment of Advanced Colorectal Cancer', *The Oncologist*, vol. 12, no. 4, pp. 443–450, Apr. 2007.

[87] K. J. Kim *et al.*, 'Inhibition of vascular endothelial growth factor-induced angiogenesis suppresses tumour growth in vivo', *Nature*, vol. 362, no. 6423, pp. 841–844, Apr. 1993.

[88] B. Olofsson *et al.*, 'Vascular endothelial growth factor B (VEGF-B) binds to VEGF receptor-1 and regulates plasminogen activator activity in endothelial cells', *PNAS*, vol. 95, no. 20, pp. 11709–11714, Sep. 1998.

[89] D. Bellomo *et al.*, 'Mice lacking the vascular endothelial growth factor-B gene (Vegfb) have smaller hearts, dysfunctional coronary vasculature, and impaired recovery from cardiac ischemia', *Circ. Res.*, vol. 86, no. 2, pp. E29-35, Feb. 2000.

[90] M. Reichelt *et al.*, 'Vascular endothelial growth factor-B and retinal vascular development in the mouse', *Clinical & Experimental Ophthalmology*, vol. 31, no. 1, pp. 61–65, 2003.

[91] V. Louzier *et al.*, 'Role of VEGF-B in the lung during development of chronic hypoxic pulmonary hypertension', *American Journal of Physiology-Lung Cellular and Molecular Physiology*, vol. 284, no. 6, pp. L926–L937, Jun. 2003.

[92] F. Zhang *et al.*, 'VEGF-B is dispensable for blood vessel growth but critical for their survival, and VEGF-B targeting inhibits pathological angiogenesis', *PNAS*, vol. 106, no. 15, pp. 6152–6157, Apr. 2009.

[93] C. E. Wright, 'Effects of vascular endothelial growth factor (VEGF)A and VEGFB gene transfer on vascular reserve in a conscious rabbit hindlimb ischaemia model', *Clinical and Experimental Pharmacology and Physiology*, vol. 29, no. 11, pp. 1035–1039, 2002.

[94] T. Tammela and K. Alitalo, 'Lymphangiogenesis: Molecular Mechanisms and Future Promise', *Cell*, vol. 140, no. 4, pp. 460–476, Feb. 2010.

[95] J. Welti, S. Loges, S. Dimmeler, and P. Carmeliet, 'Recent molecular discoveries in angiogenesis and antiangiogenic therapies in cancer', *J Clin Invest*, vol. 123, no. 8, pp. 3190–3200, Aug. 2013.

[96] M. J. Karkkainen, T. Mäkinen, and K. Alitalo, 'Lymphatic endothelium: a new frontier of metastasis research', *Nature Cell Biology*, vol. 4, pp. E2–E5, Jan. 2002.

[97] S. Van de Veire *et al.*, 'Further Pharmacological and Genetic Evidence for the Efficacy of PlGF Inhibition in Cancer and Eye Disease', *Cell*, vol. 141, no. 1, pp. 178–190, Apr. 2010.

[98] M. Autiero *et al.*, 'Role of PlGF in the intra- and intermolecular cross talk between the VEGF receptors Flt1 and Flk1', *Nature Medicine*, vol. 9, no. 7, pp. 936–943, Jul. 2003.

[99] R. L. Kendall and K. A. Thomas, 'Inhibition of vascular endothelial cell growth factor activity by an endogenously encoded soluble receptor', *PNAS*, vol. 90, no. 22, pp. 10705–10709, Nov. 1993.

[100] J. Waltenberger, L. Claesson-Welsh, A. Siegbahn, M. Shibuya, and C. H. Heldin, 'Different signal transduction properties of KDR and Flt1, two receptors for vascular endothelial growth factor.', *J. Biol. Chem.*, vol. 269, no. 43, pp. 26988–26995, Oct. 1994.

[101] J. Krueger *et al.*, 'Flt1 acts as a negative regulator of tip cell formation and branching morphogenesis in the zebrafish embryo', *Development*, vol. 138, no. 10, pp. 2111–2120, May 2011.

[102] H. Gerhardt *et al.*, 'VEGF guides angiogenic sprouting utilizing endothelial tip cell filopodia', *The Journal of Cell Biology*, vol. 161, no. 6, pp. 1163–1177, Jun. 2003.

[103] D. M. Roberts, J. B. Kearney, J. H. Johnson, M. P. Rosenberg, R. Kumar, and V. L. Bautch, 'The Vascular Endothelial Growth Factor (VEGF) Receptor Flt-1 (VEGFR-1) Modulates Flk-1 (VEGFR-2) Signaling During Blood Vessel Formation', *The American Journal of Pathology*, vol. 164, no. 5, pp. 1531–1535, May 2004.

[104] S. Hiratsuka, O. Minowa, J. Kuno, T. Noda, and M. Shibuya, 'Flt-1 lacking the tyrosine kinase domain is sufficient for normal development and angiogenesis in mice', *PNAS*, vol. 95, no. 16, pp. 9349–9354, Aug. 1998.

[105] B. K. Ambati *et al.*, 'Corneal avascularity is due to soluble VEGF receptor-1', *Nature*, vol. 443, no. 7114, pp. 993–997, Oct. 2006.

[106] S. Hiratsuka *et al.*, 'MMP9 induction by vascular endothelial growth factor receptor-1 is involved in lung-specific metastasis', *Cancer Cell*, vol. 2, no. 4, pp. 289–300, Oct. 2002.

[107] M. Shibuya, 'Vascular Endothelial Growth Factor (VEGF) and Its Receptor (VEGFR) Signaling in Angiogenesis', *Genes Cancer*, vol. 2, no. 12, pp. 1097–1105, Dec. 2011.

[108] A. Sawano, T. Takahashi, S. Yamaguchi, M. Aonuma, and M. Shibuya, 'Flt-1 but not KDR/Flk-1 tyrosine kinase is a receptor for placenta growth factor, which is related to vascular endothelial growth factor.', *Cell Growth Differ*, vol. 7, no. 2, pp. 213–221, Feb. 1996.

[109] L. B. Jakeman, J. Winer, G. L. Bennett, C. A. Altar, and N. Ferrara, 'Binding sites for vascular endothelial growth factor are localized on endothelial cells in adult rat tissues.', *Journal of Clinical Investigation*, vol. 89, no. 1, pp. 244–253, Jan. 1992.

[110] S. J. Kattman, T. L. Huber, and G. M. Keller, 'Multipotent Flk-1+ Cardiovascular Progenitor Cells Give Rise to the Cardiomyocyte, Endothelial, and Vascular Smooth Muscle Lineages', *Developmental Cell*, vol. 11, no. 5, pp. 723–732, Nov. 2006.

[111] S.-H. Jeon *et al.*, 'Mechanisms underlying TGF-β1-induced expression of VEGF and Flk-1 in mouse macrophages and their implications for angiogenesis', *Journal of Leukocyte Biology*, vol. 81, no. 2, pp. 557–566, 2007.

[112] D. Tvorogov *et al.*, 'Effective Suppression of Vascular Network Formation by Combination of Antibodies Blocking VEGFR Ligand Binding and Receptor Dimerization', *Cancer Cell*, vol. 18, no. 6, pp. 630–640, Dec. 2010.

[113] K. Holmes, O. L. Roberts, A. M. Thomas, and M. J. Cross, 'Vascular endothelial growth factor receptor-2: Structure, function, intracellular signalling and therapeutic inhibition', *Cellular Signalling*, vol. 19, no. 10, pp. 2003–2012, Oct. 2007.

[114] S. Koch, S. Tugues, X. Li, L. Gualandi, and L. Claesson-Welsh, 'Signal transduction by vascular endothelial growth factor receptors', *Biochemical Journal*, vol. 437, no. 2, pp. 169–183, Jul. 2011.

[115] K. N. Meadows, P. Bryant, and K. Pumiglia, 'Vascular Endothelial Growth Factor Induction of the Angiogenic Phenotype Requires Ras Activation', *J. Biol. Chem.*, vol. 276, no. 52, pp. 49289–49298, Dec. 2001.

[116] S. Cébe-Suarez, A. Zehnder-Fjällman, and K. Ballmer-Hofer, 'The role of VEGF receptors in angiogenesis; complex partnerships', *Cell. Mol. Life Sci.*, vol. 63, no. 5, p. 601, Feb. 2006.

[117] K. Holmqvist *et al.*, 'The Adaptor Protein Shb Binds to Tyrosine 1175 in Vascular Endothelial Growth Factor (VEGF) Receptor-2 and Regulates VEGF-dependent Cellular Migration', *J. Biol. Chem.*, vol. 279, no. 21, pp. 22267–22275, May 2004.

[118] K. Holmqvist, M. Cross, D. Riley, and M. Welsh, 'The Shb adaptor protein causes Src-dependent cell spreading and activation of focal adhesion kinase in murine brain endothelial cells', *Cellular Signalling*, vol. 15, no. 2, pp. 171–179, Feb. 2003.

[119] M. Laramée *et al.*, 'The Scaffolding Adapter Gab1 Mediates Vascular Endothelial Growth Factor Signaling and Is Required for Endothelial Cell Migration and Capillary Formation', *J. Biol. Chem.*, vol. 282, no. 11, pp. 7758–7769, Mar. 2007.

[120] L. Lamalice, F. Houle, and J. Huot, 'Phosphorylation of Tyr1214 within VEGFR-2 Triggers the Recruitment of Nck and Activation of Fyn Leading to SAPK2/p38 Activation and Endothelial Cell Migration in Response to VEGF', *J. Biol. Chem.*, vol. 281, no. 45, pp. 34009–34020, Nov. 2006.

[121] K. Ballmer-Hofer, A. E. Andersson, L. E. Ratcliffe, and P. Berger, 'Neuropilin-1 promotes VEGFR-2 trafficking through Rab11 vesicles thereby specifying signal output', *Blood*, p. blood-2011-01-328773, Jan. 2011.

[122] A. Salikhova *et al.*, 'Vascular Endothelial Growth Factor and Semaphorin Induce Neuropilin-1 Endocytosis via Separate Pathways', *Circ Res*, vol. 103, no. 6, pp. e71–e79, Sep. 2008.

[123] M. Nakayama *et al.*, 'Spatial regulation of VEGF receptor endocytosis in angiogenesis', *Nature Cell Biology*, vol. 15, no. 3, pp. 249–260, Mar. 2013.

[124] R. Soldi, S. Mitola, M. Strasly, P. Defilippi, G. Tarone, and F. Bussolino, 'Role of αvβ3 integrin in the activation of vascular endothelial growth factor receptor-2', *The EMBO Journal*, vol. 18, no. 4, pp. 882–892, Feb. 1999.

[125] S. Tugues *et al.*, 'Tetraspanin CD63 Promotes Vascular Endothelial Growth Factor Receptor 2-β1 Integrin Complex Formation, Thereby Regulating Activation and Downstream Signaling in Endothelial Cells in Vitro and in Vivo', *J. Biol. Chem.*, vol. 288, no. 26, pp. 19060–19071, Jun. 2013.

[126] G. B. Whitaker, B. J. Limberg, and J. S. Rosenbaum, 'Vascular Endothelial Growth Factor Receptor-2 and Neuropilin-1 Form a Receptor Complex That Is Responsible for the Differential

Signaling Potency of VEGF165 and VEGF121', *J. Biol. Chem.*, vol. 276, no. 27, pp. 25520–25531, Jul. 2001.

[127] B. Favier *et al.*, 'Neuropilin-2 interacts with VEGFR-2 and VEGFR-3 and promotes human endothelial cell survival and migration', *Blood*, vol. 108, no. 4, pp. 1243–1250, Aug. 2006.

[128] K. Alitalo, T. Tammela, and T. V. Petrova, 'Lymphangiogenesis in development and human disease', *Nature*, vol. 438, pp. 946–953, Dec. 2005.

[129] D. J. Dumont *et al.*, 'Cardiovascular Failure in Mouse Embryos Deficient in VEGF Receptor-3', *Science*, vol. 282, no. 5390, pp. 946–949, Oct. 1998.

[130] E. F. Plow, J. Meller, and T. V. Byzova, 'Integrin function in vascular biology: a view from 2013', *Curr Opin Hematol*, vol. 21, no. 3, pp. 241–247, May 2014.

[131] C. J. Avraamides, B. Garmy-Susini, and J. A. Varner, 'Integrins in angiogenesis and lymphangiogenesis', *Nature Reviews Cancer*, vol. 8, no. 8, pp. 604–617, Aug. 2008.

[132] I. D. Campbell and M. J. Humphries, 'Integrin Structure, Activation, and Interactions', *Cold Spring Harb Perspect Biol*, p. a004994, Jan. 2011.

[133] J. W. Tamkun *et al.*, 'Structure of integrin, a glycoprotein involved in the transmembrane linkage between fibronectin and actin', *Cell*, vol. 46, no. 2, pp. 271–282, Jul. 1986.

[134] R. O. Hynes, 'Integrins', *Cell*, vol. 110, no. 6, pp. 673–687, Sep. 2002.

[135] E. Ruoslahti and M. D. Pierschbacher, 'New perspectives in cell adhesion: RGD and integrins', *Science*, vol. 238, no. 4826, pp. 491–497, Oct. 1987.

[136] V. M. Belkin, A. M. Belkin, and V. E. Koteliansky, 'Human smooth muscle VLA-1 integrin: purification, substrate specificity, localization in aorta, and expression during development.', *The Journal of Cell Biology*, vol. 111, no. 5, pp. 2159–2170, Nov. 1990.

[137] E. C. Lee, M. M. Lotz, G. D. Steele, and A. M. Mercurio, 'The integrin alpha 6 beta 4 is a laminin receptor.', *The Journal of Cell Biology*, vol. 117, no. 3, pp. 671–678, May 1992.

[138] J.-P. Xiong *et al.*, 'Crystal Structure of the Extracellular Segment of Integrin αVβ3', *Science*, vol. 294, no. 5541, pp. 339–345, Oct. 2001.

[139] J.-P. Xiong *et al.*, 'Crystal Structure of the Extracellular Segment of Integrin αVβ3 in Complex with an Arg-Gly-Asp Ligand', *Science*, vol. 296, no. 5565, pp. 151–155, Apr. 2002.

[140] L. Seguin, J. S. Desgrosellier, S. M. Weis, and D. A. Cheresh, 'Integrins and cancer: regulators of cancer stemness, metastasis, and drug resistance', *Trends in Cell Biology*, vol. 25, no. 4, pp. 234–240, Apr. 2015.

[141] D. G. Stupack, X. S. Puente, S. Boutsaboualoy, C. M. Storgard, and D. A. Cheresh, 'Apoptosis of adherent cells by recruitment of caspase-8 to unligated integrins', *J Cell Biol*, vol. 155, no. 3, pp. 459–470, Oct. 2001.

[142] A. L. Berrier and K. M. Yamada, 'Cell–matrix adhesion', *Journal of Cellular Physiology*, vol. 213, no. 3, pp. 565–573, 2007.

[143] C. K. Miranti and J. S. Brugge, 'Sensing the environment: a historical perspective on integrin signal transduction', *Nature Cell Biology*, vol. 4, no. 4, pp. E83–E90, Apr. 2002.

[144] A. Pozzi and R. Zent, 'Integrins: Sensors of Extracellular Matrix and Modulators of Cell Function', *NEE*, vol. 94, no. 3, pp. e77–e84, 2003.

[145] H. B. Schiller and R. Fässler, 'Mechanosensitivity and compositional dynamics of cell–matrix adhesions', *EMBO reports*, vol. 14, no. 6, pp. 509–519, Jun. 2013.

[146] R. O. Hynes, 'Integrins: Versatility, modulation, and signaling in cell adhesion', *Cell*, vol. 69, no. 1, pp. 11–25, Apr. 1992.

[147] M. H. Ginsberg, X. Du, and E. F. Plow, 'Inside-out integrin signalling', *Current Opinion in Cell Biology*, vol. 4, no. 5, pp. 766–771, Oct. 1992.

[148] R. Barrow-McGee *et al.*, 'Beta 1-integrin–c-Met cooperation reveals an inside-in survival signalling on autophagy-related endomembranes', *Nature Communications*, vol. 7, no. 1, Dec. 2016.

[149] M. Huang *et al.*, 'EGFR-dependent pancreatic carcinoma cell metastasis through Rap1 activation', *Oncogene*, vol. 31, no. 22, pp. 2783–2793, May 2012.

[150] H. L. Goel and A. M. Mercurio, 'Enhancing integrin function by VEGF/neuropilin signaling', *Cell Adhesion & Migration*, vol. 6, no. 6, pp. 554–560, Nov. 2012.

[151] J. D. Hood, R. Frausto, W. B. Kiosses, M. A. Schwartz, and D. A. Cheresh, 'Differential αv integrin–mediated Ras-ERK signaling during two pathways of angiogenesis', *The Journal of Cell Biology*, vol. 162, no. 5, pp. 933–943, Sep. 2003.

[152] N. D. Franceschi, H. Hamidi, J. Alanko, P. Sahgal, and J. Ivaska, 'Integrin traffic – the update', *J Cell Sci*, vol. 128, no. 5, pp. 839–852, Mar. 2015.

[153] J. S. Desgrosellier and D. A. Cheresh, 'Integrins in cancer: biological implications and therapeutic opportunities', *Nature Reviews Cancer*, vol. 10, no. 1, pp. 9–22, Jan. 2010.

[154] P. C. Brooks, R. A. Clark, and D. A. Cheresh, 'Requirement of vascular integrin alpha v beta 3 for angiogenesis', *Science*, vol. 264, no. 5158, pp. 569–571, Apr. 1994.

[155] K. Mulgrew *et al.*, 'Direct targeting of αvβ3 integrin on tumor cells with a monoclonal antibody, Abegrin™', *Mol Cancer Ther*, vol. 5, no. 12, pp. 3122–3129, Dec. 2006.

[156] E. Borges, Y. Jan, and E. Ruoslahti, 'Platelet-derived Growth Factor Receptor β and Vascular Endothelial Growth Factor Receptor 2 Bind to the β3Integrin through Its Extracellular Domain', *J. Biol. Chem.*, vol. 275, no. 51, pp. 39867–39873, Dec. 2000.

[157] G. H. Mahabeleshwar, W. Feng, D. R. Phillips, and T. V. Byzova, 'Integrin signaling is critical for pathological angiogenesis', *Journal of Experimental Medicine*, vol. 203, no. 11, pp. 2495–2507, Oct. 2006.

[158] X. Z. West *et al.*, 'Integrin β3 Crosstalk with VEGFR Accommodating Tyrosine Phosphorylation as a Regulatory Switch', *PLOS ONE*, vol. 7, no. 2, p. e31071, Feb. 2012.

[159] J. D. Humphries, A. Byron, and M. J. Humphries, 'Integrin ligands at a glance', *Journal of Cell Science*, vol. 119, no. 19, pp. 3901–3903, Sep. 2006.

[160] D. R. Senger and G. E. Davis, 'Angiogenesis', *Cold Spring Harb Perspect Biol*, vol. 3, no. 8, p. a005090, Aug. 2011.

[161] D. G. Stupack and D. A. Cheresh, 'ECM Remodeling Regulates Angiogenesis: Endothelial Integrins Look for New Ligands', *Sci. STKE*, vol. 2002, no. 119, pp. pe7–pe7, Feb. 2002.

[162] B. Masson-Gadais, F. Houle, J. Laferrière, and J. Huot, 'Integrin αvβ3 requirement for VEGFR2-mediated activation of SAPK2/p38 and for Hsp90-dependent phosphorylation of focal adhesion kinase in endothelial cells activated by VEGF', *Cell Stress Chaperones*, vol. 8, no. 1, pp. 37–52, Jan. 2003.

[163] T. V. Byzova *et al.*, 'A Mechanism for Modulation of Cellular Responses to VEGF: Activation of the Integrins', *Molecular Cell*, vol. 6, no. 4, pp. 851–860, Oct. 2000.

[164] G. H. Mahabeleshwar, W. Feng, K. Reddy, E. F. Plow, and T. V. Byzova, 'Mechanisms of Integrin–Vascular Endothelial Growth Factor Receptor Cross-Activation in Angiogenesis', *Circ Res*, vol. 101, no. 6, pp. 570–580, Sep. 2007.

[165] S. Loges *et al.*, 'Cilengitide inhibits proliferation and differentiation of human endothelial progenitor cells in vitro', *Biochemical and Biophysical Research Communications*, vol. 357, no. 4, pp. 1016–1020, Jun. 2007.

[166] R. E. Nisato, J.-C. Tille, A. Jonczyk, S. L. Goodman, and M. S. Pepper, 'αvβ3 and αvβ5 integrin antagonists inhibit angiogenesis in vitro', *Angiogenesis*, vol. 6, no. 2, pp. 105–119, Jun. 2003.

[167] L. Oliveira-Ferrer *et al.*, 'Cilengitide induces cellular detachment and apoptosis in endothelial and glioma cells mediated by inhibition of FAK/src/AKT pathway', *Journal of Experimental & Clinical Cancer Research*, vol. 27, no. 1, pp. 1–13, 2008.

[168] M. A. Buerkle, S. A. Pahernik, A. Sutter, A. Jonczyk, K. Messmer, and M. Dellian, 'Inhibition of the alpha-v integrins with a cyclic RGD peptide impairs angiogenesis, growth and metastasis of solid tumours *in vivo*', *British Journal of Cancer*, vol. 86, no. 5, pp. 788–795, Mar. 2002.

[169] S. Yamada, X.-Y. Bu, V. Khankaldyyan, I. Gonzales-Gomez, J. G. McComb, and W. E. Laug, 'EFFECT OF THE ANGIOGENESIS INHIBITOR CILENGITIDE (EMD 121974) ON GLIOBLASTOMA GROWTH IN NUDE MICE', *Neurosurgery*, vol. 59, no. 6, pp. 1304–1312, Dec. 2006.

[170] P. C. Brooks *et al.*, 'Integrin αvβ3 antagonists promote tumor regression by inducing apoptosis of angiogenic blood vessels', *Cell*, vol. 79, no. 7, pp. 1157–1164, Dec. 1994.

[171] S. Strömblad, J. C. Becker, M. Yebra, P. C. Brooks, and D. A. Cheresh, 'Suppression of p53 activity and p21WAF1/CIP1 expression by vascular cell integrin alphaVbeta3 during angiogenesis.', *J Clin Invest*, vol. 98, no. 2, pp. 426–433, Jul. 1996.

[172] S. Strieth, M. E. Eichhorn, A. Sutter, A. Jonczyk, A. Berghaus, and M. Dellian, 'Antiangiogenic combination tumor therapy blocking αv-integrins and VEGF-receptor-2 increases therapeutic effects in vivo', *International Journal of Cancer*, vol. 119, no. 2, pp. 423–431, 2006.

[173] T. Taga *et al.*, 'αv-Integrin antagonist EMD 121974 induces apoptosis in brain tumor cells growing on vitronectin and tenascin', *International Journal of Cancer*, vol. 98, no. 5, pp. 690–697, 2002.

[174] R. O. Hynes, 'Integrins: Bidirectional, Allosteric Signaling Machines', *Cell*, vol. 110, no. 6, pp. 673–687, Sep. 2002.

[175] K. M. Hodivala-Dilke *et al.*, 'β3-integrin–deficient mice are a model for Glanzmann thrombasthenia showing placental defects and reduced survival', *J Clin Invest*, vol. 103, no. 2, pp. 229–238, Jan. 1999.

[176] E. A. Morgan *et al.*, 'Dissection of platelet and myeloid cell defects by conditional targeting of the β3-integrin subunit', *The FASEB Journal*, vol. 24, no. 4, pp. 1117–1127, Nov. 2009.

[177] L. E. Reynolds *et al.*, 'Enhanced pathological angiogenesis in mice lacking β3 integrin or β3 and β5 integrins', *Nature Medicine*, vol. 8, no. 1, pp. 27–34, Jan. 2002.

[178] S. D. Robinson, L. E. Reynolds, L. Wyder, D. J. Hicklin, and K. M. Hodivala-Dilke, 'Beta3-integrin regulates vascular endothelial growth factor-A-dependent permeability', *Arterioscler. Thromb. Vasc. Biol.*, vol. 24, no. 11, pp. 2108–2114, Nov. 2004.

[179] A. R. Reynolds *et al.*, 'Stimulation of tumor growth and angiogenesis by low concentrations of RGD-mimetic integrin inhibitors', *Nature Medicine*, vol. 15, no. 4, pp. 392–400, Apr. 2009.

[180] V. Steri *et al.*, 'Acute Depletion of Endothelial β3-Integrin Transiently Inhibits Tumor Growth and Angiogenesis in MiceNovelty and Significance', *Circulation Research*, vol. 114, no. 1, pp. 79–91, Jan. 2014.

[181] S. D. Robinson *et al.*, 'αvβ3 Integrin Limits the Contribution of Neuropilin-1 to Vascular Endothelial Growth Factor-induced Angiogenesis', *J. Biol. Chem.*, vol. 284, no. 49, pp. 33966–33981, Dec. 2009.

[182] T. S. Ellison *et al.*, 'Suppression of β3-integrin in mice triggers a neuropilin-1-dependent change in focal adhesion remodelling that can be targeted to block pathological angiogenesis', *Disease Models & Mechanisms*, vol. 8, no. 9, pp. 1105–1119, Sep. 2015.

[183] G. D'Amico *et al.*, 'Endothelial-Rac1 Is Not Required for Tumor Angiogenesis unless αvβ3-Integrin Is Absent', *PLOS ONE*, vol. 5, no. 3, p. e9766, Mar. 2010.

[184] B. Geiger, A. Bershadsky, R. Pankov, and K. M. Yamada, 'Transmembrane crosstalk between the extracellular matrix and the cytoskeleton', *Nature Reviews Molecular Cell Biology*, vol. 2, no. 11, pp. 793–805, Nov. 2001.

[185] D. R. Critchley, M. R. Holt, S. T. Barry, H. Priddle, L. Hemmings, and J. Norman, 'Integrin-mediated cell adhesion: the cytoskeletal connection.', *Biochem Soc Symp*, vol. 65, pp. 79–99, 1999.

[186] K. Burridge, K. Fath, T. Kelly, G. Nuckolls, and C. Turner, 'Focal Adhesions: Transmembrane Junctions Between the Extracellular Matrix and the Cytoskeleton', *Annual Review of Cell Biology*, vol. 4, no. 1, pp. 487–525, 1988.

[187] C. A. Whittaker, K.-F. Bergeron, J. Whittle, B. P. Brandhorst, R. D. Burke, and R. O. Hynes, 'The echinoderm adhesome', *Developmental Biology*, vol. 300, no. 1, pp. 252–266, Dec. 2006.

[188] R. Zaidel-Bar, S. Itzkovitz, A. Ma'ayan, R. Iyengar, and B. Geiger, 'Functional atlas of the integrin adhesome', *Nature Cell Biology*, vol. 9, no. 8, pp. 858–867, Aug. 2007.

[189] H. B. Schiller *et al.*, 'β_1- and α_v-class integrins cooperate to regulate myosin II during rigidity sensing of fibronectin-based microenvironments', *Nature Cell Biology*, vol. 15, no. 6, pp. 625–636, Jun. 2013.

[190] T. M. Scales and M. Parsons, ‘Spatial and temporal regulation of integrin signalling during cell migration’, *Current Opinion in Cell Biology*, vol. 23, no. 5, pp. 562–568, Oct. 2011.

[191] J.-C. Kuo, X. Han, C.-T. Hsiao, J. R. Yates Iii, and C. M. Waterman, ‘Analysis of the myosin-II-responsive focal adhesion proteome reveals a role for β-Pix in negative regulation of focal adhesion maturation’, *Nature Cell Biology*, vol. 13, no. 4, pp. 383–393, Apr. 2011.

[192] E. Zamir, B. Z. Katz, S. Aota, K. M. Yamada, B. Geiger, and Z. Kam, ‘Molecular diversity of cell-matrix adhesions’, *Journal of Cell Science*, vol. 112, no. 11, pp. 1655–1669, Jun. 1999.

[193] M. Nagano, D. Hoshino, N. Koshikawa, T. Akizawa, and M. Seiki, ‘Turnover of Focal Adhesions and Cancer Cell Migration’, *International Journal of Cell Biology*, 2012. [Online]. Available: https://www.hindawi.com/journals/ijcb/2012/310616/abs/. [Accessed: 21-Jan-2019].

[194] R. Zaidel-Bar, M. Cohen, L. Addadi, and B. Geiger, ‘Hierarchical assembly of cell–matrix adhesion complexes’, *Biochemical Society Transactions*, vol. 32, no. 3, pp. 416–420, Jun. 2004.

[195] H. Wolfenson, I. Lavelin, and B. Geiger, ‘Dynamic Regulation of the Structure and Functions of Integrin Adhesions’, *Developmental Cell*, vol. 24, no. 5, pp. 447–458, Mar. 2013.

[196] N. O. Carragher and M. C. Frame, ‘Focal adhesion and actin dynamics: a place where kinases and proteases meet to promote invasion’, *Trends in Cell Biology*, vol. 14, no. 5, pp. 241–249, May 2004.

[197] S. Tojkander, G. Gateva, and P. Lappalainen, ‘Actin stress fibers – assembly, dynamics and biological roles’, *J Cell Sci*, p. jcs.098087, Jan. 2012.

[198] D. S. Courson and R. S. Rock, ‘Actin crosslink assembly and disassembly mechanics for alpha-actinin and fascin’, *J. Biol. Chem.*, p. jbc.M110.123117, Jun. 2010.

[199] C. A. Otey and O. Carpen, ‘α-actinin revisited: A fresh look at an old player’, *Cell Motility*, vol. 58, no. 2, pp. 104–111, 2004.

[200] C. E. Turner, ‘Paxillin interactions’, *Journal of Cell Science*, vol. 113, no. 23, pp. 4139–4140, Jan. 2000.

[201] C. E. Turner, ‘Paxillin and focal adhesion signalling’, *Nature Cell Biology*, vol. 2, no. 12, pp. E231–E236, Dec. 2000.

[202] B. T. Goult, J. Yan, and M. A. Schwartz, ‘Talin as a mechanosensitive signaling hub’, *J Cell Biol*, vol. 217, no. 11, pp. 3776–3784, Nov. 2018.

[203] D. A. Calderwood, I. D. Campbell, and D. R. Critchley, ‘Talins and kindlins: partners in integrin-mediated adhesion’, *Nature Reviews Molecular Cell Biology*, vol. 14, no. 8, pp. 503–517, Aug. 2013.

[204] S. J. Monkley *et al.*, ‘Disruption of the talin gene arrests mouse development at the gastrulation stage’, *Developmental Dynamics*, vol. 219, no. 4, pp. 560–574, 2000.

[205] S. H. Lo, E. Weisberg, and L. B. Chen, ‘Tensin: A potential link between the cytoskeleton and signal transduction’, *BioEssays*, vol. 16, no. 11, pp. 817–823, 1994.

[206] S. H. Lo, ‘Tensin’, *The International Journal of Biochemistry & Cell Biology*, vol. 36, no. 1, pp. 31–34, Jan. 2004.

[207] K. Burridge and P. Mangeat, ‘An interaction between vinculin and talin’, *Nature*, vol. 308, no. 5961, pp. 744–746, Apr. 1984.

[208] W. H. Ziegler, R. C. Liddington, and D. R. Critchley, ‘The structure and regulation of vinculin’, *Trends in Cell Biology*, vol. 16, no. 9, pp. 453–460, Sep. 2006.

[209] C. Grashoff *et al.*, ‘Measuring mechanical tension across vinculin reveals regulation of focal adhesion dynamics’, *Nature*, vol. 466, no. 7303, pp. 263–266, Jul. 2010.

[210] T.-L. Shen *et al.*, ‘Conditional knockout of focal adhesion kinase in endothelial cells reveals its role in angiogenesis and vascular development in late embryogenesis’, *J Cell Biol*, vol. 169, no. 6, pp. 941–952, Jun. 2005.

[211] B. Tavora *et al.*, ‘Endothelial FAK is required for tumour angiogenesis’, *EMBO Molecular Medicine*, vol. 2, no. 12, pp. 516–528, Dec. 2010.

[212] M. Guarino, ‘Src signaling in cancer invasion’, *Journal of Cellular Physiology*, vol. 223, no. 1, pp. 14–26, 2010.

[213] S. A. Courtneidge, ‘Role of Src in Signal Transduction Pathways’, *Biochemical Society Transactions*, vol. 30, no. 2, pp. 11–17, Apr. 2002.

[214] J. R. Wiener, K. Nakano, R. P. Kruzelock, C. D. Bucana, R. C. Bast, and G. E. Gallick, ‘Decreased Src Tyrosine Kinase Activity Inhibits Malignant Human Ovarian Cancer Tumor Growth in a Nude Mouse Model’, *Clin Cancer Res*, vol. 5, no. 8, pp. 2164–2170, Aug. 1999.

[215] J. B. Bolen, A. Veillette, A. M. Schwartz, V. DeSeau, and N. Rosen, ‘Activation of pp60c-src protein kinase activity in human colon carcinoma’, *PNAS*, vol. 84, no. 8, pp. 2251–2255, Apr. 1987.

[216] A. E. Ottenhoff-Kalff, G. Rijksen, E. A. C. M. van Beurden, A. Hennipman, A. A. Michels, and G. E. J. Staal, ‘Characterization of Protein Tyrosine Kinases from Human Breast Cancer: Involvement of the c-src Oncogene Product’, *Cancer Res*, vol. 52, no. 17, pp. 4773–4778, Sep. 1992.

[217] ‘Cell Migration lab - cell adhesion’. [Online]. Available: http://www.reading.ac.uk/cellmigration/adhesion.htm. [Accessed: 13-Nov-2018].

[218] P. Hu and B.-H. Luo, ‘Integrin bi-directional signaling across the plasma membrane’, *Journal of Cellular Physiology*, vol. 228, no. 2, pp. 306–312, 2013.

[219] B. D. Hoffman, C. Grashoff, and M. A. Schwartz, ‘Dynamic molecular processes mediate cellular mechanotransduction’, *Nature*, vol. 475, no. 7356, pp. 316–323, Jul. 2011.

[220] K. O. Simon and K. Burridge, ‘Interactions between Integrins and the Cytoskeleton: Structure and Regulation’, in *Integrins*, D. A. Cheresh and R. P. Mecham, Eds. San Diego: Academic Press, 1994, pp. 49–78.

[221] I. Kaverina, K. Rottner, and J. V. Small, ‘Targeting, Capture, and Stabilization of Microtubules at Early Focal Adhesions’, *The Journal of Cell Biology*, vol. 142, no. 1, pp. 181–190, Jul. 1998.

[222] M. Gonzales *et al.*, ‘Structure and Function of a Vimentin-associated Matrix Adhesion in Endothelial Cells’, *MBoC*, vol. 12, no. 1, pp. 85–100, Jan. 2001.

[223] O. Rossier *et al.*, ‘Integrins β_1 and β_3 exhibit distinct dynamic nanoscale organizations inside focal adhesions’, *Nature Cell Biology*, vol. 14, no. 10, pp. 1057–1067, Oct. 2012.

[224] E. H. J. Danen, P. Sonneveld, C. Brakebusch, R. Fässler, and A. Sonnenberg, 'The fibronectin-binding integrins α5β1 and αvβ3 differentially modulate RhoA–GTP loading, organization of cell matrix adhesions, and fibronectin fibrillogenesis', *The Journal of Cell Biology*, vol. 159, no. 6, pp. 1071–1086, Dec. 2002.

[225] P. Roca-Cusachs, N. C. Gauthier, A. del Rio, and M. P. Sheetz, 'Clustering of α5β1 integrins determines adhesion strength whereas αvβ3 and talin enable mechanotransduction', *PNAS*, vol. 106, no. 38, pp. 16245–16250, Sep. 2009.

[226] D. J. Webb, J. T. Parsons, and A. F. Horwitz, 'Adhesion assembly, disassembly and turnover in migrating cells – over and over and over again', *Nature Cell Biology*, vol. 4, no. 4, pp. E97–E100, Apr. 2002.

[227] L. Contois, A. Akalu, and P. C. Brooks, 'Integrins as "functional hubs" in the regulation of pathological angiogenesis', *Seminars in Cancer Biology*, vol. 19, no. 5, pp. 318–328, Oct. 2009.

[228] P. C. Brooks, S. Strömblad, R. Klemke, D. Visscher, F. H. Sarkar, and D. A. Cheresh, 'Antiintegrin alpha v beta 3 blocks human breast cancer growth and angiogenesis in human skin.', *J Clin Invest*, vol. 96, no. 4, pp. 1815–1822, Oct. 1995.

[229] H. Athanassiou *et al.*, 'Randomized phase II study of temozolomide and radiotherapy compared with radiotherapy alone in newly diagnosed glioblastoma multiforme', *J Clin Oncol*, vol. 23, 2005.

[230] R. Stupp *et al.*, 'Cilengitide combined with standard treatment for patients with newly diagnosed glioblastoma with methylated MGMT promoter (CENTRIC EORTC 26071-22072 study): a multicentre, randomised, open-label, phase 3 trial', *The Lancet Oncology*, vol. 15, no. 10, pp. 1100–1108, Sep. 2014.

[231] H. B. Schiller, C. C. Friedel, C. Boulegue, and R. Fässler, 'Quantitative proteomics of the integrin adhesome show a myosin II-dependent recruitment of LIM domain proteins', *EMBO reports*, vol. 12, no. 3, pp. 259–266, Mar. 2011.

[232] S. J. Atkinson *et al.*, 'The β3-integrin endothelial adhesome regulates microtubule-dependent cell migration', *EMBO reports*, p. e44578, May 2018.

[233] M. E. Eichhorn, A. Kleespies, M. K. Angele, K.-W. Jauch, and C. J. Bruns, 'Angiogenesis in cancer: molecular mechanisms, clinical impact', *Langenbeck's Archives of Surgery*, vol. 392, no. 3, pp. 371–379, 2007.

[234] C. Cremolini *et al.*, 'FOLFOXIRI plus bevacizumab versus FOLFIRI plus bevacizumab as first-line treatment of patients with metastatic colorectal cancer: updated overall survival and molecular subgroup analyses of the open-label, phase 3 TRIBE study', *The Lancet Oncology*, vol. 16, no. 13, pp. 1306–1315, Oct. 2015.

[235] J. M. L. Ebos and R. S. Kerbel, 'Antiangiogenic therapy: impact on invasion, disease progression, and metastasis', *Nature Reviews Clinical Oncology*, vol. 8, no. 4, pp. 210–221, Apr. 2011.

[236] S. L. Goodman and M. Picard, 'Integrins as therapeutic targets', *Trends in Pharmacological Sciences*, vol. 33, no. 7, pp. 405–412, Jul. 2012.

[237] K. Ley, J. Rivera-Nieves, W. J. Sandborn, and S. Shattil, 'Integrin-based Therapeutics: Biological Basis, Clinical Use and New Drugs', *Nat Rev Drug Discov*, vol. 15, no. 3, pp. 173–183, Mar. 2016.

[238] R. C. Turaga *et al.*, 'Rational design of a protein that binds integrin αvβ3 outside the ligand binding site', *Nature Communications*, vol. 7, p. 11675, May 2016.

[239] S. Raab-Westphal, J. F. Marshall, and S. L. Goodman, 'Integrins as Therapeutic Targets: Successes and Cancers', *Cancers (Basel)*, vol. 9, no. 9, Aug. 2017.

[240] N. Ferrara, K. J. Hillan, H.-P. Gerber, and W. Novotny, 'Case history: Discovery and development of bevacizumab, an anti-VEGF antibody for treating cancer', *Nature Reviews Drug Discovery*, vol. 3, no. 5, pp. 391–400, May 2004.

[241] N. Wang, R. K. Jain, and T. T. Batchelor, 'New Directions in Anti-Angiogenic Therapy for Glioblastoma', *Neurotherapeutics*, vol. 14, no. 2, pp. 321–332, Apr. 2017.

[242] 'FDA Commissioner announces Avastin decision', U.S. Food and Drug Administration, News Release, Nov. 2011.

[243] L. D. Sasich and S. R. Sukkari, 'The US FDAs withdrawal of the breast cancer indication for Avastin (bevacizumab)', *Saudi Pharm J*, vol. 20, no. 4, pp. 381–385, Oct. 2012.

[244] 'EPAR summary for the public, Avastin (bevacizumab)', EMEA, London, EPAR EMEA/H/C/000582, EMA/302947/2017, Jun. 2017.

[245] K. J. Gotink and H. M. W. Verheul, 'Anti-angiogenic tyrosine kinase inhibitors: what is their mechanism of action?', *Angiogenesis*, vol. 13, no. 1, pp. 1–14, Mar. 2010.

[246] 'Angiogenesis Inhibitors Fact Sheet', *Cancer.gov*. National Cancer Institute, Apr-2018.

[247] S. De Falco, 'Antiangiogenesis therapy: an update after the first decade', *Korean J Intern Med*, vol. 29, no. 1, pp. 1–11, Jan. 2014.

[248] B. Sennino and D. M. McDonald, 'Controlling escape from angiogenesis inhibitors', *Nature Reviews Cancer*, vol. 12, no. 10, pp. 699–709, Oct. 2012.

[249] S. Tugues, S. Koch, L. Gualandi, X. Li, and L. Claesson-Welsh, 'Vascular endothelial growth factors and receptors: Anti-angiogenic therapy in the treatment of cancer', *Molecular Aspects of Medicine*, vol. 32, no. 2, pp. 88–111, Apr. 2011.

[250] A. Patnaik *et al.*, 'A Phase Ib study evaluating MNRP1685A, a fully human anti-NRP1 monoclonal antibody, in combination with bevacizumab and paclitaxel in patients with advanced solid tumors', *Cancer Chemotherapy and Pharmacology*, vol. 73, no. 5, pp. 951–960, May 2014.

[251] R. Stupp and C. Ruegg, 'Integrin Inhibitors Reaching the Clinic', *JCO*, vol. 25, no. 13, pp. 1637–1638, May 2007.

[252] B. P. Eliceiri and D. A. Cheresh, 'The role of αv integrins during angiogenesis: insights into potential mechanisms of action and clinical development', *J Clin Invest*, vol. 103, no. 9, pp. 1227–1230, May 1999.

[253] B. P. Eliceiri and D. A. Cheresh, 'The role of alphav integrins during angiogenesis.', *Mol Med*, vol. 4, no. 12, pp. 741–750, Dec. 1998.

[254] B. Felding-Habermann *et al.*, 'Integrin activation controls metastasis in human breast cancer', *PNAS*, vol. 98, no. 4, pp. 1853–1858, Feb. 2001.

[255] J. Schnittert, R. Bansal, G. Storm, and J. Prakash, 'Integrins in wound healing, fibrosis and tumor stroma: High potential targets for therapeutics and drug delivery', *Advanced Drug Delivery Reviews*, vol. 129, pp. 37–53, Apr. 2018.

[256] C. Mas-Moruno, F. Rechenmacher, and H. Kessler, 'Cilengitide: The First Anti-Angiogenic Small Molecule Drug Candidate. Design, Synthesis and Clinical Evaluation', *Anticancer Agents Med Chem*, vol. 10, no. 10, pp. 753–768, Dec. 2010.

[257] R. Stupp *et al.*, 'Phase I/IIa study of cilengitide and temozolomide with concomitant radiotherapy followed by cilengitide and temozolomide maintenance therapy in patients with newly diagnosed glioblastoma', *J. Clin. Oncol.*, vol. 28, no. 16, pp. 2712–2718, Jun. 2010.

[258] C. Delbaldo *et al.*, 'Phase I and pharmacokinetic study of etaracizumab (Abegrin™), a humanized monoclonal antibody against αvβ3 integrin receptor, in patients with advanced solid tumors', *Invest New Drugs*, vol. 26, no. 1, pp. 35–43, Feb. 2008.

[259] S. J. DeNardo *et al.*, 'Neovascular Targeting with Cyclic RGD Peptide (cRGDf-ACHA) to Enhance Delivery of Radioimmunotherapy', *Cancer Biotherapy and Radiopharmaceuticals*, vol. 15, no. 1, pp. 71–79, Feb. 2000.

[260] M. Pickarski, A. Gleason, B. Bednar, and L. T. Duong, 'Orally active αvβ3 integrin inhibitor MK-0429 reduces melanoma metastasis', *Oncology Reports*, vol. 33, no. 6, pp. 2737–2745, Jun. 2015.

[261] M. A. Rosenthal *et al.*, 'Evaluation of the safety, pharmacokinetics and treatment effects of an alpha(nu)beta(3) integrin inhibitor on bone turnover and disease activity in men with hormone-refractory prostate cancer and bone metastases', *Asia Pac J Clin Oncol*, vol. 6, no. 1, pp. 42–48, Mar. 2010.

[262] J. H. Hutchinson *et al.*, 'Nonpeptide alphavbeta3 antagonists. 8. In vitro and in vivo evaluation of a potent alphavbeta3 antagonist for the prevention and treatment of osteoporosis', *J. Med. Chem.*, vol. 46, no. 22, pp. 4790–4798, Oct. 2003.

[263] M. G. Murphy, K. Cerchio, S. A. Stoch, K. Gottesdiener, M. Wu, and R. Recker, 'Effect of L-000845704, an αVβ3 Integrin Antagonist, on Markers of Bone Turnover and Bone Mineral Density in Postmenopausal Osteoporotic Women', *J Clin Endocrinol Metab*, vol. 90, no. 4, pp. 2022–2028, Apr. 2005.

[264] P. Hersey *et al.*, 'A randomized phase 2 study of etaracizumab, a monoclonal antibody against integrin αvβ3, ± dacarbazine in patients with stage IV metastatic melanoma', *Cancer*, vol. 116, no. 6, pp. 1526–1534, 2010.

[265] M. Sharma, R. C. Turaga, Y. Yuan, F. Mishra, and Z.-R. Liu, 'Abstract 2124: Therapeutic targeting of cancer-associated fibroblasts by a novel protein, ProAgio, effectively decreases TNBC growth and metastasis to the lungs', *Cancer Res*, vol. 78, no. 13 Supplement, pp. 2124–2124, Jul. 2018.

[266] T. J. Kim *et al.*, 'Combined anti-angiogenic therapy against VEGF and integrin alphabeta in an orthotopic model of ovarian cancer', *Cancer Biology & Therapy*, vol. 8, no. 23, pp. 2261–2270, Dec. 2009.

[267] N. Papo, A. P. Silverman, J. L. Lahti, and J. R. Cochran, 'Antagonistic VEGF variants engineered to simultaneously bind to and inhibit VEGFR2 and αvβ3 integrin', *PNAS*, vol. 108, no. 34, pp. 14067–14072, Aug. 2011.

[268] Q. Qiu *et al.*, 'Small molecular peptide-ScFv αvβ3 conjugates specifically inhibit lung cancer cell growth in vitro and in vivo', *Am J Cancer Res*, vol. 6, no. 12, pp. 2846–2858, Dec. 2016.

[269] D. Krilleke *et al.*, 'Molecular Mapping and Functional Characterization of the VEGF164 Heparin-binding Domain', *J. Biol. Chem.*, vol. 282, no. 38, pp. 28045–28056, Sep. 2007.

[270] L. E. Reynolds and K. M. Hodivala-Dilke, 'Primary Mouse Endothelial Cell Culture for Assays of Angiogenesis', in *Breast Cancer Research Protocols*, Humana Press, Totowa, NJ, 2006, pp. 503–509.

[271] K. Maasho, A. Marusina, N. M. Reynolds, J. E. Coligan, and F. Borrego, 'Efficient gene transfer into the human natural killer cell line, NKL, using the Amaxa nucleofection system™', *Journal of Immunological Methods*, vol. 284, no. 1, pp. 133–140, Jan. 2004.

[272] M. Ishiyama, Y. Miyazono, K. Sasamoto, Y. Ohkura, and K. Ueno, 'A highly water-soluble disulfonated tetrazolium salt as a chromogenic indicator for NADH as well as cell viability', *Talanta*, vol. 44, no. 7, pp. 1299–1305, Jul. 1997.

[273] 'Tumor Angiogenesis: Therapeutic Implications | NEJM', *New England Journal of Medicine*. [Online]. Available: https://www.nejm.org/doi/pdf/10.1056/NEJM197111182852108. [Accessed: 14-Sep-2018].

[274] P. C. Brooks, R. A. Clark, and D. A. Cheresh, 'Requirement of vascular integrin alpha v beta 3 for angiogenesis', *Science*, vol. 264, no. 5158, pp. 569–571, Apr. 1994.

[275] L. E. Reynolds *et al.*, 'Enhanced pathological angiogenesis in mice lacking β_3 integrin or β_3 and β_5 integrins', *Nature Medicine*, vol. 8, no. 1, pp. 27–34, Jan. 2002.

[276] G. Eisele *et al.*, 'Cilengitide treatment of newly diagnosed glioblastoma patients does not alter patterns of progression', *J Neurooncol*, vol. 117, no. 1, pp. 141–145, Mar. 2014.

[277] Atkinson S. A., 'The Role of the Integrin β3 Adhesome in Angiogenesis', PhD Thesis, University of East Anglia, Norwich, UK, 2018.

[278] S. D. Robinson and K. M. Hodivala-Dilke, 'The role of β3-integrins in tumor angiogenesis: context is everything', *Current Opinion in Cell Biology*, vol. 23, no. 5, pp. 630–637, Oct. 2011.

[279] S. Tyanova *et al.*, 'The Perseus computational platform for comprehensive analysis of (prote)omics data', *Nature Methods*, vol. 13, no. 9, pp. 731–740, Sep. 2016.

[280] M. Ashburner *et al.*, 'Gene Ontology: tool for the unification of biology', *Nature Genetics*, 01-May-2000. [Online]. Available: https://www.nature.com/articles/ng0500_25. [Accessed: 22-Jun-2018].

[281] M. Kanehisa, M. Furumichi, M. Tanabe, Y. Sato, and K. Morishima, 'KEGG: new perspectives on genomes, pathways, diseases and drugs', *Nucleic Acids Res*, vol. 45, no. D1, pp. D353–D361, Jan. 2017.

[282] V. G. Tusher, R. Tibshirani, and G. Chu, 'Significance analysis of microarrays applied to the ionizing radiation response', *PNAS*, vol. 98, no. 9, pp. 5116–5121, Apr. 2001.

[283] ‘mRNA export through an additional cap-binding complex consisting of NCBP1 and NCBP3 | Nature Communications’. [Online]. Available: https://www.nature.com/articles/ncomms9192. [Accessed: 01-Jul-2018].

[284] R. L. Gendron, L. C. Adams, and H. Paradis, ‘Tubedown-1, A novel acetyltransferase associated with blood vessel development’, *Developmental Dynamics*, vol. 218, no. 2, pp. 300–315.

[285] D. Ursic, J. C. Sedbrook, K. L. Himmel, and M. R. Culbertson, ‘The essential yeast Tcp1 protein affects actin and microtubules.’, *MBoC*, vol. 5, no. 10, pp. 1065–1080, Oct. 1994.

[286] C. Magnon *et al.*, ‘Canstatin Acts on Endothelial and Tumor Cells via Mitochondrial Damage Initiated through Interaction with αvβ3 and αvβ5 Integrins’, *Cancer Res*, vol. 65, no. 10, pp. 4353–4361, May 2005.

[287] J. D. Paul *et al.*, ‘SLIT3–ROBO4 activation promotes vascular network formation in human engineered tissue and angiogenesis in vivo’, *Journal of Molecular and Cellular Cardiology*, vol. 64, pp. 124–131, Nov. 2013.

[288] Z. B. Wu *et al.*, ‘Heat Shock Protein 47 Promotes Glioma Angiogenesis’, *Brain Pathology*, vol. 26, no. 1, pp. 31–42, Jan. 2016.

[289] R. J. Steagall, A. E. Rusiñol, Q. A. Truong, and Z. Han, ‘HSPA12B Is Predominantly Expressed in Endothelial Cells and Required for Angiogenesis’, *Arteriosclerosis, Thrombosis, and Vascular Biology*, Sep. 2006.

[290] K.-H. Tung *et al.*, ‘CHC promotes tumor growth and angiogenesis through regulation of HIF-1α and VEGF signaling’, *Cancer Letters*, vol. 331, no. 1, pp. 58–67, Apr. 2013.

[291] Y. Matsuda, M. Hagio, and T. Ishiwata, ‘Nestin: A novel angiogenesis marker and possible target for tumor angiogenesis’, *World J Gastroenterol*, vol. 19, no. 1, pp. 42–48, Jan. 2013.

[292] T. M. Svitkina, A. B. Verkhovsky, and G. G. Borisy, ‘Plectin sidearms mediate interaction of intermediate filaments with microtubules and other components of the cytoskeleton.’, *The Journal of Cell Biology*, vol. 135, no. 4, pp. 991–1007, Nov. 1996.

[293] R. Bhattacharya *et al.*, ‘Recruitment of vimentin to the cell surface by β3 integrin and plectin mediates adhesion strength’, *J Cell Sci*, vol. 122, no. 9, pp. 1390–1400, May 2009.

[294] P. Soellner, R. A. Quinlan, and W. W. Franke, ‘Identification of a distinct soluble subunit of an intermediate filament protein: tetrameric vimentin from living cells’, *Proc. Natl. Acad. Sci. U.S.A.*, vol. 82, no. 23, pp. 7929–7933, Dec. 1985.

[295] B. Trüeb, B. Gröbli, M. Spiess, B. F. Odermatt, and K. H. Winterhalter, ‘Basement membrane (type IV) collagen is a heteropolymer.’, *J. Biol. Chem.*, vol. 257, no. 9, pp. 5239–5245, May 1982.

[296] J. D. Paul *et al.*, ‘SLIT3–ROBO4 activation promotes vascular network formation in human engineered tissue and angiogenesis in vivo’, *Journal of Molecular and Cellular Cardiology*, vol. 64, pp. 124–131, Nov. 2013.

[297] R. J. Steagall, A. E. Rusiñol, Q. A. Truong, and Z. Han, ‘HSPA12B Is Predominantly Expressed in Endothelial Cells and Required for Angiogenesis’, *Arteriosclerosis, Thrombosis, and Vascular Biology*, vol. 26, no. 9, pp. 2012–2018, Sep. 2006.

[298] K.-H. Tung *et al.*, 'CHC promotes tumor growth and angiogenesis through regulation of HIF-1α and VEGF signaling', *Cancer Letters*, vol. 331, no. 1, pp. 58–67, Apr. 2013.

[299] K. Michalczyk and M. Ziman, 'Nestin structure and predicted function in cellular cytoskeletal organisation.', *Histol Histopathol*, vol. 20, no. 2, pp. 665–671, Apr. 2005.

[300] 'Plectin sidearms mediate interaction of intermediate filaments with microtubules and other components of the cytoskeleton', *J Cell Biol*, vol. 135, no. 4, pp. 991–1007, Nov. 1996.

[301] Z. B. Wu *et al.*, 'Heat Shock Protein 47 Promotes Glioma Angiogenesis', *Brain Pathology*, vol. 26, no. 1, pp. 31–42.

[302] Y.-P. Shih, P. Sun, A. Wang, and S. H. Lo, 'Tensin1 positively regulates RhoA activity through its interaction with DLC1', *Biochimica et Biophysica Acta (BBA) - Molecular Cell Research*, vol. 1853, no. 12, pp. 3258–3265, Dec. 2015.

[303] L. Zan *et al.*, 'Src regulates angiogenic factors and vascular permeability after focal cerebral ischemia–reperfusion', *Neuroscience*, vol. 262, pp. 118–128, Mar. 2014.

[304] A. G. Porter and R. U. Jänicke, 'Emerging roles of caspase-3 in apoptosis', *Cell Death and Differentiation*, vol. 6, no. 2, pp. 99–104, Feb. 1999.

[305] B. Eckes *et al.*, 'Impaired wound healing in embryonic and adult mice lacking vimentin', *J Cell Sci*, vol. 113, no. 13, pp. 2455–2462, Jul. 2000.

[306] J. R. van Beijnum *et al.*, 'Gene expression of tumor angiogenesis dissected: specific targeting of colon cancer angiogenic vasculature', *Blood*, vol. 108, no. 7, pp. 2339–2348, Oct. 2006.

[307] A. Kern, J. Eble, R. Golbik, and K. Kühn, 'Interaction of type IV collagen with the isolated integrins α1β1 and α2β1', *European Journal of Biochemistry*, vol. 215, no. 1, pp. 151–159, Jul. 1993.

[308] D. S. Kuo, C. Labelle-Dumais, and D. B. Gould, 'COL4A1 and COL4A2 mutations and disease: insights into pathogenic mechanisms and potential therapeutic targets', *Hum Mol Genet*, vol. 21, no. R1, pp. R97–R110, Oct. 2012.

[309] M. H. Kulke *et al.*, 'Phase II Study of Recombinant Human Endostatin in Patients With Advanced Neuroendocrine Tumors', *JCO*, vol. 24, no. 22, pp. 3555–3561, Aug. 2006.

[310] Y. Sun *et al.*, 'Results of phase III trial of rh-endostatin (YH-16) in advanced non-small cell lung cancer (NSCLC) patients', *JCO*, vol. 23, no. 16_suppl, pp. 7138–7138, Jun. 2005.

[311] T. Arnesen *et al.*, 'A novel human NatA Nα-terminal acetyltransferase complex: hNaa16p-hNaa10p (hNat2-hArd1)', *BMC Biochem*, vol. 10, p. 15, May 2009.

[312] P. V. Damme *et al.*, 'Proteome-derived peptide libraries allow detailed analysis of the substrate specificities of Nα-acetyltransferases and point to hNaa10p as the posttranslational actin Nα-acetyltransferase', *Molecular & Cellular Proteomics*, p. mcp.M110.004580, Jan. 2011.

[313] H. Paradis, T. Islam, S. Tucker, L. Tao, S. Koubi, and R. L. Gendron, 'Tubedown associates with cortactin and controls permeability of retinal endothelial cells to albumin', *Journal of Cell Science*, vol. 121, no. 12, pp. 1965–1972, Jun. 2008.

[314] Y. Kaneko *et al.*, 'Nestin Overexpression Precedes Caspase-3 Upregulation in Rats Exposed to Controlled Cortical Impact Traumatic Brain Injury', *Cell Med*, vol. 4, no. 2, pp. 55–63, Jul. 2012.

[315] S. Dupont *et al.*, 'Role of YAP/TAZ in mechanotransduction', *Nature*, vol. 474, no. 7350, pp. 179–183, Jun. 2011.

[316] A. J. Engler, S. Sen, H. L. Sweeney, and D. E. Discher, 'Matrix Elasticity Directs Stem Cell Lineage Specification', *Cell*, vol. 126, no. 4, pp. 677–689, Aug. 2006.

[317] P. Moreno-Layseca and C. H. Streuli, 'Signalling pathways linking integrins with cell cycle progression', *Matrix Biology*, vol. 34, pp. 144–153, Feb. 2014.

[318] J. D. Humphries, A. Byron, and M. J. Humphries, 'Integrin ligands at a glance', *Journal of Cell Science*, vol. 119, no. 19, pp. 3901–3903, Oct. 2006.

[319] E. R. Horton *et al.*, 'Definition of a consensus integrin adhesome and its dynamics during adhesion complex assembly and disassembly', *Nature Cell Biology*, vol. 17, no. 12, pp. 1577–1587, Dec. 2015.

[320] D. Llić *et al.*, 'Reduced cell motility and enhanced focal adhesion contact formation in cells from FAK-deficient mice', *Nature*, vol. 377, no. 6549, p. 539, Oct. 1995.

[321] J.-L. Guan, 'Focal adhesion kinase in integrin signaling', *Matrix Biology*, vol. 16, no. 4, pp. 195–200, Oct. 1997.

[322] R. Zaidel-Bar and B. Geiger, 'The switchable integrin adhesome', *J Cell Sci*, vol. 123, no. 9, pp. 1385–1388, May 2010.

[323] J. D. Humphries, M. R. Chastney, J. A. Askari, and M. J. Humphries, 'Signal transduction via integrin adhesion complexes', *Current Opinion in Cell Biology*, vol. 56, pp. 14–21, Feb. 2019.

[324] J.-M. Dong *et al.*, 'Proximity biotinylation provides insight into the molecular composition of focal adhesions at the nanometer scale', *Sci. Signal.*, vol. 9, no. 432, pp. rs4–rs4, Jun. 2016.

[325] M. C. Jones, P. T. Caswell, and J. C. Norman, 'Endocytic recycling pathways: emerging regulators of cell migration', *Current Opinion in Cell Biology*, vol. 18, no. 5, pp. 549–557, Oct. 2006.

[326] G. P. F. Nader, E. J. Ezratty, and G. G. Gundersen, 'FAK, talin and PIPKIγ regulate endocytosed integrin activation to polarize focal adhesion assembly', *Nature Cell Biology*, vol. 18, no. 5, pp. 491–503, May 2016.

[327] C. P. Blobel, 'ADAMs: key components in EGFR signalling and development', *Nature Reviews Molecular Cell Biology*, vol. 6, no. 1, pp. 32–43, Jan. 2005.

[328] L. C. Bridges and R. D. Bowditch, 'ADAM-Integrin Interactions: Potential Integrin Regulated Ectodomain Shedding Activity', Mar-2005. [Online]. Available: https://uea.library.ingentaconnect.com/content/ben/cpd/2005/00000011/00000007/art00004. [Accessed: 11-Sep-2018].

[329] T. Lieber, S. Kidd, and M. W. Young, 'kuzbanian-mediated cleavage of Drosophila Notch', *Genes Dev.*, vol. 16, no. 2, pp. 209–221, Jan. 2002.

[330] M. B. Marron *et al.*, 'Regulated Proteolytic Processing of Tie1 Modulates Ligand Responsiveness of the Receptor-tyrosine Kinase Tie2', *J. Biol. Chem.*, vol. 282, no. 42, pp. 30509–30517, Oct. 2007.

[331] P. W. Janes *et al.*, 'Adam Meets Eph: An ADAM Substrate Recognition Module Acts as a Molecular Switch for Ephrin Cleavage In trans', *Cell*, vol. 123, no. 2, pp. 291–304, Oct. 2005.

[332] A. Luque, D. R. Carpizo, and M. L. Iruela-Arispe, 'ADAMTS1/METH1 Inhibits Endothelial Cell Proliferation by Direct Binding and Sequestration of VEGF165', *J. Biol. Chem.*, vol. 278, no. 26, pp. 23656–23665, Jun. 2003.

[333] F. Vázquez *et al.*, 'METH-1, a Human Ortholog of ADAMTS-1, and METH-2 Are Members of a New Family of Proteins with Angio-inhibitory Activity', *J. Biol. Chem.*, vol. 274, no. 33, pp. 23349–23357, Aug. 1999.

[334] S. Kumar, N. Rao, R. Ge, S. Kumar, N. Rao, and R. Ge, 'Emerging Roles of ADAMTSs in Angiogenesis and Cancer', *Cancers*, vol. 4, no. 4, pp. 1252–1299, Nov. 2012.

[335] K. Demircan *et al.*, 'Increased mRNA expression of ADAMTS metalloproteinases in metastatic foci of head and neck cancer', *Head & Neck*, vol. 31, no. 6, pp. 793–801, Jun. 2009.

[336] S. Porter *et al.*, 'Dysregulated Expression of Adamalysin-Thrombospondin Genes in Human Breast Carcinoma', *Clin Cancer Res*, vol. 10, no. 7, pp. 2429–2440, Apr. 2004.

[337] Y.-P. Hsu, C. A. Staton, N. Cross, and D. J. Buttle, 'Anti-angiogenic properties of ADAMTS-4 in vitro', *International Journal of Experimental Pathology*, vol. 93, no. 1, pp. 70–77, Feb. 2012.

[338] G. Murphy, 'Tissue inhibitors of metalloproteinases', *Genome Biology*, vol. 12, no. 11, p. 233, Nov. 2011.

[339] A. Amour *et al.*, 'The in vitro activity of ADAM-10 is inhibited by TIMP-1 and TIMP-3', *FEBS Letters*, vol. 473, no. 3, pp. 275–279, May 2000.

[340] J. Carlos Rodríguez-Manzaneque *et al.*, 'ADAMTS1 cleaves aggrecan at multiple sites and is differentially inhibited by metalloproteinase inhibitors', *Biochemical and Biophysical Research Communications*, vol. 293, no. 1, pp. 501–508, Apr. 2002.

[341] G. J. Wayne *et al.*, 'TIMP-3 Inhibition of ADAMTS-4 (Aggrecanase-1) Is Modulated by Interactions between Aggrecan and the C-terminal Domain of ADAMTS-4', *J. Biol. Chem.*, vol. 282, no. 29, pp. 20991–20998, Jul. 2007.

[342] B. Anand-Apte *et al.*, 'A review of tissue inhibitor of metalloproteinases-3 (TIMP-3) and experimental analysis of its effect on primary tumor growth', *Biochem. Cell Biol.*, vol. 74, no. 6, pp. 853–862, Dec. 1996.

[343] J. H. Qi *et al.*, 'A novel function for tissue inhibitor of metalloproteinases-3 (TIMP3): inhibition of angiogenesis by blockage of VEGF binding to VEGF receptor-2', *Nature Medicine*, vol. 9, no. 4, pp. 407–415, Apr. 2003.

[344] A. Bretscher, K. Edwards, and R. G. Fehon, 'ERM proteins and merlin: integrators at the cell cortex', *Nature Reviews Molecular Cell Biology*, vol. 3, no. 8, pp. 586–599, Aug. 2002.

[345] A. H. Chishti *et al.*, 'The FERM domain: a unique module involved in the linkage of cytoplasmic proteins to the membrane', *Trends in Biochemical Sciences*, vol. 23, no. 8, pp. 281–282, Aug. 1998.

[346] C. Chen, H. Chi, L. Min, and Z. Junhua, 'Downregulation of guanine nucleotide-binding protein beta 1 (GNB1) is associated with worsened prognosis of clearcell renal cell carcinoma and is related to VEGF signaling pathway', *J BUON*, vol. 22, no. 6, pp. 1441–1446, Dec. 2017.

[347] T. Jiang *et al.*, 'CD146 is a co-receptor for VEGFR-2 in tumor angiogenesis', *Blood*, p. blood-2012-01-406108, Jan. 2012.

[348] A. Ouhtit *et al.*, 'Towards understanding the mode of action of the multifaceted cell adhesion receptor CD146', *Biochimica et Biophysica Acta (BBA) - Reviews on Cancer*, vol. 1795, no. 2, pp. 130–136, Apr. 2009.

[349] T. Hosaka *et al.*, 'Vasohibin-1 Expression in Endothelium of Tumor Blood Vessels Regulates Angiogenesis', *The American Journal of Pathology*, vol. 175, no. 1, pp. 430–439, Jul. 2009.

[350] A. Mariotti, P. A. Kedeshian, M. Dans, A. M. Curatola, L. Gagnoux-Palacios, and F. G. Giancotti, 'EGF-R signaling through Fyn kinase disrupts the function of integrin α6β4 at hemidesmosomes: role in epithelial cell migration and carcinoma invasion', *J Cell Biol*, vol. 155, no. 3, pp. 447–458, Oct. 2001.

[351] L. Seetharam, N. Gotoh, Y. Maru, G. Neufeld, S. Yamaguchi, and M. Shibuya, 'A unique signal transduction from FLT tyrosine kinase, a receptor for vascular endothelial growth factor VEGF.', *Oncogene*, vol. 10, no. 1, pp. 135–147, Jan. 1995.

[352] E. A. Jaffe, L. W. Hoyer, and R. L. Nachman, 'Synthesis of von Willebrand Factor by Cultured Human Endothelial Cells', *PNAS*, vol. 71, no. 5, pp. 1906–1909, May 1974.

[353] R. Nachman, R. Levine, and E. A. Jaffe, 'Synthesis of Factor VIII Antigen by Cultured Guinea Pig Megakaryocytes', *J Clin Invest*, vol. 60, no. 4, pp. 914–921, Oct. 1977.

[354] J. J. Cook, M. Trybulec, E. C. Lasz, S. Khan, and S. Niewiarowski, 'Binding of glycoprotein IIIa-derived peptide 217–231 to fibrinogen and von Willebrand factors and its inhibition by platelet glycoprotein IIb/IIIa complex', *Biochimica et Biophysica Acta (BBA) - Protein Structure and Molecular Enzymology*, vol. 1119, no. 3, pp. 312–321, Mar. 1992.

[355] S. Kaur, G. Martin-Manso, M. L. Pendrak, S. H. Garfield, J. S. Isenberg, and D. D. Roberts, 'Thrombospondin-1 inhibits vascular endothelial growth factor receptor-2 signaling by disrupting its association with CD47', *J. Biol. Chem.*, p. jbc.M110.172304, Oct. 2010.

[356] D. F. Mosher, M. J. Doyle, and E. A. Jaffe, 'Synthesis and secretion of thrombospondin by cultured human endothelial cells.', *The Journal of Cell Biology*, vol. 93, no. 2, pp. 343–348, May 1982.

[357] A. R. Reynolds *et al.*, 'Elevated Flk1 (Vascular Endothelial Growth Factor Receptor 2) Signaling Mediates Enhanced Angiogenesis in β3-Integrin–Deficient Mice', *Cancer Res*, vol. 64, no. 23, pp. 8643–8650, Dec. 2004.

[358] E. Fuchs and K. Weber, 'Intermediate Filaments: Structure, Dynamics, Function and Disease', *Annual Review of Biochemistry*, vol. 63, no. 1, pp. 345–382, 1994.

[359] E. E. Charrier and P. A. Janmey, 'Mechanical properties of intermediate filament proteins', *Methods Enzymol*, vol. 568, pp. 35–57, 2016.

[360] H. Herrmann and U. Aebi, 'INTERMEDIATE FILAMENTS : Molecular Structure, Assembly Mechanism, and Integration Into Functionally Distinct Intracellular Scaffolds', *Annual Review of Biochemistry*, vol. 73, no. 1, pp. 749–789, Jun. 2004.

[361] L. Chang, Y. Shav-Tal, T. Trcek, R. H. Singer, and R. D. Goldman, 'Assembling an intermediate filament network by dynamic cotranslation', *J Cell Biol*, vol. 172, no. 5, pp. 747–758, Feb. 2006.

[362] M. B. Omary, P. A. Coulombe, and W. H. I. McLean, ‘Intermediate Filament Proteins and Their Associated Diseases’, *New England Journal of Medicine*, vol. 351, no. 20, pp. 2087–2100, Nov. 2004.

[363] J. Schweizer *et al.*, ‘New consensus nomenclature for mammalian keratins’, *J Cell Biol*, vol. 174, no. 2, pp. 169–174, Jul. 2006.

[364] J. D. Gorham, E. B. Ziff, and H. Baker, ‘Differential spatial and temporal expression of two type III intermediate filament proteins in olfactory receptor neurons’, *Neuron*, vol. 7, no. 3, pp. 485–497, Sep. 1991.

[365] W. T. Clarke *et al.*, ‘Syncoilin modulates peripherin filament networks and is necessary for large-calibre motor neurons’, *Journal of Cell Science*, p. jcs.059113, Jan. 2010.

[366] K. P. García-Pelagio *et al.*, ‘Myopathic changes in murine skeletal muscle lacking synemin’, *Am J Physiol Cell Physiol*, vol. 308, no. 6, pp. C448–C462, Mar. 2015.

[367] H. Jacomy, Q. Zhu, S. Couillard-Després, J.-M. Beaulieu, and J.-P. Julien, ‘Disruption of Type IV Intermediate Filament Network in Mice Lacking the Neurofilament Medium and Heavy Subunits’, *Journal of Neurochemistry*, vol. 73, no. 3, pp. 972–984, Sep. 1999.

[368] A. M. Kachinsky, J. A. Dominov, and J. B. Miller, ‘Intermediate filaments in cardiac myogenesis: nestin in the developing mouse heart.’, *J Histochem Cytochem.*, vol. 43, no. 8, pp. 843–847, Aug. 1995.

[369] G. Goulielmos *et al.*, ‘Filensin and phakinin form a novel type of beaded intermediate filaments and coassemble de novo in cultured cells.’, *The Journal of Cell Biology*, vol. 132, no. 4, pp. 643–655, Feb. 1996.

[370] R. Foisner and G. Wiche, ‘Intermediate filament-associated proteins’, *Current Opinion in Cell Biology*, vol. 3, no. 1, pp. 75–81, Feb. 1991.

[371] H. Herrmann, H. Bär, L. Kreplak, S. V. Strelkov, and U. Aebi, ‘Intermediate filaments: from cell architecture to nanomechanics’, *Nature Reviews Molecular Cell Biology*, vol. 8, no. 7, pp. 562–573, Jul. 2007.

[372] H. Svachova, S. Sevcikova, and R. Hajek, ‘Heterogeneity and Plasticity of Multiple Myeloma’, in *Multiple Myeloma - A Quick Reflection on the Fast Progress*, R. Hajek, Ed. InTech, 2013.

[373] W. W. Franke, E. Schmid, M. Osborn, and K. Weber, ‘Intermediate-sized filaments of human endothelial cells.’, *The Journal of Cell Biology*, vol. 81, no. 3, pp. 570–580, Jun. 1979.

[374] H. Herrmann *et al.*, ‘Structure and Assembly Properties of the Intermediate Filament Protein Vimentin: The Role of its Head, Rod and Tail Domains’, *Journal of Molecular Biology*, vol. 264, no. 5, pp. 933–953, Dec. 1996.

[375] R. D. Goldman, S. Khuon, Y. H. Chou, P. Opal, and P. M. Steinert, ‘The function of intermediate filaments in cell shape and cytoskeletal integrity.’, *The Journal of Cell Biology*, vol. 134, no. 4, pp. 971–983, Aug. 1996.

[376] T. Katsumoto, A. Mitsushima, and T. Kurimura, ‘The role of the vimentin intermediate filaments in rat 3Y1 cells elucidated by immunoelectron microscopy and computer-graphic reconstruction’, *Biology of the Cell*, vol. 68, no. 1, pp. 139–146, Jan. 1990.

[377] Y. Byun, F. Chen, R. Chang, M. Trivedi, K. J. Green, and V. L. Cryns, 'Caspase cleavage of vimentin disrupts intermediate filaments and promotes apoptosis', *Cell Death and Differentiation*, vol. 8, no. 5, pp. 443–450, May 2001.

[378] W. W. Franke, C. Grund, C. Kuhn, B. W. Jackson, and K. Illmensee, 'Formation of Cytoskeletal Elements During Mouse Embryogenesis: III. Primary Mesenchymal Cells and the First Appearance of Vimentin Filaments', *Differentiation*, vol. 23, no. 1, pp. 43–59, Dec. 1982.

[379] S. H. Lang *et al.*, 'Enhanced expression of vimentin in motile prostate cell lines and in poorly differentiated and metastatic prostate carcinoma', *The Prostate*, vol. 52, no. 4, pp. 253–263, Sep. 2002.

[380] M. J. C. Hendrix, E. A. Seftor, Y.-W. Chu, K. T. Trevor, and R. E. B. Seftor, 'Role of intermediate filaments in migration, invasion and metastasis', *Cancer Metast Rev*, vol. 15, no. 4, pp. 507–525, Dec. 1996.

[381] F. C. Ramaekers, D. Haag, A. Kant, O. Moesker, P. H. Jap, and G. P. Vooijs, 'Coexpression of keratin- and vimentin-type intermediate filaments in human metastatic carcinoma cells', *PNAS*, vol. 80, no. 9, pp. 2618–2622, May 1983.

[382] A. D. Bershadsky, I. S. Tint, and T. M. Svitkina, 'Association of intermediate filaments with vinculin-containing adhesion plaques of fibroblasts', *Cell Motility*, vol. 8, no. 3, pp. 274–283, Jan. 1987.

[383] R. Bhattacharya *et al.*, 'Recruitment of vimentin to the cell surface by 3 integrin and plectin mediates adhesion strength', *Journal of Cell Science*, vol. 122, no. 9, pp. 1390–1400, May 2009.

[384] J. Kim *et al.*, 'Vimentin filaments regulate integrin-ligand interactions by binding to the cytoplasmic tail of integrin β3', *J. Cell. Sci.*, Apr. 2016.

[385] D. Tsuruta and J. C. R. Jones, 'The vimentin cytoskeleton regulates focal contact size and adhesion of endothelial cells subjected to shear stress', *Journal of Cell Science*, vol. 116, no. 24, pp. 4977–4984, Dec. 2003.

[386] P. M. Steinert *et al.*, 'A high molecular weight intermediate filament-associated protein in BHK-21 cells is nestin, a type VI intermediate filament protein. Limited co-assembly in vitro to form heteropolymers with type III vimentin and type IV alpha-internexin', *J. Biol. Chem.*, vol. 274, no. 14, pp. 9881–9890, Apr. 1999.

[387] U. Lendahl, L. B. Zimmerman, and R. D. G. McKay, 'CNS stem cells express a new class of intermediate filament protein', *Cell*, vol. 60, no. 4, pp. 585–595, Feb. 1990.

[388] J. Dahlstrand, V. P. Collins, and U. Lendahl, 'Expression of the Class VI Intermediate Filament Nestin in Human Central Nervous System Tumors', *Cancer Res*, vol. 52, no. 19, pp. 5334–5341, Oct. 1992.

[389] E. Cattaneo and R. McKay, 'Proliferation and differentiation of neuronal stem cells regulated by nerve growth factor', *Nature*, vol. 347, no. 6295, pp. 762–765, Oct. 1990.

[390] D. Park *et al.*, 'Nestin Is Required for the Proper Self-Renewal of Neural Stem Cells', *STEM CELLS*, vol. 28, no. 12, pp. 2162–2171, Dec. 2010.

[391] C. Wiese *et al.*, 'Nestin expression – a property of multi-lineage progenitor cells?', *CMLS, Cell. Mol. Life Sci.*, vol. 61, no. 19, pp. 2510–2522, Oct. 2004.

[392] R. C. S. Lin, D. F. Matesic, M. Marvin, R. D. G. McKay, and O. Brüstle, 'Re-expression of the intermediate filament nestin in reactive astrocytes', *Neurobiology of Disease*, vol. 2, no. 2, pp. 79–85, Apr. 1995.

[393] J. Namiki and C. H. Tator, 'Cell Proliferation and Nestin Expression in the Ependyma of the Adult Rat Spinal Cord after Injury', *J Neuropathol Exp Neurol*, vol. 58, no. 5, pp. 489–498, May 1999.

[394] T. Ishiwata, K. Teduka, T. Yamamoto, K. Kawahara, Y. Matsuda, and Z. Naito, 'Neuroepithelial stem cell marker nestin regulates the migration, invasion and growth of human gliomas', *Oncology Reports*, vol. 26, no. 1, pp. 91–99, Jul. 2011.

[395] J. Mokrý *et al.*, 'Nestin Expression by Newly Formed Human Blood Vessels', *Stem Cells and Development*, vol. 13, no. 6, pp. 658–664, Dec. 2004.

[396] N. Teranishi *et al.*, 'Identification of neovasculature using nestin in colorectal cancer', *International Journal of Oncology*, Mar. 2007.

[397] K. Sugawara *et al.*, 'Nestin as a marker for proliferative endothelium in gliomas', *Lab. Invest.*, vol. 82, no. 3, pp. 345–351, Mar. 2002.

[398] W. Kleeberger *et al.*, 'Roles for the Stem Cell–Associated Intermediate Filament Nestin in Prostate Cancer Migration and Metastasis', *Cancer Res*, vol. 67, no. 19, pp. 9199–9206, Oct. 2007.

[399] K. Vuoriluoto *et al.*, 'Vimentin regulates EMT induction by Slug and oncogenic H-Ras and migration by governing Axl expression in breast cancer', *Oncogene*, vol. 30, no. 12, pp. 1436–1448, Mar. 2011.

[400] C. L. Hyder, G. Lazaro, J. W. Pylvänäinen, M. W. G. Roberts, S. M. Rosenberg, and J. E. Eriksson, 'Nestin regulates prostate cancer cell invasion by influencing FAK and integrin localisation and functions', *J Cell Sci*, p. jcs.125062, Jan. 2014.

[401] Y. Matsuda, Z. Naito, K. Kawahara, N. Nakazawa, M. Korc, and T. Ishiwata, 'Nestin is a novel target for suppressing pancreatic cancer cell migration, invasion and metastasis', *Cancer Biology & Therapy*, vol. 11, no. 5, pp. 512–523, Mar. 2011.

[402] L. Winter and G. Wiche, 'The many faces of plectin and plectinopathies: pathology and mechanisms', *Acta Neuropathologica*, vol. 125, no. 1, pp. 77–93, Jan. 2013.

[403] K. Andrä *et al.*, 'Targeted inactivation of plectin reveals essential function in maintaining the integrity of skin, muscle, and heart cytoarchitecture', *Genes Dev.*, vol. 11, no. 23, pp. 3143–3156, Dec. 1997.

[404] T. M. Svitkina, A. B. Verkhovsky, and G. G. Borisy, 'Plectin sidearms mediate interaction of intermediate filaments with microtubules and other components of the cytoskeleton', *J. Cell Biol.*, vol. 135, no. 4, pp. 991–1007, Nov. 1996.

[405] T. Hijikata, T. Murakami, H. Ishikawa, and H. Yorifuji, 'Plectin tethers desmin intermediate filaments onto subsarcolemmal dense plaques containing dystrophin and vinculin', *Histochem Cell Biol*, vol. 119, no. 2, pp. 109–123, Feb. 2003.

[406] S. M. Homan, R. Martinez, A. Benware, and S. E. LaFlamme, 'Regulation of the Association of α6β4 with Vimentin Intermediate Filaments in Endothelial Cells', *Experimental Cell Research*, vol. 281, no. 1, pp. 107–114, Nov. 2002.

[407] S. M. Homan, A. M. Mercurio, and S. E. LaFlamme, 'Endothelial cells assemble two distinct alpha6beta4-containing vimentin-associated structures: roles for ligand binding and the beta4 cytoplasmic tail', *Journal of Cell Science*, vol. 111, no. 18, pp. 2717–2728, Sep. 1998.

[408] G. J. Seifert, D. Lawson, and G. Wiche, 'Immunolocalization of the intermediate filament-associated protein plectin at focal contacts and actin stress fibers', *Eur. J. Cell Biol.*, vol. 59, no. 1, pp. 138–147, Oct. 1992.

[409] G. Wiche, 'Cytoplasmic network arrays demonstrated by immunolocalization using antibodies to a high molecular weight protein present in cytoskeletal preparations from cultured cells*1', *Experimental Cell Research*, vol. 138, no. 1, pp. 15–29, Mar. 1982.

[410] S. Osmanagic-Myers *et al.*, 'Plectin reinforces vascular integrity by mediating vimentin-actin network crosstalk', *J Cell Sci*, p. jcs.172056, Jan. 2015.

[411] D. Bausch *et al.*, 'Plectin-1 as a novel biomarker for pancreatic cancer', *Clin Cancer Res*, vol. 17, no. 2, pp. 302–309, Jan. 2011.

[412] E. Fuchs, 'Bridging cytoskeletal intersections', *Genes & Development*, vol. 15, no. 1, pp. 1–14, Jan. 2001.

[413] M. Mirjalili *et al.*, 'Steroidal Lactones from Withania somnifera, an Ancient Plant for Novel Medicine', *Molecules*, vol. 14, no. 7, pp. 2373–2393, Jul. 2009.

[414] L.-C. Mishra, 'Scientific Basis for the Therapeutic Use of Withania somnifera (Ashwagandha): A Review', *Alternative Medicine Review*, vol. 5, no. 4, p. 13, 2000.

[415] J. Lee *et al.*, 'Withaferin A is a leptin sensitizer with strong antidiabetic properties in mice', *Nature Medicine*, vol. 22, no. 9, pp. 1023–1032, Sep. 2016.

[416] R. Maitra, M. A. Porter, S. Huang, and B. P. Gilmour, 'Inhibition of NFκB by the natural product Withaferin A in cellular models of Cystic Fibrosis inflammation', *Journal of Inflammation*, vol. 6, no. 1, p. 15, May 2009.

[417] R. Mohan *et al.*, 'Withaferin A is a potent inhibitor of angiogenesis', *Angiogenesis*, vol. 7, no. 2, pp. 115–122, Jun. 2004.

[418] Y. Yu *et al.*, 'Withaferin A targets heat shock protein 90 in pancreatic cancer cells', *Biochemical Pharmacology*, vol. 79, no. 4, pp. 542–551, Feb. 2010.

[419] S. D. Stan, E.-R. Hahm, R. Warin, and S. V. Singh, 'Withaferin A Causes FOXO3a- and Bim-Dependent Apoptosis and Inhibits Growth of Human Breast Cancer Cells In vivo', *Cancer Res*, vol. 68, no. 18, pp. 7661–7669, Sep. 2008.

[420] K. S. vel Szic *et al.*, 'Pharmacological Levels of Withaferin A (Withania somnifera) Trigger Clinically Relevant Anticancer Effects Specific to Triple Negative Breast Cancer Cells', *PLOS ONE*, vol. 9, no. 2, p. e87850, Feb. 2014.

[421] S.-H. Kim and S. V. Singh, 'Mammary Cancer Chemoprevention by Withaferin A Is Accompanied by In Vivo Suppression of Self-Renewal of Cancer Stem Cells', *Cancer Prev Res*, p. canprevres.0445.2013, May 2014.

[422] M. Kaileh *et al.*, 'Withaferin A Strongly Elicits IκB Kinase β Hyperphosphorylation Concomitant with Potent Inhibition of Its Kinase Activity', *J. Biol. Chem.*, vol. 282, no. 7, pp. 4253–4264, Feb. 2007.

[423] H. L. Pahl, ‘Activators and target genes of Rel/NF-κB transcription factors’, *Oncogene*, vol. 18, no. 49, pp. 6853–6866, Nov. 1999.

[424] J. A. Romashkova and S. S. Makarov, ‘NF-κB is a target of AKT in anti-apoptotic PDGF signalling’, *Nature*, vol. 401, no. 6748, pp. 86–90, Sep. 1999.

[425] S. Ghosh and D. Baltimore, ‘Activation in vitro of NF-κB" by phosphorylation of its inhibitor IκB"’, *Nature*, vol. 344, no. 6267, pp. 678–682, Apr. 1990.

[426] V. J. Palombella, O. J. Rando, A. L. Goldberg, and T. Maniatis, ‘The ubiquitinproteasome pathway is required for processing the NF-κB1 precursor protein and the activation of NF-κB’, *Cell*, vol. 78, no. 5, pp. 773–785, Sep. 1994.

[427] B. Grin *et al.*, ‘Withaferin A Alters Intermediate Filament Organization, Cell Shape and Behavior’, *PLOS ONE*, vol. 7, no. 6, p. e39065, Jun. 2012.

[428] P. Bargagna-Mohan *et al.*, ‘The Tumor Inhibitor and Antiangiogenic Agent Withaferin A Targets the Intermediate Filament Protein Vimentin’, *Chemistry & Biology*, vol. 14, no. 6, pp. 623–634, Jun. 2007.

[429] P. Bargagna-Mohan *et al.*, ‘Vimentin Phosphorylation Underlies Myofibroblast Sensitivity to Withaferin A In Vitro and during Corneal Fibrosis’, *PLOS ONE*, vol. 10, no. 7, p. e0133399, Jul. 2015.

[430] M. B. Omary, N.-O. Ku, G.-Z. Tao, D. M. Toivola, and J. Liao, ‘“Heads and tails” of intermediate filament phosphorylation: multiple sites and functional insights’, *Trends in Biochemical Sciences*, vol. 31, no. 7, pp. 383–394, Jul. 2006.

[431] ‘Regulatory mechanisms and functions of intermediate filaments: A study using site- and phosphorylation state-specific antibodies - Izawa - 2006 - Cancer Science - Wiley Online Library’. [Online]. Available: https://onlinelibrary.wiley.com/doi/full/10.1111/j.1349-7006.2006.00161.x. [Accessed: 17-Oct-2018].

[432] Q.-S. Zhu *et al.*, ‘Vimentin is a novel AKT1 target mediating motility and invasion’, *Oncogene*, vol. 30, no. 4, pp. 457–470, Jan. 2011.

[433] M. Inagaki, Y. Nishi, K. Nishizawa, M. Matsuyama, and C. Sato, ‘Site-specific phosphorylation induces disassembly of vimentin filaments in vitro’, *Nature*, vol. 328, no. 6131, pp. 649–652, Aug. 1987.

[434] S. D. Stan, Y. Zeng, and S. V. Singh, ‘Ayurvedic Medicine Constituent Withaferin A Causes G2 and M Phase Cell Cycle Arrest in Human Breast Cancer Cells’, *Nutrition and Cancer*, vol. 60, no. sup1, pp. 51–60, Nov. 2008.

[435] J. H. Oh and T. K. Kwon, ‘Withaferin A inhibits tumor necrosis factor-α-induced expression of cell adhesion molecules by inactivation of Akt and NF-κB in human pulmonary epithelial cells’, *International Immunopharmacology*, vol. 9, no. 5, pp. 614–619, May 2009.

[436] O. Esue, A. A. Carson, Y. Tseng, and D. Wirtz, ‘A Direct Interaction between Actin and Vimentin Filaments Mediated by the Tail Domain of Vimentin’, *J. Biol. Chem.*, vol. 281, no. 41, pp. 30393–30399, Oct. 2006.

[437] A. Bocquet, R. Berges, R. Frank, P. Robert, A. C. Peterson, and J. Eyer, ‘Neurofilaments Bind Tubulin and Modulate Its Polymerization’, *J. Neurosci.*, vol. 29, no. 35, pp. 11043–11054, Sep. 2009.

[438] P. Rudrabhatla, H. Jaffe, and H. C. Pant, 'Direct evidence of phosphorylated neuronal intermediate filament proteins in neurofibrillary tangles (NFTs): phosphoproteomics of Alzheimer's NFTs', *The FASEB Journal*, vol. 25, no. 11, pp. 3896–3905, Aug. 2011.

[439] S. D. J. Pena and C. R. Scriver, '1599 Identification of Intermediate Filament Aggregates in Cultured Skin Fibroblasts from Patients with Giant Axonal Neuropathy', *Pediatric Research*, vol. 15, no. S4, p. 709, Apr. 1981.

[440] D. H. Ausprunk and J. Folkman, 'Migration and proliferation of endothelial cells in preformed and newly formed blood vessels during tumor angiogenesis', *Microvascular Research*, vol. 14, no. 1, pp. 53–65, Jul. 1977.

[441] D. F. Lazarous *et al.*, 'Comparative Effects of Basic Fibroblast Growth Factor and Vascular Endothelial Growth Factor on Coronary Collateral Development and the Arterial Response to Injury', *Circulation*, Sep. 1996.

[442] S. Rousseau, F. Houle, J. Landry, and J. Huot, 'p38 MAP kinase activation by vascular endothelial growth factor mediates actin reorganization and cell migration in human endothelial cells', *Oncogene*, vol. 15, no. 18, pp. 2169–2177, Oct. 1997.

[443] C. Leduc and S. Etienne-Manneville, 'Intermediate filaments in cell migration and invasion: the unusual suspects', *Current Opinion in Cell Biology*, vol. 32, pp. 102–112, Feb. 2015.

[444] J. T. Thaiparambil *et al.*, 'Withaferin A inhibits breast cancer invasion and metastasis at sub-cytotoxic doses by inducing vimentin disassembly and serine 56 phosphorylation', *International journal of cancer*, vol. 129, no. 11, pp. 2744–2755, 2011.

[445] 'Vimentin Phosphorylation Underlies Myofibroblast Sensitivity to Withaferin A In Vitro and during Corneal Fibrosis'. [Online]. Available: https://journals.plos.org/plosone/article?id=10.1371/journal.pone.0133399. [Accessed: 31-Aug-2018].

[446] J. M. Dave, H. Kang, C. A. Abbey, S. A. Maxwell, and K. J. Bayless, 'Proteomic Profiling of Endothelial Invasion Revealed Receptor for Activated C Kinase 1 (RACK1) Complexed with Vimentin to Regulate Focal Adhesion Kinase (FAK)', *J. Biol. Chem.*, p. jbc.M113.512467, Sep. 2013.

[447] J. V. Shah, L. Z. Wang, P. Traub, and P. A. Janmey, 'Interaction of Vimentin With Actin and Phospholipids', *The Biological Bulletin*, vol. 194, no. 3, pp. 402–405, Jun. 1998.

[448] K. Katada *et al.*, 'Plectin promotes migration and invasion of cancer cells and is a novel prognostic marker for head and neck squamous cell carcinoma', *Journal of Proteomics*, vol. 75, no. 6, pp. 1803–1815, Mar. 2012.

[449] S. Osmanagic-Myers, M. Gregor, G. Walko, G. Burgstaller, S. Reipert, and G. Wiche, 'Plectin-controlled keratin cytoarchitecture affects MAP kinases involved in cellular stress response and migration', *J Cell Biol*, vol. 174, no. 4, pp. 557–568, Aug. 2006.

[450] J. Ševčík, L. Urbániková, J. Košťan, L. Janda, and G. Wiche, 'Actin-binding domain of mouse plectin', *European Journal of Biochemistry*, vol. 271, no. 10, pp. 1873–1884, 2004.

[451] M. Gonzales *et al.*, 'A Cell Signal Pathway Involving Laminin-5, α3β1 Integrin, and Mitogen-activated Protein Kinase Can Regulate Epithelial Cell Proliferation', *MBoC*, vol. 10, no. 2, pp. 259–270, Feb. 1999.

[452] S. Kreis, H.-J. Schönfeld, C. Melchior, B. Steiner, and N. Kieffer, 'The intermediate filament protein vimentin binds specifically to a recombinant integrin α2/β1 cytoplasmic tail complex and co-localizes with native α2/β1 in endothelial cell focal adhesions', *Experimental Cell Research*, vol. 305, no. 1, pp. 110–121, Apr. 2005.

[453] P. Bargagna-Mohan *et al.*, 'Withaferin A targets intermediate filaments GFAP and vimentin in A model of retinal gliosis', *J. Biol. Chem.*, p. jbc.M109.093765, Jan. 2010.

[454] W. Vanden Berghe, L. Sabbe, M. Kaileh, G. Haegeman, and K. Heyninck, 'Molecular insight in the multifunctional activities of Withaferin A', *Biochemical Pharmacology*, vol. 84, no. 10, pp. 1282–1291, Nov. 2012.

[455] A. Grover *et al.*, 'Hsp90/Cdc37 Chaperone/co-chaperone complex, a novel junction anticancer target elucidated by the mode of action of herbal drug Withaferin A', *BMC Bioinformatics*, vol. 12, no. 1, p. S30, Feb. 2011.

[456] H. Yang, G. Shi, and Q. P. Dou, 'The Tumor Proteasome Is a Primary Target for the Natural Anticancer Compound Withaferin A Isolated from "Indian Winter Cherry"', *Mol Pharmacol*, vol. 71, no. 2, pp. 426–437, Feb. 2007.

[457] M. I. Choudhary, S. Yousuf, S. A. Nawaz, S. Ahmed, and Atta-ur-Rahman, 'Cholinesterase Inhibiting Withanolides from Withania somnifera', *Chem. Pharm. Bull.*, vol. 52, no. 11, pp. 1358–1361, 2004.

[458] Y. Kubota, H. K. Kleinman, G. R. Martin, and T. J. Lawley, 'Role of laminin and basement membrane in the morphological differentiation of human endothelial cells into capillary-like structures.', *The Journal of Cell Biology*, vol. 107, no. 4, pp. 1589–1598, Oct. 1988.

[459] I. Arnaoutova, J. George, H. K. Kleinman, and G. Benton, 'The endothelial cell tube formation assay on basement membrane turns 20: state of the science and the art', *Angiogenesis*, vol. 12, no. 3, pp. 267–274, Sep. 2009.

[460] K. Sugawara *et al.*, 'Nestin as a Marker for Proliferative Endothelium in Gliomas', *Laboratory Investigation*, vol. 82, no. 3, pp. 345–351, Mar. 2002.

[461] S. Claxton, V. Kostourou, S. Jadeja, P. Chambon, K. Hodivala-Dilke, and M. Fruttiger, 'Efficient, inducible Cre-recombinase activation in vascular endothelium', *genesis*, vol. 46, no. 2, pp. 74–80, Feb. 2008.

[462] M. Baker *et al.*, 'Use of the mouse aortic ring assay to study angiogenesis', *Nature Protocols*, vol. 7, no. 1, pp. 89–104, Jan. 2012.

[463] A. Ventura *et al.*, 'Cre-lox-regulated conditional RNA interference from transgenes', *PNAS*, vol. 101, no. 28, pp. 10380–10385, Jul. 2004.

[464] A. Reynolds, D. Leake, Q. Boese, S. Scaringe, W. S. Marshall, and A. Khvorova, 'Rational siRNA design for RNA interference', *Nature Biotechnology*, vol. 22, no. 3, pp. 326–330, Mar. 2004.

[465] D. A. Rubinson *et al.*, 'A lentivirus-based system to functionally silence genes in primary mammalian cells, stem cells and transgenic mice by RNA interference', *Nature Genetics*, vol. 33, no. 3, pp. 401–406, Mar. 2003.

[466] N. C. Shaner, R. E. Campbell, P. A. Steinbach, B. N. G. Giepmans, A. E. Palmer, and R. Y. Tsien, 'Improved monomeric red, orange and yellow fluorescent proteins derived from

Discosoma sp. red fluorescent protein', *Nature Biotechnology*, vol. 22, no. 12, pp. 1567–1572, Dec. 2004.

[467] J. Ye, G. Coulouris, I. Zaretskaya, I. Cutcutache, S. Rozen, and T. L. Madden, 'Primer-BLAST: A tool to design target-specific primers for polymerase chain reaction', *BMC Bioinformatics*, vol. 13, no. 1, p. 134, Jun. 2012.

[468] P. M. Steinert *et al.*, 'A High Molecular Weight Intermediate Filament-associated Protein in BHK-21 Cells Is Nestin, a Type VI Intermediate Filament Protein LIMITED CO-ASSEMBLY IN VITRO TO FORM HETEROPOLYMERS WITH TYPE III VIMENTIN AND TYPE IV α-INTERNEXIN', *J. Biol. Chem.*, vol. 274, no. 14, pp. 9881–9890, Apr. 1999.

[469] R. F. Doll, J. E. Crandall, C. A. Dyer, J. M. Aucoin, and F. I. Smith, 'Comparison of promoter strengths on gene delivery into mammalian brain cells using AAV vectors.', *Gene Ther*, vol. 3, no. 5, pp. 437–447, May 1996.

[470] M. H. K. Linskens *et al.*, 'Cataloging altered gene expression in young and senescent cells using enhanced differential display', *Nucleic Acids Res*, vol. 23, no. 16, pp. 3244–3251, Aug. 1995.

[471] E. C. LeRoy and G. F. Grotendorst, 'TGF-p Inhibition of Endothelial Cell Proliferation: Alteration of EGF Binding and EGF-Induced Growth-Regulatory (Competence) Gene Expression', p. 8.

[472] 'A biomarker that identifies senescent human cells in culture and in aging skin in vivo | PNAS'. [Online]. Available: http://www.pnas.org/content/92/20/9363.short. [Accessed: 04-Dec-2018].

[473] 'Protocols to detect senescence-associated beta-galactosidase (SA-βgal) activity, a biomarker of senescent cells in culture and in vivo | Nature Protocols'. [Online]. Available: https://www.nature.com/articles/nprot.2009.191. [Accessed: 04-Dec-2018].

[474] S. Suzuki, J. Namiki, S. Shibata, Y. Mastuzaki, and H. Okano, 'The Neural Stem/Progenitor Cell Marker Nestin Is Expressed in Proliferative Endothelial Cells, but Not in Mature Vasculature':, *Journal of Histochemistry & Cytochemistry*, Apr. 2010.

[475] J. Kim *et al.*, 'Vimentin filaments regulate integrin–ligand interactions by binding to the cytoplasmic tail of integrin β3', *J Cell Sci*, vol. 129, no. 10, pp. 2030–2042, May 2016.

[476] C. Waldner, M. Roose, and G. U. Ryffel, 'Red fluorescent Xenopus laevis: a new tool for grafting analysis', *BMC Developmental Biology*, vol. 9, no. 1, p. 37, Jun. 2009.

[477] S. Graewe, S. Retzlaff, N. Struck, C. Janse, and V. Heussler, 'Going live: a comparative analysis of the suitability of the RFP derivates RedStar, mCherry and tdTomato for intravital and in vitro live imaging of Plasmodium parasites', *Biotechnology Journal*, vol. 4, no. 7, p. 895, Jun. 2009.

[478] A. B. Nair and S. Jacob, 'A simple practice guide for dose conversion between animals and human', *J Basic Clin Pharm*, vol. 7, no. 2, pp. 27–31, Mar. 2016.

[479] A. C. Sharada, F. E. Solomon, P. U. Devi, N. Udupa, and K. K. Srinivasan, 'Antitumor and Radiosensitizing Effects of Withaferin a on Mouse Ehrlich Ascites Carcinoma in vivo', *Acta Oncologica*, vol. 35, no. 1, pp. 95–100, Jan. 1996.

[480] D. Laviee and Y. Shvo, '1371. Constituents of Withania somnifera Dun. Part 1V.l The Xtructure of Withaferin A', p. 15.

[481] R. R. Kulkarni, P. S. Patki, V. P. Jog, S. G. Gandage, and B. Patwardhan, 'Treatment of osteoarthritis with a herbomineral formulation: a double-blind, placebo-controlled, cross-over study', *J Ethnopharmacol*, vol. 33, no. 1–2, pp. 91–95, Jun. 1991.

[482] S. Venkataraghavan, C. Seshadri, T. P. Sundaresan, R. Revathi, V. Rajagopalan, and K. Janaki, 'The comparative effect of milk fortified with Ashwagandha and punarnava in children – a double-blind study', Jan. 1980.

[483] K. Bone, *Clinical applications of Ayurvedic and Chinese herbs: monographs for the Western herbal practitioner*. Warwick, Qld.: Phytotherapy Press, 1996.

[484] M. Ganzera, M. I. Choudhary, and I. A. Khan, 'Quantitative HPLC analysis of withanolides in Withania somnifera', *Fitoterapia*, vol. 74, no. 1, pp. 68–76, Feb. 2003.

[485] P. C. Prabu, S. Panchapakesan, and C. D. Raj, 'Acute and Sub-Acute Oral Toxicity Assessment of the Hydroalcoholic Extract of Withania somnifera Roots in Wistar Rats', *Phytotherapy Research*, vol. 27, no. 8, pp. 1169–1178, Aug. 2013.

[486] 'Search of: withania - List Results - ClinicalTrials.gov'. [Online]. Available: https://clinicaltrials.gov/ct2/results?cond=&term=withania&cntry=&state=&city=&dist=. [Accessed: 12-Nov-2018].

[487] A. K. Sharma, I. Basu, and S. Singh, 'Efficacy and Safety of Ashwagandha Root Extract in Subclinical Hypothyroid Patients: A Double-Blind, Randomized Placebo-Controlled Trial', *J Altern Complement Med*, vol. 24, no. 3, pp. 243–248, Mar. 2018.

[488] K. N. R. Chengappa, J. S. Brar, J. M. Gannon, and P. J. Schlicht, 'Adjunctive Use of a Standardized Extract of Withania somnifera (Ashwagandha) to Treat Symptom Exacerbation in Schizophrenia: A Randomized, Double-Blind, Placebo-Controlled Study', *J Clin Psychiatry*, vol. 79, no. 5, Jul. 2018.

[489] K. N. R. Chengappa, C. R. Bowie, P. J. Schlicht, D. Fleet, J. S. Brar, and R. Jindal, 'Randomized placebo-controlled adjunctive study of an extract of withania somnifera for cognitive dysfunction in bipolar disorder', *J Clin Psychiatry*, vol. 74, no. 11, pp. 1076–1083, Nov. 2013.

[490] V. R. Ambiye, D. Langade, S. Dongre, P. Aptikar, M. Kulkarni, and A. Dongre, 'Clinical Evaluation of the Spermatogenic Activity of the Root Extract of Ashwagandha (Withania somnifera) in Oligospermic Males: A Pilot Study', *Evidence-Based Complementary and Alternative Medicine*, 2013. [Online]. Available: https://www.hindawi.com/journals/ecam/2013/571420/abs/. [Accessed: 12-Nov-2018].

[491] S. Dongre, D. Langade, and S. Bhattacharyya, 'Efficacy and Safety of Ashwagandha (Withania somnifera) Root Extract in Improving Sexual Function in Women: A Pilot Study', *BioMed Research International*, 2015. [Online]. Available: https://www.hindawi.com/journals/bmri/2015/284154/abs/. [Accessed: 12-Nov-2018].

[492] S. B. Patel, N. J. Rao, and L. L. Hingorani, 'Safety assessment of Withania somnifera extract standardized for Withaferin A: Acute and sub-acute toxicity study', *J Ayurveda Integr Med*, vol. 7, no. 1, pp. 30–37, Mar. 2016.

[493] E. Gustafsson, C. Brakebusch, K. Hietanen, and R. Fassler, 'Tie-1-directed expression of Cre recombinase in endothelial cells of embryoid bodies and transgenic mice', *Journal of Cell Science*, vol. 114, no. 4, pp. 671–676, Feb. 2001.

[494] S. A. Schnell, W. A. Staines, and M. W. Wessendorf, 'Reduction of Lipofuscin-like Autofluorescence in Fluorescently Labeled Tissue , Reduction of Lipofuscin-like Autofluorescence in Fluorescently Labeled Tissue', *J Histochem Cytochem.*, vol. 47, no. 6, pp. 719–730, Jun. 1999.

[495] W.M.S. Russell, R.L. Burch, *The Principles of Humane Experimental Technique*. London, UK: Methuen, 1959.

[496] J. Mokrý *et al.*, 'Nestin Expression by Newly Formed Human Blood Vessels', *Stem Cells and Development*, vol. 13, no. 6, pp. 658–664, Dec. 2004.

[497] F. A. Steinböck and G. Wiche, 'Plectin: A Cytolinker by Design', *Biological Chemistry*, vol. 380, no. 2, pp. 151–158, 1999.

[498] F. Heitz, T. Johansson, K. Baumgärtel, R. Gecaj, P. Pelczar, and I. M. Mansuy, 'Heritable and inducible gene knockdown in astrocytes or neurons in vivo by a combined lentiviral and RNAi approach', *Front. Cell. Neurosci.*, vol. 8, 2014.

[499] C. Lois, E. J. Hong, S. Pease, E. J. Brown, and D. Baltimore, 'Germline Transmission and Tissue-Specific Expression of Transgenes Delivered by Lentiviral Vectors', *Science*, vol. 295, no. 5556, pp. 868–872, Feb. 2002.

[500] K. Chandrasekhar, J. Kapoor, and S. Anishetty, 'A Prospective, Randomized Double-Blind, Placebo-Controlled Study of Safety and Efficacy of a High-Concentration Full-Spectrum Extract of Ashwagandha Root in Reducing Stress and Anxiety in Adults', *Indian J Psychol Med*, vol. 34, no. 3, pp. 255–262, 2012.

[501] M. Verheijen *et al.*, 'DMSO induces drastic changes in human cellular processes and epigenetic landscape in vitro', *Scientific Reports*, vol. 9, no. 1, Dec. 2019.

[502] K. S. Bauer, S. C. Dixon, and W. D. Figg, 'Inhibition of Angiogenesis by Thalidomide Requires Metabolic Activation, Which Is Species-dependent', *Biochemical Pharmacology*, vol. 55, no. 11, pp. 1827–1834, Jun. 1998.

[503] H. C. Haspel, G. M. Scicli, G. McMahon, and A. G. Scicli, 'Inhibition of Vascular Endothelial Growth Factor-Associated Tyrosine Kinase Activity with SU5416 Blocks Sprouting in the Microvascular Endothelial Cell Spheroid Model of Angiogenesis', *Microvascular Research*, vol. 63, no. 3, pp. 304–315, May 2002.

[504] H. Athanassiou *et al.*, 'Randomized phase II study of temozolomide and radiotherapy compared with radiotherapy alone in newly diagnosed glioblastoma multiforme', *J. Clin. Oncol.*, vol. 23, no. 10, pp. 2372–2377, Apr. 2005.

[505] R. Stupp *et al.*, 'Cilengitide combined with standard treatment for patients with newly diagnosed glioblastoma with methylated MGMT promoter (CENTRIC EORTC 26071-22072 study): a multicentre, randomised, open-label, phase 3 trial', *The Lancet Oncology*, vol. 15, no. 10, pp. 1100–1108, Sep. 2014.

[506] K. Andrä, B. Nikolic, M. Stöcher, D. Drenckhahn, and G. Wiche, 'Not just scaffolding: plectin regulates actin dynamics in cultured cells', *Genes Dev.*, vol. 12, no. 21, pp. 3442–3451, Nov. 1998.